

# Lawrence Berkeley National Laboratory

## Lawrence Berkeley National Laboratory

### Title

CIRCULAR INTENSITY DIFFERENTIAL SCATTERING OF CHIRAL MOLECULES

### Permalink

<https://escholarship.org/uc/item/4rd9s4sd>

### Author

Bustamante, Carlos J.

### Publication Date

1980-12-01



# Lawrence Berkeley Laboratory

UNIVERSITY OF CALIFORNIA

## CHEMICAL BIODYNAMICS DIVISION

CIRCULAR INTENSITY DIFFERENTIAL SCATTERING OF  
CHIRAL MOLECULES

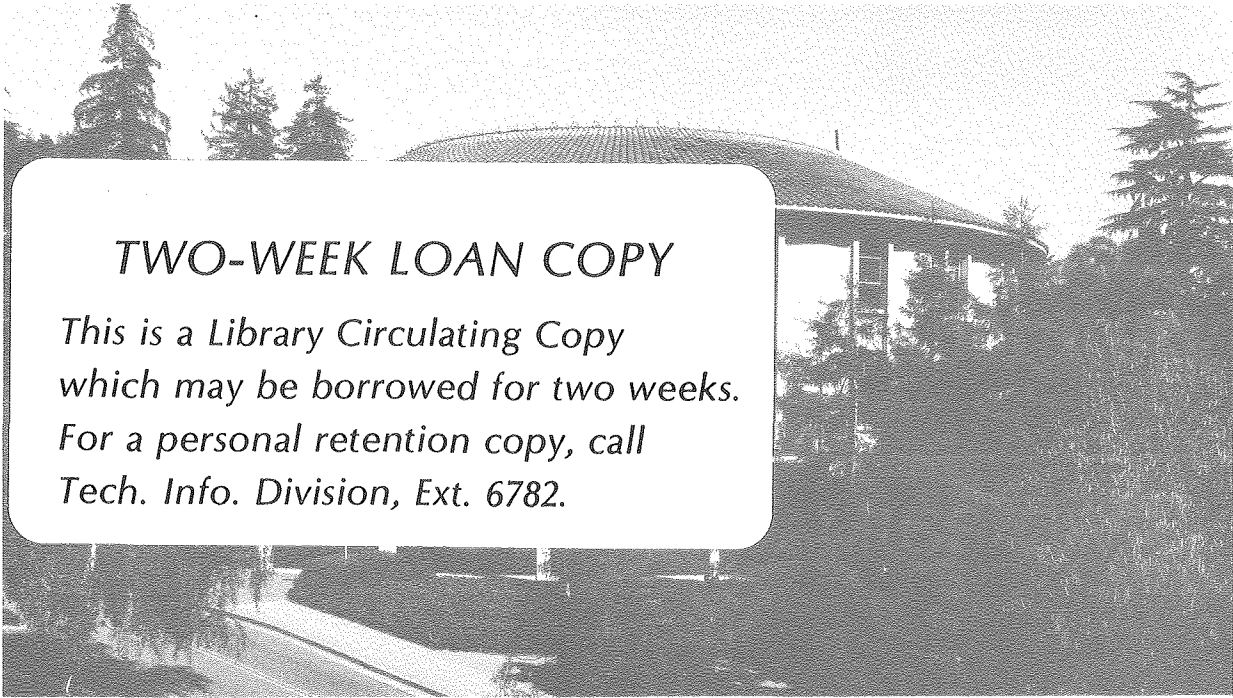
Carlos J. Bustamante  
(Ph.D. thesis)

December 1980

RECEIVED  
LAWRENCE  
BERKELEY LABORATORY

FEB 17 1981

LIBRARY AND  
CURRENTS SECTION



### TWO-WEEK LOAN COPY

*This is a Library Circulating Copy  
which may be borrowed for two weeks.  
For a personal retention copy, call  
Tech. Info. Division, Ext. 6782.*

LBL-12110 c.2

## **DISCLAIMER**

This document was prepared as an account of work sponsored by the United States Government. While this document is believed to contain correct information, neither the United States Government nor any agency thereof, nor the Regents of the University of California, nor any of their employees, makes any warranty, express or implied, or assumes any legal responsibility for the accuracy, completeness, or usefulness of any information, apparatus, product, or process disclosed, or represents that its use would not infringe privately owned rights. Reference herein to any specific commercial product, process, or service by its trade name, trademark, manufacturer, or otherwise, does not necessarily constitute or imply its endorsement, recommendation, or favoring by the United States Government or any agency thereof, or the Regents of the University of California. The views and opinions of authors expressed herein do not necessarily state or reflect those of the United States Government or any agency thereof or the Regents of the University of California.

CIRCULAR INTENSITY DIFFERENTIAL SCATTERING  
OF CHIRAL MOLECULES

CARLOS J. BUSTAMANTE

Lawrence Berkeley Laboratory  
University of California  
Berkeley, California 94720

1980

This work was supported by the U.S. Department of Energy  
under Contract W-7405-ENG-48.



## ABSTRACT

In this thesis a theory of the Circular Intensity Differential Scattering (CIDS) of chiral molecules as modelled by a helix oriented with respect to the direction of incidence of light is presented. It is shown that a necessary condition for the existence of CIDS is the presence of an asymmetric polarizability in the scatterer. The polarizability of the scatterer is assumed generally complex, so that both refractive and absorptive phenomena are taken into account.

The theory is derived within the frame of the first-Born approximation to the internal field. Under these conditions, the preferential scattering observed is characterized as FORM-CIDS, and shown to be valid for all ranges of wavelength of the incident radiation.

The symmetry laws governing the spatial distribution of the scattering intensities are derived for the case of incidence of light perpendicular to the helix axis and for a helix possessing a uniaxial tangential polarizability.

Calculations are presented for the case of a triaxial polarizability and analytical equations of the CIDS derived for a helix having a biaxial polarizability. In both cases anomalous behavior is found and their symmetry rules discussed.

It is also presented here a first correction to the

internal field by adding to the incident field the dipole radiation fields generated somewhere else in the scatterer. The main result is the presence of non-vanishing forward CIDS. This is not a form-CIDS effect.

Finally, the theory is generalized for the case of a sample of randomly oriented chiral scatterers of arbitrary geometry.

The result of this study points out the promising aspects of CIDS as a powerful technique to probe chiral regions in macromolecular aggregates.

"Learn everything about Nature  
and love it"

Guillaume Apollinaire





## DEDICATION

TO MY PARENTS:

Who first taught me to respect  
and to love knowledge.

TO SILVIA:

Because of you  
Because of our life together  
Because of Fernanda.

## ACKNOWLEDGMENTS

I would like to thank my research director Nacho Tinoco for all the support and help he has given me along these years. Perhaps more important than the day to day knowledge acquired, I learned that in science, the correct answer only comes after the correct question has been formulated. I also became aware that no work pre-exists as good or bad, great or mediocre, by itself. In any human enterprise the outcome is always the result of a will.

I want to thank in a very special way to my friend Dr. Marcos Maestre, with whom most of the scratch work of this thesis was done. His moral support has been invaluable. His endless motivation for science, almost as endless as his erudition in every subject of human knowledge, made working side by side with him a truly renacentist experience.

Professor Robert A. Harris helped me very much on every theoretical question I raised. He had always the answer.

Professor John E. Hearst kindly provided advice and answers to many questions.

Professor Wayne Hubbell was most supportive. As a T.A. for him, I truly learned Thermodynamics.

It has been a pleasure to share so many hours toge-

ther with all the members of the Tinoco's group. In particular I want to mention Barbara Dengler who was always ready to help and to listen in the hardest moments of the journey. She is to be responsible, at least in part, through her gourmet food, for some of the weight I gained since I entered the group. This responsibility must also be shared by David Koh. Through his "opinions" I learned to appreciate some of his ancient wisdom. With Helen Lok I shared many of the lunch hours I spent in the lab., and her conversation made it always a pleasure.

I want to thank my two "green" friends in the "senior graduate student office", Art Pardi and Ken Dahl, for the good time we spent together. We shared the ups and downs of our graduate work. Art, in his Californian relaxed ways and Ken, in his rather energetic approach, were a source of constant amazement to this foreigner, as I am sure I was to both of them. Art's reading of part of the manuscript of this thesis was most helpful.

At the beginning of my graduate work, and during the short period which our stay in the lab. overlapped, Alan Levin was of great help and encouragement.

I spent many hours of enlightening discussion on physics and epistemology with my close comrade, Jeff Cina, who also managed to convince me to jog up and down the Strawberry Canyon almost every day during a whole summer.

I spent very good time playing music together with Jeff Nelson. I want to thank him in particular for the many hours he put in helping me in the editing of the computer programs.

Kathi Morden and David Keller provided great companionship and comradery.

Joe Kao is a great *conversador*. We talked about many subjects, and I always learned from him about linguistics.

I am truly grateful to Kathy Hall who read most of the manuscript and made useful comments and corrections.

The preparation of this script would have not been possible without the excellent and heroic work of Stephen M. Quong, who did more than what was requested.

## INTRODUCTION

The last thirty years have witnessed the fast growth of the quantitative aspects of Biology. The great success of Biochemistry in providing better and more efficient separation methods, rapidly started to open the gigantic panorama of the molecular anatomy and physiology of the simplest living organisms.

At one side of the spectrum, biologically oriented researchers have concentrated on the study and characterization of the function of the macromolecular components of the cell. At the other side, there have been workers trying to elucidate the structural properties of these macromolecules, by means of more physically oriented experimental and theoretical methods. While the rationale of the functional approach is self-evident, the philosophy behind the structural approach is not as clear.

Certainly, nobody denies that in a body of study such as Biology, in which the emergent forms are the result of natural selection, structure is a category reducible to function. What is not as clear is what is behind the structure i.e. the dynamical play of forces and interactions that maintain and express themselves in that structure. Is it possible to reduce in turn the biological function to this inner dynamics of the structure? Hopefully yes. And

this is probably the Platonic archetype limit of the structural approach.

Experimentally, the use of a well characterized physical property can give information on the structural dynamics of the molecule which in turn, will help to build a dynamical structure of the system. Theoretically, one must resort to idealized models that approach more or less reality. It might be useful to remember at this point Plato again. Somewhere he has said that "some problems only can be treated by building myths around them..." His position is not far from Einstein's precept that "theory cannot be built on experimental results. It must be invented".

The work presented here is an attempt to establish theoretical grounds of the preferential scattering of light of circular polarization by optically active molecules, and its possible utilization to obtain structural information of these molecules.

In Chapter 1, a review of the main experimental evidence for the existence of CIDS in macromolecular aggregates and liquid crystals is done. This is followed by a general background in classical electrodynamics and the main results of the classical theory of scattering is presented.

Chapter 2 shows the derivation of the integral for-

malism of scattering theory. We then apply the results to a unidimensional oriented helix with a polarizability tangential at each point on the helix. The equations for the fields are solved along the three orthogonal directions of incidence of light. The corresponding analytical expression for the differential scattered intensity  $(I_L - I_R)$  of right and left circularly polarized incident light is derived. Also  $I_L + I_R$  and the CIDS ratio:  $(I_L - I_R)/(I_L + I_R)$  is obtained. At the end of the chapter the Stokes' parameters for the scattered light are derived.

In Chapter 3 we present numerical calculations based on the equations derived in Chapter 2. The general features of the scattering pattern are presented in polar plots of intensity vs. angle and we derive relations to determine how the parameters of the scatterer affect these patterns.

In Chapter 4 the case of an absorptive helical scatterer is considered. The equivalent to Friedel's law for CIDS is established. The symmetry rules of the scattered intensities in space are then derived. Numerical calculations are shown.

In Chapter 5, the first-Born approximation in the internal field is replaced by a dipole-dipole coupling of the radiating dipoles on the scatterer. We show that in this case a diffraction effect is responsible for non-zero CIDS in the forward direction. We present numerical



calculations of the equations obtained.

Finally, in Chapter 6, we present the spatial averaging of the classical expressions for differential and total scattering of circularly and plane polarized light respectively.

## TABLE OF CONTENTS

DEDICATION	i
ACKNOWLEDGMENTS	ii
INTRODUCTION	v
TABLE OF CONTENTS	ix
CHAPTER 1 General Review and Background	1
Section I. Differential Scattering	1
1) Experimental and theoretical results in biological systems	1
2) Liquid crystals	8
3) Theoretical treatments	10
Section II. Basic Electrodynamic Relations	11
1) The wave equation	11
2) Retarded potentials-multipole expansion of the scattering fields	17
Section III. Differential Scattering - Classical Formalism	25
Bibliography	28
CHAPTER 2 Theory	32
Section I. Introduction	32
Section II. The Integral Equation of Scattering	34
1) Derivation by the tensorial Green's function method.	34
2) First Born approximation	39

Section III.	Theory of Scattering of Radiation by a Helical Structure	40
Section IV.	Characterization of the State of Polarization of the Scattered Light	67
Section V	Discussion and Conclusions	74
	Bibliography	80
CHAPTER 3	Numerical Computations	82
Section I.	Introduction	82
Section II.	Numerical Computations	83
Section III.	Numerical Results	85
Section IV.	Symmetry Properties of the Scattering Patterns	93
	1) The zeros of the CIDS patterns	94
	2) Dependence of the zeros of the CIDS on helix geometry	97
	3) Vanishing of CIDS at specific angles of scattering	103
Section V.	Applications	106
	1) Length of helix	108
	2) Experimental results	108
Section VI.	Conclusions	116
	Bibliography	119
CHAPTER 4	The General Polarizability Tensor and Anomalous Scattering	120
Section I.	Introduction	120

Section II.	Numerical Calculation	121
	1) Equations and results	121
	2) A biaxial polarizability	132
Section III.	Symmetry Analysis	135
Section IV.	The Dispersion Dependence of the Scattering Intensities	148
Section V.	Discussion	156
	Bibliography	164
CHAPTER 5	Correction of the Internal Field by Dipole-Dipole Interaction	165
Section I.	Introduction	165
Section II.	The Dipole-Dipole interaction	166
Section III.	Numerical Calculations	172
	1) The transmission band	172
	2) Forward CIDS vs. CD	174
	3) Programming strategies	176
	4) Results	177
Section IV.	Conclusions	192
	Bibliography	194
CHAPTER 6	Spatial Averaging of Differential and Total Scattering	195
Section I	Introduction	195
Section II	Averaging of $I_L - I_R$	196
	1) The molecule-fixed and the space-fixed coordinate systems	196
	2) The Euler transformations	204
	3) Averaging of $I_L - I_R$	208

Bibliography	231
APPENDIX A	232
1) Friedel's Law	232
2) Breakdown of Friedel's Law	233
APPENDIX B	235
APPENDIX C	237
1) Program VINO	237
2) Program PAN	252
3) Program COCO	262

## Chapter 1

## GENERAL REVIEW AND BACKGROUND

## I. Differential Scattering: Review on Experimental Observations and Theoretical Treatments.

## 1) Experimental and theoretical results in biological systems.

A great amount of work on the optical properties of biological macromolecules has appeared in the literature in the last two decades. These studies have been directed towards gaining a better understanding of the structural and electronic properties of these systems, in the hope that this, in turn, will clarify their biological functions.

This has been, in part, the result of two major steps in the area: first, the development of better and more accurate measuring instruments, and second, the appearance during this period of very general and useful theories on the optical properties of macromolecules, in particular on circular dichroism (CD) and optical rotatory dispersion (ORD).<sup>1</sup> These methods were originally limited to homogeneous solutions of macromolecules. Within the last decade, they have also been applied to increasingly complex systems such as particulate aggregates of biological macromolecules, suspensions of whole or fractured membranes, nucleohistones complexes, etc. A remarkable common feature of all these systems was the presence of notorious anomalies in their CD

and ORD spectra.

Urry and co-workers<sup>2</sup> were the first people attempting an explanation of the modifications they observed in the CD of suspensions of membranes. They also recognized that the difference between the CD of aggregates of poly-glutamate versus the dispersed solution arose from Duysen's flattening effect and preferential scattering of light of opposite circular polarization, and not from a dependence of the electronic states upon aggregation. These authors presented a phenomenological analysis in an attempt to recuperate the original CD signal. Their analysis has been questioned by other authors.<sup>3</sup>

Ottaway and Wetlaufer<sup>4</sup> have applied the Rayleigh Scattering theory modified to account for the optical activity of the scattering particle. According to their calculations, very small corrections of the measured CD would be found. It is clear that this theory, due to its restrictive wavelength character (Rayleigh), cannot be applied to particles of the order or larger than the wavelength of light. Holzwarth<sup>3</sup> has classified the three major mechanisms by which scattering of the sample could affect the intrinsic CD and ORD signal:

- a) Scattering can decrease the transmission of the signal.
- b) Depolarization of the incident light occurs when it passes through the scattering sample.
- c) Differential scattering of right and left circularly

polarized light might be present and can be interpreted as differential absorption.

Schneider et al.<sup>5</sup> raised the question of whether the CD spectral distortions characteristic of membrane systems reflect a unique and common structure in these systems or are the result of the combination of scattering and Duysen's flattening effects. With this purpose these authors carried out three types of experiments: First the CD spectra of red blood cell ghosts were compared to the spectra of sonicated ghosts. They found that sonication produced a characteristic general increase in the ellipticity as compared to the intact ghosts, in particular of the band at 208 nm. Second, CD of hemoglobin in solution was compared with that of hemoglobin concentrated into red blood cells at different degrees of hemolysis. It was found that hemolysis restores the spectra of the hemoglobin in solution as compared to the flattened spectra observed for the hemoglobin inside the cells. Third, droplets (approximately 10 nm in diameter) of a solution of bovine serum albumin, when suspended in glycerol, showed large amounts of scattering. The ellipticities measured presented a similar type of distortion as the one observed in the ghost of red blood cells. These authors attributed these distortions to scattering and Duysen's flattening "artifacts" and discussed the possibility of a differential scattering contribution.

In this context, it should be noted that total scattering and Duysen's flattening have opposite effects in the CD



spectra. We can write the contribution of the scattering to the ellipticities as:

$$CD = \frac{(I_L - S) - (I_R - S)}{(I_L - S) + (I_R - S)}$$

where  $I_L$  and  $I_R$  are the transmitted intensities of the corresponding incident circular polarizations and  $S$  is the amount scattered by the sample (therefore the minus sign). Clearly, the scattering contribution cancels in the numerator but decreases the denominator, yielding an overall higher ellipticity. This, as mentioned above, is contrary to the spectral distortions observed in membranes.<sup>6</sup> Conversely, Duysen's flattening effects tend to decrease the ellipticities. Although possible total scattering effects cannot be ruled out, it seems that Duysen's flattening and differential scattering are the dominant contributions to the distortions observed. Similar conclusions were drawn by Glaser and Singer<sup>7</sup> by applying Urry's phenomenological equations to their CD data of red blood cell membranes.

Maestre et al.,<sup>8</sup> measuring the CD of bacteriophages  $T_2$ ,  $T_4$ , and  $T_6$ , found that the CD curves presented long tails extending towards the longer wavelengths of the spectrum up to the visible. These authors attributed the effect correctly to differential scattering. Dorman et al.,<sup>9,10</sup> using a set of variable acceptance detectors and an integrating capturing device (fluorscat cell) that captures all but

the back-scattered light, were able to eliminate these tails effectively.

Many CD studies of nucleohistones<sup>11,12</sup> and DNA-polylysine complexes<sup>13,14</sup> have been reported. In all cases, an important differential scattering contribution is present showing long tails toward the red and giving rise to enormous ellipticities (of the order of hundreds) within the absorption band of the complexes.<sup>15</sup> Another sample of biological material that exhibits similar manifestations are intact chloroplasts. They show remarkable dependence of the CD signal on the angular orientation of the sample with respect to the incident beam.<sup>16</sup>

Holzwarth et al.<sup>17</sup> have pointed out at the similarities between the CD spectra of T-even bacteriophages and those of the liquid crystals (large ellipticities, positive or negative tails towards longer wavelengths). These authors tried to account for the scattering contributions to the CD by the use of Mie-type calculations. The model, however, proved unable to reproduce the experimental CD curves.

In an effort to subtract the scattering artifacts plaguing the ORD and CD measurements of molecular aggregates, Schneider<sup>18</sup> has constructed the scattering amplitude matrix<sup>19</sup> for incident right and left circularly polarized light, to describe the intrinsic optical activity and all the scattering properties of the suspension. The author relates the observed optical activity of the suspension to the elements

of the matrix, through the bulk refractive index of the suspension. In order to separate the optical activity from the scattering effects, the author proposes a general (non-specified) functional dependence between the bulk optical properties of the suspension represented by the matrix elements and the true optical activity of the particles represented by their index of refraction. Unfortunately, it seems that all the information about the scattering effects of the sample is buried in this "functional dependence" whose determination is the central problem in understanding these scattering phenomena. However, even phenomenologically the analysis appears incorrect, since the formalism deals only with the forward scattering matrix, failing to recognize that non-forward total and differential scattering would also affect the differential extinction measured at the detector in the forward direction.

Other attempts to fit the classical general scattering Mie theory by means of the introduction of ad-hoc terms to account for the optical activity of the particles and the anomalies in the CD spectra of several particulate suspensions, have appeared in the literature, with quite varied degree of success.<sup>20-23</sup> The most serious attempt in this sense was carried out by C. F. Bohren,<sup>24</sup> who solved the scattering of an optically active isotropic sphere within the frame of the Mie-theory, using phenomenological coefficients to describe its differential reactions to right and

left circularly polarized light. He found in calculations for polyglutamic acid spheres that even for ratios of radius of the sphere to wavelength of  $1/8$  the differential extinction (including both absorption and scattering) peaked in the forward direction, although in this limit the scattering was negligible compared to the absorptive contribution.

The recent development of the Fluorescence Detected Circular Dichroism technique (FD CD)<sup>25</sup> has allowed Reich et al.<sup>26</sup> to measure the  $4\pi$ -radians integrated differential scattering of DNA condensates in ethanolic solutions. These authors found very little forward differential scattering. Most scattering appeared at right angles to the incident beam and moderate differential scattering occurred in the backward direction. Furthermore, CD studies of films of DNA twisted by shearing the fibers between two quartz plates<sup>27</sup> yielded enormous ellipticities whose sign was reversed by reversing the sense of the twist. The back scattering intensities measured in these studies indicated that the polarization of the reflected light was the same as that of the incoming beam. As will be seen later, this is a property of cholesteric and twisted nematic liquid crystals. To explain the large CD spectra observed in nucleohistone complexes, ethanolic precipitates of DNA, and polylysine-DNA aggregates, Maestre et al.<sup>27</sup> advanced the following conclusions: a) the anomalous CD spectra observed were the result of liquid crystal behavior with

both differential scattering and resonance transmission near the absorbance band; b) the long tails observed, being a scattering phenomenon, reflect the size and shape of the particle; c) the sign of the differential scattering contributions singled out by the FDCD technique must reflect the sense of chirality of the studied structure.

## 2) Liquid crystals.

Cholesteric mesophases are a special type of nematic liquid crystals in which the constituent molecules are optically active.<sup>28-30</sup> Under appropriate conditions, the structure possesses a screw axis normal to the preferential molecular orientations. The whole mesophase looks like a group of stacked planes each composed of well aligned parallel molecules with a definite twist angle between a given plane and the next.

When the wavelength of light corresponds to the pitch of the cholesteric helix, there are two opposite cases: First, circularly polarized light incident along the helix axis and having the same handedness as that of the helix is almost completely reflected. On the contrary, if the circular polarization of the light is opposite to the handedness of the helix, the light is almost completely transmitted. Furthermore, the polarization of the reflected light is the same as that of the incident radiation. Along its optical axes the system possesses enormous rotatory power as well as very large circular dichroism. Mauguin<sup>31</sup> has treated

this problem theoretically seeking to explain the large ORD signal measured in the twisted nematic phase, when light is incident along the optical axis. An equivalent treatment can be done by using Jones calculus,<sup>30</sup> in which each plane of the cholesteric phase is treated as a thin birefringent medium with the principal axes of the successive planes twisted by a fixed angle. By calculating the phase retardation matrix which describes the modification of the incident electric vector in passing through each plane, it is possible to obtain for N successive planes, the retarder-rotator matrix  $\underline{J}$  such that:

$$\underline{D}' = \underline{J}\underline{D}$$

where  $\underline{D}$  and  $\underline{D}'$  are the incident and emergent displacement vectors of the light.

Similar treatments have been presented by Oseen<sup>32</sup> and de Vries<sup>33</sup> by solving the wave equation for propagation along the optical axis of a medium described by a continuous spiral dielectric tensor. In all cases only forward intensities (transmission) and reflection bands were derived. By allowing the birefringent planes (in the Mauguin layer theory) or the dielectric tensor (Oseen, de Vries) to be dichroic as well as birefringent, and assuming that the birefringent and dichroic axes coincide, the observed CD of these cholesterics have been reproduced very successfully. Analytical solutions for the scattering of polarized light as a function of wavelength and directions in space have not

been presented. The observed CD signals can be interpreted as manifestations of differential scattering reflecting the long range organization of the crystal and not as intrinsic dichroism, since the disordered mesophase presents CD signals 2 or 3 orders of magnitude smaller. Numerical calculations along the lines described above have been carried out for light incident at oblique angles with respect to the optical axis and for wavelengths close to the pitch of the helix, by Berreman and Scheffer.<sup>34</sup> Only transmission and reflection bands have been studied. No analytical solutions for the amplitudes of the scattered fields have yet been found.<sup>30</sup> Approximate expressions for the intensities of polarized diffraction maxima observed when plane polarized light is incident perpendicular to the optical axis have been derived by the Raman-Nath theory of the diffraction of light by ultrasonic waves.<sup>35</sup>

### 3) Theoretical treatments.

Some very general treatments of scattering of circularly polarized light have appeared in the literature.<sup>36</sup> Atkins and Barron<sup>37</sup> have given general expressions for the differential scattering of light both for Rayleigh and Raman processes, from a quantum mechanical point of view. These authors were able to obtain explicit expressions by constructing the scattering matrix and relating it to molecular parameters. In their treatment the wavelength of light was large

compared to the dimensions of the molecules and no absorptive phenomena were taken into account. Later, Barron and Buckingham<sup>38</sup> presented both a classical and quantum mechanical analysis for the elastic and inelastic differential scattering of circularly polarized light. Harris and McClain<sup>39,40</sup> have presented a theory for the polarization of light scattered by polymers emphasizing its applicability for wavelengths shorter than the polymer dimensions. These authors construct the Perrin matrix for the scattering of light according to Stokes' formalism<sup>41</sup> and relate this phenomenological treatment to molecular parameters. The wavelength is assumed to be large compared to the size of the monomers, but not necessarily large relative to the polymer. The treatment is general; it does not explicitly consider any particular geometry.

## II. Basic Electrodynamic Relations.

### 1) The wave equation.

The behavior of the electromagnetic fields and their interaction with charged particles is the subject of study of electrodynamics. Between the years of 1860-1870, J. C. Maxwell formulated his unified theory of all electromagnetic phenomena that culminated in the fundamental relations of classical electrodynamics. These are called the Maxwell equations and their microscopic formulations have the form:



$$\nabla \times \underline{\tilde{e}} + \frac{1}{c} \frac{\partial \underline{\tilde{b}}}{\partial t} = 0 \quad (1a)$$

$$\nabla \times \underline{\tilde{b}} - \frac{1}{c} \frac{\partial \underline{\tilde{e}}}{\partial t} = \frac{4\pi}{c} \underline{\tilde{j}}(x, t) \quad (1b)$$

$$\nabla \cdot \underline{\tilde{b}} = 0 \quad (1c)$$

$$\nabla \cdot \underline{\tilde{e}} = 4\pi \xi(x, t) \quad (1d)$$

where  $\xi$  and  $\underline{\tilde{j}}$  are the microscopic charge and current densities, and include all charges free and bound;  $\underline{\tilde{e}}$  and  $\underline{\tilde{b}}$  are the microscopic electric and magnetic fields. To obtain the corresponding macroscopic relations, a space averaging on all charges at a given instant of time must be carried out. In this process the averaged charge density can be shown<sup>42</sup> to take the form:

$$\begin{aligned} \bar{\xi}(x, t) = & \bar{\xi}_{\text{free}} + \bar{\xi}_{\text{bound}}(x, t) - \nabla \cdot \underline{\tilde{P}}(x, t) + \\ & \sum_{\alpha\beta} \frac{\partial^2}{\partial x_\alpha \partial x_\beta} \theta_{\alpha\beta}(x, t) + \dots \end{aligned} \quad (2)$$

where  $\bar{\xi}_{\text{free}}$  and  $\bar{\xi}_{\text{bound}}$  are the averaged densities of free and bound charges, respectively,  $\underline{\tilde{P}}$  is macroscopic polarization (i.e., the averaged dipole moment of all bound charges) and  $\theta_{\alpha\beta}$  the corresponding macroscopic quadrupole density. Given that  $\langle \underline{\tilde{b}} \rangle_{\text{av}} \rightarrow \underline{\tilde{B}}$  and  $\langle \underline{\tilde{e}} \rangle_{\text{av}} \rightarrow \underline{\tilde{E}}$ , then substituting Equation (2) into expression (1d) and averaging:

$$\nabla \cdot \underline{\underline{E}} = 4\pi(\underline{\underline{\xi}}_{\text{free}} + \underline{\underline{\xi}}_{\text{bound}} - \nabla \cdot \underline{\underline{P}} + \sum_{\alpha\beta} \frac{\partial^2}{\partial x_\alpha \partial x_\beta} \Theta_{\alpha\beta} + \dots)$$

from which a new associated displacement vector can be defined as:

$$\underline{D}_\alpha = \underbrace{\sum_{\beta} \epsilon_{\alpha\beta} E_\beta}_{\text{constitutive linear relation}} = E_\alpha + \underbrace{4\pi P_\alpha}_{\text{macroscopically averaged electric dipole}} - 4\pi \sum_{\beta} \frac{\partial}{\partial x_\beta} \underbrace{\Theta_{\alpha\beta}}_{\text{macroscopically averaged electric quadrupole}} \quad (3)$$

The corresponding averaging process for the current density yields the macroscopic magnetic field

$$\underline{H}_\alpha = \underbrace{\sum_{\beta} \mu'_{\alpha\beta} B_\beta}_{\text{constitutive linear relation}} = B_\alpha - 4\pi \underbrace{(M_\alpha + \dots)}_{\text{macroscopically averaged magnetic dipole}} \quad (4)$$

where  $\epsilon_{\alpha\beta}$  is the electric permittivity and  $\mu'_{\alpha\beta}$  the inverse magnetic permeability.

The last two equations are the constitutive relations that express the relationship between the principal ( $\underline{E}, \underline{B}$ ) and the derived fields ( $\underline{D}, \underline{H}$ ) in material media.  $\underline{B}$  is usually called the magnetic displacement and  $\underline{H}$  the magnetic field.

We can now write the macroscopic Maxwell equations for material media equivalent to expression (1):

$$\nabla \times \underline{\tilde{E}} + \frac{1}{c} \frac{\partial \underline{\tilde{B}}}{\partial t} = 0 \quad (5a)$$

$$\nabla \times \underline{\tilde{H}} - \frac{1}{c} \frac{\partial \underline{\tilde{D}}}{\partial t} = \frac{4\pi}{c} \underline{\tilde{J}}_{\text{free}} \quad (5b)$$

$$\nabla \cdot \underline{\tilde{B}} = 0 \quad (5c)$$

$$\nabla \cdot \underline{\tilde{D}} = 4\pi \xi_{\text{free}} \quad (5d)$$

where all quantities involved are macroscopic averages. It can be shown that for electro-neutral molecules the contribution of the bound charge density of expression (2) vanishes and therefore only free charges and currents appear explicitly in the macroscopic equations. The bound charges and currents appear instead through the higher moments of the charge and current distributions ( $\underline{\tilde{P}}$ ,  $\underline{\tilde{M}}$ ,  $\underline{\tilde{\Theta}}$ ).

Notice that even for zero values of both currents and charge densities, Equations (5) possess nontrivial solutions. This is in fact the way Maxwell theory accounts for the existence of electromagnetic radiation in the absence of charges in space.<sup>43</sup> It must be clear, on the other hand, that  $\underline{\tilde{E}}$  and  $\underline{\tilde{B}}$  are the fundamental fields, whereas their associated fields  $\underline{\tilde{D}}$  and  $\underline{\tilde{H}}$  are introduced to take into account the average contribution of the bound charges.

It is convenient to introduce potentials in terms of which the electric and magnetic fields can be obtained, so that Maxwell equations are replaced by a smaller number of second order differential equations.

Since  $\nabla \cdot \vec{B} = 0$ , we can define  $\vec{B}$  in terms of a vector potential  $\vec{A}$ :

$$\vec{B} = \nabla \times \vec{A} \quad (6)$$

Then from Equation (5a),  $\nabla \times (\vec{E} + \frac{1}{c} \frac{\partial \vec{A}}{\partial t}) = 0$ . The quantity in parenthesis, having a vanishing curl, can be written as the gradient of a scalar function (potential), so that:

$$\vec{E} = - \frac{1}{c} \frac{\partial \vec{A}}{\partial t} - \nabla \phi \quad (7)$$

If the medium is homogeneous  $\epsilon_{\alpha\beta}$  and  $\mu'_{\alpha\beta}$  in (3) and (4) are scalars and Equations (5b) and (5d) become:

$$\epsilon \nabla \cdot \vec{E} = 4\pi \rho_{\text{free}} \quad (8a)$$

$$\frac{1}{\mu} \nabla \times \vec{B} - \frac{\epsilon}{c} \frac{\partial \vec{E}}{\partial t} = 4\pi \vec{J}_{\text{free}} \quad (8b)$$

with  $\mu = (\mu')^{-1}$ . Taking the divergency of (7) and using Equation (8a):

$$\nabla^2 \phi + \frac{1}{c} \frac{\partial}{\partial t} \nabla \cdot \vec{A} = \frac{4\pi}{\epsilon} \rho_{\text{free}}, \quad (9)$$

also, substituting (6) into (8b):

$$\nabla (\nabla \cdot \vec{A} + \frac{\mu \epsilon}{c} \frac{\partial \phi}{\partial t}) = \nabla^2 \vec{A} + \mu \frac{4\pi}{c} \vec{J}_{\text{free}} - \frac{\mu \epsilon}{c^2} \frac{\partial^2 \vec{A}}{\partial t^2} \quad (10)$$

The definitions of the field in terms of the potentials do not determine these fields uniquely, since the same fields would be obtained if  $\underline{A} \rightarrow \underline{A}' = \underline{A} + \Delta\Lambda$ , and  $\Phi \rightarrow \Phi' = \Phi - \frac{1}{c} \frac{\partial \Lambda}{\partial t}$ , where  $\Lambda$  is some arbitrary scalar. This lack of uniqueness of the potentials allows for the possibility to choose them in such a way as to satisfy a supplementary condition (Gauge), according to the nature of the problem being solved. In this case we impose the often called Lorentz condition:

$$\nabla \cdot \underline{A} + \frac{\mu\epsilon}{c} \frac{\partial}{\partial t} \Phi = 0$$

which combine with (9) and (10) to give the second order differential equations that are completely equivalent to the Maxwell equations. They are frequently called the wave equations:

$$\nabla^2 \Phi - \frac{\epsilon\mu}{c^2} \frac{\partial^2 \Phi}{\partial t^2} = \frac{4\pi\rho_{\text{free}}}{\epsilon} ; \quad \nabla^2 \underline{A} - \frac{\epsilon\mu}{c^2} \frac{\partial^2 \underline{A}}{\partial t^2} = \mu \frac{4\pi}{c} \underline{J}_{\text{free}} \quad (11)$$

For constant fields these equations give the usual static solutions (Poisson for the scalar potential and a corresponding one for the vector potential). For problems involving the emission of electromagnetic radiation by time dependent charge and current densities, we are interested in the solutions to these equations as fully written above.

The wave-equations (11) are very important for the general theory of scattering. The differential formulation, despite its inherent difficulty in interpretation, has the advantage of allowing for the search of solutions in regions of the space, to which supplementary initial and boundary conditions (at the frontier between regions) are added to obtain unique solutions. Let us suppose that a given body

possessing both bound and free charges is occupying a finite region of space. An incident electromagnetic radiation impinges upon the body and it is required to obtain the scattered field far away from the region occupied by the scatterer. Away from this region  $\rho = 0$ ,  $\underline{J} = 0$ , and  $\mu\epsilon = 1$  so that first, the corresponding homogeneous wave equations in vacuo must be solved. Next, the solution within the region of the scatterer must be obtained, for which we need to solve Equations (11) as fully written. Having both solutions, it is then possible to apply the adequate conditions at the boundary between the two regions and an initial condition, such as the form of the incident electromagnetic field at time  $t = 0$ . In this way, the scattering problem can, in principle, be solved from the differential equations. Notice that if the scatterer is a nonconducting dielectric,  $\rho_{\text{free}} = \underline{J}_{\text{free}} = 0$  when seeking the inner solution.

2) Retarded potentials - multipole expansion of the scattering fields.

A completely formal solution to the wave equations (11) can be found by linearly combining the solution to the homogeneous equation and a particular solution of the inhomogeneous one. It is a well known result of electrodynamics that the particular solution to the inhomogeneous equations is given by the so-called "retarded potentials" and that the general solutions of the inhomogeneous equations are:

$$\begin{aligned}\phi(\underline{r}', t') &= \int \frac{\rho(\underline{r}, t' - \frac{\mu\epsilon R}{c})}{R} dV + \phi_0 \\ A(\underline{r}', t') &= \frac{\mu\epsilon}{c} \int \frac{J(\underline{r}, t' - \frac{\mu\epsilon R}{c})}{R} dV + A_0\end{aligned}\tag{12}$$

An important point should be made clear here. In the way Equations (12) have been obtained from (5) through (11), it is apparent that  $\rho$  and  $\underline{J}$  appearing in these equations are the free charge and current densities. These are clearly zero for nonconducting material. However, it is possible to write Equations (5) for nonconducting material in terms of the fundamental fields  $\underline{E}$  and  $\underline{B}$  so that they maintain their general form but  $\rho_{\text{free}}$  and  $\underline{J}_{\text{free}}$  being replaced by  $\rho_{\text{bound}}$  and  $\underline{J}_{\text{bound}}$ . The equivalent wave equation (11), as well as the corresponding general solutions (12) can then be obtained explicitly in terms of  $\rho_{\text{bound}}$  and  $\underline{J}_{\text{bound}}$  valid for nonconducting dielectric media. In this way, Equations (12) represent the general formal solutions for the scattered fields in conduction or dielectric media.

In Equation (12),  $\underline{r}'$  is the observation point,  $\underline{r}$  is the region where the scattered is bounded and  $R = |\underline{r}' - \underline{r}|$  (See Fig. 1).

$A_0$  and  $\phi_0$  are the solutions to the homogeneous wave equations but more generally they are chosen so that the conditions of the particular problem are satisfied. These conditions are commonly those imposed for far distances.

For example, suppose that a given radiation impinges upon the systems of charges from outside. Here the field that results from the interaction can be different from the incident exterior field only in the radiation originated by the system itself. At large distances this radiation must have the form of waves that propagate away from the system, which corresponds to the retarded potential part of Equation (12), whereas  $\phi_0$  and  $\underline{A}_0$  in this equation must be recognized as the external fields.

We can now make the assumption that the charge and current densities vary harmonically with time, so that

$$\rho(t) = \rho e^{2\pi i \nu t}$$

$$\underline{J}(t) = \underline{J} e^{2\pi i \nu t}$$

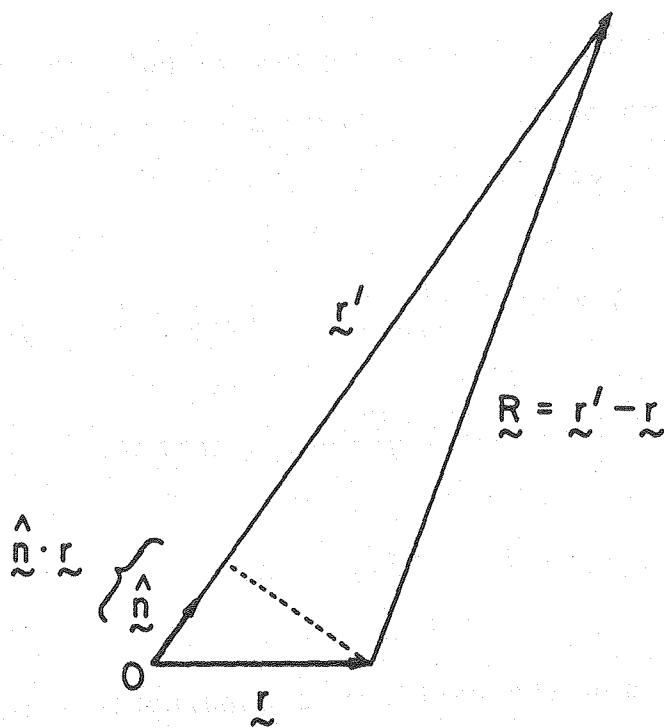
Since in most physical problems  $\rho$  and  $\underline{J}$  are restricted to finite regions of space whose dimensions are small compared to  $k^{-1}$  (with  $k = 2\pi\nu/c$ ), this suggests a development of the retarded potential formula according to powers of  $k$ . In the expressions:

$$\phi(\underline{r}', t') = e^{2\pi i \nu t'} \int \frac{\rho e^{-ikR}}{R} dV$$

in the far field or radiation zone,  $R = r' - \hat{n} \cdot \underline{r}$  with  $\hat{n} = \frac{\underline{r}'}{|\underline{r}'|}$  (see Fig. 1) so that:



Figure 1. The distance approximation involved in the radiation zone is shown.  $0$  is an arbitrary origin of coordinates within the molecule.  $\underline{r}$  is the position of the scattering element and  $\underline{r}'$  is the location of the observer.  $\hat{\underline{n}}$  is a unit vector along  $\underline{r}'$ . If  $|\underline{r}'| \gg |\underline{r}|$ , then clearly  $|\underline{R}| \sim |\underline{r}'| - \hat{\underline{n}} \cdot \underline{r}$ .



XBL 8012-12964

$$\phi(\underline{r}', t') = e^{i(2\pi\nu t' - kr')} \int \frac{e^{i\hat{\mathbf{k}}\hat{\mathbf{n}}\cdot\underline{r}}}{(\underline{r}' - \hat{\mathbf{n}}\cdot\underline{r})} dV .$$

Now we do a double Taylor expansion both for the exponential and the denominator and collecting the terms with the same power of  $k$  it can be shown<sup>44</sup> that:

$$\begin{aligned} \phi(\underline{r}', t') = & \frac{e^{i(2\pi\nu t' - kr')}}{r'} \left\{ \int \rho dV + ik\left(1 - \frac{i}{kr'}\right) \int \rho \underline{r} \cdot \hat{\mathbf{n}} dV \right. \\ & - \frac{k^2}{3} \left[ \left(1 - \frac{3i}{kr'}\right) \left(\frac{3}{2} \hat{\mathbf{n}} \cdot \int \rho \underline{r} \underline{r} dV \cdot \hat{\mathbf{n}} - \frac{1}{2} \int \rho r^2 dV\right) \right. \\ & \left. \left. + \frac{1}{2} \int \rho r^2 dV \right] + \dots \right\} \end{aligned}$$

But  $\int \rho dV = 0$  and the dipole and quadrupole moments are defined as:

$$\underline{\underline{P}} = \int \rho \underline{r} dV \quad \text{and} \quad \underline{\underline{\Theta}} = \int \rho \underline{r} \underline{r} dV .$$

Therefore, the potentials up to the second power in  $k$  are:

$$\begin{aligned} \phi(\underline{r}', t') = & \frac{e^{i(2\pi\nu t' - kr')}}{r'} \left\{ ik\left(1 - \frac{i}{kr'}\right) \hat{\mathbf{n}} \cdot \underline{\underline{P}} - \frac{1}{2} k^2 \left[ \hat{\mathbf{n}} \cdot \underline{\underline{\Theta}} \cdot \hat{\mathbf{n}} \right. \right. \\ & \left. \left. - \frac{i}{kr'} (3\hat{\mathbf{n}} \cdot \underline{\underline{\Theta}} \cdot \hat{\mathbf{n}}) \right] \right\} \quad (13) \end{aligned}$$

$$\begin{aligned} A(\underline{r}', t) = & \frac{e^{i(2\pi\nu t' - kr')}}{r'} \left\{ ik\underline{\underline{P}} - ik\left(1 - \frac{i}{kr'}\right) \hat{\mathbf{n}} \underline{\underline{X}} \underline{\underline{M}} \right. \\ & \left. - \frac{1}{2} k^2 \left(1 - \frac{i}{kr'}\right) \hat{\mathbf{n}} \cdot \underline{\underline{\Theta}} \right\} \end{aligned}$$

where  $\tilde{M}$  is the magnetic dipole moment and is defined as:

$$\tilde{M} = \frac{1}{2c} (\tilde{r} \times \tilde{J})$$

Expression (13) describes, therefore, the interaction of the incident radiation with a system of charges and currents through the induction by the external fields of a series of moments of the distributions. An observer placed at  $\tilde{r}'$  at time  $t'$  will therefore receive the radiation contributions of the electric dipole (the most important), the magnetic dipole, and the quadrupole induced in the scatterer by the incident electromagnetic field.

It can be shown<sup>45</sup> that the amplitudes of the different oscillating moments induced in the system can be written (keeping only linear terms in the fields):

$$P_{\alpha}^{(0)} = \alpha_{\alpha\beta} E_{\beta i}^{(0)} + \frac{1}{ck} G_{\alpha\beta} \dot{B}_{\beta i}^{(0)} + \frac{1}{3} A_{\alpha\beta\gamma} (\nabla_{\beta} E_{\gamma i}^{(0)})$$

$$M_{\alpha}^{(0)} = -G_{\beta\alpha} E_{\beta i}^{(0)} + \dots \quad (14)$$

$$\Theta_{\alpha\beta}^{(0)} = A_{\gamma\alpha\beta} E_{\gamma i}^{(0)} + \dots$$

where the subscripts "i" indicate the amplitudes of the incident fields. In Equations (14) tensor notation has been used, meaning that the expressions with repeated sub-indices must be summed over their three spatial components.

Expressions (14) can be formally obtained by doing a time dependent perturbation derivation of the induced moments in a molecule perturbed by an external field.<sup>45</sup> Classically, however, Equation (11) is still valid and we can see that  $\alpha_{\alpha\beta}$  represents a symmetric polarizability.  $G_{\beta\alpha}$  is the coefficient of the term which is proportional to the time derivative of the magnetic field (i.e., proportional to the curl of  $\underline{E}$ ) and therefore responsible for natural optical activity. This term can be formally derived from the anti-symmetric part of the polarizability.  $A_{\alpha\beta\gamma}$  is the hyper-polarizability connected to the gradient of the electric field. Each of these polarizabilities can be, in general, complex and therefore they contain both the absorptive and refractive properties of the molecular system.

Our derivation up to this point has been based in the choice of the Lorentz Gauge:  $(\nabla \cdot \underline{A} - \frac{\epsilon\mu}{c} \frac{\partial\phi}{\partial t}) = 0$ ; this allowed us to obtain the wave equation and has the additional advantage of rendering completely relativistically invariant equations. However, in dealing with radiation problems, we are interested in obtaining solutions for the electric and magnetic field that are transverse to the direction of propagation. The Lorentz Gauge gives transverse magnetic fields but the electric vector has components parallel and perpendicular to the  $\underline{k}$  vector. To obtain completely transverse fields that are uniquely determined, we can use the Coulomb or radiation gauge:  $\nabla \cdot \underline{A} = 0$  and the additional condition

$\phi = 0$ , so that the Lorentz condition is still satisfied and all our derivations are still valid. In this radiation gauge then:  $\vec{H} = \nabla \times \vec{A}$  and  $\vec{E} = -\frac{1}{c} \frac{\partial \vec{A}}{\partial t}$ . Keeping only the dipole term in (13), we can write, for light scattered along the y-axis:

$$\vec{E}(\vec{r}', t') = -\frac{ik\omega}{cr'} p e^{-i(\omega t' - ky)} \quad (15)$$

with  $\omega = 2\pi\nu$ . From (14):

$$\begin{aligned} E_{\alpha} = & -\frac{i\omega^2}{c^2 r} \left\{ \alpha_{\alpha\beta} E_{\beta i}^{(0)} + \frac{G_{\alpha\beta}}{ck} \dot{B}_{\beta i}^{(0)} + \frac{1}{3} A_{\alpha\beta\gamma} \right. \\ & \left. (\nabla_{\beta} E_{\gamma i})^0 + \dots \right\} \times e^{-i(\omega t - ky)} \quad (16) \end{aligned}$$

where the primes have been dropped for simplicity.

### III. Differential Scattering - Classical Formalism.

Suppose the light is incident along the z-axis; then the signal recorded at the photomultiplier is proportional to the time-averaged flux of energy given by the real part of the complex Poynting vector:

$$\langle \vec{S} \rangle = \frac{c}{16\pi} (\vec{E}_S^{(0)} \times \vec{H}_S^{(0)*} + \vec{E}_S^{(0)*} \times \vec{H}_S^{(0)})$$

where the subscripts "S" indicate the amplitudes of the scattered fields, with  $\vec{B} = \mu\vec{H}$  as before. The components of  $\vec{S}$  associated with electric vectors  $E_z$  and  $E_x$  can be written:

$$S_z = \frac{c}{16\pi\mu} (E_{zS}^{(0)} B_{xS}^{(0)*} + E_{zS}^{(0)*} B_{xS}^{(0)}) =$$

$$\frac{c}{8\pi\mu} E_{zS}^{(0)} E_{zS}^{(0)*}$$

$$S_x = \frac{-c}{16\pi\mu} (E_{xS}^{(0)} B_{zS}^{(0)*} + E_{xS}^{(0)*} B_{zS}^{(0)}) =$$

$$- \frac{c}{8\pi\mu} E_{xS}^{(0)} E_{xS}^{(0)*}$$

If the incident radiation is right (plus sign) and left (minus sign) circularly polarized,

$$\tilde{E}_i^{(0)\pm} = \frac{1}{\sqrt{2}} E_i^{(0)} (\tilde{i} \pm i\tilde{j})$$

with  $\tilde{i}$ ,  $\tilde{j}$ ,  $\tilde{k}$  a set of units vector along the x, y, and z directions, then the differential scattered intensities are (with  $\mu = 1$ ):

$$S_z^+ - S_z^- = \frac{\omega^4 E_i^{(0)2}}{8\pi c^3 r^2} \text{Im} \{ \alpha_{zy} \alpha_{zx}^* + \alpha_{zy} G_{zy}^* + \alpha_{zx} G_{zx}^* -$$

$$\alpha_{zy} G_{xx}^* + \alpha_{zx} G_{yx}^* \} \quad (17)$$

where the term proportional to  $(\nabla_\beta E_{\gamma i})^0$  has been neglected. Equation (17) shows that within the dipole approximation for the scattered field (15), the differential scattering intensity can be directly related to the symmetric and anti-symmetric parts of the polarizability of the molecular system.

The possibility of nonvanishing differential scattering within the dipole radiation field depends therefore on the symmetry properties of the polarizability tensor of the molecule and on the validity of neglecting the second term in the right-hand side of (16). In the next chapter we will treat with more detail the condition imposed on the polarizability of a molecule, for the existence of finite differential scattering intensities in the radiation field.



Bibliography

1. Tinoco, I., Jr. (1962) Advances in Chemical Physics 4, 113-160.
2. Urry, D. W., Krivacic, J. (1970) Proc. Natl. Acad. Sci. USA 65, 845-852.
3. Holzwarth, G., " The Ultraviolet Optical activity of Membranes " (Unpublished Manuscript , 1970).
4. Ottaway, C. A., Wetlaufer, D. B. (1970) Arch. Biochem. Biophys. 139, 257.
5. Schneider, A. S., Schneider, M.-J. T., Rosenheck, K. (1970) Proc. Natl. Acad. Sci. USA 66, 793-798.
6. Urry, D. W., Ji, T. H. (1968) Arch. Biochem. Biophys. 128, 802.
7. Glaser, M., Singer, S. J. (1971) Biochemistry 10, 1780-1787.
8. Maestre, M. F., Gray, D. M., Cook, R. B. (1971) Biopolymers 10, 2537-2553.
9. Dorman, B. P., Hearst, J. E., Maestre, M. F. (1973) in Methods in Enzymology 27, 767-796, ed. Hirs, C. H. W., Timasheff, S. N. (Academic Press: New York).
10. Dorman, B. P., Maestre, M. F. (1973) Proc. Natl. Acad. Sci. USA 70, 255-259.
11. Fasman, G. D., Cowman, M. K. (1978) The All Nucleus Chromatin, Pt. B, H. Busch, pp. 55-57 (Academic Press: N.Y.).
12. Fasman, G. D., Schaffhauser, G., Goldsmith, L., Adler, A. (1970) Biochemistry 9, 2814-2822.

13. Shir, Y. A., Eichborn, G. L. (1977) Biopolymers 16, 225-230.
14. Carrol, D. (1972) Biochemistry 11, 426-433.
15. Tinoco, I., Jr., Bustamante, C., Maestre, M. F. (1980) Ann. Rev. Biophys. Bioeng. 9, 107-141.
16. Philipson, K. D., Sauer, K. (1973) Biochemistry 12, 3454-3458.
17. Holzwarth, G., Gordon, D. G., McGinnes, J. E., Dorman, B. P., Maestre, M. F. (1974) Biochemistry 13, 126-132.
18. Schneider, A. S. (1971) Chem. Phys. Lett. 8, 604-608.
19. Van de Hulst, H. C. (1957) Light Scattering of Small Particles (Wiley: New York).
20. Rosenheck, K., Schneider, A. S. (1973) Proc. Natl. Acad. Sci. USA 70, 3458.
21. Gitter-Amir, A., Rosenheck, K., Schneider, A. S. (1976) Biochemistry 15, 3131-3137.
22. Gordon, D. J., Holzwarth, G. (1971) Proc. Natl. Acad. Sci. USA 68, 2365-2369.
23. Gordon, D. J. (1972) Biochemistry 11, 413-420.
24. Bohren, C. F. (1975) Ph.D. Thesis, Department of Physics, University of Arizona.
25. Turner, D. H., Tinoco, I., Jr., Maestre, M. F. (1974) J. Am. Chem. Soc. 96, 4340-4342.
26. Reich, C., Maestre, M. F., Edmondson, S., Gray, D. M. (1980) Biochemistry, in press.
27. Maestre, M. F., Reich, C. (1980) Biochemistry, in press.

28. Baur, G., Steib, A., Meir, G. (1974) Liquid Crystals and Ordered Fluids 2, eds. Johnson, J. F., Porter, R. S. (Plenum: New York).
29. De Gennes, P. G. (1974) The Physics of Liquid Crystals (Clarendon: Oxford)
30. Chandrasekhar, S. (1974) Liquid Crystals (Cambridge University Press: London)
31. Mauguin, M.C. (1911) Bull. Soc. Franc. Miner. Crist. 34, 71.
32. Oseen, C. W. (1933) Trans. Faraday Soc. 29, 883
33. DeVries, H. (1951) Acta Cryst. 4, 219.
34. Berreman, D. W., Scheffer, T. J. (1970) Phys. Rev. Lett. 25, 577.
35. Chandrasekhar, S., Shashidhara Prasad, J. (1969) Physics of the Solid State, eds. Balakrishna, S., Krishnamurthi, M., Rao, B. R. (Academic Press: New York) p. 77.
36. Barron, L.D., Buckingham, A. D. (1975) Ann. Rev. Phys. Chem. 26, 381.
37. Atkins, P. W., Barron, L. D. (1969) Mol. Phys. 16, 453-466.
38. Barron, L.D., Buckingham, A. D. (1971) Mol. Phys. 20, 1111-1119.
39. Harris, R. A., McClain, W. M. (1977) J. Chem. Phys. 67, 269-270.
40. Harris, R. A., McClain, W. M. (1977) J. Chem. Phys. 67, 265-268.

41. Perrin, F. (1942) J. Chem. Phys. 10, 415.
42. Jackson, J. D. (1975) Classical Electrodynamics  
(John Wiley & Sons, Inc.: New York).
43. Landau, L. D., Lifshitz, E. M. (1975) The Classical  
Theory of Fields (Pergamon Press: New York).
44. Condon, E. U., Shortley, G. H. (1951) (Cambridge  
University Press: London).
45. Buckingham, A. D. (1967) Advances in Chemical Physics  
12, 107-142.

## Chapter 2

## THEORY

## I. Introduction.

In the previous chapter a review has been done of the main experimental evidence for the presence of differential light scattering phenomena in systems of biological origin, as well as in the cholesteric and twisted nematic mesophases of liquid crystals. Some of the theoretical attempts in characterizing this phenomenon have also been discussed. Clearly, between the macroscopic phenomenological approaches<sup>1-3</sup> and the completely general theoretical treatments<sup>4,5</sup> that have appeared in the literature, a link is necessary: a theory that will make use of the molecular properties involved in the differential scattering and will directly correlate the properties of this scattering phenomenon with the structure of the chiral molecules. The model must allow for analytical solutions so that the physics of the process is not buried in implicit expressions.

Chiral media interact differently with the light of opposite circular polarization. The existence of different refractive indices for right and left circularly polarized light gives rise to the well known phenomena of circular birefringence and circular dichroism. These are connected, respectively, to differences in the real and imaginary parts

of the refractive index for the two circular polarizations.

As shown in the previous chapter, classical electrodynamics describes light scattering as the result of the radiation emitted by changes in the charge distribution of a system, induced by an oscillating electromagnetic field. In the dipole radiation approximation, these changes are described by the polarizability of the medium, which contains all the symmetry properties necessary to account for the differential scattering of light. An appropriate measure of this is the ratio of the difference of scattered intensities between left and right circularly polarized light to its sum

$$(I_L - I_R) / (I_L + I_R)$$

where  $I_L$  and  $I_R$  are the scattered intensities for the two polarizations of the incident light. Atkins and Barron<sup>4</sup> have suggested that this ratio be called Circular Intensity Differential Scattering (CIDS). The above definition is valid for both elastic and inelastic scattering.

We have chosen an oriented helix as the simplest chiral structure whose CIDS can be obtained analytically. This geometry has many advantages: (a) It can be described in a mathematically simple way, (b) its chirality can easily be reversed to study its effect on the CIDS, (c) it is a preferred form of packing adopted by biological superstructures

and by cholesteric liquid crystals.

In the first part of this chapter the derivation of an integral equation of scattering will be accomplished as a simple way of obtaining the scattering amplitude of an arbitrarily shaped structure. In the second part the integral formalism will be applied to obtain the CIDS of helical structures.

## II. The Integral Equation of Scattering.

### 1) Derivation by the tensorial Green's function method.

As mentioned in Chapter 1, all scattering problems can (in principle) be solved using the Maxwell equation, which in the absence of free sources and assuming harmonic time dependence ( $\mu = 1$ ) are:

$$\nabla \times \vec{E} = \frac{i\omega}{c} \vec{H} \quad (1)$$

$$\nabla \times \vec{H} = -\frac{i\omega}{c} \vec{D} = -\frac{i\omega \epsilon(\vec{r})}{c} \vec{E} \quad (2)$$

where  $\epsilon$  is the dielectric constant of the medium and is a continuous function with the possible exception of surface discontinuities. It is assumed that all scattering centers can be enclosed within a finite region. The wave equations for  $\vec{E}$  and  $\vec{H}$  are then:

$$\nabla \times \nabla \times \vec{E} - \epsilon(\vec{r}) k^2 \vec{E} = 0 \quad k^2 = \frac{\omega^2}{c^2} \quad (3a)$$

and

$$\nabla \times \left[ \frac{1}{\epsilon(\underline{r})} \nabla \times \underline{H} \right] - k^2 \underline{H} = 0 \quad (3b)$$

We will work with the equation for  $\underline{E}$  and regard  $\underline{H}$  as determined by (2). Next we impose the coulomb gauge:

$$\nabla \cdot (\epsilon \underline{E}) = 0$$

so that

$$\nabla \cdot \underline{E} = - \frac{1}{\epsilon} \underline{E} \cdot \nabla \epsilon$$

which substituted in (3a) gives:

$$\nabla^2 \underline{E} + \nabla \left[ \frac{1}{\epsilon(\underline{r})} \underline{E} \cdot \nabla \epsilon(\underline{r}) \right] + \epsilon(\underline{r}) k^2 \underline{E} = 0 \quad (4)$$

The solution of this equation, subject to appropriate boundary conditions both at infinity and at the surface of the scatterer, is very difficult for geometries other than spherical, cylindrical, etc. The alternative is to transform this equation into an integral form. Here we will follow closely the method of Levine and Schwinger.<sup>6</sup> The first Green's Identity can be written as:

$$\int_S \underline{n} \cdot [\underline{B} \times \nabla \times \underline{A} - \underline{A} \times \nabla \times \underline{B}] ds = \int_V \underline{A} \cdot (\nabla \times \nabla \times \underline{B} - \underline{B} \cdot (\nabla \times \nabla \times \underline{A})) dV \quad (5)$$



Next we introduce the Green's function,  $\Gamma$  (in general, a tensor), satisfying the equation:

$$\nabla \times \nabla \times \Gamma(\underline{r}, \underline{r}') - k^2 \Gamma(\underline{r}, \underline{r}') = \underline{1} \delta(|\underline{r} - \underline{r}'|) \quad (6)$$

with  $\underline{1} = \underline{i}\underline{i} + \underline{j}\underline{j} + \underline{k}\underline{k}$  ( $\underline{i}$ ,  $\underline{j}$ ,  $\underline{k}$  three orthogonal unit vectors along  $x$ ,  $y$  and  $z$  directions). By taking the scalar product of (6) with an arbitrary vector  $\underline{j}(\underline{r}')$ , we see that  $\Gamma(\underline{r}, \underline{r}') \cdot \underline{j}(\underline{r}')$  is the field at ( $\underline{r}$ ) due to a vector point source located at  $\underline{r}'$ . Taking the divergence of (5) on both sides we obtain:

$$k^2 \nabla \cdot \Gamma = -\nabla \delta(|\underline{r} - \underline{r}'|) = \nabla' \delta(|\underline{r} - \underline{r}'|)$$

after which (5) can be rewritten as:

$$(\nabla^2 + k^2) \Gamma = -\left(1 - \frac{1}{k^2} \nabla \nabla'\right) \delta(|\underline{r} - \underline{r}'|) \quad (7)$$

Introducing the scalar Green's function:

$$G(\underline{r}, \underline{r}') = \frac{e^{-ik|\underline{r} - \underline{r}'|}}{4\pi|\underline{r} - \underline{r}'|}$$

which satisfies

$$(\nabla^2 + k^2) G(\underline{r}, \underline{r}') = -\delta(|\underline{r} - \underline{r}'|) \quad (8)$$

Then replacing this definition for  $\delta(|\underline{r}-\underline{r}'|)$  in (7) and since the operator  $(\nabla^2+k^2)$  commutes with  $(1-\frac{1}{k^2}\nabla\nabla')$  we obtain

$$\underline{\Gamma}(\underline{r},\underline{r}') = \underline{\Gamma}(\underline{r}',\underline{r}) = (1-\frac{1}{k^2}\nabla\nabla')G(\underline{r},\underline{r}') \quad (9a)$$

Note that:

$$\underline{\Gamma}(\underline{r},\underline{r}') = \underline{\Gamma}^T(\underline{r}',\underline{r}) = \underline{\Gamma}(\underline{r}',\underline{r}) \quad (9b)$$

where  $\underline{\Gamma}^T$  is the transpose of  $\underline{\Gamma}$ .

Now we apply Green's theorem (5) to  $\underline{E}(\underline{r}')$  and  $\underline{\Gamma}(\underline{r}',\underline{r}) \cdot \underline{e}$ , where  $\underline{e}$  is an arbitrary constant vector. Integrating over all space:

$$\begin{aligned} \underline{E}(\underline{r}) \cdot \underline{e} &= \underline{E}_{inc} \cdot \underline{e} + \int_V (k^2[\epsilon(\underline{r}')-1]\underline{E}(\underline{r}') \\ &\quad \cdot \underline{\Gamma}(\underline{r}',\underline{r}) \cdot \underline{e}) dV' \end{aligned}$$

where the integral over the surface at infinity provides the incident field. The last expression can be also written:

$$\underline{E}(\underline{r}) = \underline{E}_{inc} + \int_V k^2[\epsilon(\underline{r}')-1]\underline{E}(\underline{r}') \cdot \underline{\Gamma}(\underline{r}',\underline{r}) dV'$$

and from (9b)

$$\underline{E}(\underline{r}) = \underline{E}_{inc}(\underline{r}) + \int_V k^2[\epsilon(\underline{r}')-1]\underline{\Gamma}(\underline{r},\underline{r}') \cdot \underline{E}(\underline{r}') dV'$$

We see, therefore, that the field at a position  $\underline{r}$  is the sum of the incident fields plus a superposition of the fields at each point  $\underline{r}'$  by sources of strength  $k^2(\epsilon(\underline{r})-1) \cdot \underline{E}(\underline{r}')$ . Notice that Equation (10) incorporates all boundary conditions of the problem and, since no derivatives of  $\epsilon(\underline{r})$  or  $\underline{E}$  are involved, this expression is valid even in the presence of discontinuities of  $\epsilon(\underline{r})$ .

Substituting (9a) into (10):

$$\begin{aligned} \underline{E}(\underline{r}) = & \underline{E}_{\text{inc}}(\underline{r}) + k^2 \int_V [\epsilon(\underline{r}')-1] \underline{E}(\underline{r}') G(\underline{r}, \underline{r}') \\ & - \nabla \int_V \nabla' G(\underline{r}, \underline{r}') \cdot \underline{E}(\underline{r}') [\epsilon(\underline{r}')-1] dV' \end{aligned} \quad (11)$$

Now we notice that:

$$G(\underline{r}, \underline{r}') \cong \frac{e^{-ikr}}{4\pi r} (e^{+ik \cdot \underline{r}'}), \quad r \rightarrow \infty$$

where  $\underline{k}$  is the outgoing wave vector. The first integral of (10) then becomes:

$$\int_V G(\underline{r}, \underline{r}') k^2 [\epsilon(\underline{r}')-1] \underline{E}(\underline{r}') dV' \approx \frac{e^{-ikr} k^2}{4\pi} \cdot$$

$$\int_V e^{+ik \cdot \underline{r}'} (\epsilon-1) \underline{E} dV'$$

The second integral becomes:

$$\frac{e^{-ikr}}{r} \frac{k^2}{4\pi} \left( \frac{k \cdot k}{k^2} \right) \cdot \int_V e^{ik \cdot \underline{r}'} (\epsilon-1) \underline{E}(\underline{r}') dV'$$

so that the scattered field in the radiation or far field zone<sup>7</sup> is (exchanging  $r$  and  $r'$  for simplicity):

$$\underline{\underline{E}}(\underline{\underline{r}}') = \left(1 - \frac{\underline{\underline{k}}\underline{\underline{k}}}{k^2}\right) e^{-i\underline{\underline{k}}\underline{\underline{r}}'} \left(\frac{k^2}{4\pi r'}\right) \int_V e^{i\underline{\underline{k}}\cdot\underline{\underline{r}}} [\epsilon(\underline{\underline{r}}) - 1] \cdot \underline{\underline{E}}(\underline{\underline{r}}) dV \quad (12)$$

where  $\underline{\underline{E}}(\underline{\underline{r}}')$  is the scattered field at position  $\underline{\underline{r}}'$  and the integral extends over the whole volume occupied by the scatterer. This is the result we were seeking. Equation (12), as said before, is only valid in the far field approximation (i.e., for  $r' \gg r$ ). It is not a solution of the differential equation (4), since the electric field appears at both sides of the expression. We must now transform it into a solution of (4).

## 2) First Born approximation.

To transform (12) into a solution of the wave equation (4), we identify the electric field appearing in the integrand with the incident field. This is called the first Born approximation and is valid for small values of  $\epsilon - 1$ . Since  $(\epsilon - 1)/4\pi$  is equal to the polarizability tensor per unit volume ( $\alpha$ ) the microscopic equivalent of Equation (12) is:

$$\underline{\underline{E}}(\underline{\underline{r}}') = \left(1 - \frac{\underline{\underline{k}}\underline{\underline{k}}}{k^2}\right) e^{-i\underline{\underline{k}}\underline{\underline{r}}'} \left(\frac{k^2}{4\pi r'}\right) \int_V e^{i(\underline{\underline{k}} - \underline{\underline{k}}_0) \cdot \underline{\underline{r}}} \underline{\underline{E}}_0 \cdot \underline{\underline{\alpha}}(\underline{\underline{r}}) dV \quad (13)$$

$\underline{E}_0$  and  $\underline{k}_0$  are the amplitude and wave-vector of the incident radiation, respectively, and the integration is to be carried out over the volume occupied by the scatterer. It should be noticed that in the far field approximation, the scattered field at any point has the character of a spherical wave. Equation (13) is now a solution to (3) and gives the scattered field at position  $\underline{r}'$  as the superposition of all the contributions of dipole radiation induced by the incident field and it automatically incorporates through  $\underline{r}$  the boundary conditions at the surface of the scatterer.

Figure 1 shows the spatial relations of these quantities, for a scatterer with the shape of a helix.

### III. Theory of Scattering of Radiation by a Helical Structure

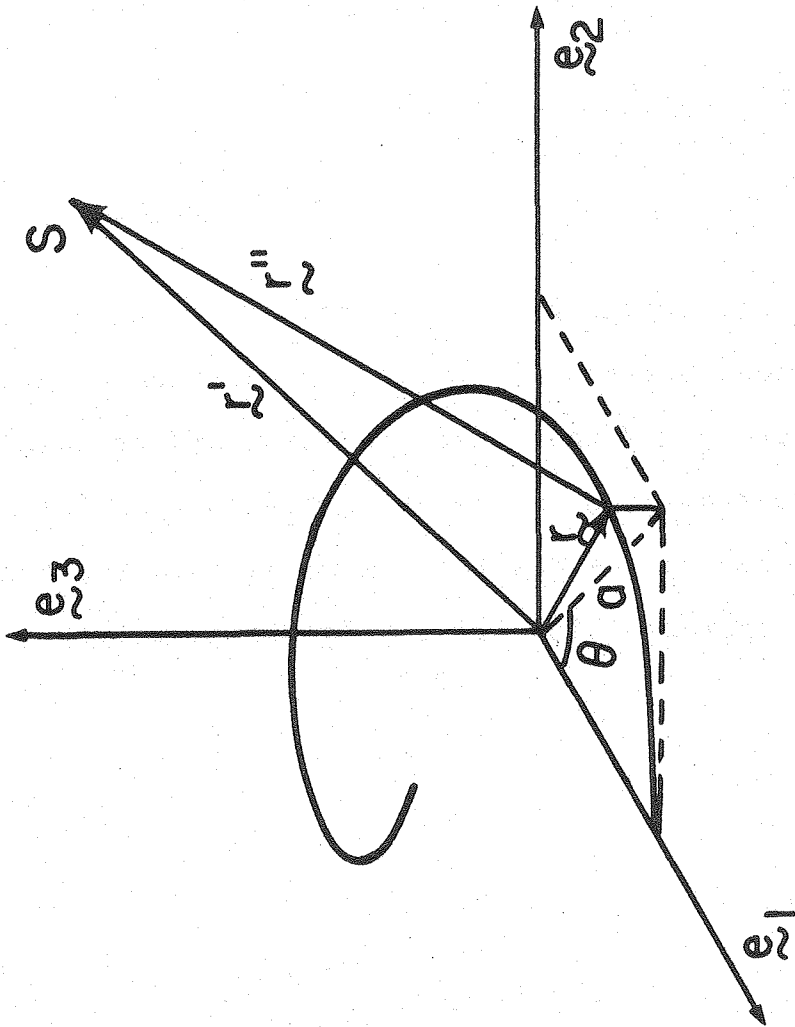
A helix can be described parametrically as:

$$\underline{r} = \underline{e}_1 a \cos\theta + \underline{e}_2 a \sin\theta + \underline{e}_3 P\theta/2\pi \quad (14)$$

where  $a$  is the radius and  $P$  the pitch of the helix;  $\underline{e}_1$ ,  $\underline{e}_2$  and  $\underline{e}_3$  are a set of unit orthogonal vectors. The helix can be thought of as a thin wire in a helical shape; it is essentially a one dimensional helix. Our next task is to write down the polarizability of the helix. At each point along its length we define a Cartesian coordinate system (see Figure 2) whose unit vectors are normal to the helix ( $\underline{n}$ ), tangent to it ( $\underline{t}$ ) and perpendicular ( $\underline{p}$ ) to these two and given by:

Figure 1. A segment of the helix of radius  $a$ , showing the relations between  $\underline{r}$ , the vector position of the scatterer;  $\underline{r}'$  the vector position of the point of observation S and  $\underline{r}''$  the distance from the scatterer to the observation point. In the far field approximation  $|\underline{r}' - \underline{r}|$  is approximately  $r'$ .

XBL 797-10654



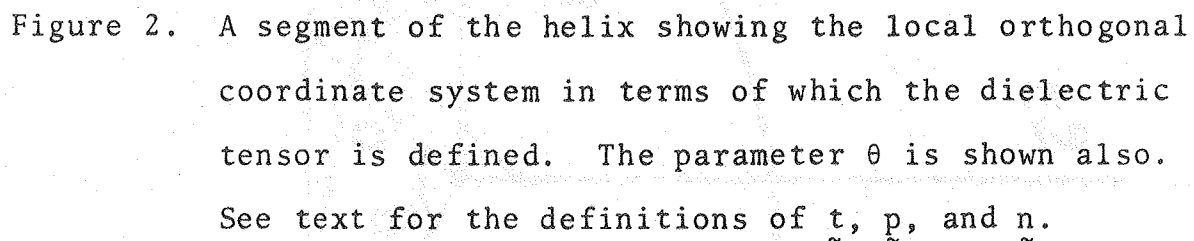
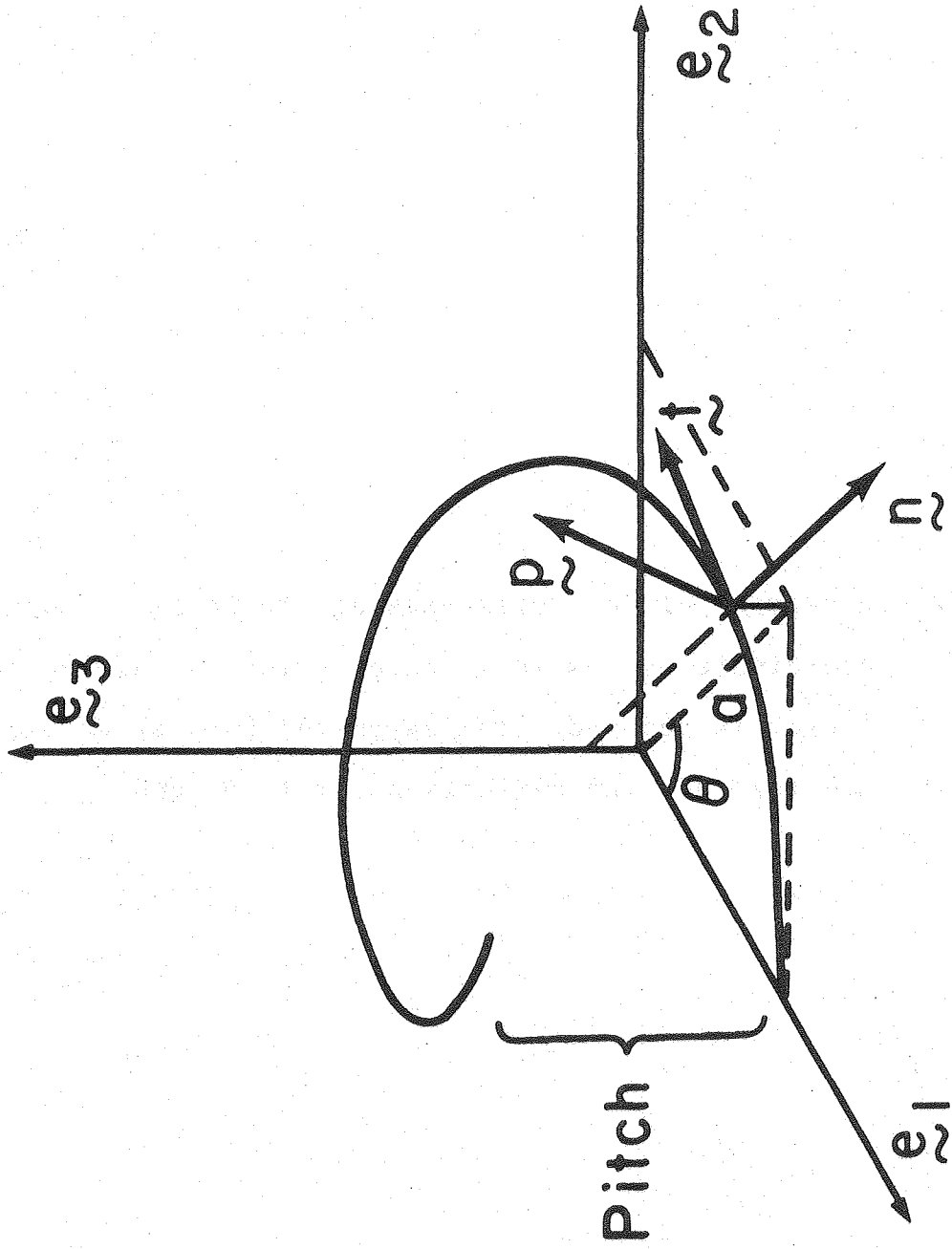


Figure 2. A segment of the helix showing the local orthogonal coordinate system in terms of which the dielectric tensor is defined. The parameter  $\theta$  is shown also. See text for the definitions of  $\underline{t}$ ,  $\underline{p}$ , and  $\underline{n}$ .



XBL 806-10470



$$\tilde{n} = \tilde{e}_1 \cos\theta + \tilde{e}_2 \sin\theta$$

$$\tilde{t} \equiv \frac{1}{M} \frac{dr}{d\theta} = -\tilde{e}_1 (a/M) \sin\theta + \tilde{e}_2 (a/M) \cos\theta + \tilde{e}_3 (P/2\pi M)$$

$$\tilde{p} = \tilde{n} \times \tilde{t} = \tilde{e}_1 (P/2\pi M) \sin\theta - \tilde{e}_2 (P/2\pi M) \cos\theta + \tilde{e}_3 (a/M)$$

(15)

where M is a normalization constant given by:

$$M = (a^2 + P^2/4\pi^2)^{1/2}$$

In the local cartesian system, therefore, the polarizability can be written as:

$$\tilde{\alpha} = \alpha_{tt} \tilde{t}\tilde{t} + \alpha_{nn} \tilde{n}\tilde{n} + \alpha_{pp} \tilde{p}\tilde{p} + \alpha_{tn} \tilde{t}\tilde{n} + \dots$$

Evaluation of the integral (13) requires the differential of volume of the helix; this can easily be shown to be:

$$dV = A_h M d\theta$$

where  $A_h$  is the cross-sectional area of the helix. Equation (13) for the helix can now be written as:

$$\tilde{E}(\tilde{r}') = B \int_0^{2\pi} \exp[i(\tilde{k} - \tilde{k}_0) \cdot \tilde{r}] \tilde{\alpha} \cdot \tilde{j} d\theta$$

$$B = A_h M \quad (16)$$

$$\tilde{F} = (1 - \tilde{k}k/k^2)(k^2/r')E_0 \exp(ikr') \quad (16)$$

where  $\ell$  is the number of turns of the helix and  $j$  describes the state of polarization of the incident radiation. We see that the amplitude of the scattered electric field is proportional to the length of the helix. Notice also that the product  $\tilde{\alpha} \cdot \tilde{j}$  of the polarizability and the polarization vector of the incident radiation which appears in the integrand will determine the amplitude of the scattered wavelet at each point on the helix. In this context, the scattered electric field appears as the Fourier transform of the  $\tilde{\alpha} \cdot \tilde{j}$  product, i.e., a transformation from the real space to the reciprocal space.

Let us consider first the integration of the exponential function in Equation (16). As an example, we choose radiation incident along  $\tilde{e}_2$ ; the exponential is:

$$\begin{aligned} \exp[i(\tilde{k} - \tilde{k}_0) \cdot \tilde{r}] = \exp\{i[k_x a \cos\theta + k_y a \sin\theta + \\ \Delta k_z P\theta/2\pi - (2\pi/\lambda) a \sin\theta]\} \end{aligned} \quad (17)$$

where

$$k_x = \tilde{e}_1 \cdot \tilde{k}; \quad k_y = \tilde{e}_2 \cdot \tilde{k} \quad \text{and} \quad \Delta k_z = (\tilde{k} - \tilde{k}_0) \cdot \tilde{e}_3.$$

Introducing two new parameters defined as  $R^2 = k_x^2 + k_y^2$

and  $\tan \psi = k_y/k_x$  (see Figure 2), we rewrite (17) as:

$$\exp\{i[R\cos(\psi-\theta) + \Delta k_z P\theta/2\pi]\} \exp[-i(2\pi a/\lambda)\sin\theta] \quad (18)$$

Next we use Bessel function expansions of the exponentials:

$$\begin{aligned} \exp\{iR\cos(\psi-\theta)\} &= \sum_{n=-\infty}^{\infty} J_n(Ra) \exp[-in(\psi-\theta)] \exp(in\pi/2) \\ \exp[-i(2\pi a/\lambda)\sin\theta] &= \sum_{m=-\infty}^{\infty} J_m(2\pi a/\lambda) \exp(-im\theta) \end{aligned} \quad (19)$$

where  $J_n$  is the cylindrical Bessel function of order  $n$ .

The integral of the exponential function in Equation (18)

is now:

$$\begin{aligned} I &= \sum_{nm} J_n(Ra) J_m(2\pi a/\lambda) \exp[in(\pi/2-\psi)] \int_0^{2\pi\ell} \exp[i(n-m+ \\ &\Delta k_z P/2\pi)\theta] d\theta \end{aligned} \quad (20)$$

For  $\ell \gg 1$ , the only terms that contribute significantly to this integral are those for which the argument of the exponential function vanishes, therefore  $m = (\Delta k_z P/2\pi) + n = \nu + n$ , and the last expression becomes:

$$I = 2\pi\ell \sum_n J_n(Ra) J_{\nu+n}(2\pi a/\lambda) \exp[-in(\psi-\pi/2)] \quad (21)$$

Graff's theorem<sup>8</sup> provides a further simplification:

$$J_\nu(\omega)\exp(i\nu\chi) = \sum_{n=-\infty}^{\infty} J_n(\nu)J_{\nu+n}(u)\exp(in\alpha) \quad (22)$$

in which the relationships among the variables are given by the Gegenbauer relations<sup>8</sup> (see Figures 3 and 4):

$$\begin{aligned} \omega &= (u^2 + v^2 - 2uv \cos\alpha) \\ u - v \cos\alpha &= \omega \cos\chi \\ v \sin\alpha &= \omega \sin\chi \end{aligned} \quad (23)$$

So that (21) can be written as:

$$\begin{aligned} I &= \int_0^{2\pi\ell} \exp[i(\underline{k} - \underline{k}_0) \cdot \underline{r}] = 2\pi\ell J_\nu(Qa) \exp\{i(\Delta k_z P/2\pi) \cdot \\ &(\psi^* + \pi/2)\} \end{aligned} \quad (24)$$

where:

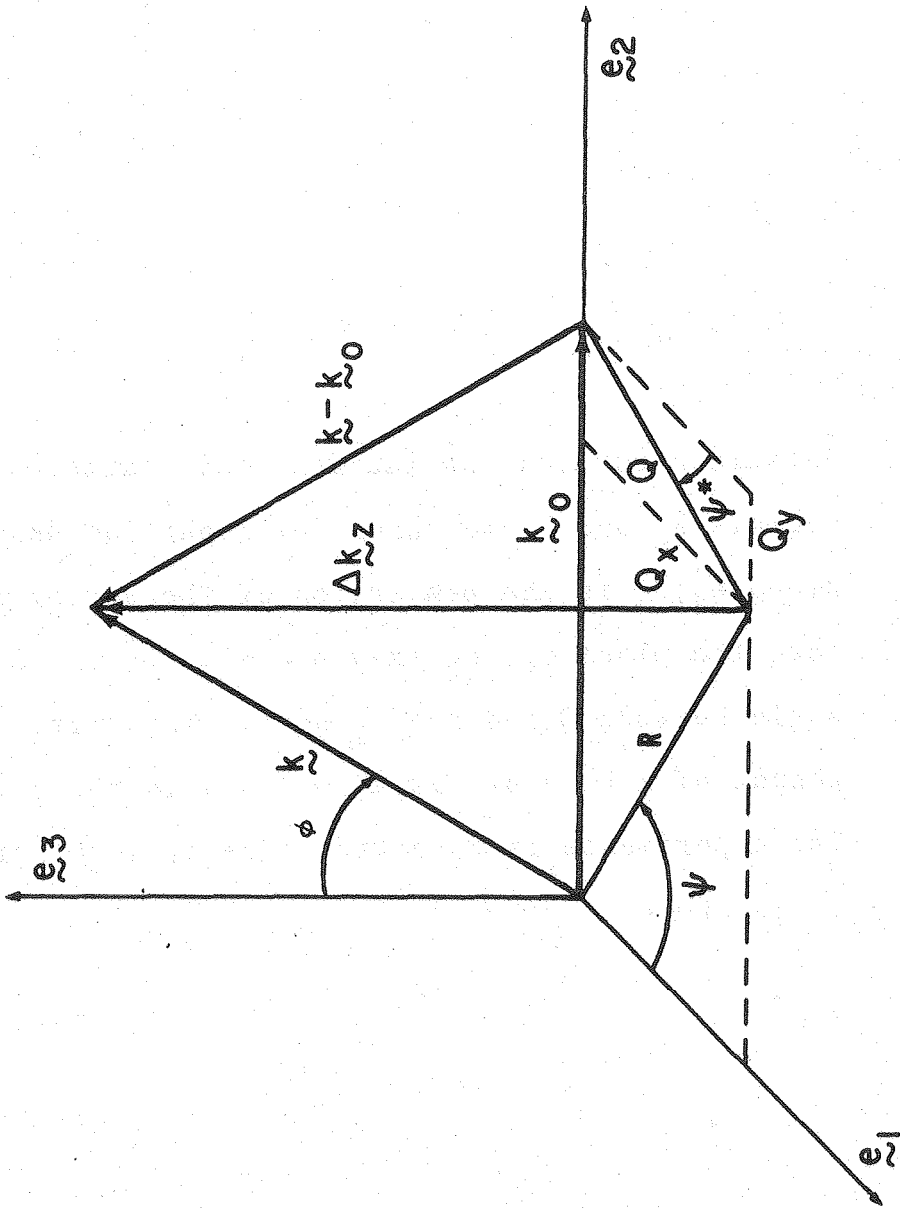
$$\Delta k_z P/2\pi = \nu; \nu = 0, \pm 1, \pm 2,$$

and  $\alpha = (\pi/2 - \psi)$

$$\psi^* = (\chi - \pi/2) \quad (24a)$$

Connections between the physical variables can now be obtained from relations (23):

Figure 3. Relations between the incident and scattered vectors  $\underline{k}_0$  and  $\underline{k}$  are shown for light incident along  $\underline{e}_2$ ; Q is the projection of the vector  $\underline{k}-\underline{k}_0$  onto the plane  $\underline{e}_1, \underline{e}_2$  (x-y plane).  $\psi^*$  is the angle between Q and the  $\underline{e}_1$ -axis. The third component of  $\underline{k}-\underline{k}_0 = \Delta k_z$  is also shown in the figure. The experimentally observed angle of scattering,  $\psi$ , is shown.



XBL 797-10652

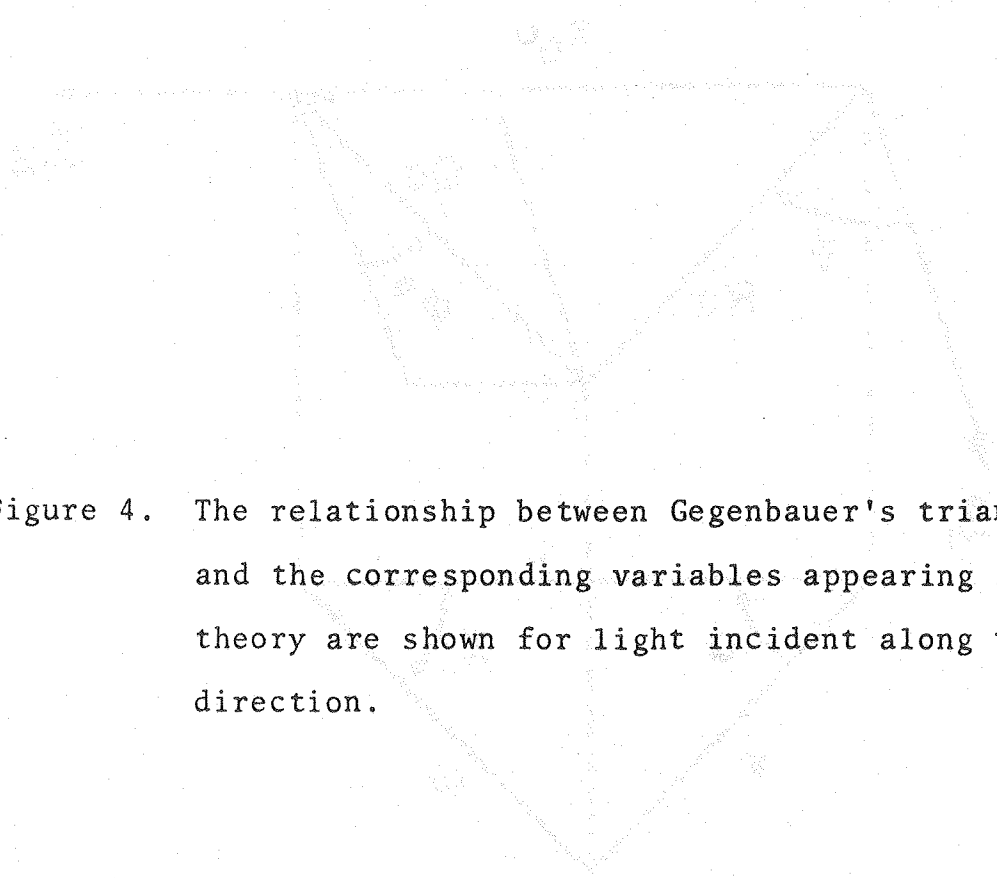
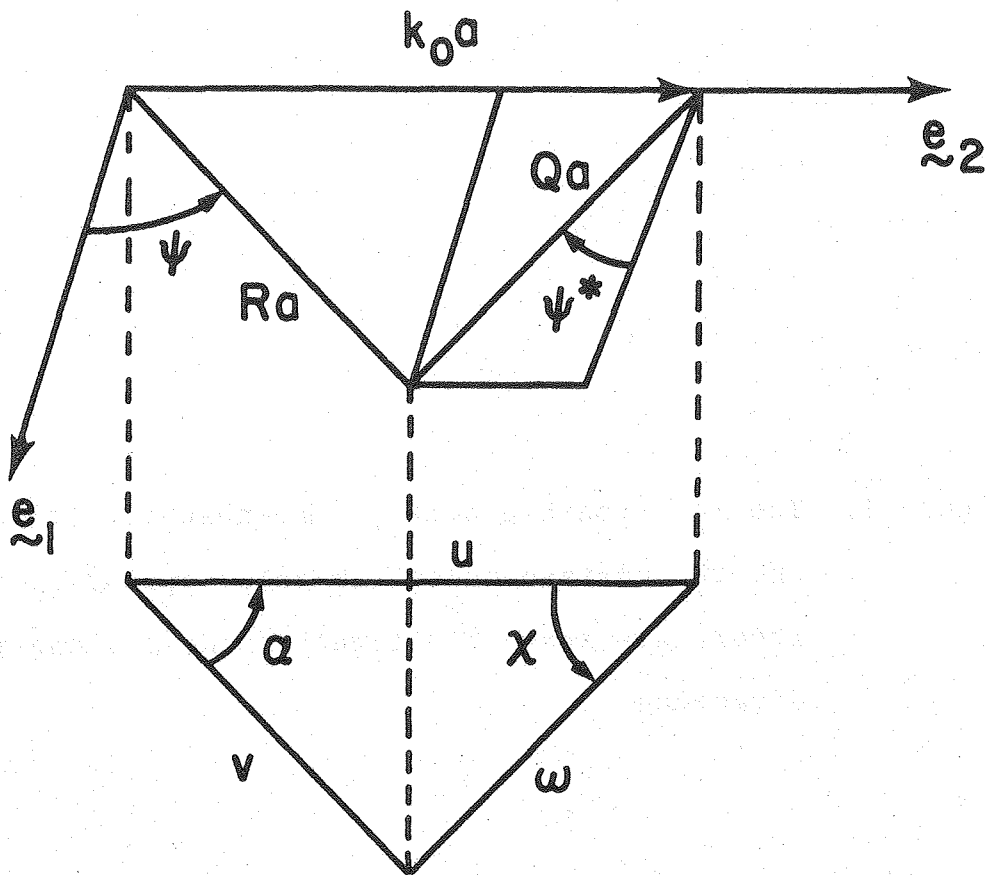


Figure 4. The relationship between Gegenbauer's triangle and the corresponding variables appearing in the theory are shown for light incident along the  $e_2$  direction.





For incidence along  $\underline{e}_2$ ,

$$\cos \psi^* = (R/Q_2) \cos \psi$$

$$Q_2 = (2\pi/\lambda)(1 + \sin^2 \phi - 2 \sin \phi \sin \psi)^{1/2} \quad (25)$$

For incidence along  $\underline{e}_1$ ,

$$\sin \psi^* = (-R/Q_1) \sin \psi$$

$$Q_1 = (2\pi/\lambda)(1 + \sin^2 \phi - 2 \sin \phi \cos \psi)^{1/2} \quad (26)$$

For incidence along  $\underline{e}_3$  (the helix axis),

$$Q_3 = R$$

$$\psi^* = \psi \quad (27)$$

where  $R = (2\pi/\lambda)\sin\phi$  and relations (24a) have been used. Figure 4 depicts congruently the variables of Equations (21) and (22). It is seen that  $0 \leq \psi \leq 2\pi$  is the azimuthal angle of scattering;  $0 \leq \phi \leq 180$  is the polar angle of scattering. These two are the experimentally measured parameters in terms of which the whole scattering field can be subtended. Angle  $\psi^*$  is a parameter which can be related to the physically observed  $\psi$  through Equations (25) and (26). Physically, it is the angle between the projection of  $\Delta \underline{k}$  on the  $\underline{e}_1$ - $\underline{e}_2$

plane, i.e.,  $Q$  and  $\underline{e}_1$  (for incidence along  $\underline{e}_2$ , see Figure 3) or  $\underline{e}_2$  (for incidence along  $\underline{e}_1$ , not depicted here). In the first case it becomes more negative as  $\psi$  becomes more positive:

first and fourth quadrant  $0^\circ \leq \psi^* \leq -90^\circ$

second and third quadrant  $-90^\circ \leq \psi^* \leq 180^\circ$

For incidence along  $\underline{e}_1$  it becomes more positive as  $\psi$  increases positively:

first and second quadrant  $-90^\circ \leq \psi^* \leq 0^\circ$

third and fourth quadrant  $0^\circ \leq \psi^* \leq 90^\circ$

Equation (24) must now be analyzed carefully. It shows that if  $\ell \gg 1$  (i.e., for large helices) there is a selection rule that quantizes the allowed values that the  $\underline{e}_3$  component of  $\Delta \underline{k} \equiv \underline{k} - \underline{k}_0$  can take in space:

$$\Delta k_z = 2\pi\nu/P, \nu = \text{integer} \quad (28)$$

Since in general  $\Delta k_z = (2\pi/\lambda) \cos\phi$  (see Figure 3), the maximum magnitude of  $\Delta k_z$  is  $2\pi/\lambda$ , and therefore Equation (28) only has solutions for  $\Delta k_z$  when  $P \geq \lambda$ . This indicates that for a long helix ( $\ell \gg 1$ ) whose pitch is at least the wavelength of the incident radiation, a discrete scattering

pattern will be found. For a short helix ( $l \approx 1$ ), or for a pitch smaller than the wavelength, a continuous scattering pattern is obtained. The planes in space where nonvanishing scattering intensities are to be found are called the scattering layer lines. Equations (24) and (28) imply that for a given layer line ( $\nu$ ), only Bessel functions of order  $\nu$  contribute to the scattering intensity. This is the result originally obtained by Cochran, Crick and Vand<sup>9</sup> for the scattering of unpolarized radiation by a helix. It is clearly seen that their solution corresponds to the case of a helix possessing a spherically symmetric polarizability,  $\alpha = \alpha \underline{1}$ .

For a general polarizability tensor, the trigonometric factors appearing in the integrand are written in exponential form. These alter the selection rule in Equation (28) with the result that, for a given layer line,  $\nu$ , Bessel functions of order  $\nu$ ,  $\nu \pm 1$ ,  $\nu \pm 2$ , etc., may contribute to the scattering amplitude. These extra trigonometric factors affecting the selection rules are the result of taking into account the polarization of the incident light. It is this new result that determines the spatial symmetry properties of the scattering of polarized light by a helical structure, and determines the differential behavior for light of opposite circular polarization. The latter, it can be seen now, results from the fact that different kinds of incident polarization are changed differently when the polarizability of the scatterer is asymmetric.

For a thin wire in helix form, we can take the polarizability to have only a tangential component, so that  $\alpha = \alpha_{tt}$ ; this is an exact result in the limit of an infinitely thin wire (a one-dimensional helix). Using Equation (15) and substituting into Equation (16), we can obtain the scattered amplitudes. For light polarized along  $\underline{e}_3$  and incident along  $\underline{e}_1$  (use minus sign) or  $\underline{e}_2$  (use plus sign), and for  $P \geq \lambda$ ,  $\ell \gg 1$ ,

$$\begin{aligned} \tilde{E}(\underline{r}') = B\alpha_t (P/4\pi M^2) \ell F \cdot \{ ia [J_{n+1}(Qa) \xi_{n+1}^{\pm} - J_{n-1}(Qa) \cdot \\ \xi_{n-1}^{\pm}] \underline{e}_1 + a [J_{n+1}(Qa) \xi_{n+1}^{\pm} + J_{n-1}(Qa) \cdot \\ \xi_{n-1}^{\pm}] \underline{e}_2 + (P/\pi) J_n(Qa) \xi_n^{\pm} \underline{e}_3 \} \end{aligned} \quad (29a)$$

with  $\xi_n^{\pm} = \exp[in(\psi \pm \pi/2)]$

and  $n = (\Delta k_z P/2\pi)$  (29b)

The equation for the scattered field amplitude on layer line  $n$  for light incident along  $\underline{e}_1$ , polarized  $\underline{e}_2$  (for  $P \geq$  and  $\ell \gg 1$ ) is:

$$\begin{aligned} \tilde{E}(\underline{r}') = B\alpha_t (a/4M^2) \ell F \cdot \{ ia [J_{n+2}(Qa) \xi_{n+2}^{-} - J_{n-2}(Qa) \cdot \\ \xi_{n-2}^{-}] \underline{e}_1 + a [J_{n+2}(Qa) \xi_{n+2}^{-} + 2J_n(Qa) \cdot \end{aligned}$$

$$\xi_n^- + J_{n-2}(Qa)\xi_{n-2}^-]e_2 + (P/\pi)[J_{n+1}(Qa)\xi_{n+1}^- + J_{n-1}(Qa)\xi_{n-1}^-]e_3\} \quad (30)$$

and for incident along  $e_2$ , polarized along  $e_1$  (for  $P \geq \lambda$  and  $\ell \gg 1$ ) is:

$$\begin{aligned} \tilde{E}(\tilde{r}') = B\alpha_t(a/4M^2)\ell F \cdot \{ & -a[J_{n+2}(Qa)\xi_{n+2}^+ - 2J_n(Qa)\xi_n^+ \\ & + J_{n-2}(Qa)\xi_{n-2}^+]e_1 + ai[J_{n+2}(Qa)\xi_{n+2}^+ \\ & - J_{n-2}(Qa)\xi_{n-2}^+]e_2 + (P/\pi)i[J_{n+1}(Qa)\xi_{n+1}^+ \\ & - J_{n-1}(Qa)\xi_{n-1}^+]e_3\} \quad (31) \end{aligned}$$

where  $\xi^\pm$  has the same meaning as in Equation (29a). For light incident along  $e_3$ ,  $\psi = \psi^*$ . Therefore, the equations for incidence  $e_3$ , polarization  $e_1$  are identical to Equation (31), but with  $R$  and  $\psi$  replacing  $Q$  and  $\psi^*$ , respectively. Again, for incidence  $e_3$ , polarization  $e_2$ , the equations are the same as (30), with  $R$ ,  $\psi$  and  $\xi^+$  instead of  $Q$ ,  $\psi^*$  and  $\xi^-$ . Clearly  $n = 0$  corresponds to the zeroth layer line.

The maximum number of layer lines that can be observed is obtained from the selection rule (29b). The total number of layer lines (including both those above and below the zero layer line) is:

$$2\{P/\lambda\} + 1 \quad (32)$$

where  $\{P/\lambda\}$  means the integral part of  $P/\lambda$ . Equation (16) can be integrated in general without the restrictions of  $P \geq \lambda$  and  $\ell \gg 1$ .

In this general case, i.e., without the above restrictions and for a tangential polarizability, the amplitudes for the scattering field can be written as an infinite sum of all order Bessel functions. For incidence along  $\underline{e}_2$  (plus sign) or  $\underline{e}_1$  (minus sign), and polarization along  $\underline{e}_3$ :

$$\begin{aligned} \underline{\tilde{E}}(\underline{r}') = & \frac{P}{2\pi M^2} \underline{\tilde{K}} \cdot \left\{ \left[ -ia \sum_{n=-\infty}^{\infty} J_n(Qa) S_n^{(1)} (-1)^{\ell(n+1)} \right] \underline{e}_1 \right. \\ & + \left[ aP \sum_{n=-\infty}^{\infty} J_n(Qa) T_n S_n^{(1)} (-1)^{\ell(n+1)} \right] \underline{e}_2 \\ & \left. + \left[ \frac{P}{2\pi} \sum_{n=-\infty}^{\infty} J_n(Qa) (\pi T_n)^{-1} (-1)^{n\ell} \right] \underline{e}_3 \right\} \cdot \\ & \sin(P\ell\Delta k_z/2) \exp(i n(\psi^* \pm \pi/2)) \quad (33) \end{aligned}$$

with

$$T_n = (\Delta k_z/2\pi - n/P)$$

$$S_n^{(1)} = \{\pi P [(\Delta k_z/2\pi - n/P)^2 - 1/P^2]\}^{-1}$$

$$\underline{\tilde{K}} = \alpha_t \underline{BF}$$

For incidence  $\underline{e}_2$ , polarization  $\underline{e}_1$ :

$$\begin{aligned}
 \underline{E}(\underline{r}') &= (a/2M^2)K \cdot \left\{ -a \left[ \sum_{n=-\infty}^{\infty} J_n(Qa) (PT_n S_n^{(2)} \right. \right. \\
 &\quad \left. \left. - (\pi T_n)^{-1} (-1)^{n\ell} \right] \underline{e}_1 - \left[ a \sum_{n=-\infty}^{\infty} J_n(Qa) \cdot \right. \right. \\
 &\quad \left. \left. S_n^{(2)} (-1)^{n\ell} \right] \underline{e}_2 - \left[ \frac{P}{\pi} \sum_{n=-\infty}^{\infty} J_n(Qa) \cdot \right. \right. \\
 &\quad \left. \left. S_n^{(1)} (-1)^{\ell(n+1)} \right] \underline{e}_3 \right\} \sin(P\ell\Delta k_z/2) e^{in(\psi^* + \pi/2)}
 \end{aligned} \tag{34}$$

For incidence  $\underline{e}_1$ , polarization  $\underline{e}_2$ :

$$\begin{aligned}
 \underline{E}(\underline{r}') &= (a/2M^2)K \cdot \left\{ [-ia \sum_{n=-\infty}^{\infty} J_n(Qa) S_n^{(2)} (-1)^{n\ell} \right] \underline{e}_1 \\
 &\quad + \left[ a \sum_{n=-\infty}^{\infty} J_n(Qa) (PT_n S_n^{(2)} + (\pi T_n)^{-1} \right. \\
 &\quad \left. (-1)^{n\ell} \right] \underline{e}_2 + \left[ \frac{P}{\pi} \sum_{n=-\infty}^{\infty} J_n(Qa) PT_n S_n^{(1)} \cdot \right. \\
 &\quad \left. (-1)^{\ell(n+1)} \right] \underline{e}_3 \right\} \sin(P\ell\Delta k_z/2) e^{in(\psi^* - \pi/2)}
 \end{aligned} \tag{35}$$

where  $S_n^{(2)} = \{\pi P [(\Delta k_z/2\pi - n/P)^2 - 4/P^2]\}^{-1}$ , and  $S_n^{(1)}$  and  $T_n$  are given as in Equation (33).

The case of incidence along  $\underline{e}_3$ , polarization  $\underline{e}_1$ , is the same as Equation (33) with  $\psi$  and  $R$  replacing  $\psi^*$  and  $Q$ , respectively, and the plus sign being used. For incidence  $\underline{e}_3$ , polarization  $\underline{e}_2$ , the expression is the same as Equation (35), with  $R$  and  $\exp[in(\psi + \pi/2)]$  replacing  $Q$  and  $\exp[in(\psi^* - \pi/2)]$ ,



respectively. Equations (33), (34), and (35) are the general expressions for the scattered electric field. Hence, for  $P \leq \lambda$  according to these equations, the scattering pattern is continuous in space. Moreover, even for the case  $P \geq \lambda$ , the equations predict a continuous pattern, if the length of the helix is comparable to the wavelength of light. This feature is depicted in the general equations by factors such as:

$$S_n^{(2)} (-1)^{n\ell} \sin(P\ell\Delta k_z)$$

that can be expanded to yield:

$$\frac{\sin\pi P\ell(-n/P+\Delta k_z/2\pi-2/P)}{\pi(-n/P+\Delta k_z/2\pi-2/P)} - \frac{\sin\pi P\ell(-n/P+\Delta k_z/2\pi+2/P)}{\pi(-n/P+\Delta k_z/2\pi+2/P)}$$

that behave as Dirac-delta sequences centered at  $\Delta k_z = (n/P \pm 2/P)$ . They predict continuous scattering patterns, for helices of a length comparable to the wavelength of light for any ratio of  $P/\lambda$ , in which the magnitudes of the scattered intensities between layer lines are of the same magnitude as those at the layer lines themselves. For  $\ell \rightarrow \infty$ , these sequences tend to Dirac-delta functions and quantize the allowed scattered directions provided that  $P/\lambda \geq 1$ . Therefore, these equations reduce to Equations (29), (30), and (31) for the case of  $P \geq \lambda$  and  $\ell \gg 1$ . The expressions for the scattered fields from right and left circularly polarized light can be obtained from linear

combinations of those obtained for plane-polarized radiation. Once obtained (the scattered fields for right and left circularly polarized light) the corresponding scattered intensities can be obtained. For left circularly polarized light, the scattered field is:

$$\underline{\underline{E}}_L(\underline{\underline{r}}') = (E_0 k^2 B \alpha_t / r') (1 - \underline{\underline{k}} \underline{\underline{k}} / k^2) \underline{\underline{E}}_{L,0}$$

where  $\underline{\underline{E}}_{L,0}$  is the scattered field without the transversality correction.

The intensity measured at the detector is:

$$I_L = [|\underline{\underline{E}}_L(\underline{\underline{r}}') - \underline{\underline{k}}(\underline{\underline{k}} \cdot \underline{\underline{E}}_L(\underline{\underline{r}}')) / k^2| \cdot |\underline{\underline{E}}_L^*(\underline{\underline{r}}') - \underline{\underline{k}}(\underline{\underline{k}} \cdot \underline{\underline{E}}_L^*(\underline{\underline{r}}')) / k^2|]$$

$$I_L = |\underline{\underline{E}}_L|^2 - (\underline{\underline{k}} \cdot \underline{\underline{E}}_L^*)(\underline{\underline{k}} \cdot \underline{\underline{E}}_L) / k^2$$

Equivalent expressions can be obtained for the right circularly polarized incident light, so that the CIDS can now be written as:

$$CIDS = \frac{|\underline{\underline{E}}_L|^2 - |\underline{\underline{E}}_R|^2 - [(\underline{\underline{k}} \cdot \underline{\underline{E}}_L^*)(\underline{\underline{k}} \cdot \underline{\underline{E}}_L) - (\underline{\underline{k}} \cdot \underline{\underline{E}}_R^*)(\underline{\underline{k}} \cdot \underline{\underline{E}}_R)] / k^2}{|\underline{\underline{E}}_L|^2 - |\underline{\underline{E}}_R|^2 - [(\underline{\underline{k}} \cdot \underline{\underline{E}}_R^*)(\underline{\underline{k}} \cdot \underline{\underline{E}}_R) + (\underline{\underline{k}} \cdot \underline{\underline{E}}_L^*)(\underline{\underline{k}} \cdot \underline{\underline{E}}_L)] / k^2}$$

In the special case of  $P \geq \lambda$  and  $\ell \gg 1$ , the calculation can be carried out analytically.

The expressions for CIDS along the three perpendicular directions  $\underline{\underline{e}}_1$ ,  $\underline{\underline{e}}_2$ , and  $\underline{\underline{e}}_3$  are therefore:

For  $e_2$ -incidence:

$$\begin{aligned}
 I_L - I_R = & CC^* \{ (aP/2\pi M^4) \{ (H+G)a^2 + (P^2/2\pi^2)U^- \} \cos\psi' \\
 & + (aP/4\pi M^4) \{ (aP/2\pi) [X^-/2 \sin(2\psi' - \psi) - Z^- \cdot \\
 & \sin\psi] \sin 2\phi - (P^2 U^- / \pi^2) \cos\psi' \cos^2\phi + a^2 [V^- \cdot \\
 & \cos\psi' + 2U^- \cos\psi \cos(\psi' - \psi) + Y^- \cos(2\psi - 3\psi')] \cdot \\
 & \sin^2\phi \} \} \quad (36a)
 \end{aligned}$$

and

$$\begin{aligned}
 I_L + I_R = & CC^* \{ (1/4M^4) \{ (a^2 P^2 / 2\pi^2) (3Z^+ - 2N \cos 2\psi') \\
 & + (P^4 / 4\pi^4) (0 - S^+) + a^4 (0 - X^+ \cos 2\psi') \} - (1/ \\
 & 8M^4) \{ (a^2 P^2 / \pi^2) [Z^+ - 2N (\cos(2\psi' - 2\psi) \sin^2\phi \\
 & + \cos 2\psi' \cos^2\phi)] + a^4 [2(0 - S^+) \cos^2\psi + S^+ + 2I \cos \\
 & (4\psi' - 2\psi) - 2X^+ \cos\psi \cos(2\psi' - \psi)] \sin^2\phi + (P^4 / \pi^4) \cdot \\
 & ((0 - S^+) / 2) \cos^2\phi + (aP^3 / \pi^3) U^+ \sin(\psi - \psi') \sin 2\phi \\
 & + (a^3 P / \pi) [Y^+ \sin(3\psi' - \psi) + V^+ \sin(\psi - \psi') - 2U^+ \cdot
 \end{aligned}$$

$$\sin\psi'\cos\psi]\sin2\phi\}} \quad (36b)$$

$$C = \ell k^2 E_0 B \alpha_t / |r'| \quad \text{with } \psi' = (\psi^* + \pi/2)$$

For incidence along  $e_1$ :

$$\begin{aligned} I_L - I_R = & CC^* \{ (aP/2\pi M^4) \{ (H+G)a^2 + (P^2/2\pi^2)U^- \} \sin\psi' \\ & + (aP/4\pi M^4) \{ (aP/2\pi) [ (X^-/2) \cos(2\psi' - \psi) \\ & - Z^- \cos\psi ] \sin2\phi + (P^2 U^- / \pi^2) \sin\psi' \cdot \cos^2\phi - a^2 \cdot \\ & [ V^- \sin\psi' + 2U^- \sin\psi \cos(\psi' - \psi) + Y^- \cos(2\psi - 3\psi') ] \\ & \sin^2\phi \} \} \quad (37a) \end{aligned}$$

and

$$\begin{aligned} I_L + I_R = & CC^* \{ (1/4M^4) \{ (a^2 P^2 / 2\pi^2) (3Z^+ + 2N \cos 2\psi') \\ & + (P^4 / 4\pi^4) (0 - S^+) + a^4 (0 + 2X^+ \cos\psi') \} - (1/8M^4) \cdot \\ & \{ (a^2 P^2 / \pi^2) [ Z^+ - 2N (\cos(2\psi' - 2\psi) \sin^2\phi - \cos 2\psi' \cdot \\ & \cos^2\phi) ] + a^4 [ 2(0 - S^+) \sin^2\psi + S^+ - 2I \cos(4\psi' - 2\psi) \\ & - 2X^+ \sin\psi \sin(2\psi' - \psi) ] \sin^2\phi + (P^4 / \pi^4) ((0 - S^+) / 2) \cdot \\ & \cos^2\phi + (aP^3 / \pi^3) U^+ \sin(\psi - \psi') \sin 2\phi + (a^3 P / \pi) [ Y^+ \cdot \end{aligned}$$

$$\cdot \sin(\psi - 3\psi') + V^+ \sin(\psi - \psi') + 2U^+ \cos\psi' \sin\psi \} \quad (37b)$$

with  $\psi' = (\psi^* - \pi/2)$ .

For  $e_3$ -incidence:

$$I_L - I_R = CC^* \{ a^2 [(S^- + X^-) \sin^2 \phi - 2S^-] + (aP/\pi) T^- \sin 2\phi - (P^2/\pi^2) Z^- \sin^2 \phi \} \quad (38a)$$

$$I_L + I_R = CC^* \{ a^2 [(O + X^+) \sin^2 \phi + 2O] + (aP/\pi) T^+ \sin 2\phi + (P^2/\pi^2) Z^+ (1 + \cos^2 \phi) \} \quad (38b)$$

with:  $G = J_{n-1} (J_n - J_{n-2})$

$$H = J_{n+1} (J_{n+2} - J_n)$$

$$I = J_{n+2} J_{n-2}$$

$$N = J_{n+1} J_{n-1}$$

$$O = 2J_n^2 + J_{n+2}^2 + J_{n-2}^2$$

$$S^\pm = (J_{n+2}^2 \pm J_{n-2}^2)$$

$$T^\pm = (2/Qa) [(n-1)J_{n-1}^2 \pm (n+1)J_{n+1}^2]$$

$$U^\pm = J_n (J_{n+1} \pm J_{n-1})$$

$$V^{\pm} = (J_{n-1}J_{n-2} \pm J_{n+1}J_{n+2})$$

$$X^{\pm} = 2J_n(J_{n+2} \pm J_{n-2})$$

$$W^{\pm} = J_{n+2}(J_{n+1} \pm J_{n-1})$$

$$Y^{\pm} = (J_{n-1}J_{n+2} \pm J_{n+1}J_{n-2})$$

$$Z^{\pm} = (J_{n+1}^2 \pm J_{n-1}^2)$$

$$\psi' = (\psi^* + \pi/2)$$

Equations (38) show that the expression for the CIDS for light incident along the helix axis is independent of the azimuthal angle  $\psi$  or  $\psi^*$ . This cylindrical symmetry does not hold along the other two directions of incidence. The corresponding formulas for the case  $P < \lambda$  and  $\ell \sim 1$  are combinations of all the sums in Equations (33), (34) and (35), and numerical calculations must be used. From the equations obtained for the CIDS, we notice that the actual value of the tangential polarizability cancels when taking the ratio of the scattered intensities.

As a result, these equations for CIDS cannot take into account the dispersion properties of the scatterer, and will fail to describe the CIDS of helical structures at wavelengths inside an absorption band. Effects resulting from band shapes are also neglected in this model. This is the result of

having combined two different approximations: a) the assumption that the polarizability is purely uniaxial:  $\alpha_{\approx} = \alpha_{t\sim\sim}$ , and b) the approximation of replacing the "local field" in the integral Equation (12) by the incident field. Relaxing either of these will result in a polarizability-dependent CIDS. In fact, a polarizability of the form:  $\alpha_{\approx} = \alpha_{t\sim\sim} + \alpha_{n\sim\sim}$  will not cancel when the ratio for CIDS is taken and will be able to describe band effects. In general, it is useful to choose a complex polarizability. The real part characterizes the dispersive contribution to the differential scattering, whereas the imaginary part allows for absorptive behavior of the scatterer. Use of complex polarizabilities does not take into account intrinsic optical activity; we are still only considering form CIDS in which the geometric arrangement of frequency-dependent polarizabilities determines the optical properties. Only when actual coupling of the radiating elements of the scatterer are taken into account can we properly speak of intrinsic CIDS. This case will be treated in Chapter 5 of this thesis, by allowing dipole-dipole interaction among the dipoles induced along the scatterer by the incident electromagnetic radiation. We have only considered here form CIDS in which the ratio of scattered intensities are independent of the magnitude of the polarizability.

From Equations (13) and (16) it is seen that the crucial feature in the model that accounts for the differential

behavior of the scatterer with light of opposite circular polarization is the product  $\underline{\alpha} \cdot \underline{j}$  appearing in the integrand. For a spherically symmetric polarizability,  $\underline{\alpha} \equiv \alpha \underline{1}$ , and therefore, different states of polarization will be left unchanged when taking their product with the polarizability. This product  $\underline{1} \cdot \underline{j}$ , being independent of the variable of integration, can be taken outside the integral and as a result, when the field amplitudes are squared to obtain the intensities, the difference between these intensities for right and left circularly polarized light will vanish, yielding no CIDS. Thus, differential scattering of light of opposite polarization is the result of (and a measure of) the asymmetry of the dielectric properties of the scatterer.

#### IV. Characterization of the State of Polarization of the Scattered Light.

A complete characterization of the scattered radiation must include both its intensity and polarization. Nothing has been said so far about the polarization of the scattered light for a given state of polarization of the incident radiation. It is interesting to establish the effect of the geometry and the dielectric properties of the scatterer in determining the final state of polarization of light. In the most general case, the polarization vector of monochromatic light traveling along a given direction describes an ellipse in space.<sup>10</sup> Indeed, if  $x$  and  $y$  are two arbitrary sets of



axes and the light is propagating along the z-axis, then the components of the electric field are (in complex notation)

$$E_x = a_1 e^{i(\alpha + \delta_1)}$$

and

$$E_y = a_2 e^{i(\alpha + \delta_2)}$$

from which we can obtain easily:

$$\left(\frac{E_x}{a_1}\right)^2 + \left(\frac{E_y}{a_2}\right)^2 - 2\left(\frac{E_x}{a_1}\right)\left(\frac{E_y}{a_2}\right)\cos\delta = \sin^2\delta \quad (39)$$

where  $\delta = \delta_2 - \delta_1$  is the phase difference between the two components of the electric field. Equation (39) is the equation of an ellipse. The following relations can be shown to hold:

$$a^2 + b^2 = a_1^2 + a_2^2$$

$$\tan 2\psi = (\tan 2\alpha)\cos\delta$$

$$\sin 2\chi = (\sin 2\alpha)\sin\delta$$

with  $a$  and  $b$  the semi-axes of the ellipse;  $\psi$  is the angle between the  $x$  direction and the major axis of the ellipse (its inclination is  $\tan\alpha = a_2/a_1$ ); and  $\tan\chi = \pm b/a$ , where  $\chi$  is proportional to the ellipticity of the light wave. Its sign indicates the sense of rotation of the polarization vector describing the ellipse. Therefore, characterizing the polarization

of light is equivalent to determining the polarization ellipse. For this we need three independent parameters, e.g., the amplitudes  $a_1$  and  $a_2$ , the phase difference  $\delta$  or the two axes of the ellipse ( $a$  and  $b$ ), and the angle  $\psi$  that specifies the orientation of the ellipse. In 1852 G. G. Stokes<sup>11</sup> introduced four parameters that are combinations of the first three independent variable mentioned above. They are of practical use because they all have the same dimensions and are frequently called the Stokes' parameters. In our notation they are:

$$I = |E_x|^2 + |E_y|^2 = a_1^2 + a_2^2$$

$$Q = |E_x|^2 - |E_y|^2 = a_1^2 - a_2^2$$

$$U = E_x E_y^* + E_x^* E_y = 2a_1 a_2 \cos \delta$$

$$V = i(E_x E_y^* - E_x^* E_y) = 2a_1 a_2 \sin \delta$$

Because these four parameters are defined out of only three independent variables, there is a relation connecting all of them; this is:

$$I^2 = Q^2 + U^2 + V^2 \quad (40)$$

$I$  represents the total intensity.  $Q$  is the excess in intensity of light transmitted by a polarizer which accepts linear polarization in the  $x$ -direction over a polarizer that

accepts linear polarization along the y-direction. U has a meaning equivalent to Q, but with the polarizers oriented at  $45^\circ$  and  $135^\circ$  from the x-axis. V describes the excess in intensity of light transmitted by a device that accepts right circularly polarized light over that which accepts the opposite polarization. Since in scattering phenomena light is dispersed in all directions, the definition of the Stoke's parameters should be the same regardless of the direction of propagation of the scattered light. To accomplish this, it is necessary to choose a reference frame that will be equivalent for all possible directions of propagation of the scattered light. It is common use to define these parameters relative to the scattering plane,<sup>12</sup> i.e., the plane which contains both the incident and scattered wave vector. The scattered electric field is therefore written in terms of its component ( $E_{\parallel}$ ) in the scattering plane, but perpendicular to  $\underline{k}$ , and its out-of-plane component ( $E_{\perp}$ ). Defining in-plane ( $\underline{p}$ ) and out-of-plane ( $\underline{n}$ ) unit vectors along these components,

$$\underline{n} = (\underline{k} \times \underline{k}_0) / |\underline{k} \times \underline{k}_0|$$

$$\underline{p} = (\underline{k} \times \underline{n}) / |\underline{k} \times \underline{n}|$$

we obtain

$$E_{\perp} = \underline{n} \cdot \underline{E} \quad \text{and} \quad E_{\parallel} = \underline{p} \cdot \underline{E} \quad (41)$$

The directions of the components are chosen so that  $\underline{n} \times \underline{p}$  is along the direction of propagation of the outgoing wave.

The scattering fields to be used in Equation (41) are the fields without the transversality correction ( $\underline{1} - \underline{k}\underline{k}/k^2$ ).

The Stokes' parameters can now be written as:

$$\begin{aligned}
 I &= \underline{E} \cdot (\underline{pp} + \underline{nn}) \cdot \underline{E}^* = \underline{E} \cdot (\underline{1} - \underline{k}\underline{k}/k^2) \cdot \underline{E}^* \\
 Q &= \underline{E} \cdot (\underline{pp} - \underline{nn}) \cdot \underline{E}^* \\
 U &= \underline{E} \cdot (\underline{pn} + \underline{np}) \cdot \underline{E}^* \\
 V &= i \underline{E} \cdot (\underline{pn} - \underline{np}) \cdot \underline{E}^* \tag{42}
 \end{aligned}$$

$$\underline{n} = (-\cos \psi \underline{e}_1 + \cos \psi \sin \psi \underline{e}_3) / (1 - \sin^2 \psi \sin^2 \phi)^{1/2}$$

and

$$\begin{aligned}
 \underline{p} = [ &-\cos \psi \sin \psi \sin^2 \phi \underline{e}_1 + (1 - \sin^2 \psi \sin^2 \phi) \underline{e}_2 \\
 &-\sin \psi \sin \phi \cos \phi \underline{e}_3] / (1 - \sin^2 \psi \sin^2 \phi)^{1/2}
 \end{aligned}$$

from which we obtain the matrices needed to compute the Stokes parameters in (41). Here we will write down these matrices for light incident along  $\underline{e}_2$  and polarized along  $\underline{e}_1$ , only:

$$\underline{\underline{(1-kk/k^2)}} = \begin{bmatrix} 1-\cos^2\psi\sin^2\phi & -\sin\psi\cos\psi\sin^2\phi & -\cos\psi\sin\phi\cos\phi \\ -\sin\psi\cos\psi\sin^2\phi & 1-\sin^2\psi\sin^2\phi & -\sin\psi\sin\phi\cos\phi \\ -\cos\psi\sin\phi\cos\phi & -\sin\psi\sin\phi\cos\phi & \sin^2\phi \end{bmatrix} \quad (43)$$

$$\underline{\underline{pp-nn}} = \begin{bmatrix} \cos^2\psi\sin^2\psi\sin^4\phi & -\cos\psi\sin\psi\sin^2\phi & \cos\phi\sin\phi\cos\psi(\sin^2\psi \\ -\cos^2\phi/(1-\sin^2\psi \\ \sin^2\phi) & & \sin^2\phi+1)/(1-\sin^2\psi \\ & & \sin^2\phi) \\ -\cos\psi\sin\psi\sin^2\phi & 1-\sin^2\psi\sin^2\phi & -\sin\psi\sin\phi\cos\phi \\ \cos\phi\sin\phi\cos\psi & -\sin\psi\sin\phi\cos\phi & \sin^2\phi(\sin^2\psi\cos^2\phi- \\ (\sin^2\psi\sin^2\phi+1)/ & & \cos^2\psi)/(1-\sin^2\phi \\ (1-\sin^2\psi\sin^2\phi) & & \sin^2\psi) \end{bmatrix} \quad (44)$$

$$\underline{\underline{pn+np}} = \begin{bmatrix} 2\cos\psi\sin\psi\sin^2\phi & -\cos\phi & \sin\psi\sin\phi(\cos^2\phi- \\ \cos\phi/(1-\sin^2\psi \\ \sin^2\phi) & & \cos^2\psi\sin^2\phi)/(1- \\ & & \sin^2\psi\sin^2\phi) \\ -\cos\phi & 0 & \cos\psi\sin\phi \\ \sin\psi\sin\phi(\cos^2\phi & \cos\psi\sin\phi & -2\sin\psi\cos\psi\sin^2\phi \\ -\cos^2\psi\sin^2\phi)/ & & \cos\phi/(1-\sin^2\psi \\ (1-\sin^2\psi\sin^2\phi) & & \sin^2\phi) \end{bmatrix} \quad (45)$$

$$i(\underline{p}\underline{n}-\underline{n}\underline{p}) = \begin{bmatrix} 0 & i \cos\phi & -i \sin\psi \sin\phi \\ -i \cos\phi & 0 & +i \cos\psi \sin\phi \\ +i \sin\psi \sin\phi & -i \cos\psi \sin\phi & 0 \end{bmatrix} \quad (46)$$

These matrices, plus the scattered fields, contain all the necessary information to describe the state of polarization of radiation scattered by a helix when incident along  $\underline{e}_2$  and polarized along  $\underline{e}_1$ . From Equations (42) we obtain (for  $P \geq \lambda$  and  $\ell \gg 1$ ):

$$\begin{aligned} I = CC^* \{ & (a^4/16M^4) [(S^+ (1+\cos^2\phi) + 2(O-S^+-X^+) \cos 2\psi') (1- \\ & \cos^2\psi \sin^2\phi) + X^+ \sin 2\psi' \sin 2\psi - I \cos(4\psi' - 2\psi) \sin^2\phi] + \\ & (P^2 a^2/16M^4 \pi^2) [Z^+ - 2N \cos 2\psi'] \sin^2\phi + (a^3 P/16\pi M^4) [Y^+ \\ & \sin(\psi - 3\psi') + V^+ \sin(\psi' - \psi) - 2U^+ \sin\psi' \cos\psi] \sin 2\phi \} \quad (47) \end{aligned}$$

$$\begin{aligned} U = CC^* \{ & (a^4/16M^4) [(2O-S^+ + 2I \cos 4\psi' - 2X^+ \cos 2\psi') \sin 2\psi \sin^2\phi \\ & \cos\phi / (1 - \sin^2\psi \sin^2\phi) + (X^+ \sin 2\psi' - 2I \sin 4\psi') \cos\phi] - \\ & (a^2 P^2/16\pi^2 M^4) [(Z^+ - 2N \cos 2\psi') \sin 2\psi \sin^2\phi \cos\phi / (1 - \sin^2\psi \\ & \sin^2\phi)] + (a^3 P/8\pi M^4) [(Y^+ \sin 3\psi' - (V^+ + 2U^+) \sin\psi') \sin\psi \\ & \sin\phi (\cos^2\phi - \cos^2\psi \sin^2\phi) / (1 - \sin^2\psi \sin^2\phi) + (V^+ \cos\psi' \end{aligned}$$

$$-Y^+ \cos 3\psi') \cos \psi \sin \phi] \} \quad (48)$$

$$V = CC^* \{ (-a^4/8M^4) [S^+ + X^- \cos 2\psi - 2I \cos 4\psi'] \cos \phi + (-a^3 P / 8\pi M^3) [-Y^- \sin(\psi + 3\psi') + (W^- + 2U^-) \cos \psi' \sin \psi - 2V^- \sin \psi' \cos \psi] \sin \phi \} \quad (49)$$

where the symbols used here have the same meaning as in Equation (38). Because of expression (40), the fourth parameter is automatically determined by the three written above.

#### V. Discussion and Conclusions.

In this chapter we have presented analytical expressions for the circular intensity differential scattering (CIDS) of a chiral structure (an oriented helix) possessing a polarizability tangent to the helix. The general expressions for the scattered fields, for any ratio of helix pitch to wavelength ( $P/\lambda$ ) are Equations (33), (34), and (35); they may be simplified when  $P \geq \lambda$  and the number of turns of the helix is large ( $l \gg 1$ ) to give Equations (29), (30), and (31). In this latter case, a selection rule for the allowed directions of scattered intensities is obtained as given by Equation (28). This is related to the Bragg scattering law found for unpolarized X-ray scattering from helices and for light scattering from liquid crystals. It is similar to the

resonance relations for the interactions of helical antennae with circularly polarized radio waves.<sup>13</sup> A helix long with respect to the wavelength of light, whose pitch is greater than the wavelength, interacts like a set of slits with the light. Interference strongly limits the scattered rays to specific angles, and a diffraction pattern is observed. The intensities between layer lines become more important as the size of the helix is reduced relative to the wavelength of light. When both the wavelength of light and the length of the helix are of the same order of magnitude, the equations predict a continuous scattering pattern even when the pitch is greater than the wavelength. As the length of the helix increases, these equations approach the discrete solutions which quantize the allowed scattered directions and lead to layer lines.

A remarkable property of the CIDS measurement is that since it involves a ratio, it may give values of  $(I_L - I_R) / (I_L + I_R)$  of the order of 1 even when each of the values for  $I$  are very small. The technique thus depends on the ability of an instrument to differentiate  $I_L$  and  $I_R$  from the stray light components in the system.

The expressions obtained for the CIDS of a helix show that the numerator involves helix parameters and differences in product of the Bessel functions. The latter are important in determining many of the symmetry features of the scattering patterns. It is worth pointing out that the scattering of plane polarized light in general shows imaginary components in



the scattered field, indicating that the scattered light is always elliptically polarized. This is true for the scattering from a helix, regardless of the type of polarization of the incoming light. For polarizability which is only tangential to the helix, the equations show that the scattering is symmetric with respect to the incoming light beam, i.e., it shows mirror image symmetry in the layer lines above and below the zero layer line. This behavior is no longer true for the case of a general, complex polarizability in which the scattering pattern shows antisymmetric properties. For light incident along the helix axis the scattering pattern shows cylindrical symmetry, the equations for this direction of incidence being independent of the azimuthal angle  $\psi$ .

The total scattering ( $I_L + I_R$ ) is positive definite and has no zeros, except for special cases such as helices with infinite pitch or zero radius. In addition, for light incident along the axis of an infinite helix there are certain angles which give zeros for both  $I_L$  and  $I_R$ . A closer analysis of the equations describing the scattering for light perpendicular to the helix axis shows that the CIDS vanishes in the forward direction for all values of pitch, radius, and wavelength of light. This is contrary to the experimental observations of liquid crystals and phenomenological computations of differential scattering done by Bohren<sup>14</sup> using the Mie-theory. Form-CIDS is a diffraction phenomenon and since the scattered electric field is the

superposition of many waves originated at the scatterer, their relative phase is what determines the interference or diffraction of the incident wave. This phase change<sup>14</sup> (see Figure 5) is given by  $e^{i(\Delta\mathbf{k}\cdot\mathbf{r})}$  appearing in all the equations. It can be seen from the figure that in the forward direction, no interference takes place; the result is zero differential forward scattering. It will be seen in Chapter 5 of this thesis that allowing coupling among the induced dipoles on the chiral molecule produces finite differential scattering intensities in the forward direction.

It is apparent, through the results of these equations, that the existence of nonvanishing form-CIDS of a chiral object is related to the asymmetry of its polarizability. CIDS is then a measure of that asymmetry. In general, spherically symmetric polarizabilities yield no CIDS. Finally, we have seen that combining two approximations (uni-axiality in the polarizability and first Born-approximation in the local field) results in CIDS independent of both the position and shape of the absorption bands. In Chapter 4, by relaxing the first of these two approximations, the general case of an absorptive chiral scatterer will be treated.

Figure 5. Phase difference between two wavelets originated at two different scatters placed at 0 and at the position  $\underline{r}$  (labeled 0') from the first.  $\underline{k}$  and  $\underline{k}_0$  are the scattered and incident wave-vectors, respectively.  $2\beta$  is the scattering angle. The path difference between the two wavelets is  $\hat{k} \cdot \underline{r} - \hat{k}_0 \cdot \underline{r} = \Delta \hat{k} \cdot \underline{r}$ . In the forward direction the path difference vanishes.



Bibliography

1. Urry, D. W., Krivacic, J. (1970) Proc. Natl. Acad. Sci. USA 65, 845-852.
2. Ottaway, C. A., Wetlaufer, D. B. (1970) Arch. Biochem. Biophys. 139, 257.
3. Schneider, A. S. (1971) Chem. Phys. Lett. 8, 604-608.
4. Atkins, P. W., Barron, L. D. (1969) Mol. Phys. 16, 453-466.
5. Barron, L. D., Buckingham, A. D. (1971) Mol. Phys. 20, 1111-1119.
6. Levine, H., Schwinger, J. (1950) Commun. Appd. Math. [1], 3, 355-391.
7. Saxon, D. S. (1955) "Lectures on the Scattering of Light", Sci. Rep. No. 9, Contract AF 19(122)-239, Dept. Meteorol., University of California, Los Angeles, 100 pp.
8. Abramowitz, M., Stegun, I. A. (1965) Handbook of Mathematical Functions (Dover: New York).
9. Cochran, W., Crick, F. H. C., Vand, V. (1952) Acta Cryst. 5, 581.
10. Born, M., Wolf, E. (1975) Principles of Optics (Pergamon Press: Oxford).
11. Shurcliff, W. A. (1962) Polarized Light (Harvard University Press: Cambridge, Mass.).
12. Van de Hulst, H. C. (1957) Light Scattering by Small Particles (John Wiley & Sons: New York).

13. Kraus, J. D. (1950) Antennas (McGraw-Hill: New York).
14. Cantor, C. R., Schimmel, P. R. (1980) Biophysical Chemistry, Vol. 2 (Freeman: San Francisco).

## Chapter 3

## NUMERICAL COMPUTATIONS

## I. Introduction.

In Chapter 2 a general theory on the circular intensity differential of scattering (CIDS) of chiral structures, as modeled by helices, has been derived. The theory has been obtained as a function of the helix parameters, and the angle of scattering and is valid for all wavelengths of light. In this chapter, a detailed analysis of the properties of the differential scattering patterns of a helical structure along with numerical calculations for different parameters will be presented. All the calculations shown deal with helical structures whose interactions with the incident radiation take place through a uniaxial polarizability, its axis being directed along the tangent to the helix.

According to the theory derived in the last chapter, a necessary condition for the existence of CIDS is that the scatterer must have an asymmetric polarizability. As a result, the numerical calculations for this simplified model illustrate a number of symmetry properties of the differential scattering patterns, whose physical basis will be derived and discussed here.

The organization of this chapter is as follows: In part II the numerical methods and strategies used in perform-

ing the computations are described. Part III shows some of the results of the calculations. Here the general characteristics of the differential scattering patterns are outlined in the form of simple rules. In part IV a detailed analysis of the symmetry properties of the CIDS is presented. We obtain a general expression that accounts for the functional dependence of the differential scattering patterns on the helix parameters and the wavelength of light. In part V the practical use of the technique as a probe for chiral structures is discussed. The relation between the differential intensities and the length and molecular weight of the chiral regions of a structure is pointed out, and a comparison with experimental measurements on a bacterial membrane is made. The theory of differential scattering for helical structures as derived in the last chapter seems to be in good qualitative agreement with the experimental data.

## II. Numerical Computations.

All the computations presented here correspond to the scattering properties of a very thin (uni-dimensional) helix. The polarizability is defined (see Chapter 2, Section II) as a tensor with three principal axes: along the tangent to the helix,  $\underline{t}$ , along the normal direction,  $\underline{n}$ , and along the remaining orthogonal direction,  $\underline{p}$ , so that  $\underline{\alpha} = \alpha_{\underline{t}\underline{t}} + \alpha_{\underline{n}\underline{n}} + \alpha_{\underline{p}\underline{p}}$ . To simplify the results and facilitate their



interpretation while preserving the significant scattering behavior,  $\alpha_n$  and  $\alpha_p$  are set equal to zero. In Chapter 2, two different sets of equations were derived to describe the CIDS of a chiral structure. Equations (36), (37) and (38) are the completely analytical solutions valid for wavelengths of light ( $\lambda$ ) smaller than or equal to the pitch ( $P$ ) of the helix, and when the length of the helix is much larger than the wavelength of light. In this case, the scattering patterns are discrete, the polar angle of scattering is limited to certain allowed values, and gives rise to layer lines of scattered intensities in space. For the case  $P < \lambda$ , Equations (33), (34) and (35) in Chapter 2, valid for all ratios of  $P/\lambda$  and for helices of arbitrary length, must be used and the intensities can be obtained through numerical computations. As shown in Chapter 2, if  $P < \lambda$ , the scattering pattern is continuous in space.

Two different computer programs corresponding to these two sets of equations have been written: PROGRAM CIDSY uses the analytical expressions of CIDS for light incident along the  $C_2$ -axis; PROGRAM VINO uses Equations (33-35) for the same direction of incidence, with the infinite sums appearing in these expressions being carried out to terms of order  $\pm 40$ .

The overlapping regions of  $P/\lambda$  served as a check on the calculations performed by the two programs. A third program, PAN, that computes the CIDS for light incident

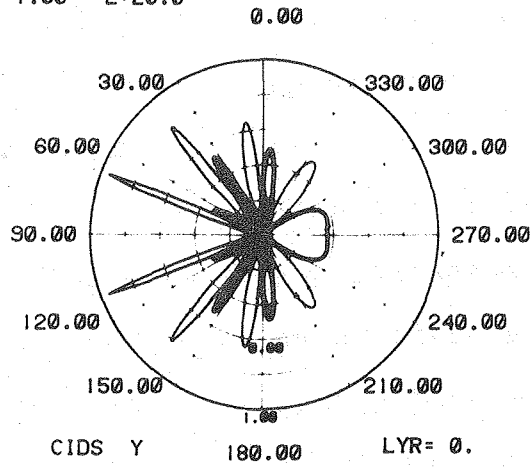
along the helix axis, has been also written. A listing of PROGRAMS VINO and PAN can be seen in the Appendices to this thesis. The calculated scattering patterns were used to study the properties of interactions of helices with circularly polarized light. These patterns are presented as polar plots of intensity vs. angle,  $\psi$  (which measures the angle between the incident and the scattered radiation), for each layer line (in the case  $P \geq \lambda$ ) or for different chosen values of the altitude  $\phi$  (for the case of  $P > \lambda$ ). The plots were generated with the graphics subroutine library IDDS of the Lawrence Berkeley Laboratory, and the output obtained optionally in microfiche, 35 mm film, or paper plots with the Cal-comp. The Bessel functions of order 0 to  $\pm 40$  were calculated from Sandia Corporation subroutines (Sand-75-0147) to obtain the intensities at one degree increments of  $\psi$  for each layer line, or for each value of the altitude. Both total intensity of scattering and CIDS =  $(I_L - I_R)/(I_L + I_R)$ , where  $I_L$  and  $I_R$  are the scattered intensities for incident left and right circularly polarized light, will be presented here. All the computations have been carried out in the Computer Center of the Lawrence Berkeley Laboratory.

### III. Numerical Results.

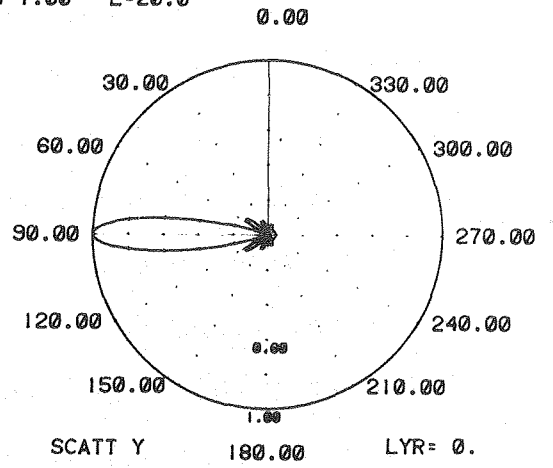
Figure 1 gives the CIDS and total scattering for a helix whose pitch is ten times the wavelength, whose radius

Figure 1. Polar plots of circular intensity differential scattering (CIDS  $y$ ) and total scattering intensity (SCATT  $y$ ) of a helix for light incident along the  $y$  ( $e_2$ )-axis (from right to left in the figures).  $P$  = pitch of the helix,  $R$  = radius,  $L$  = number of turns of helix, and  $W$  = wavelength of light. The thick lines indicate negative values of the CIDS, the light ones, positive. LYR denotes the number of the layer line being plotted. The total scattering is scaled to the maximum scattering intensity in the zero layer line; the CIDS values  $(I_L - I_R) / (I_L + I_R)$ , are not scaled.

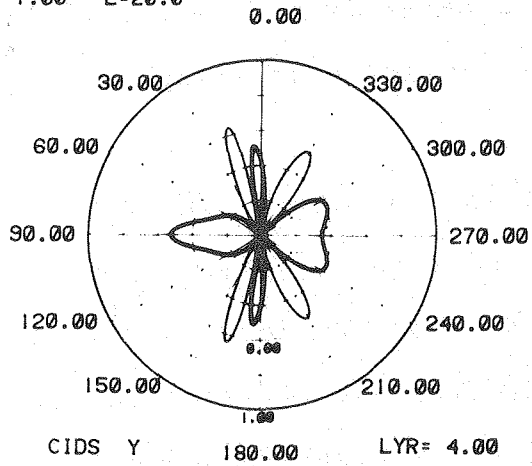
P=10.0 R=1.00  
W=1.00 L=20.0



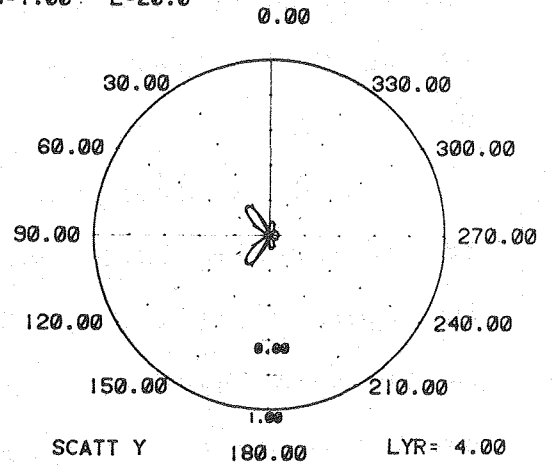
P=10.0 R=1.00  
W=1.00 L=20.0



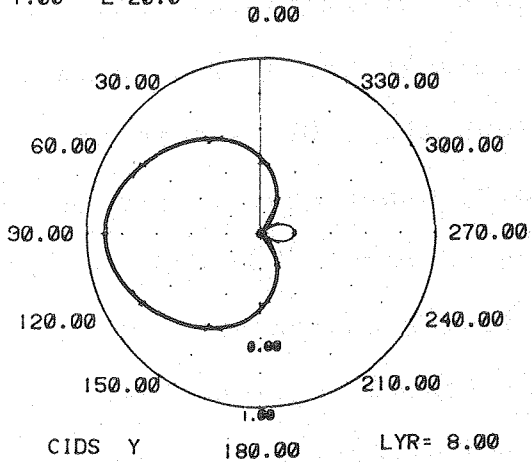
P=10.0 R=1.00  
W=1.00 L=20.0



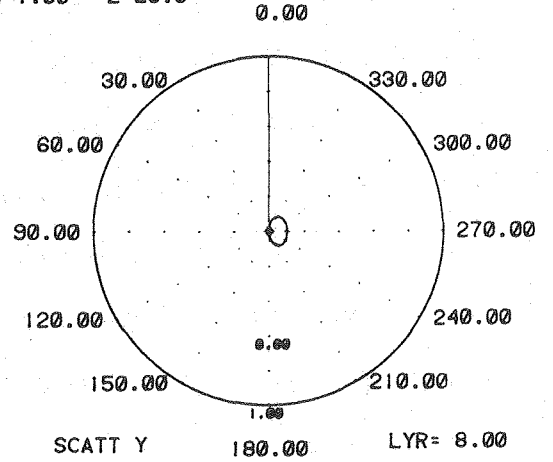
P=10.0 R=1.00  
W=1.00 L=20.0



P=10.0 R=1.00  
W=1.00 L=20.0



P=10.0 R=1.00  
W=1.00 L=20.0



is equal to the wavelength and whose length is twenty times the wavelength. The scattering patterns are given for layer lines 0, 4, 8. CIDS is a ratio whose absolute magnitude is equal to one or less, therefore the actual value of CIDS is plotted with dark lines representing negative values of CIDS and light lines representing positive values. The total intensity, whose magnitude depends on instrumental parameters, is plotted relative to the maximum intensity in the zero layer line. In this figure and in subsequent ones, the light is incident perpendicular to the helix axis from the right (along  $270^\circ$ ), therefore, the forward scattering is along  $90^\circ$  in the figures.

The first thing to note is that the differential scattering for circularly polarized light is large. For example, in Figure 1, at angles of  $\pm 25^\circ$  from the forward direction, in the zero layer line essentially only left circularly polarized light is scattered for a right-handed helix; the CIDS is close to 1. In general, the magnitudes of CIDS do not correlate with the magnitudes of the total scattering. The total scattering is a maximum in the forward direction for the zero layer line, whereas the CIDS is zero in this direction. Figure 1 illustrates other general properties of the differential scattering pattern. The CIDS in the zero layer line shows the following characteristics: A large and broad, negative back-scattering lobe, zero differential scattering in the forward direction, 15 zeros, 14 of

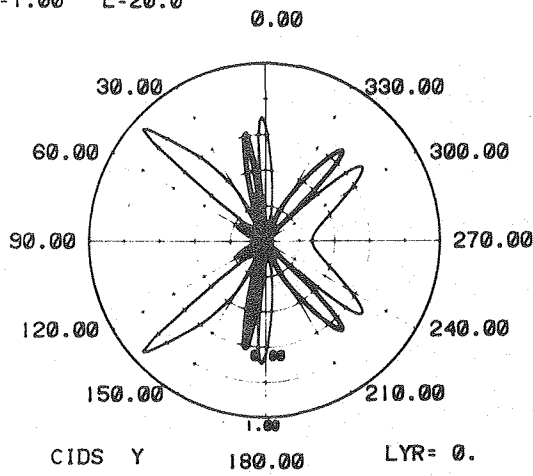
which involve a change of sign. As the number of the layer line increases, the number of the scattering lobes (zeros) is reduced, and the sign of the back-scattering lobe alternates between positive and negative for the first few layer lines. The patterns for both total and differential scattering are symmetric with respect to the direction determined by the incident light. The patterns are also symmetric above and below the zero layer line; that is, the scattering in the  $-1$  layer line is identical to that in the  $+1$  layer line. The differential scattering always contains much more structure than the total scattering. Thus, a small variation in the parameters of the helix will produce large changes in the CIDS, whereas the total scattering will change very slightly both in magnitude and direction of the scattering lobes. Moreover, the total scattering will not give information about the sense of the helix, but the sign of the CIDS is a direct measure of the sense of the helix.

Figure 2 illustrates the scattering patterns as the wavelength increases relative to the pitch and radius. The helices are the same as Fig. 1 except that the ratio of pitch/wavelength is now 1,  $1/2$ ,  $1/4$ ; only the patterns corresponding to the zero layer line are shown. Note that the CIDS is still large ( $>0.5$ ) for a pitch and radius equal to one-fourth the wavelength. General characteristics of the scattering patterns including those illustrated in Figures 1 and 2 are:

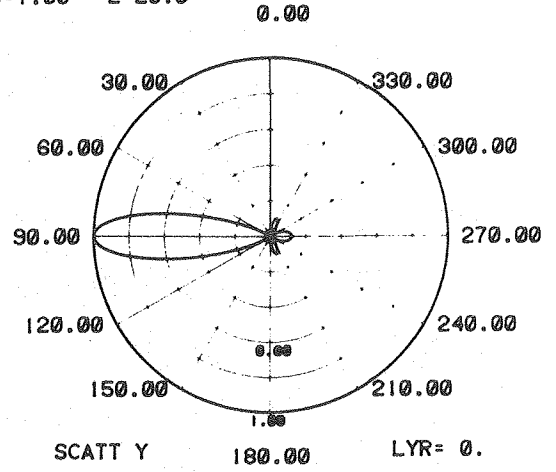
(a) There is no differential forward scattering in the zero

Figure 2. Polar plots of CIDS and total scattering for increasing values of the wavelength of light while keeping the same ratio of pitch/radius of the helix. The labels are the same as in Figure 1. In the case of pitch less than wavelength (absence of discrete layer lines), LYR has been replaced by the ALT, indicating the altitude angle measured from the  $(\underline{e}_2, \underline{e}_1)$  plane. Note that CIDS is greater than 0.5 even for a wavelength four times larger than the pitch and radius.

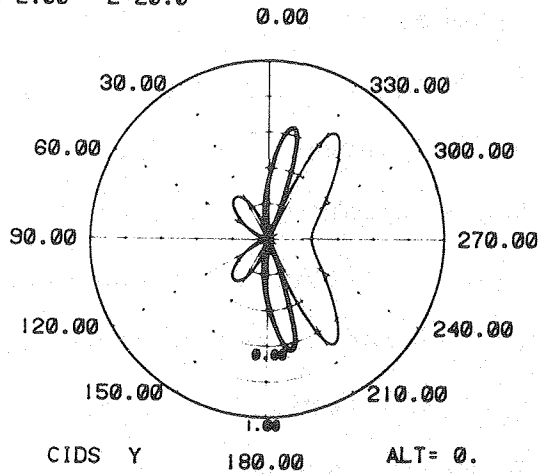
P=1.00 R=1.00  
W=1.00 L=20.0



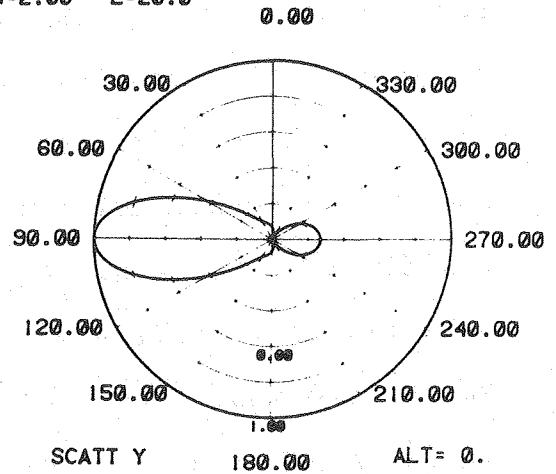
P=1.00 R=1.00  
W=1.00 L=20.0



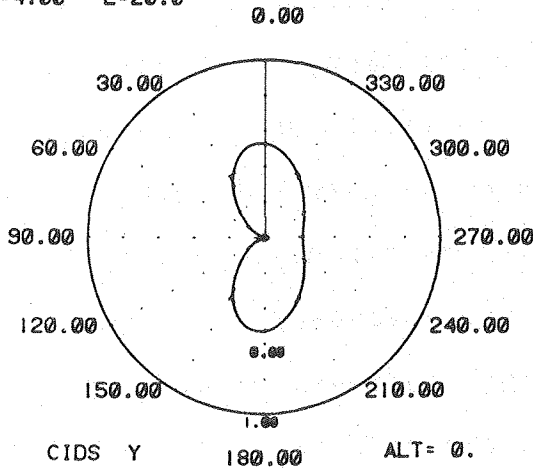
P=1.00 R=1.00  
W=2.00 L=20.0



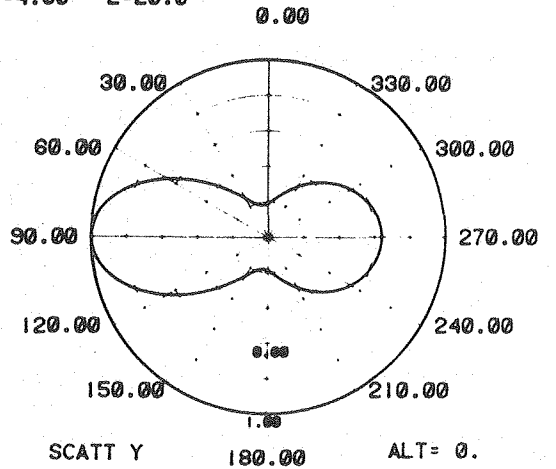
P=1.00 R=1.00  
W=2.00 L=20.0



P=1.00 R=1.00  
W=4.00 L=20.0



P=1.00 R=1.00  
W=4.00 L=20.0





layer line; this is true for any dimension of the helix. For all other layer lines the differential forward scattering is not zero. (b) The pattern of layer lines is symmetric about the zero layer line. An equivalent statement is that the scattering is symmetrical above and below the scattering plane perpendicular to the helix axis. (c) The number of lobes of the scattering pattern for the zero layer line is independent of the ratio of pitch/wavelength, but it is an increasing function of the ratio of radius/wavelength. The lobes alternate in sign. The number of lobes decreases in going from the zero layer line to the higher order layer lines. (d) For each layer line the envelope of the differential scattering pattern, i.e., a measure of the differential scattering at all angles in that layer line, depends markedly on the ratios of pitch and radius to wavelength. Maxima and minima in differential scattering occur as a function of these ratios. The minima are analogous to the "invisible" particles described by Kerker<sup>1</sup> and Chew and Kerker<sup>2</sup> for total scattering. (e) Differential back scattering, and differential scattering along the helix axis and perpendicular to the incident light, changes sign as a function of pitch/wavelength and radius/wavelength. These results are related to the sense of circular polarization of radiation scattered by helical antennae<sup>3</sup> and liquid crystals.<sup>4</sup> (f) As the wavelength increases relative to the pitch and radius of the helix, the differential scattering

decreases and its angular dependence approaches that of Rayleigh scattering. In the limit of very long wavelengths the differential scattering is zero. (g) The total scattering of the successive layer lines when projected as density spots on a plane would reproduce the well known X of the X-ray diffraction patterns of helical molecules.<sup>5</sup> (h)

Although not shown here, computations of the CIDS for light incident along the helix axis give completely symmetrical intensities with respect to angle  $\psi$  and zero forward CIDS. In fact, the zero-forward differential scattering is common to all three orthogonal directions of incidence and is a direct consequence of having used the first Born-approximation in the local incident field. The CIDS so obtained has been called in Chapter 2 form-CIDS.

In the next section we will analyze quantitatively the zeros and the signs of the CIDS in terms of the helix parameters, the layer lines and the wavelength of light.

#### IV. Symmetry Properties of the Scattering Patterns.

The polar plots of differential scattering intensities vs. azimuthal angle,  $\psi$ , show a remarkable symmetry for each layer line; the direction of incidence of the light acts as a  $C_2$  axis. Furthermore, it is seen that the patterns show a distinctive lobe structure of alternating signs with zeros between lobes. To better understand the patterns, it is appropriate to analyze the equations responsible for this behavior. The equations and notation are described in Chapter 2.

1) The zeros of the CIDS patterns.

We will analyze the patterns for long helices with pitch  $\geq$  wavelength, therefore a layer line structure will exist. The analysis will be done only for light incident along the  $e_2$ -axis, i.e., perpendicular to the axis of the helix. Since for each layer line the zeros of the CIDS are the zeros of  $I_L - I_R$ , it will suffice to consider the behavior of the numerator of the CIDS formulas. We can use the recurrence formulas for the derivatives of the Bessel functions:<sup>6</sup>

$$\frac{d}{dv} J_n(v) = J_{n-1}(v) - \frac{n}{v} J_n(v)$$

$$\frac{d}{dv} J_n(v) = -J_{n+1}(v) + \frac{n}{v} J_n(v)$$

to simplify the numerator of Equations (36a) in Chapter 2 and equate it to zero, to obtain:

$$\begin{aligned} & \frac{Pn}{\pi Q} \phi_1 \frac{\partial}{\partial(Qa)} J_n^2 + \frac{\partial}{\partial(Qa)} \{a^2 [(J_{n+1}^2 + J_{n-1}^2) \phi_2 \\ & - 2J_{n+1} J_{n-1} \phi_3] + J_n^2 (\phi_4 - \frac{2Pn}{\pi Q} \phi_5)\} = 0 \end{aligned} \quad (1)$$

where:

$$\begin{aligned}
\phi_1 &= [\sin(2\psi' - \psi) + \sin\psi] \sin 2\phi \\
\phi_2 &= \cos\psi' (\sin^2\phi - 2) \\
\phi_3 &= \cos(2\psi - 3\psi') \sin^2\phi \\
\phi_4 &= \{ [\cos\psi' - 2\cos\psi \cos(\psi' - \psi) + \cos(2\psi - 3\psi')] a^2 - \\
&\quad \frac{P^2}{\pi^2} \cos\psi' \} \times \sin^2\phi \\
\phi_5 &= \sin(2\psi' - \psi) \sin 2\phi
\end{aligned}$$

Here  $n$  specifies the layer line and the order of the Bessel functions,  $J_n(Qa)$ ;  $a$  is the radius,  $P$  is the pitch and  $Q = (2\pi/\lambda)(1 + \sin^2\phi - 2\sin\phi\sin\psi)^{1/2}$ . The angles  $\phi$  and  $\psi$  are the polar angle and the azimuthal angle of the scattering pattern; for each layer line  $\phi$  is constant and  $\psi$  varies from 0 to  $2\pi$ . The  $\phi$  depend on the scattering angles,  $\psi$ ,  $\psi'$  and  $\phi$ , where  $\psi'$  (defined in Chapter 2) depends on  $\psi$ ,  $\phi$  and wavelength. Let us consider the zero layer line, as a similar analysis applies to all the layer lines. For the zero layer line,  $\phi = 90^\circ$ ,  $n = 0$ , and after some algebraic manipulation the zeros are found to be:

$$J_1(Qa) = 0$$

$$\frac{P^2}{\pi^2} \cos\psi' J_0(Qa) + a^2 \{ J_2(Qa) [\cos\psi' - \cos(2\psi - 3\psi')]$$

$$- 2J_0(Qa) [\cos\psi' - \cos\psi \cos(\psi' - \psi)] \} = 0 \quad (2)$$

It is clear that the Bessel functions control the zeros of the scattering pattern. For the zero layer line the zeros of  $J_1$  are exact zeros and for  $P \geq 10a$ , the zeros of  $J_0$  are approximate zeros. As the radius,  $a$ , increases relative to the pitch,  $P$ , the zeros of  $J_2$  also contribute. It is interesting to point out that the theorem of interlaced zeros of Bessel functions states that Bessel functions of different orders have no common zeros.<sup>6</sup> This prevents Equation (2) from being satisfied by simultaneous nulling of  $J_0$ ,  $J_1$ , and  $J_2$ , therefore the zeros which appear are either a manifestation of the predominance of one term, or a very rare case in which both phases and Bessel functions combine to satisfy Equation (2) at particular values of  $\psi$ .

To find the values of  $\psi$  corresponding to the zeros of the Bessel functions, we need an expression for  $Qa$  vs.  $\psi$ . As  $\cos \phi$  for each layer line equals  $(n\lambda/P)$ , we can use the definition of  $Q$  above to relate  $Q$  to  $\psi$  for any layer line. For the zero layer line

$$Qa = \frac{2\sqrt{2} \pi a (1 - \sin \psi)^{1/2}}{\lambda} \quad (3)$$

For a helix with  $P = 10$ ,  $a = 1$ ,  $\lambda = 1$  as shown in Figure 1, the zeros of  $J_1(Qa)$  and  $J_0(Qa)$  determine the scattering pattern in the zero layer line. The values of  $\psi$  corresponding to these zeros are in excellent agreement with those seen in Figure 1. The trigonometric factors appearing in Equation (2) do not contribute to any of the change of sign

of the differential scattering; they mainly govern the envelope of the scattering pattern.

As the ratio of  $P/a$  decreases, we can no longer neglect the second term and some of the zeros contributed by  $J_0$  will start disappearing and a few of those due to  $J_2$  will appear. This behavior is complicated by the fact that the number of zeros of  $J_0(Qa)$ ,  $J_1(Qa)$ , and  $J_2(Qa)$  depends on the radius,  $a$ , of the helix and in fact is approximately a linear function of  $a$ . We can analyze the pattern if the pitch,  $P$ , of the helix is changed while the radius and wavelength are held constant. This is shown in Figure 3, where one sees the same zeros as in Figure 1 due to  $J_1$ , but some of the zeros from  $J_0$  disappear as  $P/a$  changes from 8 to 2.

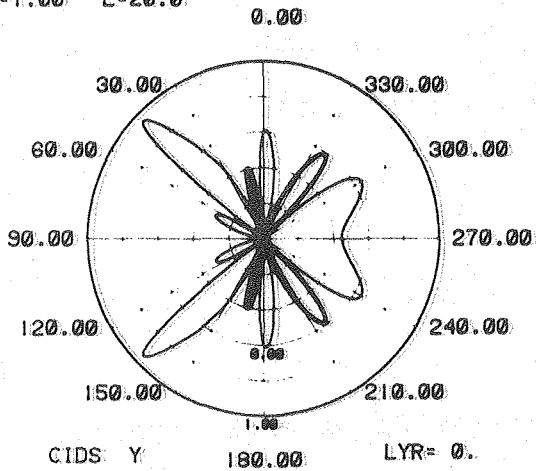
A similar analysis for the other layer lines can be done; the main difference is that higher order Bessel functions control the scattering patterns.

## 2) Dependence of the zeros of the CIDS on helix geometry.

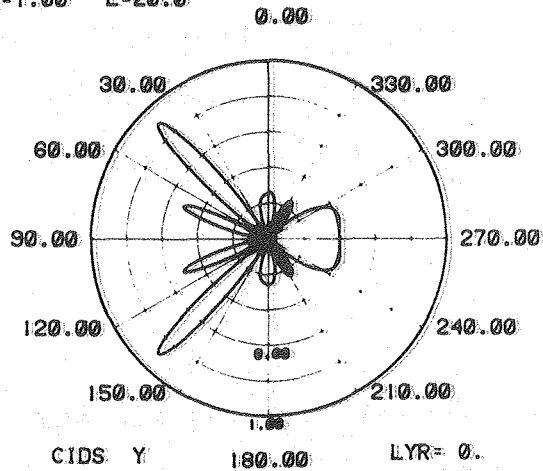
As the zeros of a few Bessel functions determine the zeros of the CIDS in each layer line, we can understand the patterns from learning how the Bessel function zeros depend on pitch, radius and wavelength. We make use of the theorem<sup>7</sup> that the number of zeros of  $z^{-\nu}J_{\nu}(z)$  between 0 and  $[m + (2\nu+1)/4]\pi$  is exactly  $m$ . However, we must realize that between 0 and  $[m \pm \epsilon + (2\nu+1)/4]\pi$  (where  $\epsilon$  is an arbitrarily small number), there may be  $m \pm 1$  zeros. That is, there is an inherent uncertainty of  $\pm 1$  in the number of zeros

Figure 3. Polar plots of CIDS for different ratios of pitch/wavelength while keeping the ratio of radius/wavelength constant. The labels are the same as before. The number of zeros in the scattering pattern increases with increasing pitch.

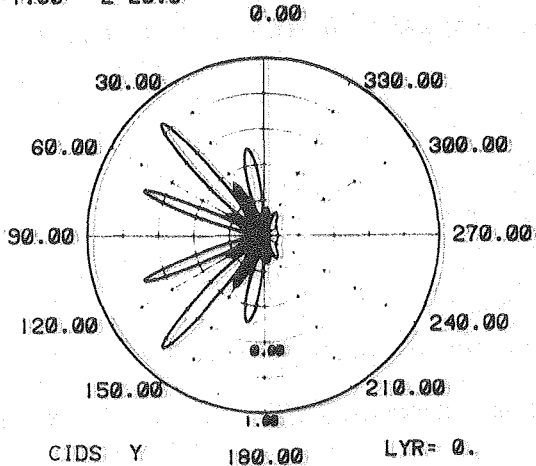
P=2.00 R=1.00  
W=1.00 L=20.0



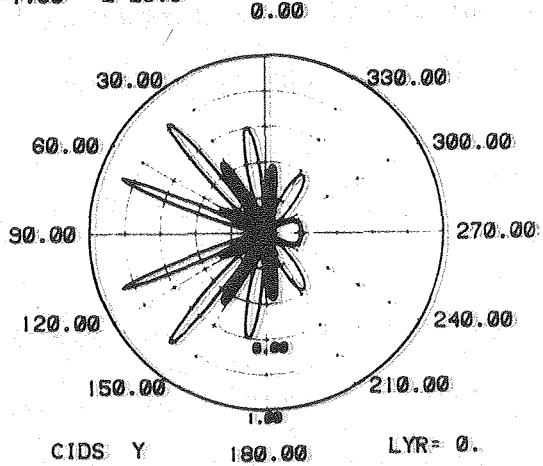
P=4.00 R=1.00  
W=1.00 L=20.0



P=6.00 R=1.00  
W=1.00 L=20.0



P=8.00 R=1.00  
W=1.00 L=20.0





calculated for a Bessel function over the range of our variable,  $Q_a$ . As we want to know how the number of zeros in the scattering pattern changes with helix parameters and wavelength, rather than the exact number of zeros, this small uncertainty is not significant.

For each layer line,  $n$ ,

$$Q_a = \frac{2\pi a}{\lambda} \left[ 2 - \frac{\lambda^2 n^2}{p^2} - 2 \left( 1 - \frac{\lambda^2 n^2}{p^2} \right)^{1/2} \sin\psi \right]^{1/2} \quad (4)$$

The maximum and minimum values of  $Q_a$  on each layer line occur when  $\sin\psi = \pm 1$ . To apply the theorem we must compare the maximum and minimum values of  $Q_a$  with  $(2\nu+1)\pi/4$ . First we obtain the number of zeros between 0 and the minimum value of  $Q_a$  by writing

$$\min Q_a = [m + (2\nu+1)/4]\pi$$

and solving for  $m$ . Similarly, we obtain the number of zeros between 0 and the maximum value of  $Q_a$ . The difference is the number of zeros in the interval  $(\min Q_a, \max Q_a)$ , i.e., in the intervals  $90^\circ \leq \psi \leq 270^\circ$ .

The number of zeros of the  $\nu$ -order Bessel function in the interval  $0 < Q_a < \min Q_a$  is:

$$m_{\nu}^{\min} = \left( \frac{1}{\pi} \min Q_a - \frac{2\nu+1}{4} \right) f_{\min}$$

and in the interval  $0 < Q_a < \max Q_a$

$$m_{\nu}^{\max} = \left( \frac{1}{\pi} \max Qa - \frac{2\nu+1}{4} \right) f_{\max}$$

The factors  $f_{\min}$  and  $f_{\max}$  are introduced to assure that the number ( $m$ ) of zeros for any given interval is always positive or zero. They are defined as Heaviside functions:

$$f_{\min} \begin{cases} 0 & \text{if } \min Qa < (2\nu+1)/4 \\ 1 & \text{otherwise} \end{cases}$$

$$f_{\max} \begin{cases} 0 & \text{if } \max Qa < (2\nu+1)/4 \\ 1 & \text{otherwise} \end{cases}$$

The number of zeros of the  $\nu$ -order Bessel function in the interval  $\min Qa < Qa < \max Qa$  will be therefore:

$$m_{\nu} = \frac{1}{\pi} (\min(Qa) f_{\max} - \min(Qa) f_{\min}) - \frac{2\nu+1}{4} (f_{\max} - f_{\min}).$$

There are three possibilities which must be considered for each layer line to estimate the number of zeros,  $m$ , of each Bessel function  $J_{\nu}$ . First, for a layer line in which  $f_{\max} = f_{\min}$  ( $\max Qa > \frac{2\nu+1}{4}$  and  $\min Qa > \frac{2\nu+1}{4}$ ) then:

$$m = \frac{1}{\pi} (\max Qa - \min Qa) = \frac{8a}{\lambda} \left( 1 - \frac{n^2 \lambda^2}{p^2} \right)^{1/2} \quad (5a)$$

Second, if  $\min Qa < (2\nu+1)/4$  and  $\max Qa < (2\nu+1)/4$ , then

$$m = 0 \quad (\min Qa \text{ and } \max Qa \leq \frac{(2\nu+1)\pi}{4}) \quad (5b)$$

Third, the intermediate case,  $m = \frac{1}{\pi} (\max Qa) - \frac{2\nu+1}{4}$  so that

$$m = \frac{4a}{\lambda} \left[ 2 - \frac{n^2 \lambda^2}{p^2} + 2 \left( 1 - \frac{n^2 \lambda^2}{p^2} \right)^{1/2} \right]^{1/2} - \frac{2\nu+1}{2}$$

$$(\min Qa \leq \frac{(2\nu+1)\pi}{4} ; \quad \max Qa > \frac{(2\nu+1)\pi}{4}) \quad (5c)$$

In obtaining the derivation of Equations (5a)-(5c) the expression for  $Qa$  given in Equation (4) has been used with  $\sin\psi = \pm 1$ . These equations provide the general results we need. They show that the number of zeros in each layer line depends linearly on  $a/\lambda$ , but depends only slightly on  $P/\lambda$ ; for the zero layer line the number of zeros is independent of  $P/\lambda$ . The number of zeros decreases with increasing layer line and becomes zero for the maximum layer line ( $n = P/\lambda$ ). In applying these equations, we should remember the restrictions. The actual number of zeros of each Bessel function is an integer near  $m \pm 1$ , and Equation (5) is derived for  $P/\lambda \geq 1$ , which is a necessary condition for the existence of layer lines.

Figure 1 clearly illustrates the decreasing number of zeros in the differential scattering pattern with increasing layer line; for the maximum layer line there are no zeros as expected. In this figure  $a/\lambda = 1$  and  $P/\lambda = 10$ , thus we know that only  $J_0$  and  $J_1$  contribute to the pattern of zeros in the

zero layer line, and we can easily calculate their number. The minimum value of  $Qa$  here is zero and the maximum is  $8\pi$ , so Equation (5c) must be used. The calculated values of  $m$  are 7.5 for  $J_0$  and 6.5 for  $J_1$ ; their sum of 14 agrees with the 14 (plus one zero at  $\psi = 90^\circ$ ) seen for the zero layer line. Figures 3 and 4 illustrate the strong dependence of the number of zeros on radius (compare Figure 4a with  $a/\lambda = 5$  with Figure 4b with  $a/\lambda = 0.5$ ) and the weak dependence on pitch (see Figure 3 with  $P/\lambda = 2, 4, 6, 8$ ), the behavior of which is correctly predicted by Equation (5b).

A few more differential and total scattering patterns for helices of different structural and electronic parameters can be found in the microfiches attached at the end of this thesis.

### 3) Vanishing of CIDS at specific angles of scattering.

It is possible to find helix parameters for which the differential scattering at certain directions in space vanishes. The differential back scattering (i.e., differential reflection) can easily be shown to possess an inversion point for certain ratios of  $P/a$  and  $a/\lambda$ , for which no reflection is observed. The differential reflection ( $\psi = -\pi/2$ ) in the zero layer line can be obtained from Equation (1). For light incident along  $e_2$  and for the case of  $P \geq \lambda$ :

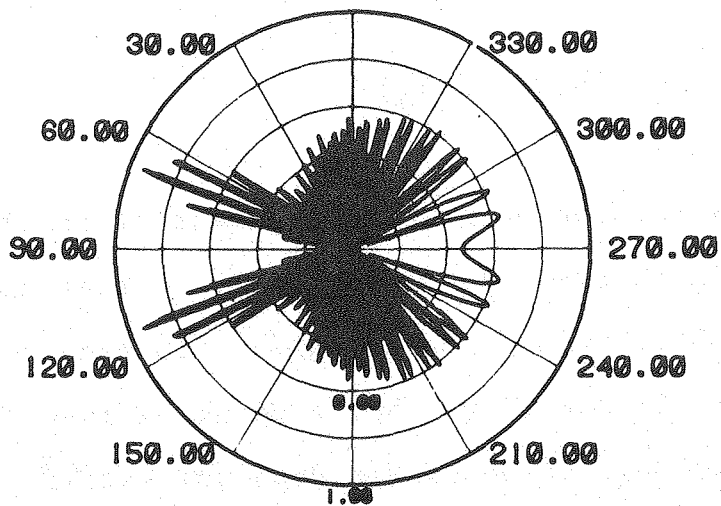
$$\frac{aP}{2\pi M^4} \{2(J_1 J_2 - J_1 J_0) a^2 + \frac{P^2}{\pi} J_1 J_0\} \quad (6)$$

Figure 4. The dependence of the number of zeros of CIDS on the ratio of radius/wavelength. In the upper figure there is no attempt to indicate the sign of the CIDS because of the large number of zeros.

P=10.0 R=5.00

W=1.00 L=20.0

0.00



CIDS Y

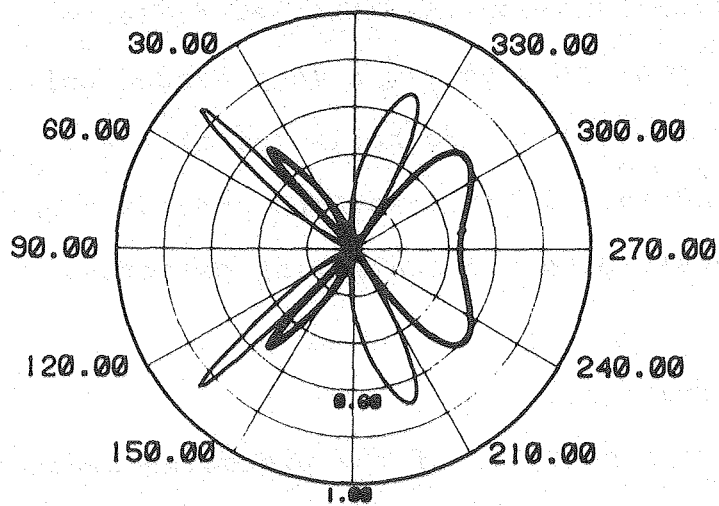
180.00

LYR= 0.

P=10.0 R= .50

W=1.00 L=20.0

0.00



CIDS Y

180.00

LYR= 0.

Setting this equation equal to zero, we obtain the value of  $P/a$  at which no differential reflection exists:

$$\frac{P}{a} = \pi\sqrt{2(1-J_2/J_0)} \quad (7)$$

At the inversion point, the argument of the Bessel functions ( $Qa$ ) is a constant equal to  $4\pi a/\lambda$ , so that the ratio obtained is an implicit function of  $(a/\lambda)$ . To prove that it is not a minimum or a maximum, but a point of inversion, we must show that this value of  $P/a$  does not satisfy the equation obtained by setting the derivative with respect to  $P$  of Equation (6) equal to zero. Although not shown here, it does not satisfy the equation, therefore  $P = \pi a\sqrt{2(1-J_2/J_0)}$  is an inversion point for the differential reflection. Notice from Equation (6) that the differential reflection has the opposite sign for a left-handed helix (pitch =  $-P$ ) than for a right-handed helix (pitch =  $P$ ). The equations we have derived in this section provide a quantitative basis for understanding the scattering patterns.

## V. Applications.

From the analysis of the preceding section, it is apparent that the CIDS signal as a function of wavelength or of the azimuthal angle of scattering can give important information about the conformation of chiral structures. In fact, it was seen that the sign of the CIDS contains the information on the

handedness of the molecule, whereas the intensity is directly related to the geometrical parameters of the chiral scatterer. As a technique, the most significant advantages of CIDS depend on the fact that it is a ratio of intensities,  $(I_L - I_R)/(I_L + I_R)$ , and that it can be positive or negative. Both of these characteristics make it more sensitive than the total scattering to structure and conformation. Right- and left-handed helices, otherwise identical, will have identical CIDS except with the opposite sign. To determine the sense of a helix from the sign of its CIDS at a chosen scattering angle, we need to know the pitch,  $P$ , and radius,  $a$ , of the helix. For long helices with  $P \geq \lambda$ , layer lines occur and the total scattering can be used to obtain  $P$  and  $a$ .<sup>8</sup> The spacing between successive layer lines is inversely proportional to  $P$ , and the angle between the arms of the characteristic X pattern produced by the scattering of a helix leads to the ratio of  $P/a$ . Thus, the geometry and the sense of the helix can be determined by the combined techniques. For helices with  $P < \lambda$ , layer lines do not occur and the usefulness of the CIDS increases relative to the total scattering. The sign and angular dependence of CIDS can provide the sense and helical parameters when the total scattering pattern is indistinguishable from that of a point or line. That is, values of CIDS of  $10^{-2}$  to  $10^{-4}$  should be measurable and interpretable, when the only geometrical information available from the total scattering



is that both  $P$  and  $a$  are less than  $\lambda/10$ .

#### 1) Length of helix.

The intensity of scattered light is proportional to the square of the length of the helix (Equation (36), Chapter 2), and therefore proportional to the square of the molecular weight of the helix. The CIDS is independent of length; it only depends on the helical geometry. The CIDS and total scattering have very different angular dependence; the maxima for CIDS tend to occur where the total intensity is small. These properties can be used to measure the amounts of helical (or chiral) structures in a mixture. For example, in cholesteric or twisted nematic liquid crystals, it is only the helical regions that give rise to the very strong circularly polarized differential scattering. In principle, it would be possible to measure the amount of helix in a protein from the CIDS.

#### 2) Experimental results.

Although the model is a very simple one, it allows immediate experimental applications as a first approximation to the measured CIDS of such structures as bacteriophages,<sup>9</sup> nucleohistones,<sup>10</sup> DNA aggregates,<sup>10</sup> membranes, chromosomes, etc. (Maestre, unpublished), all of which have been shown to have CD scattering components. The CIDS is independent of the molecular weight of the helix and for a uniaxial polarizability, even the actual value of this polarizability cancels and has no influence on the measurement. The behavior

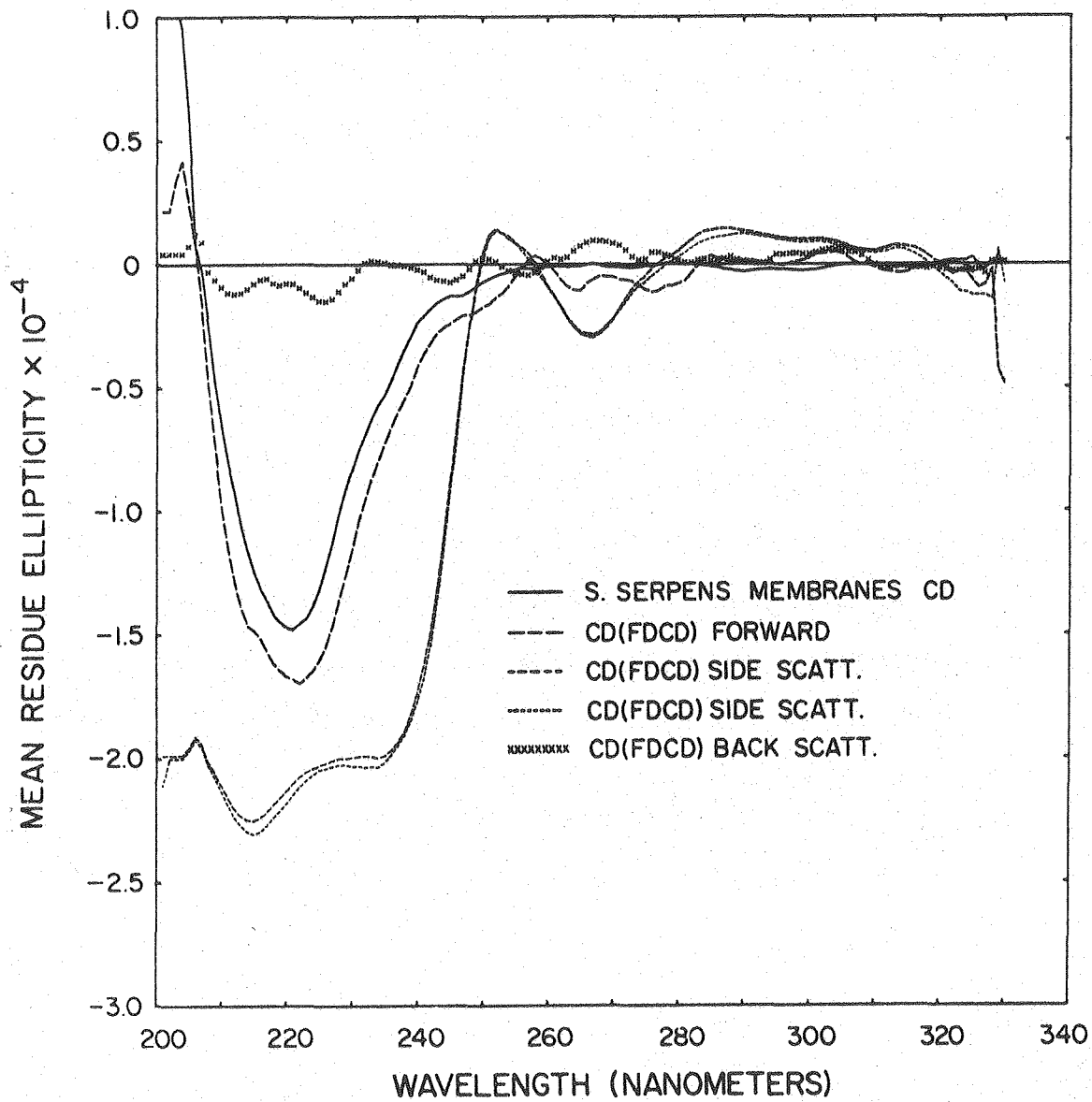
of the incoming circularly polarized light is affected only by the geometry of the helix. Thus, for example, we can obtain information about the possible supercoiling of a DNA molecule without knowing the details of the interaction of the chromophores with light.

As we have seen in this and the preceding chapter, the number of layer lines, the sign of the scattering lobes, and the number of lobes or zeros in each layer line can be used to give the main characteristics of any sample of helices. The computed values for the helical models are similar to those found experimentally.<sup>10</sup> Thus, liquid crystals with reflection coefficients of the order of 80 to 95% would give CIDS of the order of 1 (i.e., almost complete reflection for one sense of polarization). DNA films with ellipticities of nearly 4 degrees ( $A_L - A_R = 0.14$ ) have been reported and many measurements of ellipticities in the range from 0.1 to  $10^{-3}$  are routinely measured by CD scattering methods for large, optically active, biological aggregates.<sup>10</sup> Thus models which give CIDS values in the range from 1 down to  $10^{-4}$  will have applicability in the interpretation of experimental measurements. In extreme cases in which the pitch is much larger than the radius of the helix or the radius much larger than the pitch, simple formulas can be derived that will give approximate values for the scattering intensities. For the zero layer lines these formulas reduce to approximations that have been used for computational pur-

poses in the field of helical antennae.<sup>3</sup> The values obtained for these cases can be used to check the ratios of pitch to radius as determined by the number of zeros measured for the CIDS scattering envelope. If the whole scattering envelope cannot be measured, simple formulas for specific angles can be used to determine roughly the helical parameters.

Here we will discuss only one case of experimentally measured CIDS. This system has been chosen for its simplicity and because it allows easy correlation with the calculated values. These are the membranes of the bacterium Spirillum serpens, which show differential scattering for circularly polarized light when suspended in solution (Chiu, Maestre and Glaeser, in preparation). These flat, sheetlike membranes should not show CIDS, and only small corrections to the circular dichroism for Mie type scattering<sup>11</sup> is expected. However, a strong signal was measured at right angles to the incident light beam, in the wavelength range of 200-300 nm (Figure 5). Electron micrographs showed that rodlike membranes with a diameter of approximately 160 nm were mixed in with the flat membranes (Figure 6). Calculations for a helix with ratios of pitch and radius to wavelength which correspond to the experimental conditions give the scattering pattern shown in Figure 7. Although the computed CIDS is for an oriented helix with the scattering plane perpendicular to the helix axis, and the experiment is for an unoriented sample, the results can be qualitatively

Figure 5. CD plots and CIDS of Spirillum serpens membranes. Normal CD measurement is solid line. CD(FDCD) measurement is the forward scattering cone. Curves labeled "CD(FDCD) side scattering" are two different measurements of the sample at right angles. The back-scattering cone is depicted by xxxxxx. From Chiu, Maestre and Glaeser, unpublished.



XBL 807-10650

Figure 6. Electron micrograph of Spirillum membranes.

It shows both sheet-like membranes and tubular arrangements. Magnification is ~40,000. Presumably it is the cylindrical arrangement that gives the measured CD scattering. (Chiu, Maestre and Glaeser, unpublished.)



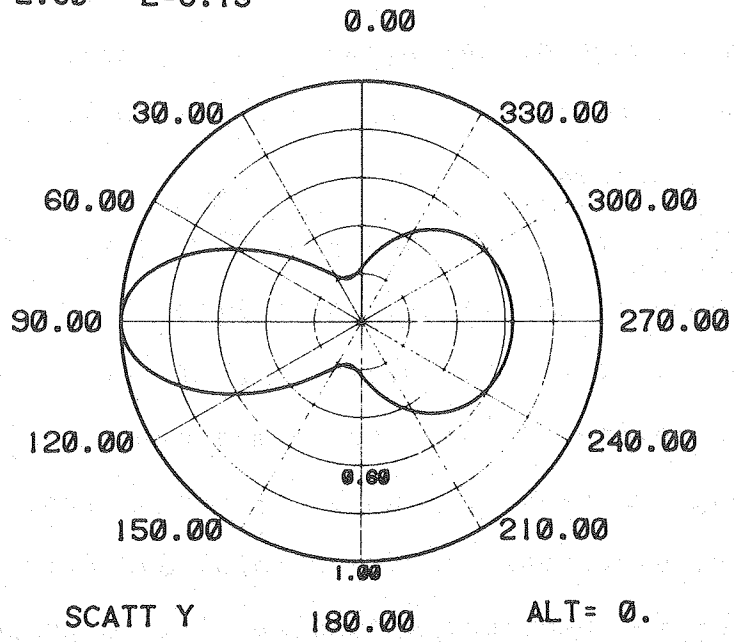
XBB 801-133

Figure 7. Total scattering and CIDS plots of a helix with geometrical parameters similar to those of the rods of Spirillum serpens as seen in the electron microscope (Figure 6). Pitch = 2.6 nm, radius = 208 nm, 6 turns and wavelength = 260 nm. The label CD/MAX indicates that the calculated values of CIDS have been scaled to 1.00; the actual maximum value calculated is  $6.7 \times 10^{-3}$ .

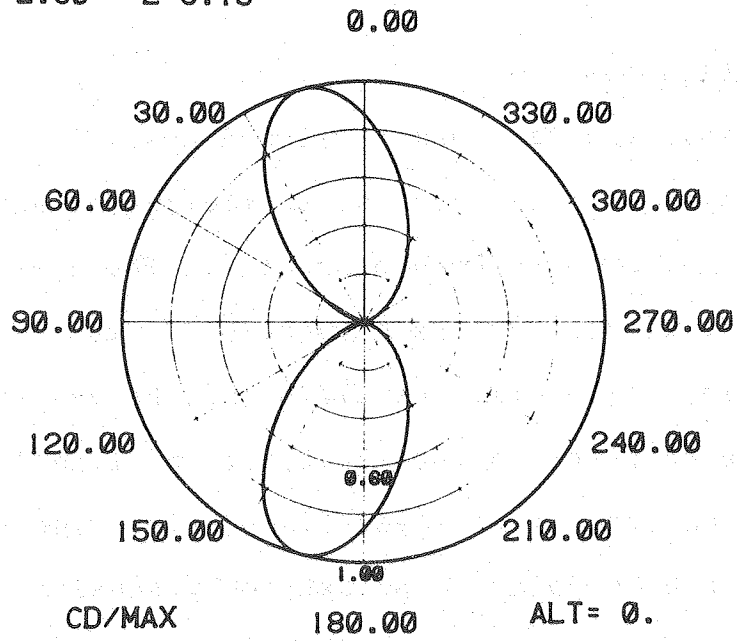




P= .01 R= .80  
 W=2.60 L=6.15



P= .01 R= .80  
 W=2.60 L=6.15



compared. The computed and experimentally observed scattering patterns agree well in the angular dependence as well as in the magnitude of the signal. It is clear that even the simple model discussed here can be usefully applied to biological structures.

We think that the theory of CIDS for chiral structures as developed in Chapter 2, in addition to the conclusions drawn in this chapter, justifies a serious effort to implement more refined techniques to measure the CIDS as a function of angle and wavelength for oriented samples.<sup>12</sup> In Chapter 6, a general theory of total and differential form-scattering for unoriented samples will be presented. It is expected that this theory would provide information on biological chiral structures in solution.

## VI. Conclusions.

In this chapter, numerical and analytical calculations of the total and differential scattering of an oriented helical structure have been presented. The numerical calculations were carried out as a function of the scattering angle in each layer line (if the pitch and the length of the helix are large compared to the wavelength of light) or at different altitude angles, if no layer lines exist. The scattering patterns have been found to be extremely sensitive to changes in the geometrical parameters of the helix. The sign of the CIDS signal is opposite for chiral objects of opposite handed-

ness, therefore CIDS can be a useful technique to determine the sense of chirality of these objects.

For values of pitch and radius greater than the wavelength, the CIDS will show lobes that alternate in sign for most layer lines; this lobular structure disappears when either pitch or radius is less than the wavelength. For the first case we have presented approximate expressions that govern the dependence of the number of lobes on the structural parameters of the helix as well as on the layer line that is being considered. These expressions show that the lobe structure of the differential scattering patterns is linearly proportional to the ratio of the radius to the wavelength of light. In general, the number of lobes decreases with increasing order of the layer line. The dependence of the number of lobes on the ratio of pitch to wavelength is weak in most layer lines and absent in the zeroth layer line. The overall symmetry of the scattering patterns is comprised of two factors: the positions of the zeros that determine the lobes are governed by the Bessel functions, whereas the envelope of the pattern is mostly determined by trigonometric functions of the scattering angle,  $\psi$ . The signs of the lobes and the positions of the zeros (the scattering pattern) will not be affected by the usual experimental difficulties associated with light scattering. Dust and other nonchiral contaminants can change the magnitudes, but not the general pattern of scattering.

It is possible to find specific directions for which

the CIDS vanishes at a given ratio of pitch,  $P$ , and radius,  $a$ , of the helix, to the wavelength of light. We have derived an expression relating the ratio of  $P/a$  as a function of wavelength of light at which differential back scattering (differential reflection) vanishes. This geometrical condition constitutes a point of inversion of sign of the differential reflection.

A wide range of samples have been experimentally studied with values of CIDS ranging from 1 (liquid crystals)<sup>4</sup> to  $10^{-4}$  (macromolecular aggregates).<sup>10</sup> Qualitative interpretation of these results can be made from our simple model. One application to rodlike structures observed in membranes of Spirillum serpens is discussed. We think that measurement of the differential scattering of polarized light and X-rays can become a very useful method for structure determination in macromolecules.

Bibliography

1. Kerker, M. (1977) J. Colloid and Interface Sci. 58, 100.
2. Chew, H., Kerker, M. (1976) J. Opt. Soc. Am. 66, 445.
3. Kraus, J. D. (1950) Antennas (McGraw-Hill: New York).
4. Chandrasekhar, S. (1977) Liquid Crystals (Cambridge University Press: London).
5. Cantor, C. R., Schimmel, P. R. (1980) Biophysical Chemistry Vol. 2 (Freeman: San Francisco).
6. Abramowitz, M., Stegun, I. A. (1965) Handbook of Mathematical Functions (Dover: New York).
7. Watson, G. N. (1958) Theory of Bessel Functions (Cambridge University Press: London).
8. Cochran, W., Crick, F. H. C., Vand, V. (1952) Acta Cryst. 5, 581.
9. Dorman, B. P., Maestre, M. F. (1972) Proc. Natl. Acad. Sci. USA 70, 255.
10. Maestre, M. F., Reich, C. (1980) Biochemistry, in press.
11. Holzwarth, G., Gordon, D. G., McGinness, J. E., Dorman, B. P., Maestre, M. F. (1974) Biochemistry 13, 126.
12. Maestre, M. F. (1981) J. Sci. Instr., submitted.

## Chapter 4

THE GENERAL POLARIZABILITY TENSOR  
AND ANOMALOUS SCATTERING

## I. Introduction.

All the theoretical work and the calculations presented so far on the CIDS of chiral structures have been restricted to the case of an oriented helix with a uniaxial (tangential) polarizability. As pointed out before, this particular choice of the polarizability has a twofold effect: 1) the values of the circular intensity scattering were independent of the magnitude of the polarizability, in particular of its wavelength dependence, and therefore the model could not take into account any absorptive phenomena; 2) all differential scattering patterns were symmetric around the direction of incidence of light (see Chapter 2).

In this chapter, numerical computations of the CIDS of a helix possessing a triaxial polarizability along the main axes of the tensor, as a function of the geometrical parameters of the chiral scatterer and the wavelength of light, are considered. The analytical expressions for the case of a biaxial polarizability will be derived and a careful analysis of the symmetry rules involved will be done. The last part of this chapter involves a discussion of the dispersion dependence of the differential scattering

intensities for the particular case of a Lorentzian-shaped polarizability.

## II. Numerical Calculations.

### 1) Equations and results.

In the numerical calculations presented here, Equations 33, 34, and 36 of Chapter 2 have been used. Since these equations give the amplitude and the intensity of the scattered electric field for a tangential polarizability, equivalent equations along the other two main axes of the polarizability have been derived. The derivation follows the same lines as in Chapter 2. Here we only write down the additional results. Perpendicular axis, incidence  $\tilde{e}_2$ , polarization  $\tilde{e}_1$

$$\begin{aligned}
 \tilde{E}(\tilde{r}') = & \frac{P}{2\pi M^2} K_P \cdot \left\{ \left[ \frac{-P}{4\pi} \sum_{n=-\infty}^{\infty} J_n(Qa) (PT_n S_n^{(2)} - (\pi T_n)^{-1}) \cdot \right. \right. \\
 & \left. \left. \cdot (-1)^{n\ell} \right] \tilde{e}_1 \right. \\
 & - \left[ \frac{iP}{4\pi} \sum_{n=-\infty}^{\infty} J_n(Qa) S_n^{(2)} (-1)^{n\ell} \right] \tilde{e}_2 \\
 & \left. + \left[ \frac{ai}{2} \sum_{n=-\infty}^{\infty} J_n(Qa) S_n^{(1)} (-1)^{\ell(n+1)} \right] \tilde{e}_3 \right\} \\
 & \sin(P\ell\Delta k_z/2) e^{in(\psi^* + \frac{\pi}{2})}
 \end{aligned} \tag{1}$$

perpendicular axis; incidence  $\tilde{e}_2$ , polarization  $\tilde{e}_3$



$$\begin{aligned}
E(r') = & \frac{a}{M} K_p \cdot \left\{ \left[ \frac{P}{2\pi} \sum_{n=-\infty}^{\infty} J_n(Qa) S_n^{(1)} (-1)^{\ell(n+1)} \right] e_1 \right. \\
& - \left[ \frac{P}{2\pi} \sum_{n=-\infty}^{\infty} J_n(Qa) P T_n S_n^{(1)} (-1)^{\ell(n+1)} \right] e_2 \\
& \left. \left[ a \sum_{n=-\infty}^{\infty} J_n(Qa) (\pi T_n)^{-1} (-1)^{n\ell} \right] e_3 \right\} \\
& \sin(P\ell\Delta k_z/2) e^{in(\psi^* + \frac{\pi}{2})}
\end{aligned} \tag{2}$$

where

$$K_p = \alpha_p B F$$

$$B = A_h M$$

$$F = (1 - k_{\perp}^2/k^2) (k^2/r') E_0 \exp(ikr')$$

where  $\ell$  is: the number of turns of the helix as before,  $Qa$  and  $M$  have the same definition as in Chapter 2,  $A_h$  the cross-sectional area of the helix, and  $\alpha_p$  is the value of the polarizability along the perpendicular axis defined in Equation (15) of Chapter 2. The equation for the scattered fields associated with the normal axis are: normal axis, incidence  $e_2$ , polarization  $e_1$ :

$$\begin{aligned}
E(r') = & \frac{1}{2} K_p \cdot \left\{ \left[ \sum_{n=-\infty}^{\infty} J_n(Qa) (P T_n S_n^{(2)} + (\pi T_n)^{-1}) \cdot \right. \right. \\
& \left. \left. (-1)^{n\ell} \right] e_1 \right\}
\end{aligned}$$

$$+ \left[ \sum_{n=-\infty}^{\infty} J_n(Qa) S_n^{(2)} (-1)^{n\ell} \right] \tilde{e}_2 \sin(P\ell\Delta k_z/2) \quad (3)$$

$$e^{in(\psi^* + \frac{\pi}{2})}$$

with  $K_n = \alpha_n BF$

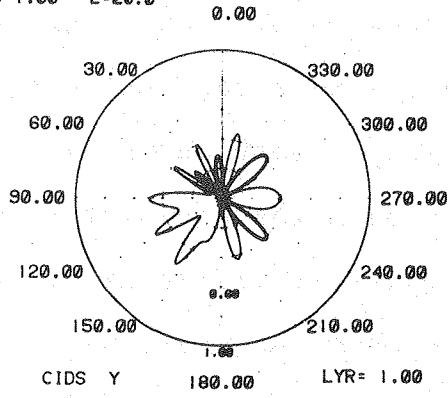
We assume now that the electrons in the scatterer are harmonically bound, so that their response to an external field can be simply expressed as:<sup>1</sup>

$$\alpha = \frac{f}{\left( \frac{1}{\lambda_0^2} - \frac{1}{\lambda^2} + \frac{i\Delta\lambda}{\lambda(\lambda_0^2 - \frac{(\Delta\lambda)^2}{4})} \right)}$$

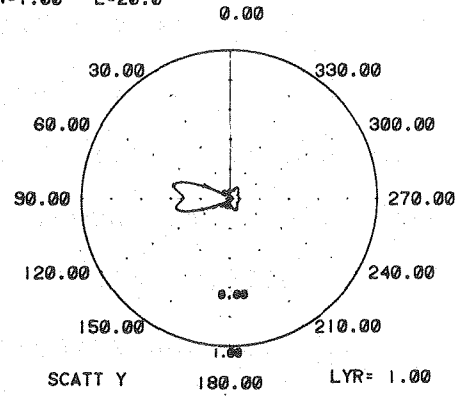
where  $f$  is the strength of the absorption band centered at wavelength  $\lambda_0$  and  $\Delta\lambda$  is equal to its width at half-height. In the numerical computations we have used polarizability tensors with two or three principal values along principal axes oriented tangent to the helix,  $\tilde{t}$ ; normal to the helix,  $\tilde{n}$ ; and perpendicular to these axes,  $\tilde{p}$  (Chapter 2). Total and differential scattering patterns were calculated as a function of the pitch and radius of the helix, the wavelength of incident light, and for various strengths ( $f$ ), widths ( $\Delta\lambda$ ), and positions ( $\lambda_0$ ) of the absorption bands along the axes defined. Figure 1 shows the results of the total and differential scattering for the case of a tri-axial polarizable helix of pitch = 3.6 and radius = 1.1;

Figure 1. Polar plots of intensity versus scattering angle  $\psi$  showing the +1, 0, and -1 layer lines (LYR) of the CIDS and total scattered intensities (SCATT Y) for light incident along the y-axis (from right to left along  $270^\circ$  on the 0 layer line). The parameters are: pitch  $P = 3.6$ , radius  $R = 1.1$ , wavelength  $W = 1.0$ , length  $L = 20$  turns and a triaxial polarizability, with a tangential absorption band  $\lambda_{0t}$  centered at 1.0, a perpendicular band  $\lambda_{0p} = 1.5$ , and a normal band  $\lambda_{0n} = 2.0$ . The strengths of the bands are all 1.0 and their half-height width chosen equal to 0.15. Heavy and light lines indicate negative and positive values of CIDS, respectively.

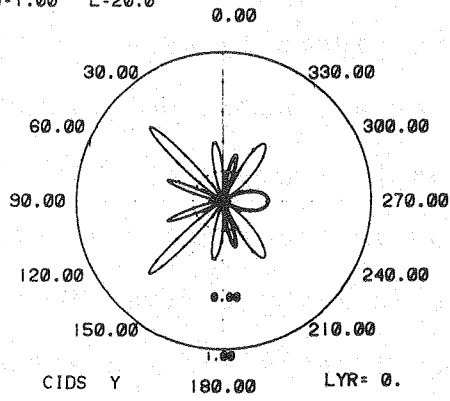
P=3.60 R=1.10  
W=1.00 L=20.0



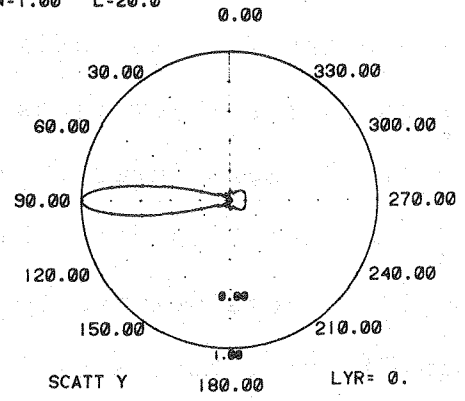
P=3.60 R=1.10  
W=1.00 L=20.0



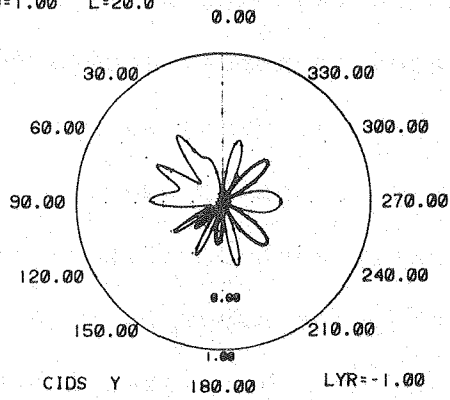
P=3.60 R=1.10  
W=1.00 L=20.0



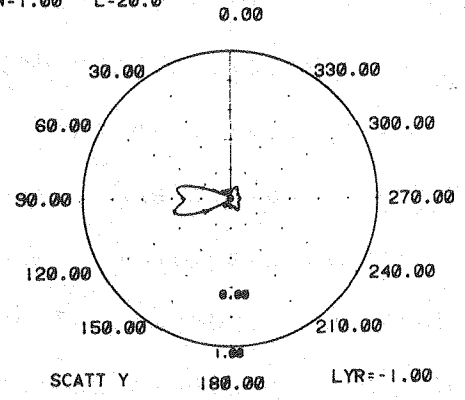
P=3.60 R=1.10  
W=1.00 L=20.0



P=3.60 R=1.10  
W=1.00 L=20.0



P=3.60 R=1.10  
W=1.00 L=20.0

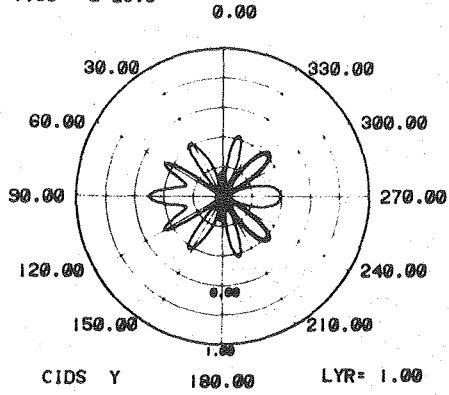


the wavelength  $\lambda = 1.0$ , and centers of bands are  $\lambda_{Ot} = 1.0$ ,  $\lambda_{On} = 2.0$ ,  $\lambda_{Op} = 1.5$ , with strengths,  $f = 1$  and widths,  $\Delta\lambda = 0.15$ . Figure 2 shows the total scattering and the CIDS for a helix of the same dimensions, but with uniaxial (tangential) polarizability. In both cases, +1, 0, and -1 layer lines are shown. The main feature of the general polarizability results is that the differential scattering patterns are now asymmetric when the wavelength of the incident radiation is within an absorption band of the polarizability. This contrasts with the uniaxial model where the  $270^\circ$ - $90^\circ$ -axis (see Figure 1) is a  $C_2$ -axis for each of the layer lines. For a general polarizability, only the zero layer line has this property. The asymmetry is seen both in the CIDS and in the total scattering; it is called anomalous scattering in X-ray diffraction. One sees in Figure 1 that the +1 and -1 layer lines are the mirror images of each other. A second feature of these general polarizability calculations is that the lobes of differential scattering have decreased in number (compared to the ones appearing in the uniaxial patterns) as well as having become sharper and restricted to smaller domains of the scattering angle  $\psi$ . Apparently each polarizability produces its independent pattern; the superposition of these patterns produces sharper and more localized lobes.

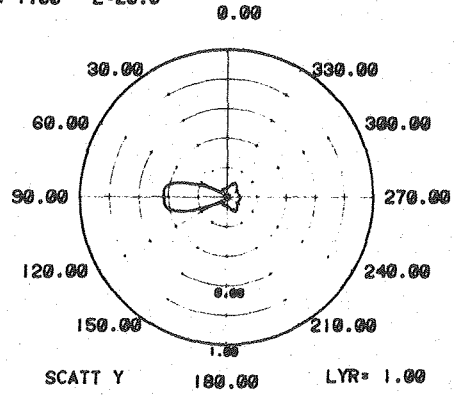
We found that the use of purely real or purely imaginary polarizabilities had the effect of producing total and

Figure 2. The corresponding polar plots of the same helix as in Figure 1 but having a uniaxial polarizability along the tangential direction with  $\lambda_{0t} = 1.0$ , band strength = 1.0, and width = 0.15 as before. Notice that both the CIDS and the total scattering away from the zero-layer line have regained their symmetry across the  $270^\circ$ - $90^\circ$  axis. As in Figure 1 the negative values are depicted with heavier lines.

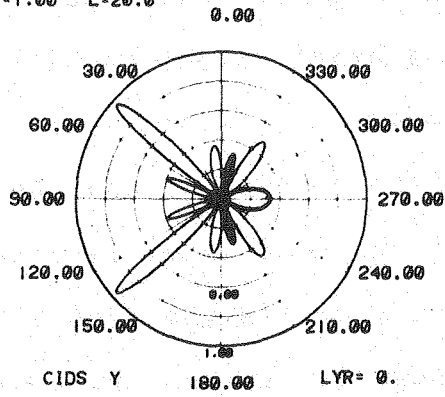
P=3.60 R=1.10  
W=1.00 L=20.0



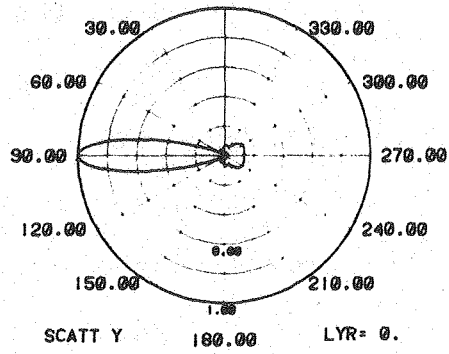
P=3.60 R=1.10  
W=1.00 L=20.0



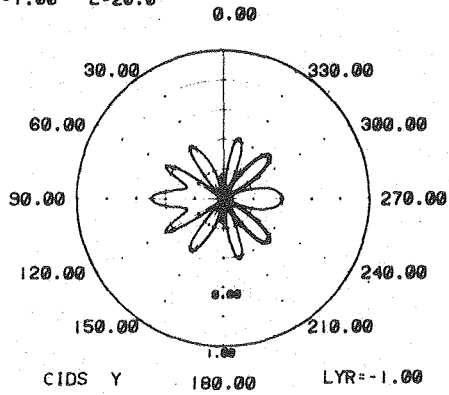
P=3.60 R=1.10  
W=1.00 L=20.0



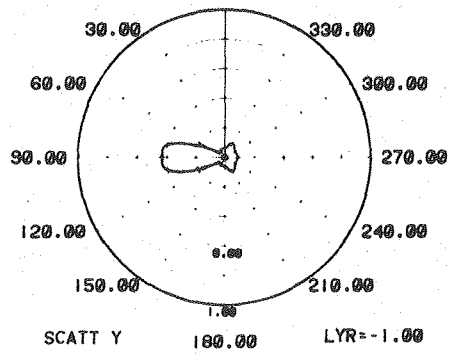
P=3.60 R=1.10  
W=1.00 L=20.0



P=3.60 R=1.10  
W=1.00 L=20.0



P=3.60 R=1.10  
W=1.00 L=20.0



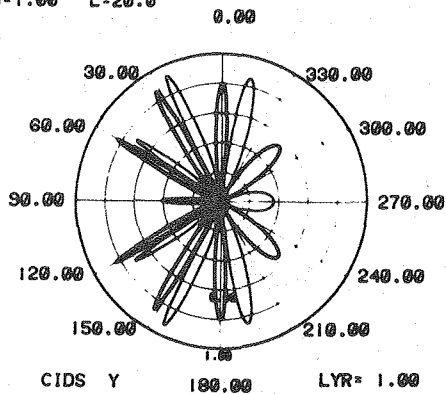
differential scattering patterns symmetric about the  $270^\circ$ - $90^\circ$  axis. This is shown in Figure 3 for a helix of the same dimensions of those used in Figure 1 and with the polarizabilities  $\alpha_t = \text{Re } \alpha_t$ ,  $\alpha_p = \text{Re } \alpha_p$ , and  $\alpha_n = \text{Re } \alpha_n$ . It should be pointed out that the number of lobes for the zeroth-layer line in Figure 3 is the same as in the corresponding layer in Figure 1, but here, three negative lobes are too small to be seen in the figure. As discussed in Chapter 3, the number of lobes of the CIDS pattern is determined by the geometry of the scatterer and not by the values and directions of the transitions in the scatterer.

In order to gain a better understanding of the symmetry laws involved in the patterns of total and differential scattering, the theory of CIDS for helical molecules is explicitly applied to the case of a biaxial polarizability. It will be shown that by writing the polarizabilities in the form  $\alpha = R \exp(i\gamma)$ , a phase change is introduced in the angular dependence of the scattering intensity, which is equal to the difference in the complex phases between the polarizabilities involved; this phase change is responsible for the antisymmetric properties observed. A detailed analysis of the symmetry of the scattering patterns will show their relations to the dispersive and absorptive properties of the polarizabilities.

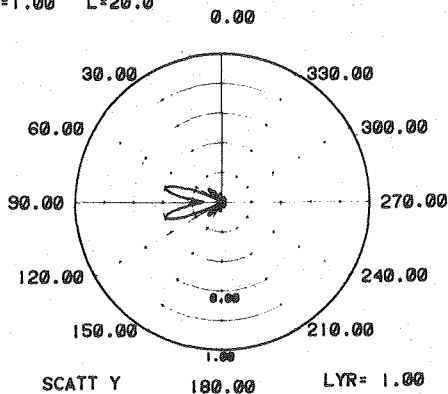


Figure 3. Polar plots for the same helix as in Figure 1, with a triaxial polarizability but with  $\alpha_t = \text{Re } \alpha_t$ ,  $\alpha_p = \text{Re } \alpha_p$ , and  $\alpha_n = \text{Re } \alpha_n$ . Everything else in the calculation was the same as in Figure 1. The CIDS and the total scattering are completely symmetric across the  $270^\circ$ - $90^\circ$  axis.

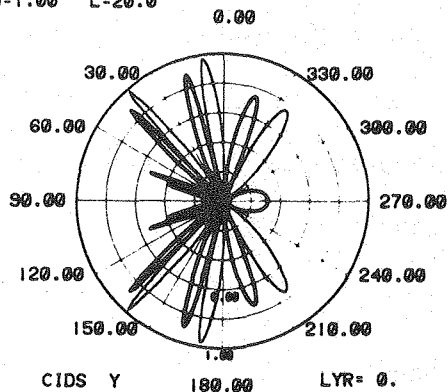
P=3.60 R=1.10  
W=1.00 L=20.0



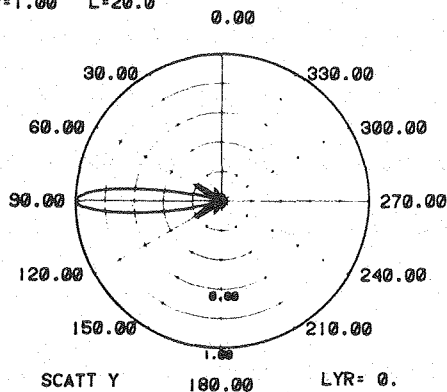
P=3.60 R=1.10  
W=1.00 L=20.0



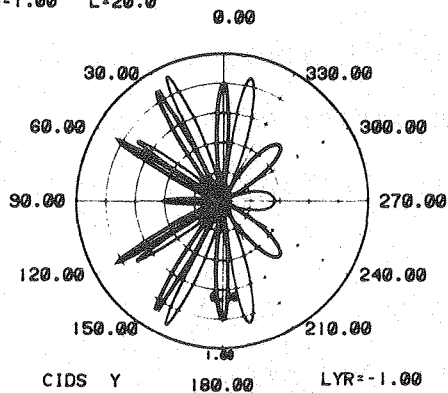
P=3.60 R=1.10  
W=1.00 L=20.0



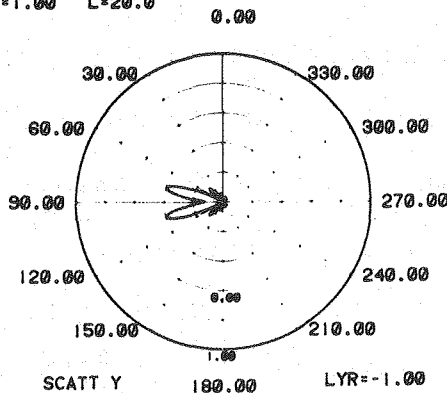
P=3.60 R=1.10  
W=1.00 L=20.0



P=3.60 R=1.10  
W=1.00 L=20.0



P=3.60 R=1.10  
W=1.00 L=20.0



2) A biaxial polarizability.

We choose a biaxial polarizability with principal axes along  $\underline{n}$  and  $\underline{t}$ . We can define the scattering matrix for the helix as:<sup>2</sup> (where  $A = (k^2 r') A_h M E_0 \exp(ikr')$ )

$$S = A(1 - \hat{\underline{k}}\hat{\underline{k}}) \int_{-\ell\pi}^{\ell\pi} e^{i\hat{\underline{k}} \cdot \underline{r}} (\alpha_{\underline{t}} \underline{t}\underline{t} + \alpha_{\underline{n}} \underline{n}\underline{n}) d\theta \quad (2)$$

where  $\hat{\underline{k}} = \underline{k}/|\underline{k}|$  is a unit vector along the direction of scattering,  $F$  includes constants and distance dependent factors,  $\ell$  is the number of turns of the helix,  $\alpha_{\underline{t}}$  and  $\alpha_{\underline{n}}$  are the magnitudes of the principal polarizabilities, and  $\underline{r}$  is the vector position of the segments in the scatterer.

Now the scattered field can formally be written as:

$$\underline{E}_{\text{scatt}}(\underline{r}') = S \underline{E}_{\text{incident}}$$

The electric field of the scattered light for right circularly polarized light and left circularly polarized incident light with polarization vector defined by  $(\underline{e}_3 + i\underline{e}_1)$  and  $(\underline{e}_3 - i\underline{e}_1)$ , respectively, and incident wave-vector  $\underline{k}_0$  along  $\underline{e}_2$  (y-axis) is:

$$\underline{E} = A(1 - \hat{\underline{k}}\hat{\underline{k}}) \cdot \int_{-\ell\pi}^{\ell\pi} e^{i\Delta\hat{\underline{k}} \cdot \underline{r}} [\alpha_{\underline{t}} \underline{t}(\underline{t} \cdot \underline{e}_3) + \alpha_{\underline{n}} \underline{n}(\underline{n} \cdot \underline{e}_3) + i(\alpha_{\underline{t}} \underline{t}(\underline{t} \cdot \underline{e}_1) + \alpha_{\underline{n}} \underline{n}(\underline{n} \cdot \underline{e}_1))] d\theta \quad (3)$$

The plus sign gives the scattered field for right circularly polarized light and the minus sign for left circularly polarized light, with  $\Delta \underline{k} = \underline{k} - \underline{k}_0$ . For a helix oriented along  $\underline{e}_3$  ( $\underline{n} \cdot \underline{e}_3 = 0$ ), we can write the terms that must be added to the ones calculated with the purely tangential polarizability (see Chapter 2) to obtain  $I_L - I_R$ . These additional terms are:

$$\begin{aligned}
 E_L E_L^* - E_R E_R^* = & 4A^2 \{ \iint \text{Im}(\alpha_t^* \alpha_n e^{i\Delta \underline{k} \cdot (\underline{r} - \underline{r}')} ) (\underline{n} \cdot \underline{t}') \\
 & (\underline{t}' \cdot \underline{e}_3) (\underline{n} \cdot \underline{e}_1) d\theta d\theta' \\
 & + \iint \text{Im}(\alpha_t \alpha_n^* e^{i\Delta \underline{k} \cdot (\underline{r} - \underline{r}')} ) (\underline{t} \cdot \hat{\underline{k}}) (\underline{t} \cdot \underline{e}_3) \\
 & (\underline{n}' \cdot \hat{\underline{k}}) (\underline{n}' \cdot \underline{e}_1) d\theta d\theta' \}
 \end{aligned} \tag{4}$$

where  $\text{Im}$  means the imaginary part of the expression should be used, and where the limits of integration have been omitted for simplicity. To perform the integrations indicated in (4), we rewrite the polarizabilities  $\alpha_t$  and  $\alpha_n$  as  $\alpha_t = R_t e^{i\gamma_t}$  and  $\alpha_n = R_n e^{i\gamma_n}$  where  $R_t$ ,  $R_n$ ,  $\gamma_t$ , and  $\gamma_n$  are real numbers.

The integration of Equation (4) allows the calculation of the contributions of the cross-terms involving both the tangential and normal axes of the polarizability, to the differential scattering. The terms that depend only on  $\underline{t}$

have been presented in Chapter 2 whereas in taking the difference the terms in  $n$  cancel as seen in Equation (4). The correction terms for  $I_L - I_R$  for a biaxial polarizability along  $t$  and  $n$  axes are therefore

$$\begin{aligned}
 A^2_{R_t R_n} \{ & \frac{aP}{4\pi M^2} [(2J_{n-1}J_{n-2} - J_n J_{n+1}) \cos(\psi' + \delta) \\
 & - (2J_{n+1}J_{n+2} - J_n J_{n-1}) \cos(\psi' - \delta)] \\
 & + \frac{k_x^2 aP}{4\pi M^2} [J_{n+1}J_{n-2} \cos(3\psi' + \delta) + (2J_n J_{n+1} - J_{n-1}J_{n-2}) \\
 & \cdot \cos(\psi' + \delta) - J_{n+2}J_{n-1} \cos(3\psi' - \delta) \\
 & - (2J_n J_{n-1} - J_{n+2}J_{n+1}) \cos(\psi' - \delta)] \\
 & + \frac{k_x k_y aP}{2\pi M^2} [J_{n+1}J_{n-2} \sin(3\psi' + \delta) - J_{n+2}J_{n-1} \sin(3\psi' - \delta) \\
 & + J_{n+1}J_n \sin(\psi' + \delta) \\
 & - J_n J_{n-1} \sin(\psi' - \delta)] \\
 & + \frac{k_y^2 aP}{4\pi M^2} [J_{n+2}J_{n-1} \cos(3\psi' - \delta) - J_{n+1}J_{n-2} \cos(3\psi' + \delta) \\
 & + J_{n+2}J_{n+1} \cos(\psi' - \delta) \\
 & - J_{n-1}J_{n-2} \cos(\psi' + \delta)]
 \end{aligned}$$

$$\frac{k_x k_z p^2}{4\pi^2 M^2} [J_{n-2} J_n \sin(2\psi' + \delta) - J_n J_{n+2} \sin(2\psi' - \delta)]$$

$$\frac{k_z k_y p^2}{4\pi^2 M^2} [J_n J_{n+2} \cos(2\psi' - \delta) - J_n J_{n-2} \cos(2\psi' + \delta)]$$

with  $\delta = \gamma_t - \gamma_n$  and the arguments of the Bessel functions, which are  $Qa$ , the angle  $\psi'$ , and the constant  $M$  have the same definition as in Chapter 2, and  $k_z$  and  $k_x$  are the  $e_3$  and  $e_1$  components of the scattered wave-vector, respectively.

### III. Symmetry Analysis.

In this section, an analysis of the symmetries involved in the scattering pattern of an absorptive chiral structure is carried out. It is clear that since the coefficients appearing in Equation (5) are different for each term, each one of them in turn must show all the symmetry behavior of the overall scattering pattern. Therefore it will be sufficient to do the analysis for only one of the terms in expression (5). Here we will do this for the term:

$$\frac{k_x k_z p^2}{4\pi^2 M^2} [J_n J_{n-2} \sin(2\psi' + (\gamma_t - \gamma_n)) - J_n J_{n+2} \sin(2\psi' - (\gamma_t - \gamma_n))] \quad (6-1) \quad (6)$$

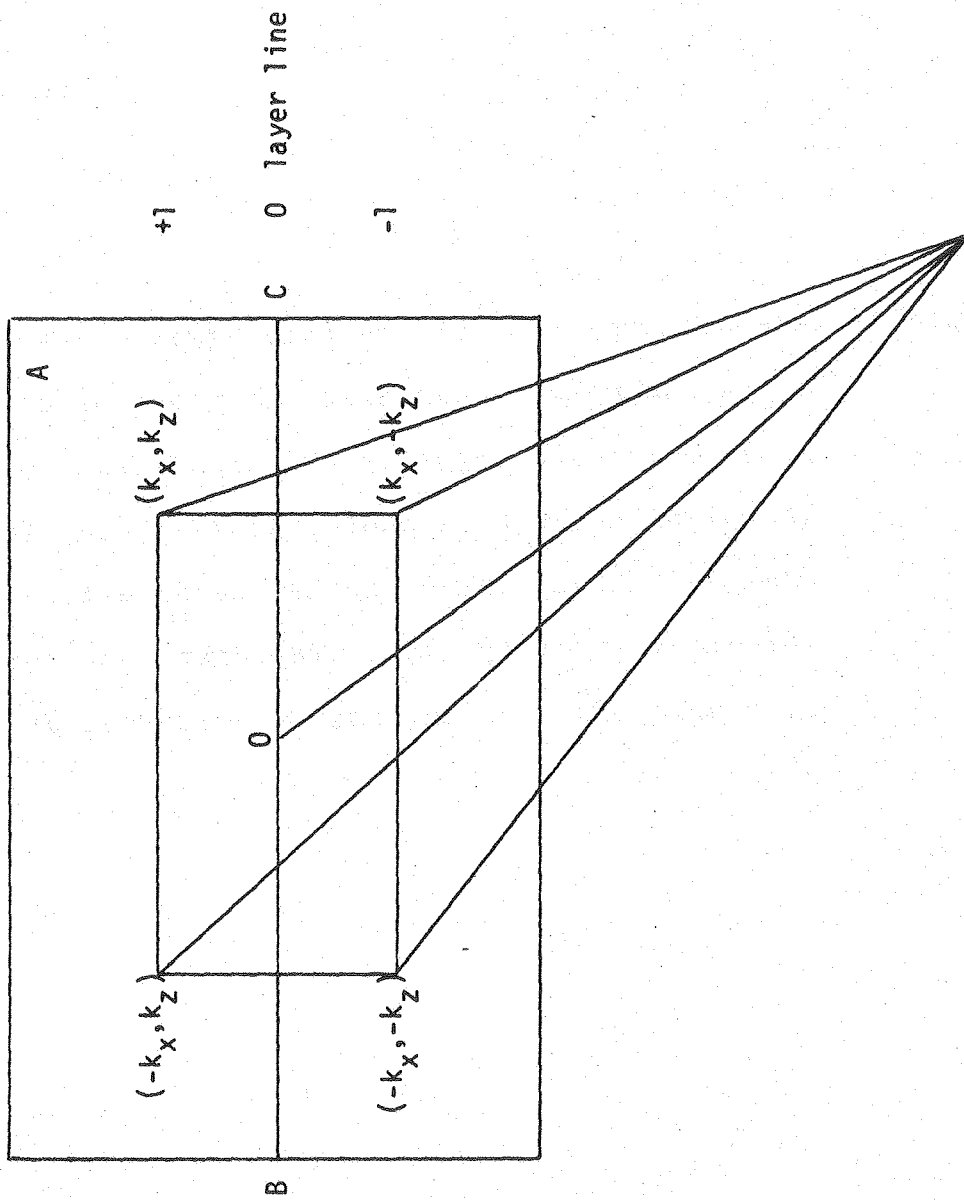
$$\sin(2\psi' - (\gamma_t - \gamma_n))]$$

(6-2)

In all the correction terms, the use of a general polarizability has the effect of introducing phase changes  $(\gamma_t - \gamma_n)$  in the trigonometric functions of the scattering angle  $\psi$  and related angles  $\psi'$ . These phase shifts are related to the scattering patterns which show differential scattering intensities in more restricted and smaller domains of the scattering angle  $\psi$  as discussed above. It is therefore clear that the new symmetry properties must be contained in the crossed terms of  $\underline{t}$  and  $\underline{n}$ , and consequently, our analysis does not have to consider the contribution to the scattering intensities of the purely tangential solution given in Chapter 2. Figure 4 shows a diagrammatic description of the symmetries involved in the differential and total anomalous scattering. The lines drawn from the scatterer to the plane A represent actual directions of the wave vector of the scattered light. Any point in the plane, therefore, where nonvanishing differential or total scattering is observed, can be described completely by the coordinates  $(k_x, k_z)$ , its sign of polarization (in the case of the differential scattering), and the observed intensity at that point. One sees that the point 0 represents an inversion point for the pattern in plane A, the differential or total scattered intensities of the point  $(k_x, k_z)$  being the same as that of  $(-k_x, -k_z)$ , and that of  $(-k_x, k_z)$  being the same as that of  $(k_x, -k_z)$ . Through our symmetry analysis of the differential scattering, we should be able to show the

Figure 4. Graphic depiction of the antisymmetry involved in the anomalous scattering of plane or circularly polarized light by a chiral structure. The plane A can be a photographic plate, for example. The point 0 labels the direction of forward scattering and it represents an inversion point for the intensities recorded at the plate.





Scatterer  
XBL 8012-13501

existence of the following properties: (a) when the polarizabilities are purely real or imaginary, the patterns must be invariant for a change of  $k_x \rightarrow -k_x$  and will also be invariant for a change  $k_z \rightarrow -k_z$ ; (b) when the polarizabilities are complex, the equations should be invariant only for a simultaneous transformation of  $k_x \rightarrow -k_x$  and  $k_z \rightarrow -k_z$ ; (c) the zeroth-layer line is completely symmetric to independent changes of  $k_x \rightarrow -k_x$  and to changes of  $k_z \rightarrow -k_z$  regardless of the use of complex polarizabilities; (d) the total scattering shows the same asymmetric behavior as the differential scattering. Equation (6) can be rewritten as:

$$\frac{k_x k_z}{4\pi^2 M^2} P^2 \{ (J_{n-2} J_n - J_n J_{n+2}) \sin 2\psi' \cos \delta + (J_{n-2} J_n + J_n J_{n+2}) \cdot$$

(7-1)
(7-2)

$$\cos 2\psi' \sin \delta \}$$

Equation (7) has the general form:

$$C_{1x} C_{1z} P_1 B_1 \cos \delta + C_{2x} C_{2z} P_2 B_2 \sin \delta$$

where C stands for coefficient, P for phase ( $\sin 2\psi'$  or  $\cos 2\psi'$  in this case) and B for the combination of Bessel functions.

For light incident along  $e_2$  (see Chapters 2 and 3), the argument of the Bessel functions (Qa) is given by:

$$Q_a = \frac{2\pi a}{\lambda} \left( 2 - \frac{\lambda^2 n^2}{p^2} - 2 \left( 1 - \frac{\lambda^2 n^2}{p^2} \right)^{1/2} \sin \psi \right)^{1/2}$$

Now, when  $k_x \rightarrow -k_x$  then  $\psi \rightarrow 180 - \psi$  and  $\psi^* \rightarrow 180 - \psi^*$ . So we see that  $Q_a$  and therefore the Bessel terms (B's) are invariant to changes of  $k_x \rightarrow -k_x$ . The transformation  $k_z \rightarrow -k_z$  implies  $n \rightarrow -n$  but since this term appears squared in the expression above,  $Q_a$  is also invariant to changes of  $k_z \rightarrow -k_z$ . However, the transformation  $k_z \rightarrow -k_z$  has an effect in the term B through the order  $n, n-2, n-4$ , etc., appearing in each of the Bessel functions. Finally, since  $\psi' = \psi^* + \pi/2$  then the transformation  $k_x \rightarrow -k_x$  will certainly affect the term P although it will be invariant to the transformation  $k_z \rightarrow -k_z$ . In what follows we will analyze the transformation properties of expression (7) when

$k_x \rightarrow -k_x$  and  $k_z \rightarrow -k_z$ .

1) term 7-1: for  $k_x \rightarrow -k_x$

a)  $C_{1x} \rightarrow -C_{1x}$

b)  $C_{1z} \rightarrow +C_{1z}$  (invariant).

c)  $B_1 \rightarrow B_1$  (invariant).

d) Since:  $\sin 2\psi' = \sin 2(\psi^* + \pi/2) = -\sin 2\psi^*$

and: when  $k_x \rightarrow -k_x$  then  $\psi^* = 180 - \psi^*$

we have  $-\sin 2\psi^* = -\sin 2(180 - \psi^*) = \sin 2\psi^*$ .

So:  $P_1 \rightarrow -P_1$

for  $k_z \rightarrow -k_z$

- a)  $C_{1x} \rightarrow C_{1x}$  (invariant).  
 b)  $C_{1z} \rightarrow -C_{1z}$   
 c)  $P_1 \rightarrow P_1$  (invariant).  
 d) Since  $n = 0$  is the zeroth layer line, we take,  
 for example:

$$\left. \begin{array}{l} k_z: n = 1 \quad J_{-1}J_1 - J_3J_1 \\ -k_z: n = -1 \quad J_{-3}J_1 - J_1J_{-1} \end{array} \right\} \text{So } B_1 \rightarrow -B_1$$

2) term 7-2: for  $k_x \rightarrow -k_x$

- a)  $C_{2x} \rightarrow -C_{2x}$   
 b)  $C_{2z} \rightarrow C_{2z}$  (invariant)  
 c)  $B_2 \rightarrow B_2$  (invariant)  
 d) Since:  $\cos 2\psi' = \cos 2(\psi^* + \pi/z) = -\cos 2\psi^*$   
 and:  $k_x \rightarrow -k_x \Rightarrow \psi^* \rightarrow 180 - \psi^*$   
 then:  $-\cos 2\psi^* \rightarrow -\cos 2\psi^*$   
 So:  $P_1 \rightarrow P_1$  (invariant)

for  $k_z \rightarrow -k_z$

- a)  $C_{2x} \rightarrow C_{2x}$  (invariant)  
 b)  $C_{2z} \rightarrow -C_{2z}$   
 c)  $P_1 \rightarrow P_1$  (invariant)  
 d)  $k_z: n = 1 \quad J_1J_{-1} + J_3J_1$   
 $-k_z: n = -1 \quad J_{-1}J_{-3} + J_1J_{-1}$  } So:  $B_1 \rightarrow B_1$   
 (invariant)

It can be shown that the above term, under the double reflexion ( $x \rightarrow -x$ ;  $z \rightarrow -z$ ), transforms as:

$$C_{1x}C_{1z}P_1B_1\cos\delta + C_{2x}C_{2z}P_2B_2\sin\delta$$

$$\begin{pmatrix} + \\ \downarrow \\ - \end{pmatrix} \begin{bmatrix} + \\ \downarrow \\ - \end{bmatrix} \begin{pmatrix} + \\ \downarrow \\ - \end{pmatrix} \begin{bmatrix} + \\ \downarrow \\ - \end{bmatrix} \quad \begin{pmatrix} + \\ \downarrow \\ - \end{pmatrix} \begin{bmatrix} + \\ \downarrow \\ - \end{bmatrix} \begin{pmatrix} + \\ \downarrow \\ + \end{pmatrix} \begin{bmatrix} + \\ \downarrow \\ + \end{bmatrix} \quad (8)$$

where the terms affected by changes of  $k_z \rightarrow -k_z$  are shown in square brackets while the ones affected by changes of  $k_x \rightarrow -k_x$  are shown in parentheses. From expressions (8) and (7) we see the term (7-1) is symmetric with respect to changes of  $k_x \rightarrow -k_x$  as well as to changes of  $k_z \rightarrow -k_z$ , whereas (7-2) is antisymmetric with respect to either of these transformations. This different behavior of the two terms is responsible for the asymmetry observed in the differential patterns. When the polarizabilities are purely real, then  $\delta = 0$ , and the asymmetric term vanishes, leaving only the term (7-1) invariant to changes  $k_x \rightarrow -k_x$  as well as to changes in  $k_z \rightarrow -k_z$ . Similarly, when purely imaginary polarizabilities are used, this means that  $\gamma_t = (2n_t + 1)\pi/2$  and  $\gamma_n = (2n_n + 1)\pi/2$  for  $n_t, n_n = 0, 1, 2$ . . . therefore the difference  $\delta \equiv \gamma_t - \gamma_n = 2(n_t - n_n)\pi/2$  and  $\sin \delta \equiv 0$ , leaving also in this case only the symmetric terms. When the polarizabilities involved are complex, it is clear from (7) that the term will still be symmetric for

the simultaneous transformation ( $k_x \rightarrow -k_x$ ;  $k_z \rightarrow -k_z$ ). Finally, in the zeroth-layer line, even though the polarizabilities might be complex, this term vanishes, either because  $k_z = 0$  in the zeroth layer line, or because the Bessel term  $B$  evaluated at  $n = 0$  vanishes. Expression (7) contains, therefore, all the antisymmetric properties depicted by the differential scattering pattern. The other terms in Equation (5) can be analyzed in an identical fashion as was the term of Equation (6). All of them show the same antisymmetric behavior for the simultaneous reflexion ( $k_x \rightarrow -k_x$ ;  $k_z \rightarrow -k_z$ ). In what follows, we indicate the symmetry transformation of the terms of expression (5) under this double reflexion.

The  $k_x^2$  - term transforms:

$$C_{1x} P_1 B_1 \cos\delta + C_{2x} P_2 B_2 \sin\delta$$

$$\begin{pmatrix} + \\ \downarrow \\ + \end{pmatrix} \begin{pmatrix} + \\ \downarrow \\ + \end{pmatrix} \begin{bmatrix} + \\ \downarrow \\ + \end{bmatrix} \quad \begin{pmatrix} + \\ \downarrow \\ + \end{pmatrix} \begin{pmatrix} + \\ \downarrow \\ - \end{pmatrix} \begin{bmatrix} + \\ \downarrow \\ - \end{bmatrix}$$

The  $k_x k_y$  - term transforms:

$$C_{1x} P_1 B_1 \cos\delta + C_{2x} P_2 B_2 \sin\delta$$

$$\begin{pmatrix} + \\ \downarrow \\ - \end{pmatrix} \begin{pmatrix} + \\ \downarrow \\ - \end{pmatrix} \begin{bmatrix} + \\ \downarrow \\ + \end{bmatrix} \quad \begin{pmatrix} + \\ \downarrow \\ - \end{pmatrix} \begin{pmatrix} + \\ \downarrow \\ + \end{pmatrix} \begin{bmatrix} + \\ \downarrow \\ - \end{bmatrix}$$

The  $k_y^2$  - term transforms:

$$C_1 P_1 B_1 \cos\delta + C_2 P_2 B_2 \sin\delta$$

$$\begin{pmatrix} + \\ \downarrow \\ + \end{pmatrix} \begin{pmatrix} + \\ \downarrow \\ + \end{pmatrix} \begin{bmatrix} + \\ \downarrow \\ + \end{bmatrix} \quad \begin{pmatrix} + \\ \downarrow \\ + \end{pmatrix} \begin{pmatrix} + \\ \downarrow \\ - \end{pmatrix} \begin{bmatrix} + \\ \downarrow \\ - \end{bmatrix}$$

The  $k_y k_z$  - term transforms:

$$C_{1z} P_1 B_1 \cos\delta + C_{2z} P_2 B_2 \sin\delta$$

$$\begin{bmatrix} + \\ \downarrow \\ - \end{bmatrix} \begin{pmatrix} + \\ \downarrow \\ + \end{pmatrix} \begin{bmatrix} + \\ \downarrow \\ - \end{bmatrix} \quad \begin{bmatrix} + \\ \downarrow \\ - \end{bmatrix} \begin{pmatrix} + \\ \downarrow \\ - \end{pmatrix} \begin{bmatrix} + \\ \downarrow \\ + \end{bmatrix}$$

The  $k$  - independent term transforms:

$$P_1 B_1 \cos\delta - P_2 B_2 \sin\delta$$

$$\begin{pmatrix} + \\ \downarrow \\ + \end{pmatrix} \begin{bmatrix} + \\ \downarrow \\ + \end{bmatrix} \quad \begin{pmatrix} + \\ \downarrow \\ - \end{pmatrix} \begin{bmatrix} + \\ \downarrow \\ - \end{bmatrix}$$

From the above results, therefore, it is clear that all the terms in Equation (5) show the same antisymmetric behavior under the simultaneous reflexion ( $k_x \rightarrow -k_x$ ;  $k_z \rightarrow -k_z$ ). Their symmetry diagrams characterize uniquely the reaction of the helix to opposite circularly polarized

light near the absorption band. Essentially, the same findings are applicable to the symmetry properties of the total scattering (see Figure 1). The correction terms for the total ( $I_L + I_R$ ) scattering can be obtained from expression (3). Squaring the amplitudes of opposite circular polarization and adding them, after some algebra, we obtain a formal expression for the correction term as:

$$\begin{aligned}
 I_L + I_R = & 2A^2 \left\{ R_n^2 \iint e^{i\Delta \mathbf{k} \cdot (\mathbf{r} - \mathbf{r}')} (\mathbf{n}' \cdot \mathbf{e}_1) (\mathbf{n} \cdot \mathbf{e}_1) \right. \\
 & [\mathbf{n} \cdot (1 - \hat{\mathbf{k}}\hat{\mathbf{k}}) \cdot \mathbf{n}'] d\theta d\theta' \\
 & + 2R_t R_n \iint \cos(\Delta \mathbf{k} \cdot (\mathbf{r} - \mathbf{r}') + (\gamma_t - \gamma_n)) (\mathbf{t} \cdot \mathbf{e}_1) \\
 & \left. (\mathbf{n}' \cdot \mathbf{e}_1) [\mathbf{n}' \cdot (1 - \hat{\mathbf{k}}\hat{\mathbf{k}}) \cdot \mathbf{t}] d\theta d\theta' \right\}
 \end{aligned} \tag{9}$$

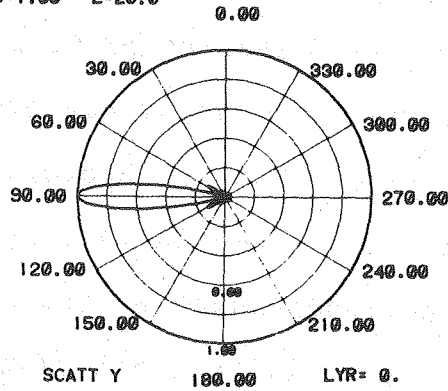
where  $\mathbf{n}'$  and  $\mathbf{n}$  indicate the dependence of the normal axes with respect to variables  $\theta'$  and  $\theta$ , respectively.

Equation (9) shows that the total scattering involves a cross-term of the values of the polarizability along the two axes  $\mathbf{t}$  and  $\mathbf{n}$ , and includes the phase difference  $\delta \equiv (\gamma_t - \gamma_n)$ ; this accounts for the antisymmetry shown by the total scattering patterns. Clearly, if the polarizability is spherically symmetric, then the phase changes  $(\gamma_t - \gamma_n)$ ,  $(\gamma_t - \gamma_p)$ , etc., will all vanish and the patterns will regain their symmetry. This behavior is indeed shown in Figure 5,

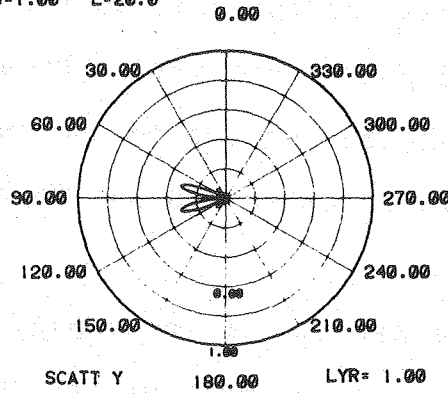


Figure 5. Polar plots for the total scattering for a helix with the same structural parameters as those of Figure 1 but possessing a spherically symmetric polarizability with  $\lambda_{0t} = \lambda_{0p} = \lambda_{0n} = 0.85$ ; band strengths = 1.0; and band widths = 0.15. The CIDS patterns are all zero. The total scattering appears symmetric as expected (see text).

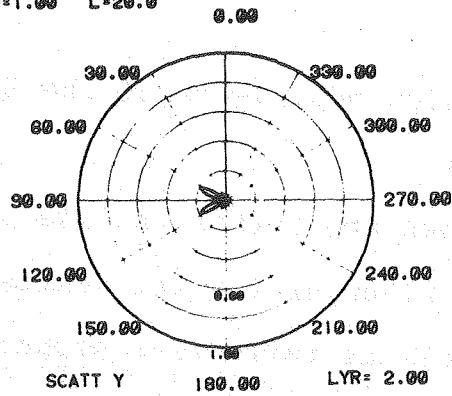
P=3.60 R=1.10  
W=1.00 L=20.0



P=3.60 R=1.10  
W=1.00 L=20.0



P=3.60 R=1.10  
W=1.00 L=20.0



XBL 8012-12858

where all three principal values of the polarizability are identical. The total scattering patterns appear symmetric, while the differential scattering patterns vanish as expected from our discussion in Chapters 2 and 3.

All the results obtained in this section are completely general and independent of the particular choice of the polarizability. In the following section, an analysis will be presented on the dispersion dependence of the differential scattering intensities for the case of a Lorentzian-shaped polarizability. The asymmetry of the polarizability will be related to the position of the absorption band with respect to the wavelength of the incident light.

Although the details of the expansions are only valid for this particular case, most of the conclusion will be valid for a Gaussian-shaped band as well.

#### IV. The Dispersion Dependence of the Scattering Intensities.

We have shown above that the use of complex polarizabilities, i.e., allowing for the scatterer to possess absorptive as well as refractive properties, has the effect of producing scattering patterns which are quite asymmetric. Indeed, the axis defined by the direction of incidence of light is a  $C_2$ -axis only for the zeroth layer line; the

remaining layer lines have lost their biaxial symmetry in the direction  $270^\circ$ - $90^\circ$  (see figures).

In all the computations we have presented, the simple harmonically bound electron model has been used for the dispersion properties of the polarizability. Here, starting from expression (1), we will derive the wavelength dependence of the scattering intensities for this Lorentzian-shaped polarizability. Expression (1) can be rewritten as:

$$\alpha = f \left( \frac{1}{\lambda^2} - \frac{1}{\lambda_0^2} \right) / \left[ \left( \frac{1}{\lambda^2} - \frac{1}{\lambda_0^2} \right)^2 - \frac{\Delta\lambda^2}{\lambda^2 \left( \lambda_0^2 - \left( \frac{\Delta\lambda}{2} \right)^2 \right)^2} \right] \quad (10)$$

$$- \frac{if\Delta\lambda}{\lambda \left( \lambda_0^2 - \left( \frac{\Delta\lambda}{2} \right)^2 \right)} / \left[ \left( \frac{1}{\lambda^2} - \frac{1}{\lambda_0^2} \right)^2 - \frac{\Delta\lambda^2}{\lambda^2 \left( \lambda_0^2 - \left( \frac{\Delta\lambda}{2} \right)^2 \right)^2} \right]$$

From this expression we see that in resonance,  $\lambda_0 = \lambda$ , and the polarizability becomes purely imaginary. In view of the results presented above, for wavelengths of light corresponding to the center of the absorption band, completely symmetric scattering patterns must be observed for  $I_L - I_R$  as well as for  $I_L + I_R$ , if the polarizability has a single absorption band common to all axes. Away from the absorption band the anomalous behavior of the scattering disappears. We must show, therefore, that the phase difference  $\delta = (\gamma_t - \gamma_n)$  responsible for the antisymmetry of the patterns,

vanishes at wavelengths far outside the absorption bands.

To demonstrate this we compare the polarizability

$\alpha = R(\cos\gamma - i \sin\gamma)$  with Equation (10) to obtain an expression for the phase angle  $\gamma$ :

$$\tan \gamma = \frac{-\Delta\lambda}{\lambda(\lambda_0^2 - [\Delta\lambda/2]^2)} \frac{(\frac{1}{\lambda_0^2} - \frac{1}{\lambda^2})}{}$$

Since  $\Delta\lambda/2 \ll \lambda_0$ , then

$$\tan \gamma = \frac{(\Delta\lambda)\lambda}{\lambda_0^2 - \lambda^2}$$

Away from the absorption band we can expand around

$\lambda_0/\lambda$ :

$$\tan \gamma \approx \gamma = -\frac{\Delta\lambda}{\lambda} \left(1 + \frac{\lambda_0^2}{\lambda^2} + \frac{\lambda_0^4}{\lambda^4} + \dots\right) \approx -\frac{\Delta\lambda}{\lambda}$$

(away from the absorption band)

Again  $\Delta\lambda/\lambda \ll 1$ , since, in general, the width of the bands spans over a restricted domain.

$$\delta \equiv (\gamma_t - \gamma_n) \approx \frac{1}{\lambda} (\Delta\lambda_n - \Delta\lambda_t) \approx 0$$

(away from the absorption band)

(11)

This is the result we were seeking. It predicts that far away from the absorptive band the antisymmetric terms (proportional to  $\sin\delta$ ) vanish, rendering completely symmetric patterns of scattering. Figures 6 and 7 show in fact that this is the case. (See details in figure captions.) By using essentially the same approximations, it can be shown from Equation (10) that away from resonance:

$$\text{Re } \alpha = \frac{f}{1 - \frac{\Delta\lambda^2}{(\lambda^2 - \lambda_0^2)\lambda_0^2}} \approx f \left( 1 + \frac{C_{\lambda_0}^2}{\lambda^2 - \lambda_0^2} \right)$$

$$\text{with } C_{\lambda_0}^2 = \frac{\Delta\lambda^2}{\lambda_0^2}$$

And in a similar fashion:

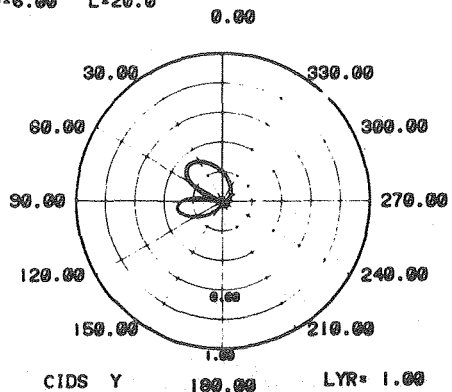
$$\text{Im } \alpha = \frac{-f \Delta\lambda}{(\lambda^2 - \lambda_0^2) \frac{2}{0} \left( i - \frac{\Delta\lambda^2}{(\lambda^2 - \lambda_0^2)\lambda_0^2} \right)}$$

$$\approx - \frac{f C_{\lambda_0}}{\lambda \lambda_0 (\lambda^2 - \lambda_0^2)} \left( 1 + \frac{C_{\lambda_0}^2}{(\lambda^2 - \lambda_0^2)} \right)$$

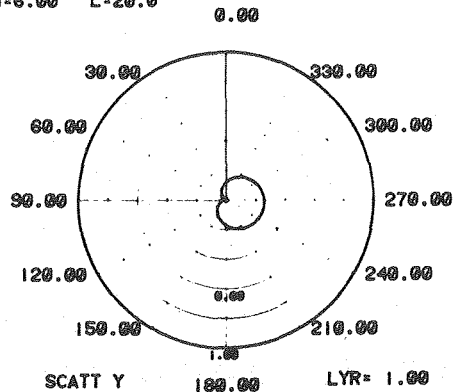
Comparing the last two expressions, we obtain:

Figure 6. Plots of CIDS and total scattering for the +1, 0, and -1 layer lines for a helix of  $P = 12$ ,  $R = 0.6$ ,  $L = 20$  turns. The wavelength of light  $W = 6.0$  coincides with the center of the tangential band ( $\lambda_{0t}$ ) and is close to the perpendicular  $\lambda_{0p} = 6.20$  and the normal band  $\lambda_{0n} = 5.00$ . The band strengths are 1.0 for all three bands and the width is 0.30. Notice that the +1 and the -1 layer lines are asymmetric for the CIDS as well as the total scattering.

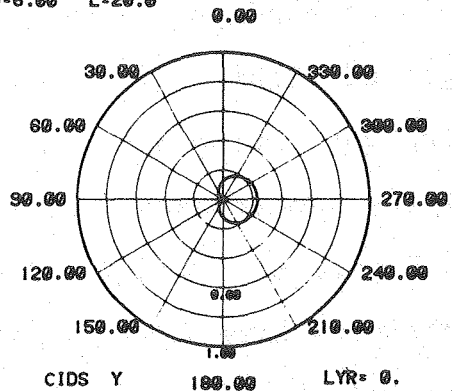
P=12.0 R= .60  
W=6.00 L=20.0



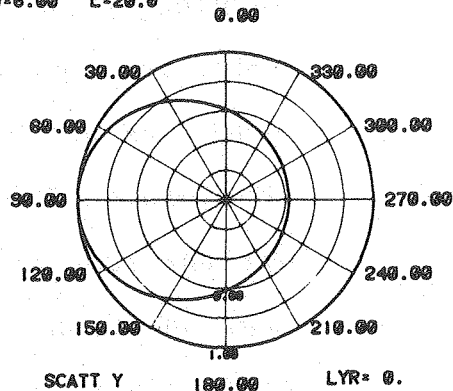
P=12.0 R= .60  
W=6.00 L=20.0



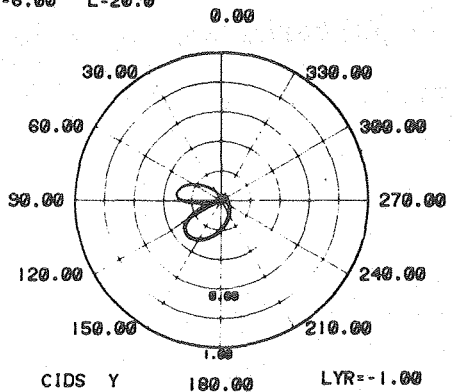
P=12.0 R= .60  
W=6.00 L=20.0



P=12.0 R= .60  
W=6.00 L=20.0



P=12.0 R= .60  
W=6.00 L=20.0



P=12.0 R= .60  
W=6.00 L=20.0

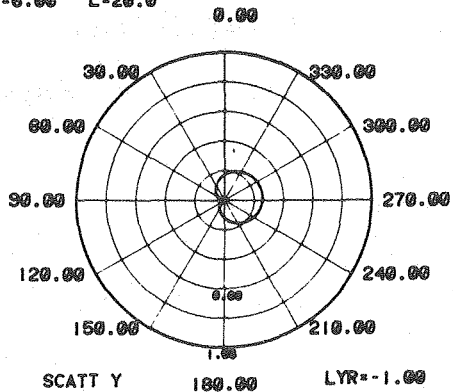
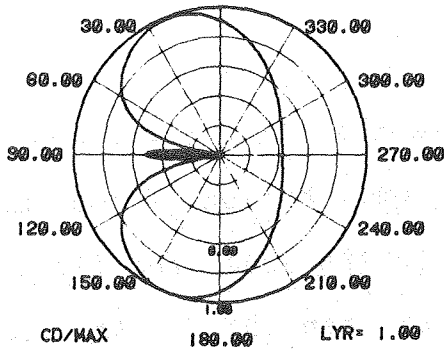




Figure 7. Equivalent plots to those of Figure 6 for the same ratios of pitch/wavelength and radius/wavelength and the same band positions. However, the wavelength of light is  $W = 10.0$ , i.e., away from any of the absorption bands of the scatterer. The widths and strengths of the bands are the same as in Figure 6. CD/MAX indicates that the CIDS intensities have been normalized to 1.0 in this case and therefore cannot be compared to the CIDS values of Figure 6 on a quantitative basis. The patterns as discussed in text are all symmetric.

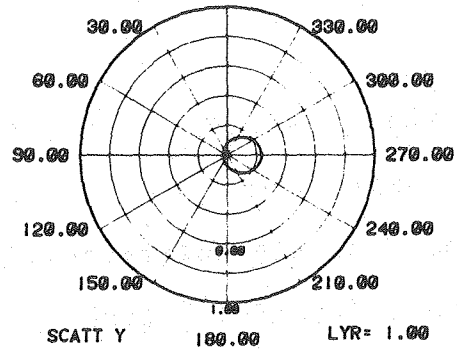
P=20.0 R=1.00  
W=10.0 L=20.0

0.00



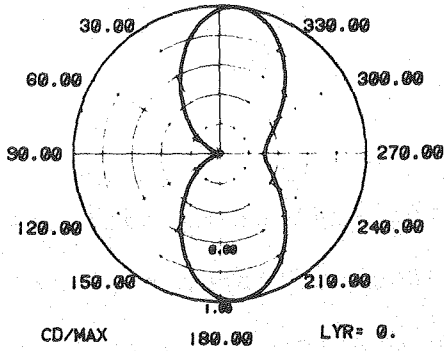
P=20.0 R=1.00  
W=10.0 L=20.0

0.00



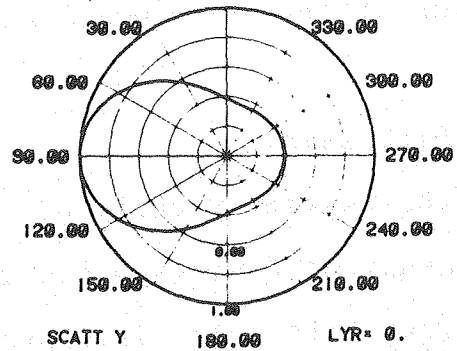
P=20.0 R=1.00  
W=10.0 L=20.0

0.00



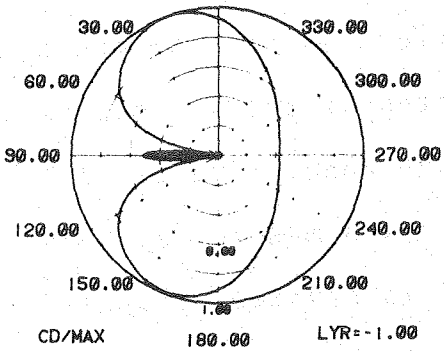
P=20.0 R=1.00  
W=10.0 L=20.0

0.00



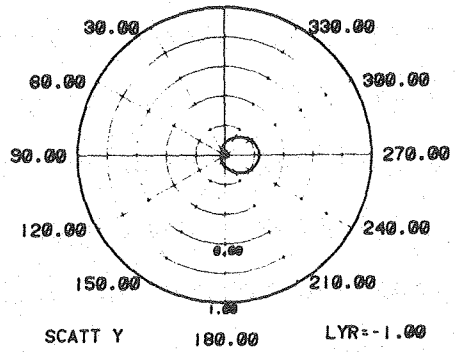
P=20.0 R=1.00  
W=10.0 L=20.0

0.00



P=20.0 R=1.00  
W=10.0 L=20.0

0.00



$$\text{Im } \alpha = \frac{C_{\lambda_0}}{\lambda \lambda_0 (\lambda^2 - \lambda_0^2)} \text{Re } \alpha \quad (12)$$

From this last expression we see that in a first approximation, away from resonance, the contribution of the imaginary part of the polarizability to the scattered fields is of the order of  $\lambda^{-4}$  times smaller than that of the real part. Therefore the imaginary part will not contribute significantly to the scattering for regions of the spectrum outside of the absorption band.

#### V. Discussion.

The asymmetry observed in the scattering patterns is the result of having chosen for the scatterer a general polarizability. As discussed in Chapter 2, this choice implies that in calculating the CIDS, the dispersion dependence of the polarizability cannot be cancelled when the CIDS ratio is taken. The effect is to make the calculated differential scattering intensities, as well as the total scattering, dependent on the absorptive properties of the scatterer. This behavior is a manifestation of "anomalous scattering" described in crystallography.<sup>3</sup> Thus, Friedel's law of symmetry of the scattered intensities above and below the equator of the diffraction pattern is violated when the wavelength of the incident radiation falls inside the absorption band of some of the scattering

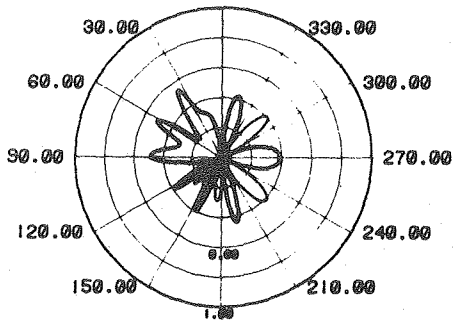
elements in the lattice. As the wavelength of light moves away from the absorption band, the asymmetry gradually disappears to eventually recover the symmetry of the pattern far away from resonance. However, the antisymmetry shown by the absorptive helix is a property peculiar to the geometry and symmetry of the scatterer studied. In this way, whereas the symmetry of the scattering patterns is a general manifestation of anomalous scattering, the antisymmetry shown by the patterns is peculiar to the highly symmetric chiral scatter discussed.

It is well known that the phenomenon of anomalous scattering is used in crystallography as a method to determine the absolute configuration of the scatterers and to recover the phases of the scattered fields.<sup>4</sup> In Figure 8 the CIDS of a left-handed helix for layer lines +1, 0, and -1 is depicted. It should be compared with the corresponding layer lines in Figure 1. It is seen that the total scattering has a reflection plane defined by the direction of the incident light, and perpendicular to the plane of the figure. The CIDS, on the other hand, gets reflected through this plane and also changes sign when a transformation from a right- to a left-handed helix is done. This effect is important, since it can immediately be used to determine the sense of the helix. Shown in Figure 9 is the effect on the scattering of light incident perpendicular to the helix axis and plane polarized first along this

Figure 8. The effect of going from a right- to a left-handed helix can be observed by comparing this figure to Figure 1. A left-handed helix is obtained by using a negative pitch ( $P = 3.6$  in this case). Everything else is the same as in Figure 1. The total intensities get reflected through a plane containing the  $270^\circ$ - $90^\circ$  axis and perpendicular to the plane of the figure, whereas the CIDS is reflected and has changed sign. The zero layer line is the same in both the CIDS and the total scattering but the sign of the CIDS is changed.

P=-3.6 R=1.10  
W=1.00 L=20.0

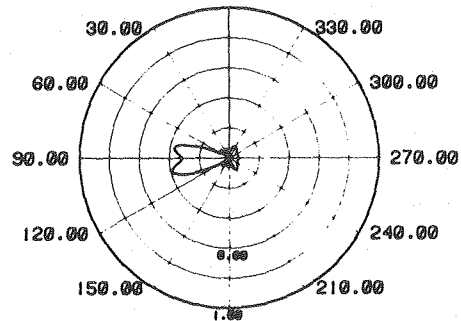
0.00



CIDS Y 100.00 LYR= 1.00

P=-3.6 R=1.10  
W=1.00 L=20.0

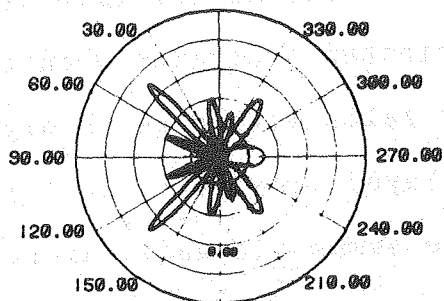
0.00



SCATT Y 100.00 LYR= 1.00

P=-3.6 R=1.10  
W=1.00 L=20.0

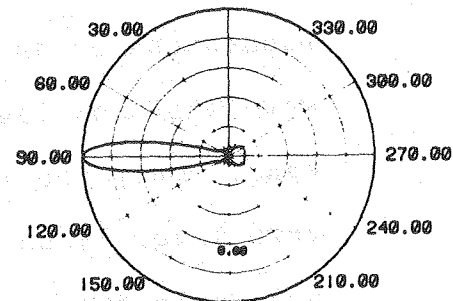
0.00



CIDS Y 100.00 LYR= 0.

P=-3.6 R=1.10  
W=1.00 L=20.0

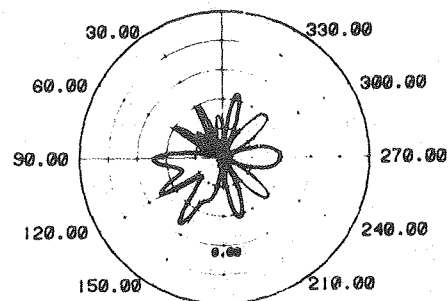
0.00



SCATT Y 100.00 LYR= 0.

P=-3.6 R=1.10  
W=1.00 L=20.0

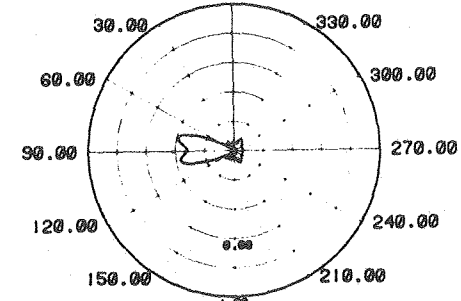
0.00



CIDS Y 100.00 LYR=-1.00

P=-3.6 R=1.10  
W=1.00 L=20.0

0.00

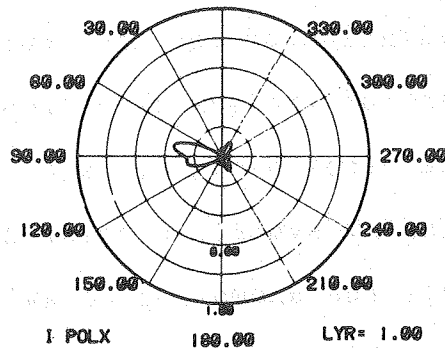


SCATT Y 100.00 LYR=-1.00

Figure 9. The figure illustrates the fact that plane polarized light can be used to determine the handedness of an oriented scatterer when the wavelength of light falls within an absorption band. Only the +1 layer line is shown. The zero layer lines are symmetric and indistinguishable for right- and left-handed helices.

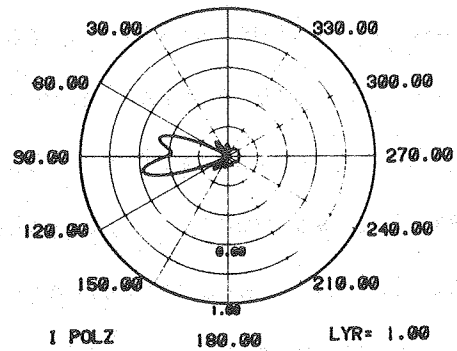
P=3.00 R=1.10  
W=1.00 L=20.0

0.00



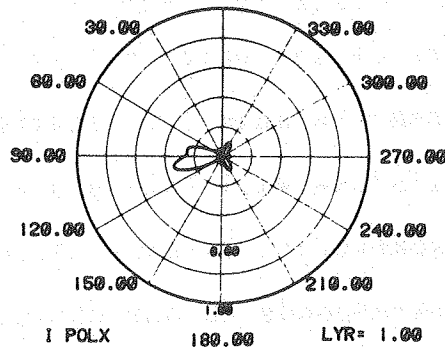
P=3.60 R=1.10  
W=1.00 L=20.0

0.00



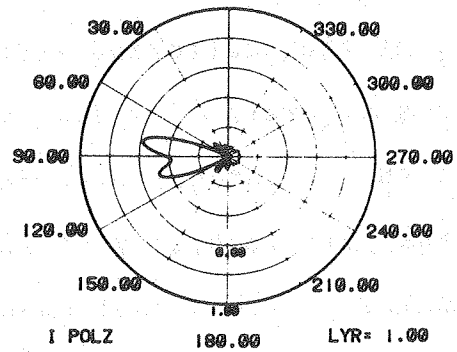
P=-3.6 R=1.10  
W=1.00 L=20.0

0.00



P=-3.6 R=1.10  
W=1.00 L=20.0

0.00



XBL 8012-12864



axis (IPOLZ) and then perpendicular to it (IPOLX). Again here the scattered intensities are asymmetric and different for the two different polarizations. For a left-handed helix the patterns invert as expected.

Anomalous scattering is a phenomenon known to be independent of the state of polarization of the incident radiation, and therefore independent of the symmetry properties of the polarizability. On the other hand, we have shown that the assumption of spherically symmetric polarizabilities in our case eliminates all the anomalous behavior of the scatterer. The reason for this apparent conflict is that anomalous scattering is independent of the symmetry properties of the polarizability only when some, but not all, of the scattering elements of the unit cell are anomalous scatterers. If all of them are anomalous scatterers, then the violations of Friedel's Law will take place only if the polarizability of the scatterers is nonspherically symmetric.<sup>5</sup> This last case corresponds to our choice for the helix. It must be pointed out that the model of absorptive scattering that has been described above must still be described as FORM-CIDS,<sup>6</sup> since no asymmetrically coupled radiation elements have been included in the model.

Qualitatively, the asymmetry observed in the scattering patterns is the result of a breakdown in the symmetry of the form contribution to the scattering. By allowing absorption bands to be present along the optical axes of

the polarizability, the helix scatters with a different efficiency, according to the position of the point in the scatterer excited by the front wave of the incident radiation. The symmetry observed in the nonabsorptive case corresponds to equal scattering efficiency of the points on the scatterer. The dispersive equations derived for the CIDS in this paper should give information about the handedness of the helical (chiral) structure as well as about the symmetry properties of the polarizability.

Bibliography

1. Rosenfeld, L., (1965) Theory of Electrons (Dover: New York).
2. Van de Hulst, H.C., (1957) Light Scattering by Small Particles (Wiley: New York).
3. Sherwood, D. (1976) Crystals, X-Rays and Proteins (Longman: New York).
4. Lipson, E., Cochran, W. (1966) The determination of Crystal Structure (G. Bell & Sons Ltd.).
5. See appendix of this thesis for a demonstration.
6. Levin, A., (1976) Ph.D. Thesis, University of California, Berkeley.

## Chapter 5

## CORRECTION OF THE INTERNAL FIELD

## BY DIPOLE-DIPOLE INTERACTION

## I. Introduction.

In Chapters 2 to 4 the theory of the form-contribution to the CIDS of chiral molecules has been presented along with numerical calculations for different parameters of the scatterer. In Chapter 2, form-CIDS is obtained by using the first-Born approximation in the internal field,<sup>1</sup> i.e., by identifying the internal field at any point in the scatterer, with the incident field. It was also shown that combining this approximation with the use of a uniaxial polarizability along a helix predicts a form-CIDS independent of the position and shape of the absorption bands of the scatterer. In Chapter 4, we were able to account for absorption band effects by using a general triaxial polarizability. Here, using a uniaxial (tangential) polarizability for a helix, we will correct the internal field, by taking into account the interaction among the dipoles induced in the scatterer. It will be shown that, in this case, the model will depend on the position and shape of the absorption bands.

In order to compare the results with those obtained in the preceding chapters, the calculations will be made for a helix of defined radius and pitch. However, an essential

difference between this model and those in the previous chapters is that, due to the nature of the dipole-dipole interaction, the distance between the dipoles must remain finite for the interaction to remain bounded. Therefore, a discontinuous helical array of point dipoles equally spaced will replace the continuous scatterer of before.

## II. The dipole-dipole interaction.

In Chapter 2, we saw that the scattered electric field at a point in space is given by the superposition of the radiation fields of the dipoles induced in the scatterer. In all derivations then, the effective perturbing field at a given point-polarizable group was assumed to be the incident field  $\underline{E}^0(\underline{r}_i)$ . This is the first Born approximation for the local field. A rather more realistic approach to describe the mutual actions between the incident field and the polarizable points in the scatterer must take into account the energy of interactions between the dipoles induced along the field. This energy takes the form:<sup>2,3</sup>

$$V_{ij} = \underline{\mu}_i \cdot \left[ \frac{1}{r_{ij}^3} - 3 \frac{\hat{r}_{ij} \hat{r}_{ij}}{r_{ij}^5} \right] \cdot \underline{\mu}_j \quad (1)$$

where  $\hat{r}_{ij}$  is the unit distance vector between the two dipoles  $\underline{\mu}_i$  and  $\underline{\mu}_j$ . Expression (1) has the form:<sup>4</sup>

$$V_{ij} = \underline{\mu}_i \cdot \underline{T}_{ij} \cdot \underline{\mu}_j$$

where  $T_{ij}$  is called the dipole interaction tensor.  $V_{ij}$  can be interpreted as the potential energy of dipole  $i$  in the field created by dipole  $j$ :

$$V_{ij} = \mu_i \cdot E_j(r_i) \quad (2)$$

From the last two expressions, we obtain:

$$E_j(r_i) = T_{ij} \cdot \mu_j \quad (3)$$

Our next step is to write the induced dipole at group  $i$  as:<sup>5</sup>

$$\mu_i = \alpha_i \cdot E^{(0)}(r_i) - \sum_{j \neq i}^N \alpha_i \cdot E_j(r_i) \quad (4)$$

where  $\alpha_i$  is the polarizability tensor of group  $i$ ,  $E^{(0)}(r_i)$  is the applied field at position  $r_i$  and  $E_j(r_i)$  has the meaning given above. Substituting (3) in (4),

$$\mu_i = \alpha_i \cdot E^{(0)}(r_i) - \sum_{j \neq i}^N \alpha_i \cdot T_{ij} \cdot \mu_j \quad (5)$$

Strictly speaking, Equation (5) constitutes a set of  $N$  linear equations, whose simultaneous solutions render the dipole induced in group  $i$ . In practice, the dipole induced at group  $j$  is approximated by:

$$\mu_j = \alpha_j \cdot E^{(0)}(r_j)$$

so that (5) becomes:

$$\underline{\mu}_i = \underline{\alpha}_i \cdot \{ \underline{E}^{(0)}(\underline{r}_i) - \sum_{j \neq i}^N T_{ij} \cdot \underline{\alpha}_j \cdot \underline{E}^{(0)}(\underline{r}_j) \} \quad (6)$$

The term in parenthesis in Equation (6) is the "corrected field" we were seeking. It says that the "effective" field at group  $i$  is given by the linear combination of the applied field and the fields caused by the electric dipoles that were induced at all the other groups, by the same initial field. The result is therefore to go from an external field to a "local" field description.

It was shown in Chapter 1 that the scattered electric field is proportional to the induced dipole and therefore from Equation (6) we can write:

$$\begin{aligned} \underline{E}_{scatt} = \frac{e^{ikr}}{4\pi r} \frac{k^2}{\underline{\underline{1}} - \underline{\underline{k}}\underline{\underline{k}}/k^2} \cdot \sum_{n=1}^N e^{i\underline{k} \cdot \underline{r}_n} \\ \underline{\alpha}_n \cdot \{ \underline{E}_0 e^{-i\underline{k}_0 \cdot \underline{r}_n} - \sum_{j \neq n}^N T_{nj} \cdot \underline{\alpha}_j \cdot \underline{E}_0 e^{-i\underline{k}_0 \cdot \underline{r}_j} \} \end{aligned} \quad (7)$$

A helical array of point dipoles can be described by:

$$\underline{r}_n = \frac{a}{M} \cos(n\theta_0) \underline{i} + \frac{a}{M} \sin(n\theta_0) \underline{j} + \frac{Pn\theta_0}{2\pi} \underline{k} \quad (8)$$

The polarizability of each group is defined now in terms of axis tangential to the helical array of these point dipoles, so that:

$$\alpha_n = \alpha_n \frac{t_n}{r_n}$$

and

$$\frac{t_n}{r_n} = -\frac{a}{M} \sin(n\theta_0) \hat{i} + \frac{a}{M} \cos(n\theta_0) \hat{j} + \frac{P}{2\pi M} \hat{k} \quad (9)$$

where  $M$  is a normalization constant defined in Chapter 2.  $\theta_0$  is the angular separation between each polarizable point along the helix, and  $n = 1, \dots, N$ . In the case of the continuous scatterer, the polarizability ( $\alpha_t$ ) was defined per unit length. Accordingly, to define a polarizability for a point dipole we must set:  $\alpha_n = \alpha_t \theta_0 M$ , where  $\theta_0 M$  is the distance between two dipoles expressed in radians. By writing  $r_{jn} = r_j - r_n$ , Equation (7) becomes:

$$E_{\text{scatt}} = F \cdot \left\{ \sum_{n=1}^N e^{i\Delta k \cdot r_n} \frac{t_n}{r_n} [\alpha_n (t_n \cdot E_0) \theta_0 M - \sum_{j \neq n} \alpha_n \alpha_j (t_j \cdot E_0) (t_n \cdot T_{nj} \cdot t_j) \theta_0^2 M^2 e^{-ik_0 \cdot r_{jn}}] \right\} \quad (10)$$

with

$$F = \frac{e^{ikr}}{4\pi r} k^2 (1 - \hat{k} \cdot \hat{k} / k^2)$$

From Equation (8), an expression for  $T_{jn}$  can be obtained and used with Equation (9) to get:

$$\frac{t_n \cdot T_{nj} \cdot t_j}{D^{2/3}} \equiv A_{jn} = \frac{1}{D} \left\{ a^2 \cos^2 \theta_{jn} + \frac{P^2}{4\pi^2} - \frac{3(a^2 \sin^2 \theta_{jn} + \frac{P^2}{4\pi^2} \theta_{jn}^2)}{D^{2/3}} \right\} \quad (11)$$



where  $\theta_{jn} = (j-n)\theta_0$  and

$$D = [2a^2(1 - \cos\theta_{jn}) + \frac{p^2}{4\pi^2} \theta_{jn}^2]^{3/2}$$

Equation (11) allows us to write the summation on  $j$  in Equation (10) in terms of  $\theta_{jn}$  and the distance vector  $\underline{r}_{jn}$ . This summation contains the interaction between each dipole and all the other dipoles induced in the scatterer. Next it can be easily seen that except for a few dipoles at both ends on the scatterer, the interaction of each dipole with all other dipoles is the same regardless of its position on the scatterer. This is true because of the symmetry of the array and because the dipole-dipole interaction, being a  $1/r^3$  interaction, is short-ranged enough so that not too many dipoles at both sides of a given group must be considered when the summation in  $j$  is evaluated. Here we will explicitly neglect those "end effects" and regard the second summation in Equation (10) as independent of  $n$ . This approximation is of course valid if  $N \gg 1$ . In the limit of  $N \rightarrow \infty$ , the neglect of the end effects does not involve any approximation. The important point for us here is that neglecting the end effects amounts to separating the two summations in Equation (9). This is of great value for performing numerical computations. Equation (10) then becomes:

$$\underline{E}_{\text{scatt}} = \underline{F} \cdot \left\{ \sum_{n=1}^N e^{i\Delta k \cdot \underline{r}_n} \underline{t}_n [(\underline{t}_n \cdot \underline{E}_0) \theta_0^M - \sum_{j \neq n}^{m \ll N} \alpha_q \alpha_j (\underline{t}_j \cdot \underline{E}_0) A_{j0} \theta_0^2 M^2 e^{-ik_0 \cdot \underline{r}_{jq}}] \right\} \quad (12)$$

where the second summation has been evaluated for say  $n = q$ . The first term in (12) has been already derived before in an equivalent way for the continuous helix. Here we will make use of (8) and (9) and write down the correction terms for the scattered fields (second term in (12)).

For incidence along  $\underline{e}_2$ , polarization along  $\underline{e}_1$ :

$$\begin{aligned} \underline{E}_{\text{scatt}}^{\text{int}} = & \sum_{n=1}^N e^{i(Qa \cos(n\theta_0 - \psi^*) + \frac{\Delta k_z P n \theta_0}{2\pi})} \left\{ -\frac{a}{M} \sin(n\theta_0) \underline{e}_1 \right. \\ & + \frac{a}{M} \cos(n\theta_0) \underline{e}_2 + \frac{P}{2\pi M} \underline{e}_3 \left. \right\} \sum_{\substack{j=1 \\ j \neq q}}^m A_{jq} \alpha^2 e^{-\frac{2\pi a}{\lambda} i \sin(j\theta_0)} \\ & (-\frac{a}{M} \sin(j\theta_0)) \theta_0^2 M^2 \end{aligned} \quad (13a)$$

For incidence along  $\underline{e}_2$ , polarization along  $\underline{e}_3$ :

$$\begin{aligned} \underline{E}_{\text{scatt}}^{\text{int}} = & \sum_{n=1}^N e^{i(Qa \cos(n\theta_0 - \psi^*) + \frac{\Delta k_z P n \theta_0}{2\pi})} \left\{ -\frac{a}{M} \sin(n\theta_0) \underline{e}_1 \right. \\ & + \frac{a}{M} \cos(n\theta_0) \underline{e}_2 + \frac{P}{2\pi M} \underline{e}_3 \left. \right\} \sum_{\substack{j=1 \\ j \neq q}}^m A_{jq} \alpha^2 e^{-\frac{2\pi a i \sin(j\theta_0)}{\lambda}} \\ & (P/2\pi M) \theta_0^2 M^2 \end{aligned} \quad (13b)$$

One final remark should be made here about Equation (12). This equation shows that the scattered field has the form of a linear plus a quadratic term in the polarizability, so that when these fields are squared and the CIDS ratio taken, the actual value of the polarizability will not cancel,

and the CIDS will depend on the position and shape of the absorption bands in the scatterer.

### III. Numerical Calculations.

#### 1) The transmission band.

A general result of the form-CIDS theory developed in Chapters 2-4 is that the CIDS in the forward direction is always zero, regardless of the geometrical and electronic properties of the scatterer. This result is still true when a general polarizability is used and the wavelength of light is within an absorption band of the scatterer. As explained in Chapter 2, when light interacts with, say, two groups,  $i$  and  $j$ , two effects take place. First, each of the groups is perturbed by the incident field and in turn radiate or "scatter" light in all directions. Second, phase shifts between the wavelets originated in different groups in the scatterer introduce a diffraction phenomenon in this scattered field. This interference effect is a function of the relative position of the two groups, and is more pronounced as the wavelength of light approaches the distance between the scattering groups. In Figure 5 of Chapter 2, it was shown that the phase difference responsible for the interference phenomenon is given by the term  $e^{i(\underline{k}-\underline{k}_0)\cdot\underline{r}}$  appearing in all scattering equations. Indeed,  $(\underline{k}-\underline{k}_0)\cdot\underline{r}$  is the path difference traveled by light scattered from two different groups. Clearly, in the forward direction  $\underline{k}-\underline{k}_0 = 0$  and

the phase difference vanishes. As a result, no diffraction phenomenon of the scattered fields takes place along the direction of the incident light. Since form-CIDS is a diffraction phenomenon, in the forward direction CIDS is unable to differentiate between two opposite handed structures. Indeed, let  $i$  and  $j$  be two similar groups in the scatterer. The scatterer field for incident right circularly polarized light can be written (through a proportionately constant  $c$ ):

$$\vec{E}_R^{\text{scatt}} = c(\alpha \cdot \vec{E}_R e^{i\Delta\vec{k} \cdot \vec{r}_i} + \alpha \cdot \vec{E}_R e^{i\Delta\vec{k} \cdot \vec{r}_j})$$

where  $\vec{E}_R$  is the amplitude of the incident field. For left circularly polarized light the scattered field is:

$$\vec{E}_L^{\text{scatt}} = c(\alpha \cdot \vec{E}_L e^{i\Delta\vec{k} \cdot \vec{r}_i} + \alpha \cdot \vec{E}_L e^{i\Delta\vec{k} \cdot \vec{r}_j})$$

In the forward direction  $\Delta\vec{k} = \vec{k} - \vec{k}_0 = 0$  and it can be shown that:

$$[(\vec{E}_L^{\text{scatt}})(\vec{E}_L^{\text{scatt}})^* - (\vec{E}_R^{\text{scatt}})(\vec{E}_R^{\text{scatt}})^*]_{\text{forward}} = 0$$

(14)

Result (14) shows that the forward form-CIDS obtained within the frame of the first-Born approximation lacks any diffraction contribution and therefore cannot give any information regarding the chiral array of the dipoles in the scatterer.

On the other hand, in the dipole coupling case of Equation (12), the scattered field for incident right (R) and left (L) circularly polarized light is of the form (for groups  $i$  and  $j$ ):

$$\begin{aligned} \vec{E}_{R,L}^{\text{scatt}} = c \{ & \alpha_{\vec{r}_i} \cdot \vec{E}_{R,L} e^{i\Delta\vec{k} \cdot \vec{r}_i} + \alpha_{\vec{r}_j} \cdot \vec{E}_{R,L} e^{i\Delta\vec{k} \cdot \vec{r}_j} \\ & - e^{i\Delta\vec{k} \cdot \vec{r}_i} \alpha_{\vec{r}_{ij}} \cdot \vec{T}_{ij} \cdot \alpha_{\vec{r}_j} \vec{E}_{R,L} e^{-i\vec{k}_0 \cdot \vec{r}_{ij}} - \dots \} \end{aligned} \quad (15)$$

Again, for forward scattering  $\Delta\vec{k} = 0$ ; however, the dipole-dipole interaction has introduced in expression (15) a phase difference proportional to the vector distance between group  $i$  and  $j$ . When  $I_L - I_R$  is obtained from (15), it can be shown that the expression is not zero. The result is that within the dipole-dipole approximation to the local field, interference in the forward direction is present and forward scattering should give information on the relative position of the dipoles. In particular, forward CIDS values carry information on the relative chiral orientations of the scattering dipoles.

## 2) Forward CIDS vs. CD.

An important point to make clear here is that the forward differential scattering intensities predicted by the dipole coupling model must not be interpreted as circular dichroism, since it is present regardless of the existence of an absorption band in the scatterer. Forward CIDS

is a purely diffraction phenomenon carrying an equivalent information to that given by CD, but not involving, as the latter, a differential absorption. Equation (12) shows that the phase difference responsible for the forward interference has the form:

$$i \frac{2\pi}{\lambda} |\underline{r}_{jq}| (\hat{k}_0 \cdot \underline{r}_{jq})$$

where " $\hat{\quad}$ " label unit vectors. Clearly for  $\lambda \gg |\underline{r}_{jq}|$ , this phase difference tends to zero and the forward CIDS should vanish in the limit of  $\lambda \rightarrow$  very large. On the other hand, if  $\lambda$  is large the terms corresponding to groups very far apart so that  $|\underline{r}_{jq}| \sim \lambda$  will not contribute significantly, since the dipole-dipole interaction term  $\underline{\alpha}_i \cdot \underline{T}_{ij} \cdot \underline{\alpha}_j$  dies off quite fast with the distance between the dipoles. The two arguments presented above are the rationale of why, in most cases, the CD signal measured in the forward direction will not be perturbed by a sizeable CIDS contribution. Only when the wavelength of light is not too large as compared to the distance between the groups, would the forward-CIDS contribute significantly to the observed CD. Some molecular arrays such as cholesteric liquid crystals<sup>6</sup> or macromolecular aggregates<sup>7</sup> seem to fulfill these requirements, showing huge ellipticities in the forward direction. When circularly polarized X-rays become available, forward CIDS intensities would be a powerful technique to determine the structure in chiral molecules.

### 3) Programming strategies.

Numerical computations to correct the scattering fields for a dipole-dipole interaction were carried out in the computer center of the Lawrence Berkeley Laboratory. In these calculations, Equations (13a) and (13b) were used, together with equivalent equations for the non-interacting fields of point dipoles in a helical array. The summations on  $n$  in these equations were carried out to  $n = 360$  to obtain reasonably symmetric patterns. The summation on index  $j$ , labeling the range of dipole-dipole interaction, was carried out from  $j = -10$  to  $j = +10$ . This last choice was proven to be good enough, since the angular distance between the discrete dipoles was never smaller than  $\theta_0 = .3$  radians or  $\sim 18$  degrees.

The program called COCO was set to obtain the value of the CIDS and total scattering for varied values of the scatterer's parameters and polarizabilities. (A listing can be seen in the appendix). The polarizabilities were chosen uniaxial along the tangent to the helical array. In all cases computed, a Lorentzian-shaped polarizability of the form:

$$\alpha = \frac{f}{\left(\frac{1}{\lambda_0^2} - \frac{1}{\lambda^2}\right) + \frac{i\Delta\lambda}{\lambda\left(\lambda_0^2 - \frac{(\Delta\lambda)^2}{4}\right)}}$$

was used, where  $f$  and  $\lambda_0$  are the strength and position of the absorption bands, respectively (see Chapter 4).

## 4) Results.

Figure 1 shows the total scattering and the CIDS for a helix of pitch  $P = 5.0$ , radius  $R = 1.0$  and for wavelength of light  $\lambda = .5$  and  $\lambda_{0t} = 3.0$ . The light is incident along the  $270^\circ$ - $90^\circ$  axis ( $e_2$ -incidence). Only the zeroth layer line is shown. The strength of the band was chosen to be  $f = .10$ . The angular distance between the point dipoles is  $\theta_0 = .3$ . As predicted by the theory, forward differential scattering is observed in the zeroth layer line. According to the discussion in the last section, the magnitude of the forward scattering depends on the relative size of the correction term with respect to the non-interaction part of the field. Figure 2 illustrates this effect for a helix of the same parameters as in Figure 1, but with the band strength  $f = .5$ .

When  $f \gg 1$  the dipole-dipole interaction term dominates and the scattering pattern becomes spherically symmetric. This result is general and valid for any combination of the structural parameters of the scatterer. For moderate values of the strength of the band, both terms in the field contribute to the scattering behavior.

In Figure 3 the effect of reducing the wavelength of light to the size of the distance between the dipoles in the scatterer is shown (see figure captions for details). It can be seen that the ratio  $R/\lambda$  (in this case, greater than 3) still controls the number of zeros of the scattering pattern,



Figure 1. Polar plot of CIDS corrected for dipole-dipole interaction of a helix made out of discrete points, polarizable along the tangent to the helix and separated by an angular distance  $\theta_0 = .3$  radians. The helix parameters are: pitch = 5.0, radius = .1, wavelength = .5, the band position  $\lambda_{0t} = 3.0$  and the band strength  $f = .1$ . The main feature is the existence of a non-vanishing forward CIDS. There are many lobes alternating in sign but the negative ones in this case are too small to be seen in the figure.

P=5.00 R=1.00 TB=3.00  
W= .50 L=20.0  
0.00

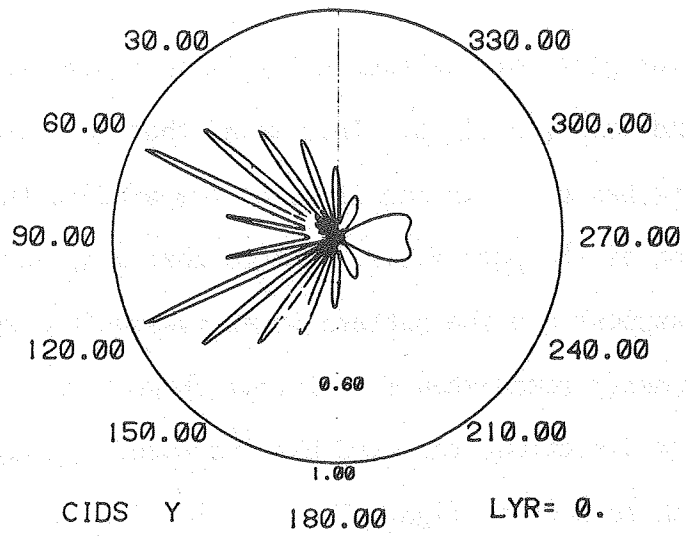
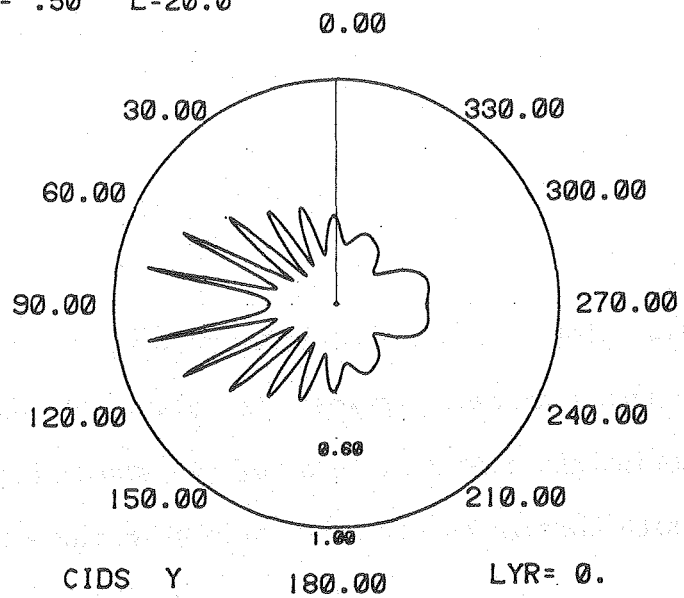


Figure 2. Polar plot for the same helix as in figure 1, but with a band strength of .5. This means that the interaction term has grown in magnitude as compared to the contribution of the pure field. Notice that many zeros have disappear and the pattern moves towards the spherical symmetry found when  $f \gg 1$  (not shown here). In the forward direction, the CIDS has increased significantly with respect to figure 1.

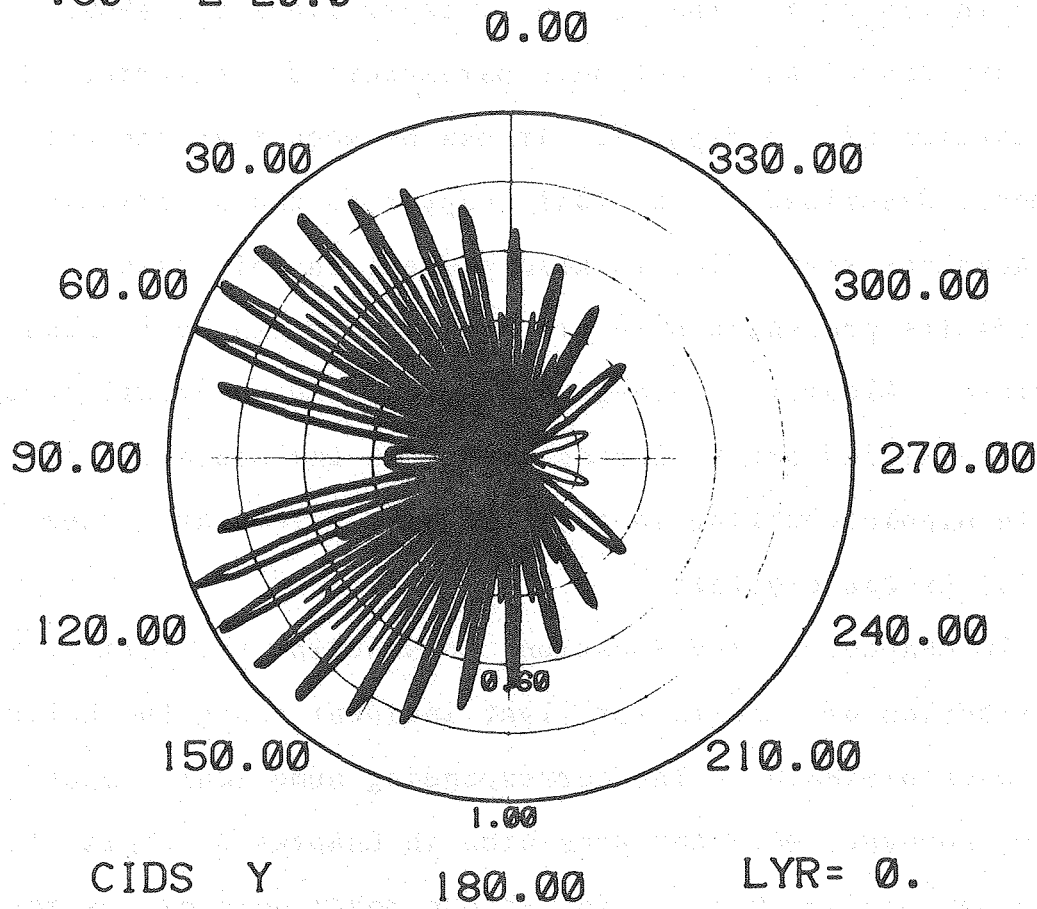
P=5.00 R=1.00 TB=3.00.  
W= .50 L=20.0



XBL 8012-12997

Figure 3. Polar plot of a helix of pitch = 10.0, radius = 1.0, wavelength = distance between the polarizable points = .3.  
Notice the number of zeros of the scattering pattern which correlates with the ratio of radius/wavelength.

P=10.0 R=1.00 TB=3.00  
W= .30 L=20.0



as found before for the form-CIDS.

In all cases studied, when  $f \ll 1$ , the form-CIDS contribution dominated. This served as an internal check in the program.

The effect of going through an absorption band is shown in Figure 4. The +1 and -1 layer lines are shown (the structural and electronic parameters are described in the caption of the figure). It can be seen that the anti-symmetry described in the last chapter as characteristic of anomalous scattering is also present in this case. The results presented here are preliminary and by no means complete. Clearly, thorough analytical and numerical studies must be carried out to characterize the influence of the dipole-dipole coupling in the CIDS of a molecular system.

#### 5) Liquid crystals.

In Chapter 2, the equations to describe the form-CIDS contribution of a helix for light incident along the helix axis were presented. The corresponding numerical computations, however, were not presented in Chapter 3. This case is of particular interest, for it can model some of the most striking effects observed in the optical activity of cholesteric liquid crystals.<sup>8</sup> Program PAN (see listing in appendix) was used to perform the calculations. For  $P/\lambda = 1$  and incidence along the helix axis, only three scattering directions in space are allowed: 1) in the back direction (reflexion), 2) the scattering perpendicular to the helix axis, and 3) in





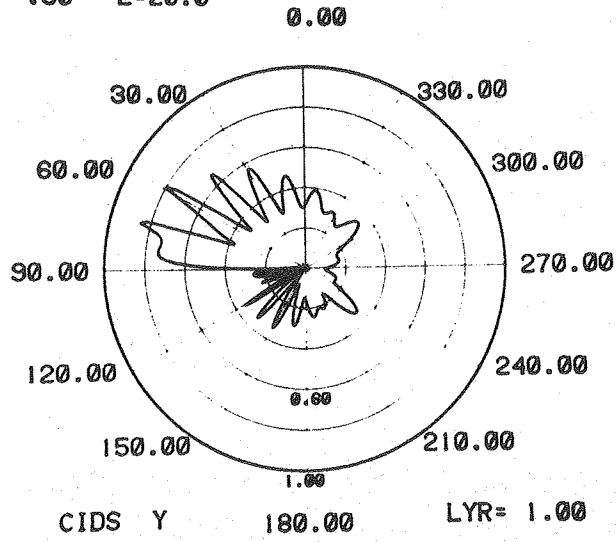
Figure 4. Polar plot of the CIDS of the same helix as in figure 1 but now with the wavelength of the incident light within the absorption band of the scatterer. Notice that the pattern is asymmetric but shows the anomalous anti-symmetry for layer lines equidistant from the in-plane scattering (zeroth layer line).





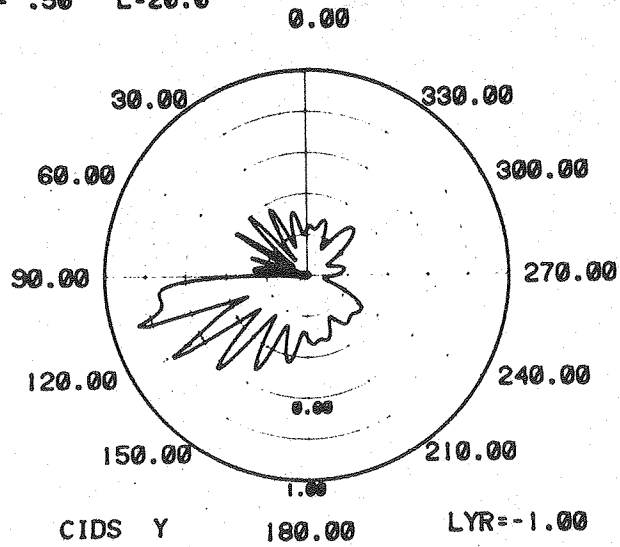
P=5.00 R=1.00  
W= .50 L=20.0

TB= .50.



P=5.00 R=1.00  
W= .50 L=20.0

TB= .50.



the forward direction (transmission). The latter is not present for the CIDS within the first Born approximation.

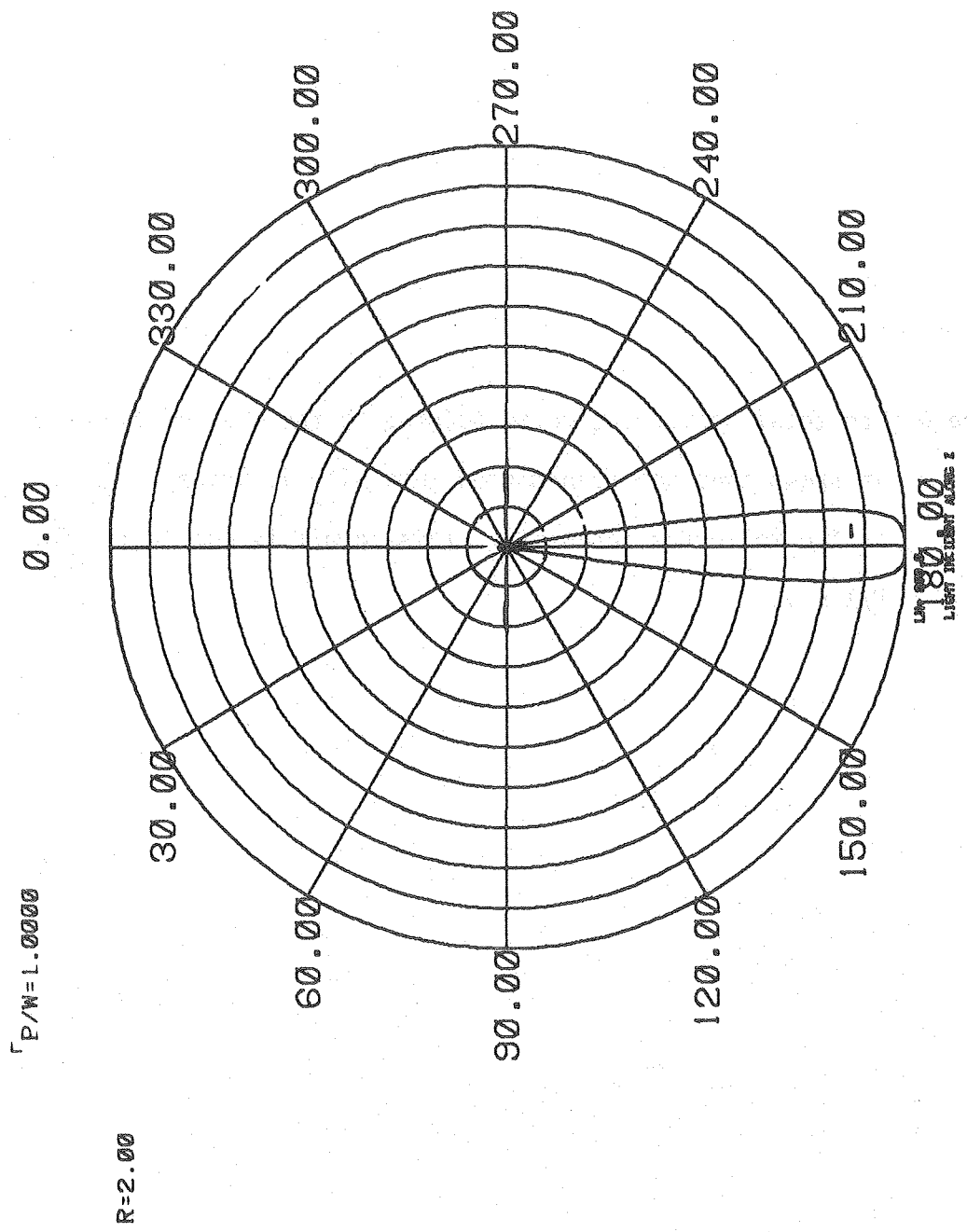
When the pitch of the helix matched the wavelength of light, it was found that only one of the circular polarizations of the light was reflected. The other polarization was not reflected at all. The polarization reflected matched the handedness of the helix, so that CIDS in the backward direction is -1 for a right-handed helix (see Figure 5) and +1 for a left-handed helix. This effect is unique for the ratio  $P/\lambda = 1$  but is independent of the radius of the helix, which seems to affect only the relative size of the perpendicular intensities. The reflexion effect described above is precisely what is found in cholesteric liquid crystals<sup>8</sup> (see also Chapter 1) for the reflexion band, when  $P/\lambda = 1$ . In the cholesteric mesophases the radius  $R$  has no meaning, of course, which is equivalent in our model to the independence of the result on the radius of the helix. The total scattering for the case just described can be seen in Figure 6. This figure shows that only three layer lines exist. The back scattering is found to be 50% of the forward scattering when  $P/\lambda = 1$ . Since:

$$I_L(0^\circ) + I_R(0^\circ) = 2(I_L(180^\circ) + I_R(180^\circ))$$

and  $I_L(180^\circ) = 0$  and  $I_L(0^\circ) = I_R(0^\circ)$ . Then, it follows that:

$$I_R(180^\circ) = I_R(0^\circ)$$

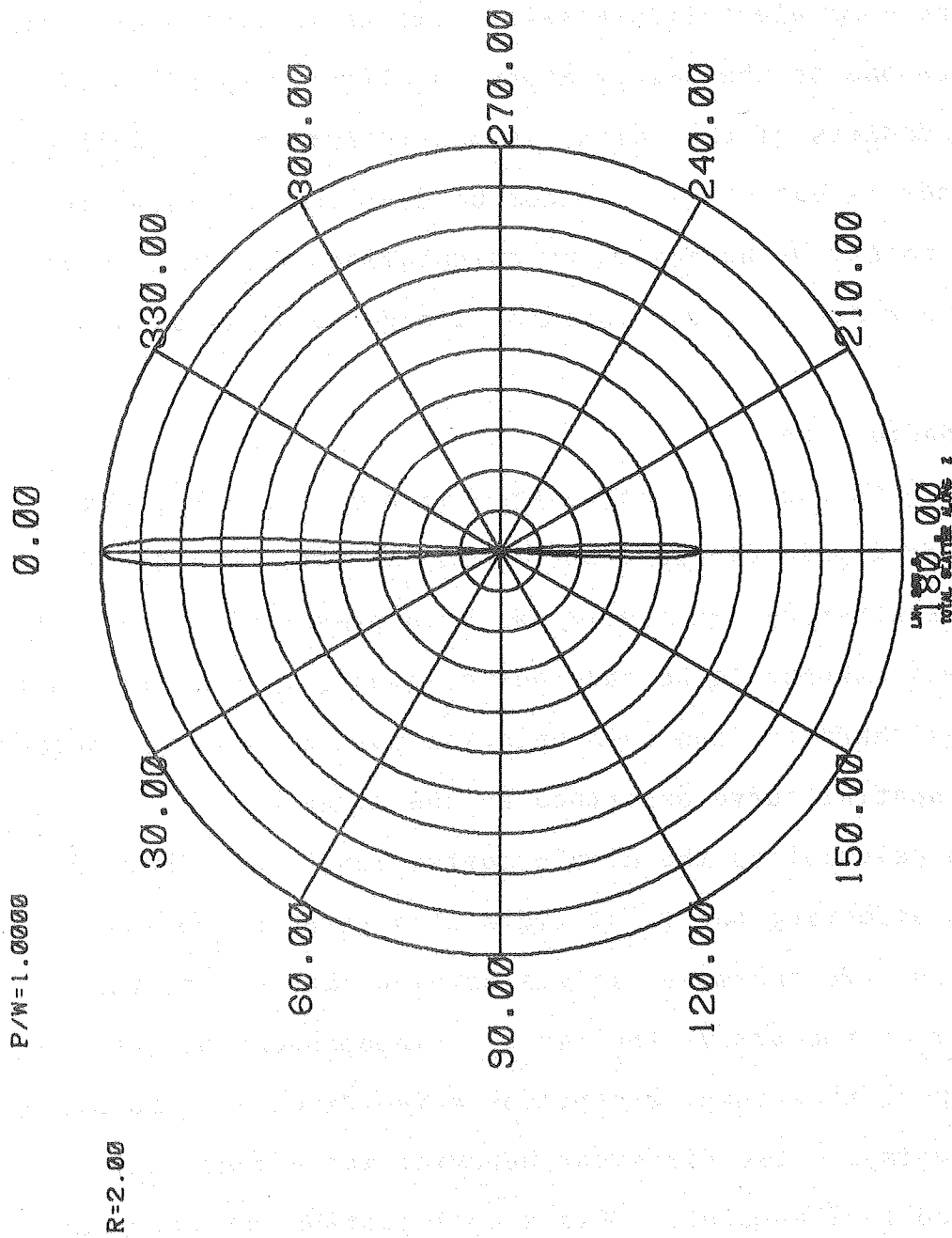
Figure 5. Polar plot of the form CIDS of a helix for light incident along the helix axis. This is a plot of intensities vs. the polar angle, for a fixed value of the azimuthal angle ( $\psi$ ). The plane of the plot is therefore perpendicular to the plane of the polar plots of figures 1 to 4. The pitch of the helix is 1.0, radius = 2.0 and the wavelength matches the pitch of the helix. Notice that CIDS = -1 for a right handed helix in the reflexion band. No form-CIDS is obtained in the forward direction.



XBL 8012-12963

Figure 6. The total scattering corresponding to the case of figure 5.

It shows that the transmitted intensity is twice as much as the reflected intensity. This result is only valid for  $P/\lambda = 1$ .



i.e., the polarization that matches the handedness of the helix is scattered in the forward and backward direction with the same intensity in the first Born approximation.

The equivalent transmission effects in liquid crystals, in which one of the polarizations of light, depending on the handedness of the helix, is mostly transmitted while the other is not at all, cannot be described by form-CIDS. At this point, we have made no calculations for the dipole coupling model of light incident along the helix axis.

#### IV. Conclusions.

In this chapter a correction of the internal field by a term of dipole-dipole coupling in the total and differential scattering of a helix has been presented. The scatterer was assumed to be made out of groups in a helical array, each one characterized by a uniaxial polarizability, tangential to the spatial curve described by the array.

In calculating the dipole correction, the number of dipoles affecting the local field at a given group was truncated. Furthermore, it was assumed that, due to the symmetry of the array, the field is independent of the position of the group, except for a few dipoles at both ends of the array, whose different behavior was effectively neglected in the model. This simplification was necessary in order to obtain simpler equations as well as to reduce the cost of the programming. The number of dipoles considered

at each side of a given group was 10. Under these conditions it has been found that the dipole-coupling correction of the internal field allows for diffraction phenomena of the scattered fields to occur in the forward direction. This appears as a phase shift in the correction terms, which does not vanish when  $\underline{k} = \underline{k}_0$ . The result is that finite CIDS values in the forward direction are predicted by this model. For wavelengths of light large compared to the distance between the coupled dipoles, the corresponding phase factors become very small and the forward CIDS vanishes.

Numerical computations of the CIDS along the axis of a helix and within the first Born approximation show that for values of the pitch close to the wavelength of light, reflexion of only one of the polarization occurs, giving CIDS reflexion bands of  $\pm 1$  depending on the handedness of the helix. This phenomenon observed in cholesteric liquid crystals seems therefore to be a purely form-effect. On the contrary, the corresponding transmission bands cannot be observed within the first-Born approximation used in the computation. These results are preliminary and the basis of more careful characterization of the "local field" corrections to the total and differential scattering of chiral molecules.



Bibliography

1. Saxon, D. S. (1955) "Lectures on the Scattering of Light", Sci. Rep. No. 9, Contract AF 19(122)-239, Dept. Metereol., University of California, Los Angeles, 100 pp.
2. Jackson, J. D., (1975) Classical Electrodynamics (John Wiley & Sons, Inc. : New York).
3. Hang, E. R., Hirschfelder, J. D., (1955) J. Chem. Phys. 23, 1779.
4. De Voe, H. (1964) J. Chem. Phys. 41, 393-400.
5. De Voe, H., (1965) J. Chem. Phys. 43, 3199-3208.
6. De Gennes, P. G. (1974) The Physics of Liquid Crystals (Clarendon: Oxford).
7. Tinoco, I., Jr., Bustamante, C., Maestre, M.F. (1980) Ann. Rev. Biophys. Bioeng. 9, 107-141.
8. Chandrasekhar, S. (1974) Liquid Crystals (Cambridge University Press: London).

## Chapter 6

SPATIAL AVERAGING OF DIFFERENTIAL  
AND TOTAL SCATTERING

## I. Introduction.

In the main body of this thesis, our objective has been to characterize and derive analytically the equations to describe the Circular Intensity Differential Scattering of a chiral molecule. As a result, we have shown the possibility of interpreting the measured differential scattered intensities in terms of the structure of the chiral scatterer. Indeed, we think CIDS will become important as a new technique to probe chiral regions in biologically relevant structures.

The effort to obtain analytical solutions from which we have learned some of the physical properties and symmetry laws involved in the total and differential scattered intensities imposed certain limitations in the treatment of Chapters 2 and 3. The main one has been that the scatterer was assumed to have a fixed orientation in space. Clearly, the experimental difficulties in orienting the samples to be studied greatly limits the potential capabilities of CIDS as a useful technique. It is therefore of prime importance to obtain spatial averages of the total and differential scattered intensities so as to provide the

theoretical basis for the interpretation of data obtained from the analysis of samples in solution. This objective will be accomplished in this chapter.

Since the measured signal at the photomultiplier for a tumbling sample is  $\langle I_L - I_R \rangle_{av}$ , our goal will be to obtain the corresponding averages for the differential and total scattering.

The total scattering intensity for a given sample is the same regardless of the two independent, orthogonal states of polarizations used to describe the incident radiation. Therefore, instead of deriving the averaged total scattered intensity for right and left circularly polarized incident radiation (i.e.:  $I_L + I_R$ ), we will derive  $I_{\parallel} + I_{\perp}$  where  $I_{\parallel}$  and  $I_{\perp}$  are the scattered intensities for incident light polarized parallel and perpendicular to the scattering plane, respectively. There are two reasons for this choice: first, the derivations of  $I_L + I_R$  are more involved than those of  $I_{\parallel} + I_{\perp}$ , and second, choosing these polarization states, it is easy to calculate also  $\langle I_{\parallel} - I_{\perp} \rangle_{av}$  from which the quantity  $\langle I_{\parallel} - I_{\perp} \rangle_{av} / \langle I_{\parallel} + I_{\perp} \rangle_{av}$ , often called the dichroic ratio, can be obtained.

## II. Averaging of $I_L - I_R$ .

- 1) The molecule-fixed and the space-fixed coordinate systems.

The field scattered by a set of polarizable groups in space, for a given incident field  $E_0$ , can be written as:

$$\tilde{E}(r') = C e^{-ikr'} (1 - \hat{k}\hat{k}) \cdot \sum_j e^{i\Delta k \cdot r_j} \tilde{\alpha}_j \cdot E_0 \quad (1)$$

where  $r_j$  is the position vector of group  $j^{\text{th}}$  defined in a suitable molecular frame,  $\tilde{\alpha}_j$  is the polarizability tensor of the  $j^{\text{th}}$ -group and  $C$  is a constant of proportionality containing some inverse distance factors. As before,  $\Delta k = k - k_0$ , i.e., the momentum transfer vector and  $k$  and  $k_0$  are the wave-vectors of the scattered and incident radiation, respectively.  $\hat{k}$  is a unit vector in the direction of the scattered light.

Now we define a molecule-fixed coordinate system, whose orthogonal unit vectors are  $i'$ ,  $j'$ , and  $k'$  (see Figure 1). The polarizability tensor of the  $j$ -group can now be written as (see Figure 1):

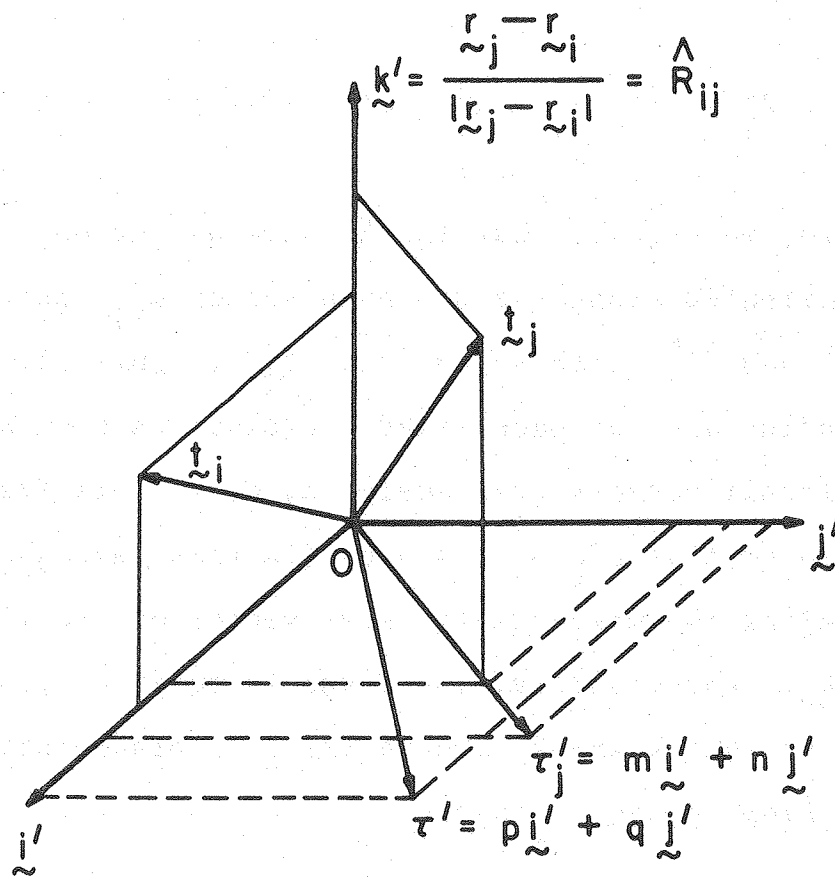
$$\tilde{\alpha}_j = \alpha_j t_{j\sim} t_{j\sim}$$

where the subindex  $j$  labels the group. The  $t$ 's are unit vectors in the molecular coordinate system whose three components along this frame determine uniquely the axes of the polarizability of group  $j$ . Since this frame is defined arbitrarily, we orient it so that (see Figure 1):

$$t_{i\sim} = \ell_{i\sim} k' + s_{i\sim} i' \quad (2a)$$

Figure 1. The molecule-fixed coordinate system with basis vectors  $\underline{i}'$ ,  $\underline{j}'$ ,  $\underline{k}'$  is shown. The frame is oriented so that the polarization vector  $\underline{t}_i$  of the group  $i^{\text{th}}$  is in the plane  $(\underline{i}', \underline{k}')$  and the polarization vector  $\underline{t}_j$  of the group  $j^{\text{th}}$  is in the plane defined by  $\underline{k}'$  and  $\underline{\tau}'_j$ . The unit vector  $\underline{\tau}'_j$  is shown in the plane  $(\underline{i}', \underline{j}')$ . Notice that  $\underline{R}_{ij}$ , the distance vector between groups  $i^{\text{th}}$  and  $j^{\text{th}}$ , is along  $\underline{k}'$ .

XBL 8012-12956



and

$$\underline{t}_j = \ell_j \underline{k}' + s_j \hat{\underline{t}}_j' \quad (2b)$$

with  $\hat{\underline{t}}_j'$  a unit vector perpendicular to  $\underline{k}'$  and defined by:

$$\hat{\underline{t}}_j' = m_i' + n_j' \quad (3)$$

Clearly

$$\ell_i^2 + s_i^2 = \ell_j^2 + s_j^2 = m^2 + n^2 \equiv 1 \quad (3a)$$

Furthermore, we require that the  $\underline{k}'$  axis of the molecular frame is oriented along the distance-vector  $\hat{R}_{ij}$  between groups  $i^{\text{th}}$  and  $j^{\text{th}}$ , with  $R_{ij} = |\underline{r}_i - \underline{r}_j|$  (Figure 1).

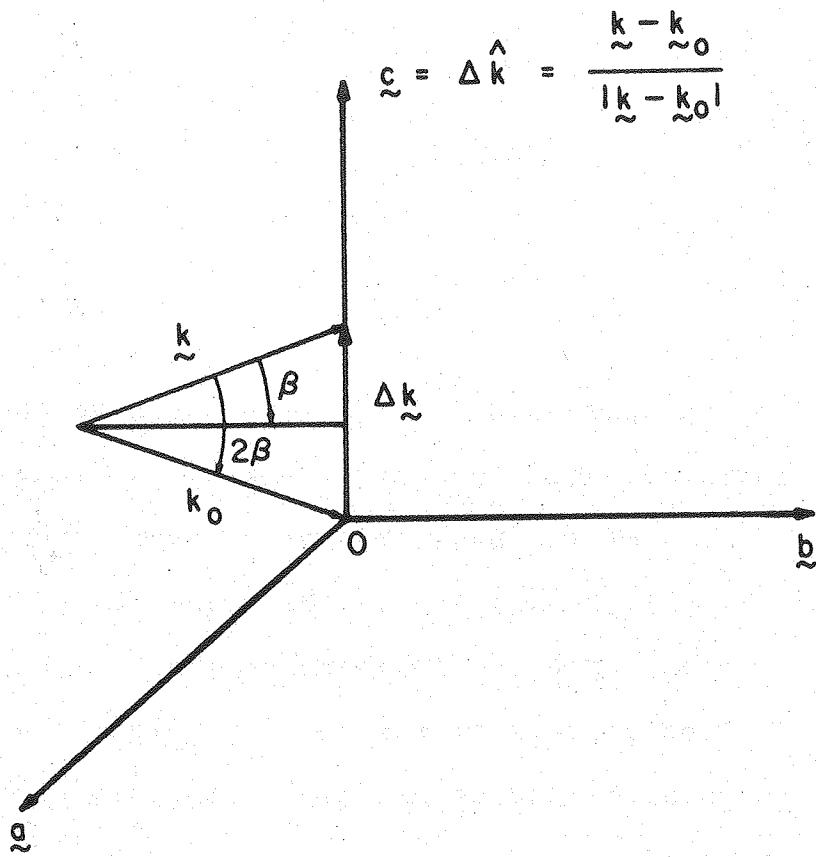
We define also a space-fixed coordinate system whose orthogonal unit vectors are labeled  $\underline{a}$ ,  $\underline{b}$ ,  $\underline{c}$ . This frame is oriented so that one of its axes (in this case the  $\underline{c}$ -axis) is along the momentum transfer vector of the light,  $\Delta \underline{k} \equiv \underline{k} - \underline{k}_0$ . Additionally, the frame is rotated around this axis so that  $\underline{k}$  and  $\underline{k}_0$  are in the  $\underline{c}$ ,  $\underline{b}$  plane (see Figure 2). From Figure 2, then:

$$\Delta \underline{k} = 4\pi/\lambda \sin\beta \underline{c} \quad (4)$$

$$\hat{\underline{k}} = \cos\beta \underline{b} + \sin\beta \underline{c}$$

Figure 2. The space-fixed frame with basis vectors  $\underline{a}$ ,  $\underline{b}$ ,  $\underline{c}$  is oriented so that  $\Delta \underline{k} = \underline{k} - \underline{k}_0$  is along the direction of the basis vector  $\underline{c}$ . The wave-vectors of light  $(\underline{k}, \underline{k}_0)$  are in the plane  $(\underline{b}, \underline{c})$  that coincides with the scattering plane. The polarization vectors of the incident light are defined parallel and perpendicular to this plane (See text).





XBL 8012-12958

$$\hat{k}_0 = \cos\beta \underline{b} - \sin\beta \underline{c}$$

where " $\hat{\quad}$ " indicates that these vectors are unit vectors along the incident and scattered directions of propagation of the light. From Figure 2, it is easy to derive the right and left circular polarization unit vectors of the incident light:

$$E_{L,R}^0 = \underline{A} \pm i\underline{B} = \frac{1}{\sqrt{2}} [\underline{a} \pm i(\sin\beta \underline{b} + \cos\beta \underline{c})] \quad (5)$$

Using the last expression, the scattered electric field for the opposite circular polarizations of the incident light can be obtained, from which the differential scattered intensity for left and right circularly polarized light takes the form:

$$I_L - I_R = 2iC^2 \sum_{ij} \alpha_j \alpha_i^* \frac{i\Delta k \cdot (\underline{r}_j - \underline{r}_i)}{[\underline{A} \times \underline{B}] \cdot (\underline{t}_j \times \underline{t}_i)} \cdot [(\underline{t}_j \cdot \underline{t}_i) - (\underline{t}_j \cdot \hat{k})(\underline{t}_i \cdot \hat{k})] \quad (6)$$

From (2) we find:

$$\underline{t}_j \times \underline{t}_i = x\underline{k}' + y\underline{l}' \quad (7)$$

where  $\hat{\underline{t}}'$  is a unit vector perpendicular to  $\underline{k}'$  and defined by:

$$\hat{\underline{t}}' \equiv p\underline{i}' + g\underline{j}' \quad (8)$$

Similarly, from (5):

$$\underline{A} \times \underline{B} = \frac{1}{2} (\sin\beta \underline{c} - \cos\beta \underline{b}) \quad (9)$$

It should be clear that the somewhat particular choice of the molecule-fixed and space-fixed frames has the advantage of rendering  $\underline{t}_i$ ,  $\underline{k}$ , and  $\underline{k}_0$  as two-component vectors in their respective frames.<sup>1</sup> This will simplify the derivations. In the next section a more important justification for this choice will be made clear.

## 2) The Euler transformations.

Our task is to perform the spatial averaging of Equation (6). The space integrations involved in the averaging process can become very difficult due to the term  $e^{i\Delta\underline{k} \cdot (\underline{r}_j - \underline{r}_i)}$  comprising the product of a space-fixed vector  $\Delta\underline{k}$  and a molecule-fixed vector ( $\underline{r}_j - \underline{r}_i \equiv R_{ij}$ ). Our choice of orienting the space-fixed coordinate system with one of its axes along  $\Delta\underline{k}$  and the molecule-fixed frame with one of its axes along  $R_{ij}$  can now be understood.

Indeed, with this choice, the product  $R_{ij} \cdot \Delta k$  is a constant for any orthogonal transformation between the two coordinate systems, with the exception of the transformation involving the angle between the polar axes ( $k'$  and  $c$ ) of these cartesian systems. In this way the factor  $e^{i\Delta k} \cdot R_{ij}$  can be dealt with in the last step of the spatial integrations evaluated in the averaging process.

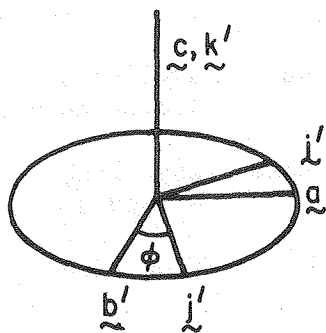
In what follows we will use the three orthogonal transformations proposed by Euler and frequently called the Euler angles<sup>2</sup> (see Figure 3) to relate the space-fixed quantities to the molecule-fixed expressions appearing in expression (6).

The transformation matrix between these frames, often called the Euler-matrix, allows us to express any product between space-fixed and molecule-fixed basis-vectors, in terms of the three Euler angles. The Euler matrix relates these basis vectors by:

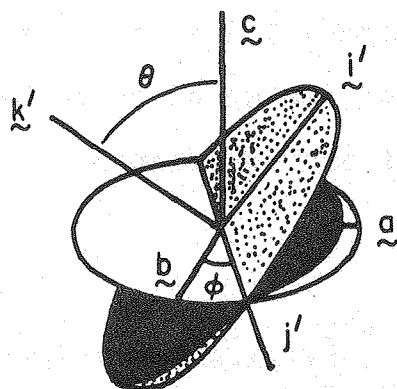
$$\underline{e}' = \xi \underline{e} \quad (10)$$

where  $\underline{e}'$  and  $\underline{e}$  denote a space-fixed and a molecule-fixed basis vector, respectively. The matrix  $\xi$ , for the three successive transformations in Figure 3, takes the form:<sup>3</sup>

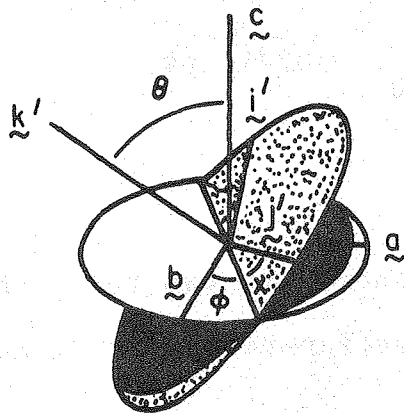
Figure 3. The three orthogonal transformations that define the Euler angles between the space-fixed and the molecule-fixed coordinate system, are seen in succession. In the text  $\underline{c}$  and  $\underline{k}'$  are called the polar-axes of these frames.



(a)



(b)



(c)

XBL 8012-12959

$$\begin{array}{r}
 \xi = \begin{array}{l} \tilde{i}' \\ \tilde{j}' \\ \tilde{k}' \end{array} = \begin{array}{l} \begin{array}{ccc} \tilde{a} & \tilde{b} & \tilde{c} \\ \cos\theta \cos\chi \cos\phi & \sin\chi \cos\phi & -\sin\theta \cos\chi \\ -\sin\chi \sin\phi & +\cos\theta \cos\chi \sin\phi & \end{array} \\ \begin{array}{ccc} -\cos\theta \sin\chi \cos\phi & \cos\chi \cos\phi & \sin\theta \sin\chi \\ -\cos\chi \sin\phi & -\cos\theta \sin\chi \sin\phi & \end{array} \\ \begin{array}{ccc} \sin\theta \cos\phi & \sin\phi \sin\theta & \cos\theta \end{array} \end{array} \quad (11)
 \end{array}$$

The spatial averaging involves the integration over the three Euler angles of the quantity to be averaged. Indeed, the averaging of any function  $f(\theta, \chi, \phi)$  can be accomplished by:

$$\begin{aligned}
 \langle f(\theta, \chi, \phi) \rangle_{av} &= \int_0^\pi \int_0^{2\pi} \int_0^{2\pi} f(\theta, \chi, \phi) \sin\theta d\theta d\chi d\phi / \\
 & \int_0^\pi \int_0^{2\pi} \int_0^{2\pi} \sin\theta d\theta d\chi d\phi \quad (12)
 \end{aligned}$$

### 3) Averaging of $I_L - I_R$ .

In expression (6) there are two terms that must be averaged. First, the nontransversal term, which with (9) and (7) becomes:

$$\begin{aligned}
 (\tilde{A} \times \tilde{B}) \cdot (\tilde{t}_j \times \tilde{t}_i) &= \frac{1}{2} [x \sin\beta (\tilde{c} \cdot \tilde{k}') - x \cos\beta (\tilde{b} \cdot \tilde{k}') \\
 & \quad + y \sin\beta (\tilde{c} \cdot \hat{\tilde{t}}') \\
 & \quad - y \cos\beta (\tilde{b} \cdot \hat{\tilde{t}}')]
 \end{aligned}$$

Using the Euler-matrix, it can be shown that the only term that does not vanish in the process of averaging is the first of the right-hand side:

$$\begin{aligned} \langle (\underline{c} \cdot \underline{k}') e^{i\Delta \underline{k} \cdot \underline{R}_{ij}} \rangle_{av} &= \int_0^\pi \frac{\sin\theta \cos\theta}{2} e^{iq \cos\theta} d\theta \\ &= i j_1(q) \end{aligned} \quad (13)$$

where  $q = \frac{4\pi}{\lambda} R_{ij} \sin\beta$  and  $j_1$  is the first-order spherical Bessel function<sup>4</sup> and is defined as:

$$j_1(q) = \frac{\sin q}{q^2} - \frac{\cos q}{q}$$

Next we average the transversality term in expression (6):

$$\langle (\underline{A} \times \underline{B}) \cdot (\underline{t}_j \times \underline{t}_i) (\underline{t}_i \cdot \hat{\underline{k}}) (\underline{t}_j \cdot \hat{\underline{k}}) e^{iq \cos\theta} \rangle_{av}$$

After expanding this expression in terms of (2), (7), and (9), we obtain:

$$\begin{aligned} &\langle \frac{1}{2} \{ x \sin\beta (\underline{c} \cdot \underline{k}') - x \cos\beta (\underline{b} \cdot \underline{k}') + y \sin\beta (\underline{c} \cdot \hat{\underline{t}}') \\ &- y \cos\beta (\underline{b} \cdot \hat{\underline{t}}') \} \{ \ell_i \ell_j (\underline{k}' \cdot \hat{\underline{k}})^2 + (\hat{\underline{t}}' \cdot \hat{\underline{k}}) (\underline{k}' \cdot \hat{\underline{k}}) \\ &+ s_i s_j (\underline{i}' \cdot \hat{\underline{k}}) (\hat{\underline{t}}_j' \cdot \hat{\underline{k}}) \} e^{iq \cos\theta} \rangle_{av} \end{aligned}$$



where  $T' \equiv (s_i \ell_j i' + \ell_i s_j j')$

It can be shown that only a few terms of this product survive the averaging process. The demonstration is tedious and here we will write down the terms that do not vanish along with their corresponding average-value:

$$1) \langle \frac{1}{2} x \ell_i \ell_j \sin \beta (c \cdot k') (\hat{k}' \cdot \hat{k})^2 e^{iq \cos \theta} \rangle_{av}$$

$$= \frac{1}{2} x \ell_i \ell_j [\sin^3 \beta i (j_1(q) - 2j_2(q)/q)$$

$$+ \sin \beta \cos^2 \beta i j_2(q)/q]$$

$$2) \langle \frac{1}{2} x s_i s_j \sin \beta (c \cdot k') (\hat{i}' \cdot \hat{k}) (\hat{\tau}'_j \cdot \hat{k}) e^{iq \cos \theta} \rangle_{av}$$

$$= \frac{1}{2} m x s_i s_j \sin \beta [\sin^2 \beta i j_2(q)/q$$

$$+ \cos^2 \beta \frac{i}{2} (j_1(q) - j_2(q)/q)]$$

$$3) \langle - \frac{1}{2} x \ell_i \ell_j \cos \beta (b \cdot k') (\hat{k}' \cdot \hat{k})^2 e^{iq \cos \theta} \rangle_{av}$$

$$= - x \ell_i \ell_j (\sin \beta - \sin^3 \beta) i j_2(q)/q$$

$$4) \langle -\frac{1}{2} x s_i s_j \cos\beta (\hat{b} \cdot \hat{k}') (\hat{i}' \cdot \hat{k}) (\hat{\tau}'_j \cdot \hat{k}) e^{iq \cos\theta} \rangle_{av}$$

$$= \frac{1}{2} x m s_i s_j \sin\beta \cos^2\beta i j_2(q)/q$$

$$5) \langle \frac{1}{2} y \sin\beta (\hat{c} \cdot \hat{\tau}') (\hat{k} \cdot \hat{\tau}') (\hat{k}' \cdot \hat{k}) e^{iq \cos\theta} \rangle_{av}$$

$$= \frac{1}{2} s_i \ell_j y (p \sin^3\beta - p m \sin\beta \cos^2\beta) i j_2(q)/q$$

$$+ \frac{1}{2} \ell_i s_j y (p m \sin^3\beta - p \sin\beta \cos^2\beta$$

$$+ g n (\sin^3\beta - \sin\beta \cos^2\beta)) i j_2(q)/q$$

$$6) \langle -\frac{1}{2} y \cos\beta (\hat{b} \cdot \hat{\tau}') (\hat{k} \cdot \hat{\tau}') (\hat{k}' \cdot \hat{k}) e^{iq \cos\theta} \rangle_{av}$$

$$= -\frac{1}{2} y \sin\beta \cos^2\beta [\ell_i s_j (p m + g n) + s_i \ell_j p]$$

$$\cdot i(j_1(q) - j_2(q)/q) \quad (14)$$

where  $j_1(q)$  is, as before, the first-order spherical Bessel function and  $j_2(q)$  is the second-order spherical Bessel function defined as:

$$j_2(q) = (3/q^3 - 1/q) \sin q - 3 \cos q / q^2 \quad (15)$$

In performing the above averagings, integrals of the form:

$$\int_0^\pi e^{iq\cos\theta} [\sin^n(\theta)] \sin\theta d\theta; \int_0^\pi e^{iq\cos\theta} [\cos^n(\theta)] \sin\theta d\theta$$

for  $n = 1, 2, 3$  must be found. In the appendix at the end of this thesis some of the integrals used in the averaging of  $I_L - I_R$  and  $I_{\parallel} + I_{\perp}$  are written along with their solutions.

It is possible to relate the coefficients such as  $l_i s_j$  or  $l_i l_j$ , etc., to the parameters of the scatterer. We will simply list the main results needed to express the answer in terms of the scatterer parameters:

$$x \equiv (\underline{t}_j \times \underline{t}_i) \cdot \hat{R}_{ij} = -s_i s_j n$$

$$y_p = n s_j l_i$$

$$y_g = s_i l_j - m s_j l_i \quad (16)$$

$$l_i l_j = (\underline{t}_i \cdot \hat{R}_{ij}) (\underline{t}_j \cdot \hat{R}_{ij})$$

$$s_i s_j m = (\underline{t}_i \times \hat{R}_{ij}) \cdot (\underline{t}_j \times \hat{R}_{ij})$$

Replacing expression (16) in the results (14) and (13), we can make use of (6) to write down, after some algebraic

manipulations, the result for the averaged  $I_L - I_R$  :

$$\langle \frac{I_L - I_R}{c^2} \rangle_{av} = \sum_{ij} \frac{\alpha_i^* \alpha_j (\underline{t}_j \times \underline{t}_i) \cdot \hat{R}_{ij} \{ [(\underline{t}_i \cdot \underline{t}_j) (j_2/q - j_1) - (\underline{t}_i \cdot \hat{R}_{ij}) (\underline{t}_j \cdot \hat{R}_{ij}) (5j_2/q - j_1)] (\sin\beta + \sin^3\beta) \}}{2} \quad (17)$$

The argument of the spherical Bessel functions is  $q$  as before. Expression (17) is the result we were seeking.

Notice that the whole expression is multiplied by a common factor :

$$(\underline{t}_j \times \underline{t}_i) \cdot \hat{R}_{ij} \equiv (\underline{t}_i \times \hat{R}_{ij}) \cdot \underline{t}_j$$

This is a form-factor that resembles the expression for the rotational strength in optical activity theory<sup>5</sup>:  $\underline{t}_i \times \hat{R}_{ij}$  is the magnetic dipole ( $\underline{m}_i$ ) associated with the transition dipole  $\underline{t}_i$  so that :

$$(\underline{t}_j \times \underline{t}_i) \cdot \hat{R}_{ij} = \underline{m}_i \cdot \underline{t}_j$$

The last expression is the product of a pseudo-vector with a vector. Pseudo-vectors or axial vectors transform by changing sign when an inversion of their coordinates is done, whereas pure or polar vectors (such as  $\underline{t}_j$ ) do not

change sign under inversion. The common factor to Equation (17) will therefore have opposite sign for two molecules that are the mirror images of each other. This feature makes CIDS more sensitive to structure than total scattering.

Equation (17) is only a function of angle  $\beta$ , while every other directional property of the incident and the scattered radiation has disappeared in the averaging. The differential scattering pattern in space is given by a "ring" structure of constant intensities, like the powder patterns observed in crystallography.<sup>6</sup> A careful limit analysis can be performed on Equation (17). The result is:

$$\lim_{\substack{q \rightarrow 0 \\ \beta \rightarrow 0}} \langle I_L - I_R \rangle_{av} = 0 \quad (18)$$

I.e., there is no forward CIDS signal for a tumbling (spatially averaged) sample. The same is true for  $\beta = 180^\circ$  (reflection band). It should be clear, however, that the above equation has been derived assuming no interaction of the induced dipole elements (transition dipoles) in the scatterer, i.e., by using the first Born approximation<sup>7</sup> in the local field.

The conclusions drawn from expression (18) will not be true if actual coupling of the radiating elements is

allowed. In this case, forward and backward CIDS should be predicted.

From the definition of  $q = \frac{4\pi}{\lambda} R_{ij} \sin\beta$  we see that as  $R_{ij}$  grows relative to  $\lambda$ ,  $q$  also increases. When  $R_{ij} > \lambda$ , then  $q \gg 1$  and  $j_2/q \ll 1$ , then we can neglect the  $j_2/q$  vs. the  $j_1$  in Equation (17). In these conditions, the  $j_1$  spherical Bessel function controls all the angular behavior of the CIDS, since the other factors,  $\sin\beta$ ,  $\sin^3\beta$ , etc., vary monotonically with respect to  $\beta$ . We can apply Equation (17) to the simplest system showing differential scattering. This is clearly a dimer. Figure 4 shows six possible dimer structures. Here we will analyze their CIDS when allowed to tumble freely in solution.

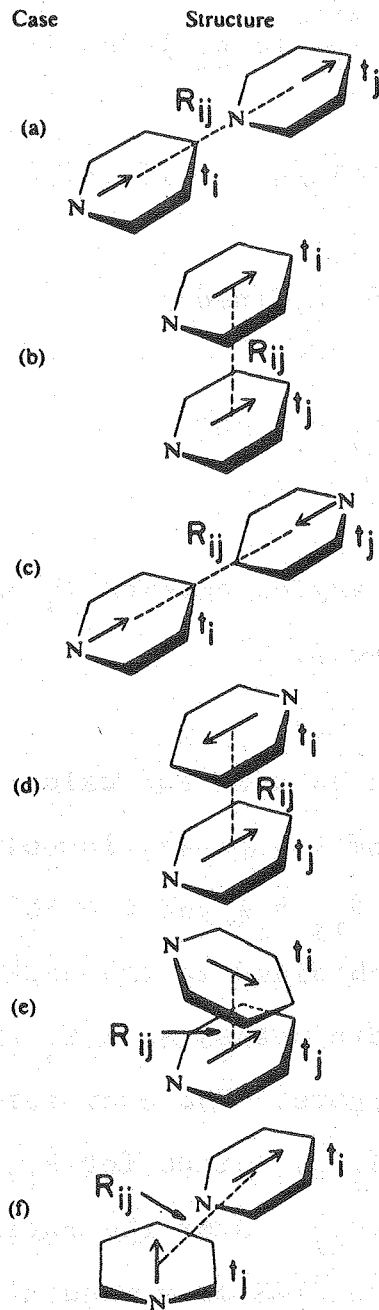
Case  $\langle I_L - I_R \rangle_{av}$

a)	0	} non chiral structures
b)	0	
c)	0	
d)	0	

$$e) \langle \frac{I_L - I_R}{c^2} \rangle_{av} = \alpha_1^* \alpha_2 \sin 2\theta (j_2/q - j_1) (\sin\beta + \sin^3\beta) \quad (19)$$

where  $\theta$  is the angle between  $\underline{t}_i$  and  $\underline{t}_j$

Figure 4. The figure shows 6 possible geometries of a dimer, to which Equation 19 (See text) is applied.  $\underline{t}_i$  and  $\underline{t}_j$  are the polarization vectors of groups  $i^{\text{th}}$  and  $j^{\text{th}}$  and  $R_{ij}$  is the distance between the centers of these two groups. a), b), c) and d) are the non-chiral geometries, and  $\langle I_L - I_R \rangle_{av}$  for these four cases is zero. e) A chiral dimer in which the angle between  $R_{ij}$  and  $\underline{t}_i$  and  $\underline{t}_j$  is  $90^\circ$ . The angle between  $\underline{t}_i$  and  $\underline{t}_j$  is  $\theta$  in the equations. f) A chiral structure in which  $R_{ij}$  is not orthogonal to either  $\underline{t}_i$  or  $\underline{t}_j$ .



XBL 8012-12960



$$f) \frac{\langle I_L - I_R \rangle_{av}}{C^2} = \frac{\alpha_1^* \alpha_2}{2} (\hat{\sigma} \cdot \hat{R}_{12}) \sin \theta \{ [\cos \theta (j_2/q - j_1) - \cos \phi_1 \cos \phi_2 (5j_2/q - j_1)] (\sin \beta + \sin^3 \beta) \} \quad (20)$$

where  $\hat{\sigma}$  is a unit vector defined by:

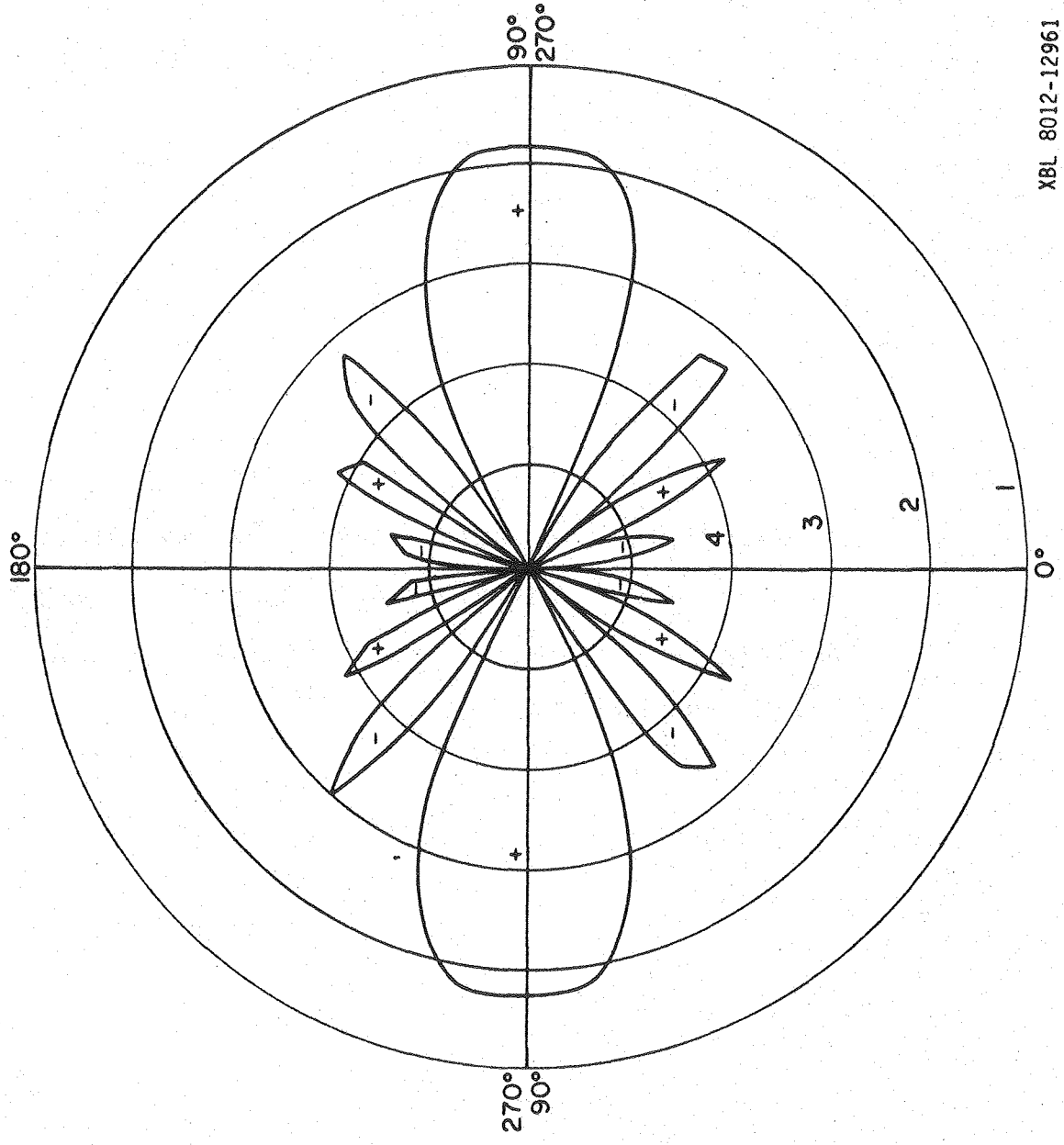
$$\hat{t}_j \times \hat{t}_i = \sin \theta \hat{\sigma}$$

and  $\phi_1$  and  $\phi_2$  are the angles between  $\hat{t}_1$  and  $\hat{R}_{12}$  and  $\hat{t}_2$  and  $\hat{R}_{12}$ , respectively.

Equation (19) can be used to calculate the CIDS of a dimer such as that of Figure 4e, in solution. This is shown in Figure 5 for  $R_{ij} = \lambda$  and  $\theta = 60^\circ$ . As predicted before, zero CIDS is obtained in the backward and forward directions. The pattern possesses a  $C_4$  axis perpendicular to the plane of the figure. The many zeros observed are mostly controlled by  $j_1(q)$ , since for  $R_{12}/\lambda = 1$ , then  $0 \leq q \leq 12$  and  $j_2/q \ll j_1$  over the entire range of  $q$ . Notice that most of the CIDS of a randomly oriented sample of dipoles is observed at right angles from the direction of incidence of light. A more complicated behavior is predicted for a trimer, a tetramer, etc. Numerical computations must be done to handle a randomly oriented sample of a polymer.

Figure 5. Polar plot of  $\langle I_L - I_R \rangle_{av}$  for the dipole of case d) in figure 4. The angle between the two polarization vectors  $\underline{t}_i$  and  $\underline{t}_j$  is  $60^\circ$ .  $R_{ij} = \lambda = 1$ . The graph depicts intensities vs increments of .1 radians in the angle  $\beta$ .

XBL 8012-12961



It is of interest to obtain an asymptotic expression for  $\langle I_L - I_R \rangle_{av}$ , valid for the case in which  $\lambda \gg R_{ij}$ . Under these circumstances,

$$q = \frac{4\pi R_{ij}}{\lambda} \sin\beta \ll 1$$

Expanding the spherical Bessel functions in terms of powers of their arguments, and keeping only the first few, we obtain:

$$\lim_{q \rightarrow 0} j_1(q) = \frac{1}{3} (q - q^3/10)$$

and

$$\lim_{q \rightarrow 0} j_2(q)/q = \frac{1}{15} (q - q^3/8)$$

Replacing in (17) the above limiting expressions, we arrive at:

$$\begin{aligned} \frac{\langle I_L - I_R \rangle_{av}}{c^2} = & \sum_{ij} \alpha_i^* \alpha_j \frac{(\underline{t}_j \times \underline{t}_i) \cdot \hat{R}_{ij}}{30} \left\{ \frac{1}{8} (\underline{t}_i \cdot \hat{R}_{ij}) (\underline{t}_j \cdot \hat{R}_{ij}) q^3 \right. \\ & \left. - 4(\underline{t}_i \cdot \underline{t}_j) q \right\} (\sin\beta + \sin^3\beta) \end{aligned}$$

If the first term is neglected as compared to the second one, the above equation becomes:

$$\frac{\langle I_L - I_R \rangle_{av}}{c^2} = -2 \sum_{ij} \alpha_i^* \alpha_j \frac{(\underline{t}_j \times \underline{t}_i) \cdot \hat{R}_{ij}}{15} (\underline{t}_i \cdot \underline{t}_j) \frac{\pi R_{ij}}{\lambda}$$

$$(\sin^2 \beta + \sin^4 \beta)$$

where the definition of  $q$  has been used. Notice that for  $R_{ij}/\lambda \ll 1$  the asymptotic expression is still an even function of  $\beta$ .

### III. The Averaging of the Total Scattering.

The scattering intensity due to a collection of polarizable points in space, each characterized by a polarizability tensor  $\alpha_i = \alpha_i \underline{t}_i \underline{t}_i$ , is:

$$\frac{I(\mathbf{r})}{c^2} = \sum_{i,j} e^{iq \cos \theta} \alpha_i^* \alpha_j [\hat{E}_0^* \cdot \underline{t}_i \underline{t}_i \cdot \underline{t}_j \underline{t}_j \cdot \hat{E}_0 - \hat{E}_0^* \cdot \underline{t}_i \underline{t}_i \cdot \hat{k} \hat{k} \cdot \underline{t}_j \underline{t}_j \cdot \hat{E}_0] \quad (21)$$

where  $\alpha_i$ ,  $\alpha_j$ ,  $\underline{t}_i$ ,  $\underline{t}_j$ ,  $\hat{k}$ ,  $q$ , and  $\theta$  have the same meaning as before.  $\hat{E}_0$  is the incident electric unit vector. For light polarized perpendicular to the scattering plane (see Figure 2):

$$\hat{E}_0 = \underline{a} \quad (22a)$$

and for light polarized parallel to the scattering plane:

$$\hat{\underline{E}}_0 = \cos\beta \underline{b} + \sin\beta \underline{c} \quad (22b)$$

The scattered intensity for light perpendicular to the scattering plane is:

$$\frac{I_{\perp}}{C^2} = \sum_{i,j} e^{iq\cos\theta} \alpha_i^* \alpha_j [(a \cdot \underline{t}_i)(a \cdot \underline{t}_j) \underline{t}_i \cdot \underline{t}_j - (a \cdot \underline{t}_i)(\underline{t}_i \cdot \hat{k})(\underline{t}_j \cdot \hat{k})(a \cdot \underline{t}_j)] \quad (23)$$

Using Equation (2), the average of the first term in Equation (23) becomes:

$$\begin{aligned} \langle (a \cdot \underline{t}_i)(a \cdot \underline{t}_j) \rangle_{av} &= \langle \ell_i \ell_j (a \cdot \hat{k}')^2 + \ell_i s_j (a \cdot \hat{k}') (a \cdot \hat{r}'_j) \\ &+ s_i \ell_j (a \cdot \hat{i}') (a \cdot \hat{k}') + s_i s_j (a \cdot \hat{i}') (a \cdot \hat{r}'_j) \rangle_{av} \end{aligned}$$

After using Equations (3) and (4) in this expression, only the following terms survive the spatial averaging:

$$\begin{aligned} \langle \ell_i \ell_j (a \cdot \hat{k}')^2 e^{iq\cos\theta} \rangle_{av} &= \ell_i \ell_j j_1(q)/q \\ \langle s_i s_j (a \cdot \hat{i}') (a \cdot \hat{r}'_j) e^{iq\cos\theta} \rangle_{av} &= \frac{1}{2} m s_i s_j (j_0(q) - j_1(q)/q) \end{aligned} \quad (24)$$

The averaging of the second term in Equation (23):

$$\langle (\underline{a} \cdot \underline{t})(\underline{a} \cdot \underline{t})(\underline{t}_i \cdot \hat{\underline{k}})(\underline{t}_j \cdot \hat{\underline{k}}) \rangle_{av}$$

is tedious and only a few terms do not vanish when the average is performed. We will omit the details of the derivation and will write down only the results. These will be included in the final averaged value of the scattered intensity perpendicular to the scattering plane:

$$\begin{aligned} \langle \frac{I_1}{C^2} \rangle_{av} = & \sum_{ij} \alpha_i^* \alpha_j \{ [\ell_i \ell_j j_1/q + 1/2 m s_i s_j (j_0 - j_1/q)] \underline{t}_i \cdot \\ & \underline{t}_j \} - \sum_{ij} \alpha_i^* \alpha_j \{ 2\ell_i^2 \ell_j^2 \sin^2 \beta (j_1/q - 4j_2/q^2) + \\ & (\ell_1^2/2 + \ell_j^2/2) [j_2/q^2 - 1/2 \sin^2 \beta (j_1/q - j_2/q^2)] \\ & + m \ell_i \ell_j s_i s_j [j_1/q + 1/2 \sin^2 \beta (16 j_2/q - \\ & 7j_1/q + j_0)] + m s_i^2 s_j^2 [1/8 (3j_2/q^2 - 2j_1/q + j_0) \\ & + 1/8 \sin^2 \beta (-15j_2/q^2 + 6j_1/7 - j_0)] + 1/8 m s_i^2 s_j^2 \\ & [(j_2/q^2 + 2j_1/q - j_0) - \sin^2 \beta (4j_2/q_2 + \\ & 2j_1/q - j_0)] \} \end{aligned}$$

(25)

where the arguments of the Bessel functions have been omitted for simplicity. In reducing the above expression, the relations (3a) have been used.

Our next task is to obtain the equivalent average for the scattered intensity of light incident parallel to the scattering plane. From Equations (21) and (22b), the quantity to be averaged is:

$$\begin{aligned}
 \frac{I_{\parallel}}{C^2} = & \sum_{ij} e^{iq\cos\theta} \alpha_i^* \alpha_j [\sin^2\beta (\underline{b}\cdot\underline{t}_i)(\underline{b}\cdot\underline{t}_j)(\underline{t}_i\cdot\underline{t}_j) + \cos^2\beta \\
 & (\underline{c}\cdot\underline{t}_i)(\underline{c}\cdot\underline{t}_j)(\underline{t}_i\cdot\underline{t}_j) + \sin\beta\cos\beta(\underline{b}\cdot\underline{t}_i) \\
 & (\underline{c}\cdot\underline{t}_j)(\underline{t}_i\cdot\underline{t}_j) + \sin\beta\cos\beta \\
 & (\underline{c}\cdot\underline{t}_i)(\underline{b}\cdot\underline{t}_j)(\underline{t}_i\cdot\underline{t}_j)] \\
 - & \sum_{ij} e^{iq\cos\theta} \alpha_i^* \alpha_j [\sin^2\beta (\underline{b}\cdot\underline{t}_i) (\underline{t}_i\cdot\hat{\underline{k}}) (\underline{t}_j\cdot\hat{\underline{k}}) (\underline{b}\cdot\underline{t}_j) \\
 & + \cos^2\beta (\underline{c}\cdot\underline{t}_i) (\underline{t}_i\cdot\hat{\underline{k}}) (\underline{t}_j\cdot\hat{\underline{k}}) (\underline{c}\cdot\underline{t}_j) \\
 & + \sin\beta\cos\beta (\underline{t}_i\cdot\hat{\underline{k}}) (\underline{t}_j\cdot\hat{\underline{k}}) [(\underline{b}\cdot\underline{t}_i) \\
 & (\underline{c}\cdot\underline{t}_j) + (\underline{b}\cdot\underline{t}_j)(\underline{c}\cdot\underline{t}_i)] \quad (26)
 \end{aligned}$$

Here again, only the results will be presented. The



relations (3b) have been used in the reduction of the expression for  $\langle I_{\parallel} \rangle_{av}$ :

$$\begin{aligned}
 \frac{I_{\parallel}}{c^2} = & \sum_{ij} \alpha_i^* \alpha_j \{ \ell_i \ell_j [j_0 - 2j_1/q + \sin^2 \beta (3j_1/q - \\
 & j_0)] + m s_i s_j [j_1/q + 1/2 \sin^2 \beta (j_0 - 3j_1/q)] \} \\
 & (\tilde{t}_i \cdot \tilde{t}_j) - \sum_{ij} \alpha_i^* \alpha_j \{ 2 \ell_i^2 \ell_j^2 [(j_1/q - 4j_2/q^2) + \\
 & (\sin^2 \beta - \sin^4 \beta) (3j_2/q^2 - j_1/q)] + 1/2 \ell_i \ell_j s_i s_j m \\
 & [16j_2/q^2 - 5j_1/q + j_0 + 2(\sin^2 \beta - \sin^4 \beta) \\
 & (j_1/q - 3j_2/q^2)] + (\ell_i^2 + \ell_j^2) [1/2 (j_1/q - \\
 & 4j_2/q^2) + 1/2 (\sin^2 \beta - \sin^4 \beta) (j_0 - 3j_2/q^2)] + \\
 & 1/2 s_i^2 s_j^2 m^2 [(j_1/q - 4j_2/q^2) + 1/4 (\sin^2 \beta - \\
 & \sin^4 \beta) (9j_2/q^2 + 2j_1/q + 3j_0)] + 1/2 s_i^2 s_j^2 n^2 [j_2/q^2 + \\
 & 1/4 (\sin^2 \beta - \sin^4 \beta) (9j_2/q^2 + 2j_1/q + 3j_0)] \} \quad (27)
 \end{aligned}$$

In order to rewrite these expressions in terms of the parameters of the scatterer we need the following relations:

$$\begin{aligned} \ell_i^2 + \ell_j^2 &= (\underline{t}_i \cdot \hat{R}_{ij})^2 + (\underline{t}_j \cdot \hat{R}_{ij})^2 \\ s_i^2 s_j^2 n^2 &= (\underline{t}_j \cdot (\hat{R}_{ij} \times \underline{t}_i))^2 \end{aligned} \quad (28)$$

These expressions, together with Equations (16) are used to write down the spatially averaged total scattered intensity as the sum of Equations (25) and (27):

$$\begin{aligned} \frac{I_{\perp} + I_{\parallel}}{C^2} &= \sum_{ij} \alpha_i \alpha_j^* \{ (\underline{t}_i \cdot \hat{R}_{ij}) (\underline{t}_i \cdot \hat{R}_{ij}) \{ [(j_0 - j_1/q) + \\ &\sin^2 \beta (3j_1/q - j_0)] (\underline{t}_i \cdot \underline{t}_j) - 2 (\underline{t}_i \cdot \hat{R}_{ij}) \\ &(\underline{t}_i \cdot \hat{R}_{ij}) [(j_1/q - 4j_2/q^2) - \sin^2 \beta j_2/q^2 + \\ &\sin^4 \beta (j_1/q - 3j_2/q^2)] \} + (\underline{t}_i \times \hat{R}_{ij}) \cdot \\ &(\underline{t}_j \times \hat{R}_{ij}) \{ 1/2 [(j_0 + j_1/q) + \sin^2 \beta (j_0 - 2j_1/q)] \\ &(\underline{t}_i \cdot \underline{t}_j) + 1/2 (\underline{t}_i \cdot \hat{R}_{ij}) (\underline{t}_j \cdot \hat{R}_{ij}) [(16j_2/q^2 - \end{aligned}$$

$$\begin{aligned}
& 3j_1/q + j_0) + \sin^2\beta(8j_2/q^2 - 3j_1/q + j_0) + \\
& 4\sin^4\beta(j_1/q - 3j_2/q^2)] \} (1 - 1/2 ((\hat{R}_{ij} \times \underline{t}_i)^2 + \\
& (\hat{R}_{ij} \times \underline{t}_j)^2)) [(5j_2/q^2 - j_1/q) + \sin^2\beta(j_0 - j_1/q) - \\
& \sin^4\beta(j_0 - 3j_2/q^2)] + ((\underline{t}_i \times \hat{R}_{ij}) \cdot (\underline{t}_j \times \hat{R}_{ij}))^2 \\
& [1/8 (-9j_2/q^2 + 2j_1/q + j_0) - 1/4 \sin^2\beta \\
& (3j_2/q^2 - 4j_1/q - j_0) - 1/8 \sin^4\beta(9j_2/q^2 + \\
& 2j_1/q + 3j_0)] + (\underline{t}_j \cdot (\hat{R}_{ij} \times \underline{t}_i))^2 [1/8 (5j_2/q^2 + \\
& 2j_1/q - j_0) + 1/4 \sin^2\beta(3j_2/q^2 + 2j_1/q + j_0) - \\
& (1/8 \sin^4\beta(3j_2/q^2 - j_1/q - j_0))] \}
\end{aligned}$$

(29)

in a similar way, the quantity  $I_{\parallel} - I_{\perp}$  can be obtained from Equations (25) and (27). Due to lack of space we will omit it here.

Equation (29) gives, therefore, the total scattering as a function of the scattering angle (28) for an ensemble

of scatterers (each described by a set of point polarizable groups), adopting all possible orientations in space.

Notice that in the expression for total scattering intensity, only three spherical Bessel functions contribute:  $j_0$ ,  $j_1$ , and  $j_2$ . This fact is important in determining the symmetry of the scattering intensities as a function of the angle  $\beta$ .

Indeed, the spherical Bessel functions have the property:<sup>4</sup>

$$j_n(-q) = (-1)^n j_n(q)$$

Since  $q = \frac{4\pi}{\lambda} R_{ij} \sin\beta$ , clearly if  $\beta \rightarrow -\beta$ , then  $q \rightarrow -q$ .

Now, there are two things to notice about Equation (29). First, only the 0<sup>th</sup>, 2<sup>nd</sup>, and 4<sup>th</sup> powers of  $\sin\beta$  appear in the equation and these factors are even on  $\beta$ . Second, all the Bessel functions appearing in Equation (29) have the form  $j_n/q^n$  which behaves also as an even function of the angle, i.e.:

$$j_n(-q)/(-q)^n = j_n(q)/q^n$$

Therefore, the whole expression (29) is even on  $\beta$ . This means that the scattering patterns must be symmetric at both sides of the direction of incidence of light. Fur-

thermore, since the only trigonometric functions appearing implicitly or explicitly in this expression are sines, and

$$\sin\beta = \sin(180-\beta)$$

the pattern is also symmetric at both across the  $270^\circ$ - $90^\circ$  axis (see Figure 5). As in the case of  $\langle I_L - I_R \rangle_{av}$ , the in-plane scattering pattern has a  $C_4$  axis of symmetry perpendicular to the plane.

Equation (29) is the equivalent to the spatially averaged scattering of a collection of point polarizable groups, originally devised by Debye<sup>8</sup> for the case of unpolarized incident radiation.

Bibliography

1. Tobias, I., Balazs, N. L. (1978) Chemical Physics 32, 93-99.
2. Goldstein, H. (1953) Classical Mechanics (Addison-Wesley: Cambridge, Mass).
3. Margenau, H., Murphy, G. M. (1949) The Mathematics of Physics and Chemistry (Van Nostrand: New York).
4. Abramowitz, M., Stegun, I. A. (1965) Handbook of Mathematical Functions (Dover: New York).
5. Condon, E. U. (1937) Rev. Mod. Phys. 9, 432.
6. Sherwood, D. (1976) Crystals, X-rays and Proteins (Longman: New York).
7. Saxon, D. S. (1955) Lectures on the Scattering of Light, Sci. Rep. No. 9, Contract AF 19(122)-239, Dept. of Meteorol., University of California, Los Angeles, 100 pp.
8. Tanford, C. (1961) Physical Chemistry of Macromolecules (Wiley: New York).

Appendix A

1) Friedel's Law.

The scattering power of an atom is described in crystallography by the atomic scattering factor:

$$f_j = \int_{\text{atom}} \rho_j(\underline{R}_j) e^{i\Delta\vec{k} \cdot \underline{R}_j} d\underline{R}_j \quad (\text{A-1})$$

where  $\rho_j(\underline{R}_j)$  is the electron charge density at point  $\underline{R}_j$  in the atom. In the limit of short wavelengths the electric charge density appearing in the above expression can be formally derived from the atomic polarizability.

If  $\rho_j(\underline{R}_j)$  is spherically symmetric (centrosymmetric), its Fourier transform ( $f_j$ ) is a real function. Near an absorption band the electron density is not spherically symmetric and therefore, in resonance  $f_j$  is in general a complex quantity:

$$f_j = f_j^0 e^{i\phi_j} \quad (\text{A-2})$$

where  $f_j^0$  and  $\phi_j$  are real.

Let us suppose a group of atoms on which external radiation incides. The scattering amplitude at a position in space in which a diffraction maximum exists, labelled by the components of the vector  $\Delta\vec{k}$  ( $h, k, l$ ) is:

$$F_{hkl} = \sum_j f_j e^{i(hx_j + ky_j + lz_j)} \quad (\text{A-3})$$

Away from the absorption band,  $f_j$  is real and the corresponding centrosymmetric point in space scatters with the amplitude:

$$F_{\bar{h}\bar{k}\bar{l}} = \sum_j f_j e^{-i(hx_j+ky_j+lz_j)} \quad (\text{A-4})$$

Then from (A-3) and (A-4):

$$F_{hkl}^* = F_{\bar{h}\bar{k}\bar{l}}$$

and

$$|F_{\bar{h}\bar{k}\bar{l}}|^2 = |F_{hkl}|^2$$

This is called Friedel's Law. It states that the intensities of the diffraction maxima corresponding to centrosymmetrically related points are equal.

## 2) Breakdown of Friedel's Law.

If one of the atoms in the group, say atom  $n^{\text{th}}$ , is in resonance with the frequency of the incident radiation, then,

$$F_{hkl} = \sum_{j \neq n} f_j e^{i(hx_j+ky_j+lz_j)} + f_n^0 e^{i(hx_n+ky_n+lz_n)} e^{i\phi_n}$$

It is clear that:

$$F_{\bar{h}\bar{k}\bar{l}} \neq F_{hkl}^*$$

and

$$|F_{\bar{h}\bar{k}\bar{l}}|^2 \neq |F_{hkl}|^2$$



so that Friedel's Law is violated. On the other hand, if all the atoms are anomalous scatterers:

$$F_{hkl} = \sum_j f_j^0 e^{i(hx_j + ky_j + lz_j)} e^{i\phi_j}$$

and

$$F_{\bar{h}\bar{k}\bar{l}} = \sum_j f_j^0 e^{-i(hx_j + ky_j + lz_j)} e^{i\phi_j}$$

but

$$|F_{hkl}|^2 = \sum_j \sum_i f_i^0 f_j^0 e^{i(h(x_j - x_i) + k(y_j - y_i) + l(z_j - z_i))} \cdot e^{i(\phi_j - \phi_i)}$$

and

$$|F_{\bar{h}\bar{k}\bar{l}}|^2 = \sum_j \sum_i f_i^0 f_j^0 e^{-i(h(x_j - x_i) + k(y_j - y_i) + l(z_j - z_i))} \cdot e^{i(\phi_j - \phi_i)}$$

Since all of the atoms are in resonance for the same frequency, then:

$$f_i^{(0)} e^{i\phi_j} = f_j^{(0)} e^{i\phi_i}$$

and again:

$$|F_{hkl}|^2 = |F_{\bar{h}\bar{k}\bar{l}}|^2$$

i.e., Friedel's Law holds in this case.

Appendix B

In performing the averages of Chapter 6, the following integrals are encountered:

$$\int x^n e^{iax} dx = e^{iax} \left[ \frac{x^n}{ia} + \sum_{k=1}^n \frac{(-1)^k n(n-1)\dots(n-k+1)}{(ia)^{k+1}} x^{(n-k)} \right]$$

These integrals appear commonly in the spatial averaging of optical properties. A list of those used in the obtaining of the equations of Chapter 6 follows:

$$\int_0^\pi e^{iq \cos\theta} \cos\theta \sin\theta d\theta = i j_1(q)$$

$$\int_0^\pi e^{iq \cos\theta} \cos\theta \sin^3\theta d\theta = i j_2(q)/q$$

$$\int_0^\pi e^{iq \cos\theta} \cos^3\theta \sin\theta d\theta = i(j_1(q) - 2j_2(q)/q)$$

$$\int_0^\pi e^{iq \cos\theta} \sin\theta d\theta = 2j_0(q)$$

$$\int_0^\pi e^{iq \cos\theta} \cos^2\theta \sin\theta d\theta = 2(j_0(q) - 2j_1(q)/q)$$

$$\int_0^\pi e^{iq \cos\theta} \cos^4\theta \sin\theta d\theta = 2(8j_2(q)/q^2 - 4j_1(q)/q + j_0(q))$$

$$\int_0^\pi e^{iq \cos\theta} \sin^3\theta d\theta = 4j_1(q)/q$$

(continued)

} appear in  
 $\langle I_L - I_R \rangle_{av}$

\*

$$\left. \begin{aligned} \int_0^\pi e^{iq \cos \theta} \cos^2 \theta \sin^3 \theta d\theta &= 4(j_1(q)/q - 4j_2(q)/q^2) \\ \int_0^\pi e^{iq \cos \theta} \sin^5 \theta d\theta &= 16j_2(q)/q^2 \end{aligned} \right\} \begin{array}{l} \text{(continued)} \\ \text{appear in} \\ \langle I_{\parallel} + I_{\perp} \rangle_{av} \end{array}$$

The spherical Bessel functions ( $j$ 's) are:

$$j_0(q) = \frac{\sin q}{q}$$

$$j_1(q) = \frac{\sin q}{q^2} - \frac{\cos q}{q}$$

$$j_2(q) = \left(\frac{3}{q^3} - \frac{1}{q}\right) \sin q - \frac{3}{2} \frac{\cos q}{q}$$

\*Integrals appear in  $\langle I_{\parallel} + I_{\perp} \rangle_{av}$ .

## Appendix C

Here follows a list of the programs VINO, PAN and COCO, used in the CIDS computations. Only a few remarks are made before the listing since the comment cards in each program made themselves explanatory.

### I. PROGRAM VINO.

Calculates  $CIDS = I_L - I_R / I_L + I_R$  and total scattering =  $I_L + I_R$  for a helix of arbitrary dimensions whose axis is oriented along the  $z$  ( $\underline{e}_3$ ) direction of an arbitrary coordinate system. Light of both circular polarizations is incident along the positive  $y$  ( $\underline{e}_2$ ) direction. No restriction is imposed to the ratio of pitch of the helix/wavelength of light. The results are printed and plotted in the form of polar plots (intensities vs. azimuthal angle) at a fixed polar angle (or layer line).

Deck set-up:

- |                     |   |
|---------------------|---|
| (1) Control cards   |   |
| (2) Program         | } Program SCATTER (version 1)<br>Subroutine POLAR |
| (3) Input deck      |   |
| (4) End-of-job-card |   |

```

VING,12,300,55000.449312,BUSTAPANTE
*NOSTAGE
SFL,100000.
FTN4.
FETCHFS,SANDIA,SAND,SANLIB.
FETCHGS,IODS/ULIBX,DATE=01NOV79,15475.
FETCHPS,GPAC9N7,GPAC,SCBN.
LINK,F=LGO,P=ULIBX,F=GFAC,P=SAN(X,PF={LC=50000}.
EXIT.
DUMP,0.
FETCHFS,IODS,SYMTAB,SYMTAEX.
GRUPP,P=ZZZSYM,P=SYMTAE.
FIN.
REWIND(FILM)
COPY(FILM,OUT)
REWIND(FILM)
COPY(FILM,MORE)
DISFOSE,FILM=3M,M=MF.
DISFCSE,MORE=3M,M=MF.
DISFCSE,CUT=MF,P=ME.
<EOF>

```

```

PROGRAM SCATTER(INPL,CUTPUT,TAPE5=INPUT,TAPE6=CUTPUT,FILM)
C*****
C*THIS PROGRAM COMPUTES THE TOTAL AND THE DIFFERENTIAL SCATTERING FOR A *
C*HELICAL SCATTERER OF ARBITRARY PITCH, RADIUS, AND LENGTH, AND FOR AN *
C*ARBITRARY RATIO OF PITCH/LAMBDA. IF PITCH IS GREATER THAN LAMBDA IT CALCULA *
C*TES THE SCATTERING INTENSITIES AT EACH LAYER LINE. IF PITCH IS SMALLER *
C*THAN LAMBDA IT CALCULATES THE SCATTERING INTENSITIES AT FIXED ANGLES IN *
C*SPACE.
C*THE INPUT PARAMETERS ARE THEREFORE WAVELENGTH, PITCH, RADIUS, ANGLE *
C*OF ALTITUDE OF SCATTERING
C*****
C
C
C
C*****
C*HERE WE DECLARE ALL VARIABLES AND ARRAYS USED IN THIS PROGRAM AND ALSO *
C*THE ALLOCATION FOR MEMORY IS DONE
C*****
COMMON FTT,FMFP,FMAN,TEC,PBO,A30
REAL NBO
DIMENSION IN(4),PA(4)
REAL LAMBDA,LAMBDA,LAMBDA,LAMBDA
REAL LENGTH
COMPLEX E(3,3,3),YPCN
COMPLEX SUMMA(3,3,3)
COMPLEX ALPHA1,ALPHA2
COMPLEX ALPHA3
COMPLEX EYZETA,EYKIS
COMPLEX C1,C2,C3,C1,C2,C3,CSTR1,CSTR2,CSTR3,CSTR1,DSTR2,DSTR3
DIMENSION QA(400,20)
LEVEL2,BJN
COMMON/GIANT/BJN(81,400)
DIMENSION CD(400),PSI(400),PSISTR(400),3J(41)
DIMENSION ILMIF(400),ILPIF(400),IL(400),IF(400),PLOTIL(400),
1PLCTIR(400)
DIMENSION PLOTSC(400)
INTEGER EXPONT,PLICY

```

```

REAL LYR
REAL ILMIR,ILPIR,LAMBDA,IL,IR
DIMENSION ANGLE(400)
DIMENSION PARAM(10)

```

```

C
C
C
C*****
C*HERE WE INITIALIZE THE VALUES NEEDED FOR COMPUTATION.
C*SIGN DETERMINES THE SENSE OF THE HELIX. SIGN=1. GIVES A RIGHT HANDED
C*HELIX. SIGN=-1 GIVES A LEFT HANDED ONE.
C*FMPT, FMPP, FMNN ARE THE STRENGTHS OF THE TANGENTIAL, PERPENDICULAR AND
C*NORMAL BANDS RESPECTIVELY.
C*LAMBOT, LAMBOP AND LAMBON ARE THE CORRESPONDING POSITIONS OF THESE BANDS
C*IN UNITS OF WAVELENGTHS.
C*GAMMAT,GAMMAP AND GAMMAN ARE THE HALF HEIGHT WIDTHS OF THE BANDS
C*NAZIMU IS THE MAXIMUM NUMBER OF LAYER LINES THAT EXIST FOR A GIVEN
C*RATIO OF P/LAMBDA. HERE A DEFAULT VALUE FOR THE CONTINUOUS CASE IS GIVEN
C*A IS THE RADIUS OF THE HELIX
C*PERIOD IS THE PITCH OF THE HELIX AND LENGTH THE NUMBER OF TURNS OF THE
C*HELIX.
C*NCPLT WILL DECIDE THE MAXIMUM NUMBER OF PLOTS TO BE GENERATED BY THE
C*PROGRAM.
C*INITIA CONTROL THE INITIALIZATION OF THE POLAR PLOTS
C*POLZ=0. GIVES SCATTERING OF LIGHT POLARIZED IN THE X DIRECTION
C*POLX=0. GIVES SCATTERING OF LIGHT POLARIZED IN THE Z DIRECTION
C*DEFAULT GIVES CIDS
C*NLYR DETERMINES THE NUMBER OF LAYER LINES COMPUTED
C*LYR DETERMINES THE ALTERNATIVE PLOTTING OF LAYER LINES OF ALTITUDE IN
C*POLAR PLOTS
C*INDEX DETERMINES THE MAXIMUM ORDER OF BESSEL FUNCTIONS USED IN THE SUMS
C*FLAG IS AN OPTION THAT WHEN EQUAL TO 1 CONTROLS THE PRINTING OF ALL
C*INTERMEDIARY CALCULATIONS. IF EQUAL TO ZERO ONLY THE FINAL RESULTS ARE
C*PRINTED
C*****
307  CONTINUE
      PI=3.1415926535897
      SIGN=1.
      FMPT=1.
      FMPP=1.0 $ FMNN=1.0
      LAMBOT=1.0
      LAMBON=1.0 $ LAMBOP= 1.0
      GAMMAT=.30
      GAMMAP=.30
      GAMMAN=.30
      NAZIMU=9
      NCPLT=2
      PERIOD=1.0 $ A=1 $ LENGTH=20 $ LAMBDA= 1
      INITIA=0
      POLX=1.0 $ POLZ=1.0
      NLYR=1
      LYR=0
      INDEX1=-20
      INDEX2=20
      FLAG=0.

```

```

C
C
C
311  CONTINUE
C*****
C*HERE THE COMMANDS FOR INPUT DATA ARE SET
C*****

```

```

READ 999,((IN(J),FA(J)),J=1,4)
PRINT 998,((IN(J),FA(J)),J=1,4)
999  FCRMAT(A9,F9.4,X,3(A9,X,F9.4,X))
998  FCRMAT(/,/,4(A9,X,F9.4,X))
DC 301 I=1,4
IF(IN(I).EQ.9HPERIOD )PERIOD= PA(I)
IF(IN(I).EQ.9HLAMEDA )LAMEDA= PA(I)
IF(IN(I).EQ.9HRADIUS )A= PA(I)
IF(IN(I).EQ.9HTANGENT )LAMBOT= PA(I)
IF(IN(I).EQ.9HNOFPAL )LAMBON= PA(I)
IF(IN(I).EQ.9HPERPENDIC)LAMBOP= PA(I)
IF(IN(I).EQ.9HLENGTH )LENGTH= PA(I)
IF(IN(I).EQ.9HLAYER )NCPLCT=1+ PA(I)
IF(IN(I).EQ.9HLAYER )ALYR= PA(I)
IF(IN(I).EQ.9HSIGN )SIGN= PA(I)
IF(IN(I).EQ.9HPOL )PCLX= PA(I)
IF(IN(I).EQ.9HPOLZ )PCLZ= PA(I)
IF(IN(I).EQ.9HINDEX1 )INDEX1= PA(I)
IF(IN(I).EQ.9HINDEX2 )INDEX2= PA(I)
IF(IN(I).EQ.9HSTCF )STCF= PA(I)
IF(IN(I).EQ.9HCOMPUTE ) GO TO 303
IF(IN(I).EQ.9HRESTART ) GO TO 307
301  CONTINUE
GC TO 311
303  CONTINUE
C
C HERE IS WHERE THE SIGN OF THE HELIX SENSE IS DETERMINED
P=PERIOD*SIGN
C SMAX DETERMINES THE NORMALIZATION FACTOR FOR THE TOTAL SCATTERING FOR EACH
C LAMEDA. IT MUST BE FCNCL IN THIS CC LOOP
SMAX=0.0
SMAXL=0.0
SMAXR=0.0
CCMAX=0.0
C
C
C
C*****
C*HERE THE LORENTZIAN-SHAPED POLARIZABILITIES ARE DEFINED *
C*****
ALPHAT=FMTT/((1/(LAMBOT**2))-(1/(LAMEDA**2))+((0.1)*GAMMAT/
1(LAMEDA*((LAMBOT**2)-((GAMMAT**2)/4))))
ALPHAP=FMP/((1/(LAMBOP**2))-(1/(LAMEDA**2))+((0.1)*GAMMAP/
1(LAMEDA*((LAMBOP**2)-((GAMMAP**2)/4))))
ALPHAN=FMPN/((1/(LAMBON**2))-(1/(LAMEDA**2))+((0.1)*GAMMAN/
1(LAMEDA*((LAMBON**2)-((GAMMAN**2)/4))))
TBO=LAMBOT $ PBO=LAMBOP $ NBO=LAMBON
C
IF(FLAG.NE.0) PRINT 1505
1505 FCRMAT(*,6X,*ALPHAT*,6X,*ALPHAN*,6X,*ALPHAP*)
IF(FLAG.NE.0) PRINT 505,ALPHAT,ALPHAN,ALPHAP
C
C
C
C*****
C*THETA IS THE POLAR ANGLE OF SCATTERING *
C*THETA IS IN RADIANS *
C*PSI IS THE AZIMUTHAL ANGLE OF SCATTERING. IT IS COMPUTED HERE EVERY *
C*DEGREE BETWEEN 0 AND 360 *
C*DISCRT=0 IS FOR CONTINUOUS CASE (PERIOD LESS THAN LAMEDA), DISCRT=1 IS *
C*FOR DISCRETE CASE (PERIOD GREATER THAN LAMEDA) *
C*DELTA Z IS THE Z PROJECTION OF THE VECTOR K-K0. ITS MAXIMUM VALUE IS *

```

```

C*2*PI/LAMBDA
C*NAZIMU FOR P GREATER OR EQUAL TO LAMBDA IS CALCULATED HERE
C*IF ONLY ONE LAYER LINE IS WANTED SET NAZIMU=2
C*****
      NANGLE=3E0
      NANGL=NANGLE+1
      DC 11 I=1,NANGL
      PSI(I)=(I-1)*PI/180.
      ANGLE(I)=PSI(I)*180./PI
11  CONTINUE
      DISCRT=0.
      IF(PERIOD.GE.LAMBDA) DISCRT=1.0
C
C
C
C COMPUTE THE MAXIMUM NO. OF LAYER LINES FOR DISCRETE CASE
C COMPUTE ALSO THE PARAMETER DELTA KZ IN TERMS OF THE PCLAF ANGLE
      IF(DISCRT.EQ.1)NAZIMU=INT(PERIOD/LAMBDA+2)
      SAFETY=25
      IF(NCPLOT.LE.NAZIMU)NAZIMU=NCPLOT
      DO 300 ITETA=2,NAZIMU
      IF(SAFETY.LE.NAZIMU)STOP
      LYR=ITETA-2
      DC 299 LP=1,2
C THIS CONTROLS THE NUMBER OF NEGATIVE LAYER LINES TO BE COMPUTED
      IF(ITETA.GT.(NLYR+2).AND.LP.EQ.2) GO TO 299
C THIS ASSURES ONLY ONE ZERO LAYER LINE COMPUTATION
      IF(LP.EQ.2 .AND.ITETA.EQ.2) GO TO 299
      IF(DISCRT.EQ.0)THETA=(PI/2.)-15.*(ITETA-2)*(PI/180.)
      IF(DISCRT.EQ.1)THETA=ACOS((ITETA-2)*LAMBDA/PERIOD)
C THIS COMPUTES NEGATIVE ALTITUDE ANGLE FOR THE CONTINUOUS CASE
      IF(LP.EQ.2.AND.DISCRT.EQ.0)THETA=(PI/2)+15.*(ITETA-2)*(PI/180)
C THIS COMPUTES ALL NEGATIVE LAYER LINES FOR DISCRETE CASE
      IF(LP.EQ.2.AND.DISCRT.EQ.1)THETA=PI-ACOS((ITETA-2)*LAMBDA/
1 PERIOD)
      IF(LP.EQ.2.AND.DISCRT.EQ.1) LYR=-LYR
      DELKZ=(2*PI/(LAMBDA))*COS(THETA)
      AFCLAF=THETA*180./PI
C
C
C
C*****
C*THE LOOP STARTING HERE AND ENDING IN 100 COMPUTE THE SCATTERING INTENSITIES *
C*FOR EACH PSI ANGLE AND FOR A GIVEN VALUE OF THE ALTITUDE OF LAYER *
C*LINE.
C*ILAM IS A PARAMETER THAT ALLOWS FOR THE VARIATION OF THE HELIX PARAM *
C*ETERS TO CALCULATE THE SCATTERING OF CONCENTRIC HELICES OF VARIOUS PITCH *
C*AND RADIUS. IF ILAM GOES FROM 1 TO 1 THEN ONLY ONE HELIX IS CALCULATED *
C*****
      DC 100 I=1,360
      DC 699 II=1,3
      DC 698 JJ=1,3
      DO 697 KK=1,3
      SUPMA(II,JJ,KK)=(0.0,0.0)
697  CONTINUE
698  CONTINUE
699  CONTINUE
C
      DO 700 ILAM=1,1
C
C
C

```



```

C*****
C*CCMPUTE THE ARGUMENTS OF THE BESSEL FUNCTICNS *
C*ALSO THE DIFERENT VALUES OF THE ANGLE PSISTR RELATED TO THE AZIMUTHAL *
C*ANGLE PSI ,ARE CALCULATED HERE *
C*R IS THE PROJECTION OF THE SCATTERED WAVE VECTOR ONTO THE PLANE X-Y *
C*****
      R=(2.*PI/LAMBDA)*SIN(THETA)
      QA(I,ILAM)=(2.0*FI*A/LAMBDA)*SGRT(1.0+(SIN(THETA))**2
1  -2.0*SIN(PSI(I))*SIN(THETA) )
      DUMMY1=QA(I,ILAM)
      IF(DUMMY1.EQ.0.) GO TO 20
      ALPHA= F*A*COS(PSI(I))/QA(I,ILAM)
      IF(ALPHA.GT.1.0)GC TO 20

C
C*TAKE NEGATIVE VALUE OF PSISTR ANGLE
C
      PSISTR(I)=-ACOS(F*A*COS(PSI(I))/QA(I,ILAM))
21  CONTINUE
      IF(FLAG.EQ.0.) GC TO 71
C*HERE COME THE PRINTING STATEMENTS FOR ....
C* POLAR ANGLE, QA, INDEXJ, PSISTR(I),
C
      PRINT35,APOLAR,(CA(I,J,ILAM),J=89,93),(PSISTR(J),J=89,93)
35  FORMAT(/,*,*APCLAFH=*,F8.4,2X,*QA=*,5(2 X,F8.4),2X,*PSISTR=*,5
1  (2X,F8.4))
71  CONTINUE
      IF(FLAG.EQ.0.) GC TO 77
      PRINT 9
9    FORMAT(* *,*PSI*, 9(1(X,*QA*),/))
      PRINT 10,ANGLE(I),QA(I,ILAM)
10   FORMAT(* *, F8.4,5X,F8.4)
77  CONTINUE

C
C
C
C*****
C*HERE WE START GENERATING THE POSITIVE AND NEGATIVE ORDER BESSEL FUNCTION*
C*          BJN(1,I).....C..BJN(41,I)..C.C.....BJN(91,I) *
C*          J=40.....C.....J40.....C..J40 *
C*****
      X=CA(I,ILAM)
      L=41
      ALPHA=0.
      CALL BESJ(X,ALPHA,L,BJ,NZ)
C          BJ(1) .....BJ(41)
C          J0 .....C.....J40
C
      NN=40
30  CONTINUE
      EXPONT=-1-NN
      L=42-NN
      BJN(NN,I) =((-1.0)**EXPONT)*BJ(L)
      NN=NN-1
      IF(NN.EQ.0) GO TO 31
      GC TO 30
31  CONTINUE
      DO 2 N=1,41
      NN=N+40
      BJN(NN,I) =BJ(N)
2    CONTINUE
C*HERE COME THE PRINTING STATEMENTS.....8
C*FOR APCLAR, ANGLE(I), CA(I),INDEX OF BESSEL FUNCTICNS (KL), AND BESSEL

```

```

C* FUNCTIONS
  IF (FLAG.EQ.0.) GO TO 72
  PRINT 3, APOLAR
3   FORMAT(* *, *APOLAR*=?,F8.4, 8(3X,*JN(X)*),/)
  PRINT 10E, (ANGLE(KLM),KLM=1,8)
106  FORMAT(/,*ANGLE*=?,8(4X,F10.7))
  PRINT 6, (QA(KLM,ILAP),KLM=1,8)
6   FORMAT(/,*INDEX,CA*=?,8(5X,F10.7))
  DC 5 K=1,81
  KL=K-41
  PRINT 4,KL,(BJN(K,KLM),KLM=1,8)
4   FORMAT(* *, I4, 8(3X, E 12.5))
5   CONTINUE
72  CONTINUE
C
C
C*****
C*PROCEED TO COMPUTE CONTINUOUS CD FOR LIGHT INCIDENT ALONG THE Y DIRECTION
C*ICN
C*COMPUTE NOW THE COMPONENTS FOR EACH OF THE POLARIZATIONS OF THE ELECTRIC VECTOR E (DIRECTION, POLARIZATION, EACH OF THE THREE COMPONENTS)
C*EXAMPLE E(2,1,3) MEANS THIRD COMPONENT OF ELECTRIC VECTOR TRAVELLING
C*DETERMINES THE COEFFICIENTS D FOR SUMMS COMPLEX FP2,FM2,FP1, ECT.
C*NOW ALL BESSEL FUNCTIONS ARE INDEXED
C*****
  DC 1000 II=1,7
  DC 1001 JJ=1,3
  DC 1002 KK=1,3
  E(II,JJ,KK)=(0.0,0.0)
1002 CONTINUE
1001 CONTINUE
1000 CONTINUE
C*SUM OF ALL ORDERS OF COEFFICIENTS TIMES BESSEL FUNCTIONS TIMES THE CORRESPONDING PHASE FACTORS. FROM -INDEX TO +INDEX WILL BE GENERATED.
  NEGIDX=41+INDEX1
  FLUIDX=41+INDEX2
  DC 200 N=NEGIDX,FLUIDX
  DUMMY=(-(N-41)/P)+(CILKZ/(2*PI))
  AP2 = DUMMY+(2./P)
  IF ((AP2 **2).LT.1.0E-20) GO TO 101
  FP2= SIN(P*PI*LENGTH*AP2)/(PI*AP2)
  GO TO 111
101  FP2= P*LENGTH
111  CONTINUE
  AM2= DUMMY-(2./P)
  IF ((AM2 **2).LT.1.0E-20) GO TO 102
  FM2=SIN(F*PI*LENGTH*AM2)/(PI*AM2)
  GO TO 112
102  FM2= P*LENGTH
112  CONTINUE
  AP0= DUMMY
  IF ((AP0 **2).LT.1.0E-20) GO TO 103
  FP0= SIN(P*PI*LENGTH*AP0)/(PI*AP0)
  GO TO 113
103  FP0= P*LENGTH
113  CONTINUE
  AP1=DUMMY+(1./P)
  IF ((AP1 **2).LT.1.0E-20) GO TO 104
  FP1= SIN(P*PI*LENGTH*AP1)/(PI*AP1)
  GO TO 114
104  FP1= P*LENGTH

```

```

114 CONTINUE
    AM1= DUMMY-(1./P)
    IF((AM1 **2).LT.1.0E-20) GO TO 105
    FM1=SIN(F*PI*LENGTH*AM1)/(PI*AM1)
    GO TO 115
105 FM1= P*LENGTH
115 CONTINUE
    B=BJN(N,I)
    PSIPRM=PI/2.0 + PSISTR(I)
    Z=(N-41)*PSIPRM
    XPCN=COS(Z)+(0.01)*SIN(Z)
    AM=SQRT(A*A+(P/(2*PI))**2)
    IF(FLAG.EQ.0) GC TO 400

C
C
C
C*****
C*
C* THESE ARE ALL PRINTING ROUTINES
C*
C*****
1499 PRINT 499, N, N-41
1499 FCRMAT(/, /,*FUNNING=*, I2, 2X,*ACTUAL ORDER=*,I4)
1499 PRINT 500
1500 FCRMAT(/,3X
1      ,* DUMMY AP2 AM2 AP1 AM1 FP2
1      FM2 FP1 FM1 FP0*)
1501 PRINT 501, DUMMY,AP2,AM2,AP1,AM1,FP2,FM2,FP1,FM1,FP0
1501 FCRMAT(* *,5(2X,F8.4),5(1X,E10.4))
1501 PRINT 502
1502 FCRMAT(/,3X, * B PSIPRM Z XPCN
1      AM*)
1503 PRINT 503, B, PSIPRM,Z, XPCN ,AM
1503 FCRMAT(* *,2(2X,F8.4),1CX,F8.4,2X,*(*,F8.4,*,*,F8.4,*)*,3X,
1      F8.4)
1600 CONTINUE

C
C
C*PRINTING OF THE COMPONENTS OF THE ELECTRIC FIELD VECTOR
C
C
C INCIDENCE Y POLARIZATION Z
C COMPUTE THE TERM E (X,Y,COMPONENTS 1,2,AND3)
1 IF( FLAG.EQ.0) GC TO 405
1 PRINT 504
1504 FCRMAT(/,* E(2,3,1) / E(2,3,2) / E(2,3,3) /
1      E(2,1,1) / E(2,1,2) / E(2,1,3)*)
1505 PRINT 505, E(2,3,1),E(2,3,2),E(2,3,3),E(2,1,1),E(2,1,2),E(2,1,3)
1505 FCRMAT(* *.6(1X,*(*,F8.4,*,*,F8.4,*)*))
1405 CONTINUE

C
C
C
C INCIDENCE Y POLARIZATION Z
1 E(2,3,1)=E(2,3,1)+(A*P/(4.*PI))*(0.01)*B*(FP1-FM1)*XPCN
1 * (ALPHAP/(AM*AM) )
1 IF(FLAG.NE.0)
1 PRINT 505, E(2,3,1),E(2,3,2),E(2,3,3),E(2,1,1),E(2,1,2),E(2,1,3)
1 E(2,3,1)=E(2,3,1)
1 +ALPHAP*(A*P/(4.*PI)*AM*AM))*(0.01)*B*(FP1-FM1)*XPCN
1 IF(FLAG.NE.0)
1 PRINT 505, E(2,3,1),E(2,3,2),E(2,3,3),E(2,1,1),E(2,1,2),E(2,1,3)

```

```

E(2,3,2)=E(2,3,2)+(A*P/(4.*PI))*B*(FP1+FM1)*XPCN*(ALPHAT/(AM*AM))
IF(FLAG.NE.0)
1PRINT505, E(2,3,1),E(2,3,2),E(2,3,3),E(2,1,1),E(2,1,2),E(2,1,3)
E(2,3,2)=E(2,3,2)
1-ALPHAP*(A*P/(4.*PI*AM*AM))*B*(FP1+FM1)*XPCN E(2,3,2)
IF(FLAG.NE.0)
1PRINT505, E(2,3,1),E(2,3,2),E(2,3,3),E(2,1,1),E(2,1,2),E(2,1,3)
E(2,3,3)=E(2,3,3)+(P*P/(4*(PI*PI)))*B*(FPC)*XPCN *(ALPHAT/(AM*AM))
IF(FLAG.NE.0)
1PRINT505, E(2,3,1),E(2,3,2),E(2,3,3),E(2,1,1),E(2,1,2),E(2,1,3)
E(2,3,3)=E(2,3,3)
1+ALPHAP*(A*A/(AM*AM))*B*FPJ*XPCN E(2,3,3)
IF(FLAG.NE.0)
1PRINT505, E(2,3,1),E(2,3,2),E(2,3,3),E(2,1,1),E(2,1,2),E(2,1,3)
E(2,3,1)=E(2,3,1)*PCLZ
E(2,3,2)=E(2,3,2)*PCLZ
E(2,3,3)=E(2,3,3)*PCLZ
C
C INCIDENCE Y POLARIZATION X
C COMPLETE THE TERMS E(2,1,COMPONENTS1,2AND3)
E(2,1,1)=E(2,1,1)+(-A*A/4.)*B*(FP2-2*FP0+FM2)*XPCN
1 *(ALPHAT/(AM**2)) E(2,1,1)
IF(FLAG.NE.0)
1PRINT505, E(2,3,1),E(2,3,2),E(2,3,3),E(2,1,1),E(2,1,2),E(2,1,3)
E(2,1,1)=E(2,1,1)
1 *(ALPHAT/4.)*B*(2.*FP0+FP2+FM2)*XPCN E(2,1,1)
IF(FLAG.NE.0)
1PRINT505, E(2,3,1),E(2,3,2),E(2,3,3),E(2,1,1),E(2,1,2),E(2,1,3)
E(2,1,1)=E(2,1,1)
1+ALPHAP*((P/(4.*PI*AM))**2)*B*(-FP2+2*FP0-FM2)*XPCN E(2,1,1)
IF(FLAG.NE.0)
1PRINT505, E(2,3,1),E(2,3,2),E(2,3,3),E(2,1,1),E(2,1,2),E(2,1,3)
E(2,1,2)=E(2,1,2)+(A*A/4.)*(0.,1.)*B*(FP2-FM2)*XPCN
1 *(ALPHAT/(AM**2)) E(2,1,2)
IF(FLAG.NE.0)
1PRINT505, E(2,3,1),E(2,3,2),E(2,3,3),E(2,1,1),E(2,1,2),E(2,1,3)
E(2,1,2)=E(2,1,2)
1 -(ALPHAT/4.)*B*(FP2-FM2)*XPCN*(0.,1.) E(2,1,2)
IF(FLAG.NE.0)
1PRINT505, E(2,3,1),E(2,3,2),E(2,3,3),E(2,1,1),E(2,1,2),E(2,1,3)
E(2,1,2)=E(2,1,2)
1-ALPHAP*((P/(4.*PI*AM))**2)*(0.,-1.)*B*(FP2-FM2)*XPCN E(2,1,2)
IF(FLAG.NE.0)
1PRINT505, E(2,3,1),E(2,3,2),E(2,3,3),E(2,1,1),E(2,1,2),E(2,1,3)
E(2,1,3)=E(2,1,3)+(A*P/(4.*PI))*(0.,1.)*B*(FP1-FM1)*XPCN
1 *(ALPHAT/(AM*AM)) E(2,1,3)
IF(FLAG.NE.0)
1PRINT505, E(2,3,1),E(2,3,2),E(2,3,3),E(2,1,1),E(2,1,2),E(2,1,3)
E(2,1,3)=E(2,1,3)
1+ALPHAP*(A*P/(4.*PI*AM*AM))*(0.,-1.)*B*(FP1-FM1)*XPCN E(2,1,3)
IF(FLAG.NE.0)
1PRINT505, E(2,3,1),E(2,3,2),E(2,3,3),E(2,1,1),E(2,1,2),E(2,1,3)
E(2,1,1)=E(2,1,1)*PCLX
E(2,1,2)=E(2,1,2)*PCLX
E(2,1,3)=E(2,1,3)*PCLX
IF(FLAG.EQ.0.) GC TC =0E
PRINT505, E(2,3,1),E(2,3,2),E(2,3,3),E(2,1,1),E(2,1,2),E(2,1,3)
406 CONTINUE
200 CONTINUE
C*THIS ADDS THE ELECTRIC FIELDS FOR A SERIES OF CONCENTRIC HELICES WITH DIFF
C*ERENT PARAMETERS FOR ONE GIVEN ANGLE OF SCATTERING.
C

```

```

      DC 701 IF=1,3
      DO 702 JF=1,3
      DC 703 KF=1,3
      SUMMA(IF,JF,KF)=SUMMA(IF,JF,KF)*E(IF,JF,KF)
703   CONTINUE
702   CCNTINUE
701   CCNTINUE
700   CONTINUE
      DC 705 II=1,3
      DO 706 JJ=1,3
      DO 707 KK=1,3
      E(II,JJ,KK)=SUMMA(II,JJ,KK)
707   CCNTINUE
706   CCNTINUE
705   CCNTINUE
C*****
C*FINISH ALL SUMS
C*****
C
C
C*****
C*CORRECT FOR TRANSVERSALITY IN THIS SECTION
C*DEFINE THE TRIGONOMETRIC VALUES OF THE COMPONENTS OF THE SCATTERED WAVE
C*VECTOR K
C*****
      SINPSI=SIN(PSI(I))
      CCSPSI=CCS(PSI(I))
      SINTET=SIN(THETA)
      CCSTET=CCS(THETA)
C*DEFINE EYEKIS= KDOT E(2,1,COMPONENTS) AND EYZETA= KDOT E(2,3,COMP)
      EYZETA=CCSPSI*SINTET*E(2,3,1)+SINPSI*SINTET*E(2,3,2)+CCSTET*
      1 E(2,3,3)
      EYEKIS=CCSPSI*SINTET*E(2,1,1)+SINPSI*SINTET*E(2,1,2)+CCSTET*
      1 E(2,1,3)
C*FINISH COMPUTING CD(I) FOR ALL PSI(I)
      IF(FLAG.NE.0)PRINT 517
517   FCFMAT(* *,*EYEKIS*,9X,*EYZETA*)
      IF(FLAG.NE.0)PRINT 505, EYEKIS, EYZETA
C
C*****
C*COMPUTE IL MINUS IR
C*****
      C1=E(2,1,1)-CCSPSI*SINTET*EYEKIS
      C2=E(2,1,2)-SINPSI*SINTET*EYEKIS
      C3=E(2,1,3)-CCSTET*EYEKIS
      D1=E(2,3,1)-CCSPSI*SINTET*EYZETA
      D2=E(2,3,2)-SINPSI*SINTET*EYZETA
      D3=E(2,3,3)-CCSTET*EYZETA
      CSTR1=CONJG(C1)
      CSTF2=CONJG(C2)
      CSTR3=CONJG(C3)
      DSTF1=CONJG(D1)
      DSTF2=CONJG(D2)
      DSTF3=CONJG(D3)
      IF(FLAG.EQ.0.) GO TO -01
C* PRINTING ROUTINES FOR INTERMEDIATE CALCULATIONS OF CD
      PRINT 506
506   FCFMAT(/,9X,*C1*,9X,*CSTR1*,9X,*C2*,9X,*CSTR2*,9X,*C3*,9X,
      1*CSTR3*)
      PRINT 505, C1,CSTR1,C2,CSTR2,C3,CSTR3
      PRINT 507

```

```

507  FCRMAT(/,*,      C1      /      DSTR1  /      D2      /
10STR2 /      D3      /      CSTR3  *)
PRINT 505, D1,DSTR1,D2,DSTR2,C3,DSTR3
401  CCNTINUE
C
ILMIF(I)=(CSTR1*C1+CSTR2*D2+CSTR3*C3-(C1*CSTR1+C2*DSTR2
1 + C3*DSTR3)) *( 2.*(G.,1.))
EZ=D1*DSTR1+D2*DSTR2+D3*CSTR3
IL(I)=EZ
EX=C1*CSTR1+C2*CSTR2+C3*CSTR3
IR(I)=EX
ILPIR(I)=(C1*CSTR1+C2*CSTR2+C3*CSTR3+D1*DSTR1+D2*DSTR2
1 + D3*DSTR3)*2.
CD(I)=ILMIF(I)/ILPIR(I)
IF(FLAG.EQ.0.) GO TO 511
PRINT 512, ILMIF(I),ILPIR(I), CD(I),IL(I),IR(I)
512  FCRMAT(/,*,*,*ILMIF=*,E16.9,2X,*ILPIR=*,E16.9,2X,*CD=*,E16.9,
12X,*IL=*,E16.9,2X,*IR=*,E16.9)
PRINT 510
510  FORMAT(/,/,/,/,/)
511  CONTINUE
100  CCNTINUE
C* THIS NEXT COMPUTATION ASSUMES THAT THE VALUE AT ANGLE OF 360 DEGREES
C* IS THE SAME AS THAT OF C DEGREES
ANGLE(361)=360.
CD(361)=CD(1) $ ILPIR(361)=ILPIR(1) $ ILMIF(361)=ILMIF(1)
1$ IL(361)=IL(1) $ IR(361)=IR(1)
C
C
C
C*****
C* HERE COME MORE PRINTING ROUTINES
C*****
PRINT 907 ,APOLAR,PERIOD,A,LENGTH,LAMBDA
907  FCRMAT(/,/,*,*,* CD AND TOTAL SCATTER FOR APCLAFM ANGLE=*,F
1 5.2,2X,*EFFICD=*,F5.2,2X,*RADIUS=*,F5.2,2X,*LENGTH=*,F10.2,2X,
1 *LAMBDA=*,F5.2)
PRINT7
7  FCRMAT(/,*,* FSI*, 8X,*CD(I)*,12X,*IL-IR*,12X,*IL+IR*
1,15X,*POLZ*,15X,*POLY*)
DC 57 K=1, NANGL
ANGL=PSI(K)*180./PI
PRINT 58 , ANGL, CD(K) , ILMIF(K), ILPIR(K),IL(K),IR(K)
58  FCRMAT(* *, F8.4, 4X, E12.5, 4(4X,E15.8))
57  CCNTINUE
C
C
C
C*****
C* DETERMINE THE MAXIMUM VALUE FOR PLOTTING SUBROUTINE
C*****
DC 109 I=1,NANGLE
CDMAX=AMAX1 (ABS(CD(I)),CDMAX)
SMAX=AMAX1 (ILPIR( I),SMAX)
SMAXL=AMAX1 (IL(I),SMAXL)
SMAXR=AMAX1 (IF(I),SMAXR)
109  CCNTINUE
IF(CDMAX.GE.0.2) CDMAX=1.
DC 1115 J=1, NANGL
CD(J)=CD(J)/CDMAX
PLOTSC(J)=ILPIR( J)/SMAX
PLOTIL(J)=IL(J)/SMAXL

```

```

      PLCTIF(J)=IR(J)/SMAYF
1115  CONTINUE
C
C
C*****
C*PLOT SCATTERING VS PSI FOR DIFFERING APOLAR ANGLES *
C*IN PLOTING SCATER=0. WILL PLOT CD, SCATER=1.0 WILL PLOT IL+IR/MAX(IL+IR) *
C*SCATER= 2.0 , PLOT IL/MAX(IL), SCATER=3 , PLCT IF/MAX(IR) *
C*****
      IF(NOPLCT.EQ.0) GC TO 600
      IF(DISCRT.EQ.0) LZR=100
      RMAX=1.0
      IF(POLX.EQ.0.OR.FCLZ.EQ.0) GC TO 605
      INITIA=INITIA+1
      APCLAR=90. - APOLAR
      PRINT 151,CDMAX,APOLAR
151  FORMAT(/,*GRAPH OF CD/CDMAX WITH CDMAX=*,F16.8,*ALTITUDE=*,F5.2)
      APCLAR=INT(APOLAR)
      SCATEF=0
      IF(CDMAX.LT.1.0) SCATER=-1
      CALL PCLAR(ANGLE,CD,RMAX),APCLAR,P,A,SCATEF,LAMBDA,LENGTH,LZR,
1  INITIA)
605  CONTINUE
C
      RMAX=1.0
      INITIA=INITIA+1
      PRINT 152, SMAX,APOLAR
152  FORMAT(/,*PLOT GRAPH FOR TOTAL SCATTER DIVIDED BY SMAX=*,
1  E16.9,2X,*APCLAR=*, F5.2)
      APCLAR=INT(APCLAR)
      SCATER=1.0
      CALL PCLAR(ANGLE,PLCTSC,RMAX,APOLAR,P,A,SCATER,LAMBDA,LENGTH,
1  LZR,INITIA)
      PRINT 153,SMAYL,AZIMUT
153  FORMAT(/,*PLOT GRAPH FOR LEFT SCATTER DIVIDED BY SMAYL=*,E16.9,
1  2X,*APOLAR=*,F5.2)
      SCATER=2.0
      CALL PCLAR(ANGLE,PLCTIL,RMAX,APCLAR,P,A,SCATER,LAMBDA,LENGTH,
1  LZR,INITIA)
      PRINT 154,SMAYR,APOLAR
154  FORMAT(/,*PLOT GRAPH FOR RIGHT SCATTER DIVIDED BY SMAYR=*,E16.9,
1  2X,*APOLAR=*,F5.2)
      SCATER=3.0
      CALL PCLAR(ANGLE,PLCTIR,RMAX,APOLAR,P,A,SCATEF,LAMBDA,LENGTH,
1  LZR,INITIA)
600  CONTINUE
C
299  CONTINUE
300  CONTINUE
      GC TO 311
      STCP
20  CONTINUE
      PSISTF(I)=0.0
      GO TO 21
      END
C
C
C
      SLBFOURINE POLAR(TH,R,RPA),APCLAR,FRATIC,RADIUS,SCATEF,W,L,LZR,
1  INITIA)
C*****

```

```

C*THIS SUBROUTINE MAKES PCLAR GRAPHS
C*THE ARGUMENT OF THE FNCTICNS ARE MEASURED IN DEGREES.
C*THE INPUT OF THE ANGLAR VARIABLE HAS TO BE ENTERED IN RADIANS
C*ANGLES ARE POSITIVE IN THE COUNTERCLOCKWISE DIRECTION.
C*AN ANGLE OF ZERO IS HORIZONTAL AND TO THE RIGHT.
C*****
COMMON FMTT,FMPP,FMNN,TB0,PB0,NB0
REAL NB0
COMMON/IGSZZZ/Z(200)
DIMENSION P(400),TH(400),Y(400)
REAL L,LYR
INTEGER STB,SPB,SNB
DIMENSION YNEG(400)
EXTERNAL FONT2
DATA IRAC/2HR=/
DATA IPITCH/2HP=/
DATA IWAVE/2HW=/
DATA ISENE/4HALT=/
DATA ILYF/4HLYF=/
DATA ILENGH/2HL=/
INTEGER BLANK
DATA BLANK/4H /
DATA IPB/3HPB=/
DATA INE/3HNB=/
DATA ITB/3HTB=/
DATA LOGL9L/3HLG=/
DATA ICCMMA/1H,/
995 FORMAT(A3,I3)
996 FORMAT(A2,F4.2)
999 FORMAT(A4,F5.2)
LCGLEN=10
ENCODE(9,999,LABEL)ISENE,APCLAR
IF(LYR.NE.100)ENCODE(9,999,LABEL)ILYF,LYF
ENCODE(6,996,LABEL2)IPITCH,FRATIO
ENCODE(6,996,LABEL3)IRAC,RADIUS
ENCODE(6,996,LABEL5)IWAVE,W
IF(L.GT.99)LOGLEN=ALOG10(L)
IF(L.LE.99)ENCODE(6,996,LABEL6)ILENGH,L
IF(L.GT.99)ENCODE(6,995,LABEL6)LOGL9L,LCGLEN
913 FORMAT(F4.2)
ENCODE(4,913,STB)FMTT
ENCODE(4,913,SPB)FMPP
ENCODE(4,913,SNB)FMNN
911 FORMAT(A3,F4.2,A1)
ENCODE(8,911,LABELT)ITB,TB0,ICMMA
ENCODE(8,911,LABELP)IPB,PB0,ICMMA
ENCODE(8,911,LABELN)INE,NB0,ICMMA
912 FORMAT(A3,A4,A1)
IF(FMTT.EQ.0)ENCODE(8,912,LABELT)ITB,BLANK,ICMMA
IF(FMPP.EQ.0)ENCODE(8,912,LABELP)IPB,BLANK,ICMMA
IF(FMNN.EQ.0)ENCODE(8,912,LABELN)INB,BLANK,ICMMA
C
C
C HERE IS WHERE THE POSITIVE VALUES ARE SEPARATED FROM NEGATIVE VALUES
DO 20 I=1,361
YNEG(I)=0.0
Y(I)=ABS(R(I))
IF(R(I).LT.0.0)YNEG(I)=ABS(R(I))
20 CONTINUE
C
C
C

```



```

C*****
C*IMPORANT IMPORANT IMPORANT
C*HERE IS WHERE THE PLOTTING ROUTINE GETS INITIALIZED ONLY ONCE
C*****
C
C
C
C INITIALIZES GRAPHIC SYSTEM
C INITIA TELLS PLOTTER TO INITIALIZE ALL ROUTINES .INITIA=1 INITIALIZES
  IF(INITIA.NE.1) GO TO 23
  CALL MCDESG(Z,6,4PCIDS)
23  CCATINUE
C
C
  CALL VECIG(Z,Font2,0)
  CALL SETSMG(Z,51,1.)
C SET UP VIEW PORT TO LEAVE 20 PERCENT BORDER
  CALL OBJCTG(Z,20.,20.,80.,80.)
C SET THETA AXIS OFFSET
  Z(185)=90.
C DEFINE THE SUBJECT SPACE FOR BOTH RADIAL AND ANGLAR VARIABLES
  CALL FSLEJG(Z,C.,C.,RMAX,360.)
C DRAWS A GRID OF 30 DEGREES OF ANGULAR SPACING AND .2 CF RADIAL UNITS
  CALL SETSMG(Z,173,0.0)
  CALL PGFIDG(Z,RMAX/5.0,30.,0.,C.)
C SETS FORMAT FOR LABELLING
  CALL SETSMG(Z,30,2.)
  CALL SETSMG(Z,45,2.0)
  FMT=5.2
C LABEL RADIAL AXIS
  CALL PCLEG(Z,.65,175.,4,4H0.60)
  CALL PCLEG(Z,1.05,175.,4,4H1.00)
C SET LARGE CHARACTER SIZE
  CALL SETSMG(Z,45,3.0)
C INDICATE THE FORMAT FOR THE LABELLING
  FMT=6.2
C LABEL THETA AXIS
  CALL PLABELG(Z,1,3(.,0,FMT)
  CALL SETSMG(Z,45,3.0)
  X8=RMAX*1.41
  CALL PCLEG(Z,X8 ,211., 9,LABEL)
  X7=RMAX*1.7
  IF(SCATER.EQ.-1)
1 CALL PCLEG(Z,X7,136.,7,7HCD/MAX )
  IF(SCATEF.EQ.0.0)
1 CALL PCLEG(Z,X7,136.,7,7HCIDS Y)
  IF(SCATER.EQ.1.0)
1 CALL PCLEG(Z,X7,136.,7,7HSCATT Y)
  IF(SCATEF.EQ.0.2.0)
1 CALL PCLEG(Z,X7,136.,7,7HI PCLZ )
  IF(SCATEF.EQ.0.3.0)
1 CALL PCLEG(Z,X7,136.,7,7HI PCLX )
  PRINT 998,LABEL,LABEL2,LABEL3,LABEL5,LABEL6
998  FCRMAT(* *,*HERE ARE THE LABELS *, 6(4X,A9))
  X3=RMAX*1.79
  CALL PCLEG(Z,X3 ,30.,6,LABEL3)
  X4=RMAX*2.2
  CALL PCLEG(Z,X4,45., 6,LABEL2)
  X5=RMAX*2.05
  CALL PCLEG(Z,X5 ,49., 6,LABEL5)
  X6=RMAX*1.61

```



## II. PROGRAM PAN.

This program calculates the CIDS and the total scattering of a helix of arbitrary dimension, for light incident along the helix axis. The calculation is made as a function of the polar angle of scattering and at a fixed value of the azimuthal angle. The results are printed and plotted in polar form (intensities vs. polar angle) and obtained in microfiche and 35 mm. film. No restrictions are imposed to the ratio of pitch/wavelength.

## Deck set-up:

- |                     |   |                             |
|---------------------|---|-----------------------------|
| (1) Control cards   | } | Program SCATTER (version 2) |
| (2) Program         |   | Subroutine POLAR            |
| (3) End-of-job-card |   |                             |

```

PAN,12,300,440402,MAESTRE-BUSTAPANTE
*USERPR
*NOSTAGE
MNF4,T.
FETCHPS,SANDIA,SAND,SANLLIB.
FETCHPS,IODS,ULIB,ULIBX.
FETCHPS,GPACBN7,GPAC,CCBN.
LINK,F=LGO,P=ULIB,F=GPAC,F=SANC,X.
EXIT.
DUMF,J.
FETCHPS,IODS,SYMTAB,SYMTABX.
GRUPP,P=OUTPUT,P=SYMTAB.
FIN.
DISFOSE,FILM=PL,PE=FE.

```

```

C*****
C*THIS PROGRAM CALCULATES CIDS AND TOTAL SCATTERING FOR AN ORIENTED HELIX *
C*OF ARBITRARY PARAMETERS WITH RESPECT TO THE DIMENSIONS OF THE WAVELENGTH *
C*OF THE INCIDENT LIGHT. THE LIGHT INCIDENTS ALONG THE AXIS OF THE HELIX *
C*THE INPUT PARAMETERS ARE WAVELENGTH, PITCH, RADIUS, ANGLE OF ALTITUDE OF *
C*SCATTERING
C*****
C
C
C*****
C*HERE WE DECLARE ALL VARIABLES AND ARRAYS USED IN THE PROGRAM AND ALSO *
C*WE MAKE THE ALLOCATION FOR MEMORY
C*****
      COMPLEX EZEYE, EZEXIS
      REAL LENGTH
      COMPLEX E(3,3,3),XPCN
      COMPLEX C1,C2,C3,D1,D2,C3,CSTR1,CSTR2,CSTR3,CSYF1,DSTR2,DSTR3
      DIMENSION QA(400)
      LEVEL2,BJN
      COMMON/GIANT/BJN(81,400)
      DIMENSION CD(400),THETA(400),BJ(41)
      DIMENSION ILMIR(400),ILPIF(400)
      DIMENSION TCD(400)
      DIMENSION PLOTSC(400)
      INTEGER EXPONT,PLCIDX
      REAL ILMIR,ILPIR,LAMBDA
      REAL MAXILM
      DIMENSION ANGLE(400)
C
C
C
C*****
C*HERE WE INITIALIZE THE VALUES NEEDED FOR COMPUTATION. *
C*AS THE PROGRAM IS WRITTEN IT CALCULATES THE SCATTERING FOR A HELIX WITH *
C*A UNIAXIAL TANGENTIAL POLARIZABILITY. IN THIS CASE THE FORM OF THE POLAR *
C*IZABILITY CANCELS WHEN THE RATIO FOR CIDS IS TAKEN. THEREFORE THE BAND *
C*PARAMETERS DO NOT APPEAR *
C*A IS THE RADIUS OF THE HELIX *
C*PERIOD IS THE PITCH OF THE HELIX AND LENGTH THE NUMBER OF TURNS OF THE *
C*HELIX. *
C*NCNPLOT WILL DECIDE THE MAXIMUM NUMBER OF PLOTS TO BE GENERATED BY THE *

```

```

C*PROGRAM.
C*INDEX DETERMINES THE MAXIMUM ORDER OF BESSEL FUNCTIONS USED IN THE SUPS
C*FLAG IS AN OPTION THAT WHEN EQUAL TO 1 CONTROLS THE PRINTING OF ALL
C*INTERMEDIARY CALCULATIONS. IF EQUAL TO ZERO ONLY THE FINAL RESULTS ARE
C*PRINTED
C*VALUE DETERMINES THE CUTOFF OF SPECIFIC LOGS IN CIDS
C*SINCE THE SCATTERING AS A FUNCTION OF THE AZIMUTHAL ANGLE IS SPHERICALLY
C*SYMMETRIC, THE GENERATION AND PLOTTING OF DATA IS DONE AT AN SPECIFIED
C*AZIMUTHAL (PSI) ANGLE WHILE THE POLAR ANGLE THETA IS VARIED FROM 0 TO
C*360 DEGREES.
C*POLAR ANGLE THETA IS IN RADIAN
C*AZIMUTHAL ANGLE PSI IS ALSO IN RADIAN
C*ANGLE IS THE POLAR ANGLE THETA EXPRESSED IN DEGREE
C*****
      SMAX=0.0
      INDEX2=40.
      INDEX1=-40.
      FLAG=0.
C*SELECT POLAR ANGLE FOR PRINTINGS WHEN FLAG=1.
      MINANG=399 & MAXANG=399
      PI=3.1415926535897
      VALUE=.0001
C*SELECT AZIMUTH ANGLE
      PSI=PI/2
      NOPL0T=0
      NOPLCT=1
      PERIOD=1 & LAMBDA=1 & A=1.0& LENGTH=2000
      LENGTH=2000
      P=PERIOD
      PRATIO=P/LAMBDA
      NANGLE=360
      DO 11 I=1,NANGLE
      THETA(I)=(I-1)*PI/180.
      ANGLE(I)=THETA(I)*180./PI
11    CONTINUE
C
C
C
C*****
C*HERE COME SOME PRINTING ROUTINES
C*****
      DO 13 J=1,NANGLE
      R=(2.*PI/LAMBDA)*SIN(THETA(J))
      R=ABS(R)
      QA(J)=R*A
13    CONTINUE
      IF(FLAG.EQ.0.) GO TO 77
      PRINT 9
9      FORMAT(/,*,*,*APCLARH*, 8(10X,*QA*),/)
      DO 18 I=1, NANGLE
      PRINT 10,ANGLE(I),QA(I)
10     FORMAT(* *, F8.4,5X,F8.4)
18    CONTINUE
77    CONTINUE
C
C
C
C*****
C*HERE WE START GENERATING THE POSITIVE AND NEGATIVE ORDER BESSEL FUNCTION*
C* THE ARGUMENT OF THE BESSEL FUNCTIONS IS NOW F*A
C*****
      DO 1 I=1,NANGLE

```

```

X=QA(I)
L=41
ALPHA=0.
CALL BESJ(X,ALPHA,L,BJ,NZ)
C          BJ(1) .....BJ(41)
C          J0 .....C.....J40
C
C          BJN(1,I).....C..BJN(41,I)..C.C.....BJN(81,I)
C          J=40.....J0.....C..J40
NN=40
30 CONTINUE
EXPONT=41-NN
L=42-NN
BJN(NN,I)=((-1.0)**EXPONT)*BJ(L)
NN=NN-1
IF(NN.EQ.0) GC TO 31
GC TO 30
31 CONTINUE
DO 2 N=1,41
NN=N+40
BJN(NN,I)=BJ(N)
2 CONTINUE
1 CONTINUE
C
C
C*****
C*THESE ARE ALL PRINTING STATEMENTS
C*****
IF(FLAG.EQ.0.) GC TO *2
PRINT 3, LENGTH
3 FCRMAT(* *,*LENGTH=*,F9.4,8(9X,*JN(X)*),/)
PRINT 106,(ANGLE(I),I=1,8)
106 FCRMAT(/,*ANGLE=*,8(LX,F10.7))
PRINT 6,(QA(I),I=1,8)
6 FCRMAT(/,*INDEX,CA=*,3(5X,F10.7))
DO 5 K=1,81
KL=K-41
PRINT 4,KL,(BJN(K,I),I=1,8)
4 FCRMAT(* *,I4,* (3X,E 12.5))
5 CONTINUE
72 CONTINUE
C
C
C*****
C*PROCEED TO COMPUTE THE CIDS FOR LIGHT INCIDENT ALONG THE Z DIRECTION *
C*          BJN(41,I)=J(SUBC) OF ARG(I) *
C*COMPUTE NOW THE COMPONENTS FOR EACH OF THE POLARIZATIONS OF THE ELECTRIC *
C*VECTOR E (DIRECTION,PCLARIZATION, EACH OF THE COMPONENTS) *
C*EXAMPLE E(3,1,2) MEANS THE SECOND COMPONENT OF ELECTRIC VECTOR POLARI *
C*ZED ALONG THE X DIRECTION AND TRAVELLING ALONG THE POSITIVE Z DIREC *
C*TION *
C*DETERMINE THE COEFFICIENTS C FOR SUMS, COMPLEX FP2,FP1, ETC *
C*****
C*COMPUTE CIDS(I) FOR ALL THEYA(I)
DO 100 I=1,360
DO 1000 II=1,3
DO 1001 JJ=1,3
DO 1002 KK=1,3
E(II,JJ,KK)=(0.0,0.0)
1002 CONTINUE

```

```

1001 CONTINUE
1000 CONTINUE
C*DELKZ IS THE PROJECTION OF THE OUTGOING WAVE VECTOR (K) ON THE Z AXIS
C*ITS MAXIMUM VALUE IS -4*PI/LAMBDA
  DELKZ=(2.*PI/(LAMEDA))*(COS(THETA(I))-1.0)
C*SUM OF ALL ORDERS OF COEFFICIENTS TIMES BESSEL FUNCTIONS TIMES THE CORRE*
C*SPONDING FACTORS, FROM -INDEX TO + INDEX WILL BE GENERATED
  NEGIDX=41+INDEX1
  PLUIDX=41+INDEX2
  DO 200 N=NEGIDX,FLUIDX
    DUMMY=(-(N-41)/P)+(DELKZ/(2*PI))
    AP2 = DUMMY+ (2./P)
    IF(AP2.EQ.0.0) GC TO 101
    FP2= SIN(P*PI*LENGTH*AP2)/(PI*AP2)
    GO TO 111
101  FP2= P*LENGTH
111  CONTINUE
    AM2= DUMMY-(2./P)
    IF( AM2.EQ.0.0) GC TO 102
    FM2=SIN(P*PI*LENGTH*AM2)/(PI*AM2)
    GO TO 112
102  FM2= P*LENGTH
112  CONTINUE
    APO= DUMMY
    IF (APO.EQ.0.0) GC TO 103
    FPO= SIN(P*PI*LENGTH*APC)/(PI*APC)
    GO TO 113
103  FPO=P*LENGTH
113  CONTINUE
    AP1=DUMMY+(1./P)
    IF(AP1.EQ.0.0) GO TO 104
    FP1= SIN(P*PI*LENGTH*AP1)/(PI*AP1)
    GO TO 114
104  FP1= P*LENGTH
114  CONTINUE
    AM1= DUMMY-(1./P)
    IF (AM1.EQ.0.0) GC TO 105
    FM1=SIN(P*PI*LENGTH*AM1)/(PI*AM1)
    GO TO 115
105  FM1= P*LENGTH
115  CONTINUE
    B=BJN(N,I)
    SINTET=SIN(THETA(I))
    COSTET=COS(THETA(I))
    CCSPSI=CCS(PHI)
    SINPSI=SIN(PHI)
C*DEFINE ANGLE PSIPRM
    PSIPRM=PSI+(PI/2.0)
    Z=(N-41)*PSIPRM
    XPCN=COS(Z)+(0.,1.)*SIN(Z)
    IF (ANGLE(I).GE.MINANG.AND.ANGLE(I).LE.MAXANG) GC TO 430
C
C
C*****
C*
C*THESE ARE ALL PRINTING ROUTINES
C*
C*****
    IF(FLAG.EQ.0) GC TO 400
430  CONTINUE
    PRINT888, ANGLE(I)

```

```

088  FORMAT(/,/ /, /, /, * *, *APOLARH=*, F5.2)
      PRINT 499, N, N-41
499  FORMAT(/, /, *RUNNING=*, I2, 2X, *ACTUAL CRDER=*, I4)
      PRINT 500
500  FORMAT(/, 9X
      1  * DUMMY  AP2      AM2      AP1      AM1      FP2
      1  FM1      FP1      FM1      FP0*)
      PRINT 501, DUMMY, AP2, AM2, AP1, AM1, FP2, FM2, FP1, FM1, FP0
501  FORMAT(* *, 5(2X, F8.4), 5(1X, E10.4))
      PRINT 502
502  FORMAT(/, 8X, * B      PSIFRM      Z      XPON      *)
      PRINT 503, B, PSIFRM, Z, XPON
503  FORMAT(* *, 2(2X, F8.4), 10X, F8.4, 2X, *(*, F8.4, *, *, F8.4, *)*)
      PRINT 504
504  FORMAT(/, *      E(3,2,1) /      E(3,2,2) /      E(3,2,3) /
      1  E(3,1,1) /      E(3,1,2) /      E(3,1,3)*)
      PRINT 505, E(3,2,1), F(3,2,2), E(3,2,3), E(3,1,1), (3,1,2), E(3,1
      1, 3)
505  FORMAT(* *, 6(1X, *(*, F8.4, *, *, F8.4, *)*))
400  CONTINUE
C
C
C
C COMPUTE THE TERM E(X,Y,COMPONENTS 1,2,AND3)
C INCIDENCE Z POLARIZATION Y
  E(3,2,1)=E(3,2,1)+(A*A/(4.))*B*(J.,1.)*B*(FP2-FM2)*XPON
  E(3,2,2)=E(3,2,2)+(A*A/(4.))*B*(2.*FP0+FP2+FM2)*XPON
  E(3,2,3)=E(3,2,3)+(A*A/(4.*PI))*B*(FP1+FM1)*XPON
C*INCIDENCE Y POLARIZATION X
C**COMPUTE THE TERMS E(3,1, COMPONENTS 1,2 AND 3)
  E(3,1,1)=E(3,1,1)+(-A*A/4.)*B*(FP2-2*FP0+FM2)*XPON
  E(3,1,2)=E(3,1,2)+(A*A/4.)*(0.,1.)*B*(FP2-FM2)*XPON
  E(3,1,3)=E(3,1,3)+(A*A/(4.*PI))*(0.,1.)*B*(FP1-FM1)*XPON
  IF(ANGLE(I).GE. MINANG.ANC.ANGLE(I).LE. MAXANG) GC TO 431
  IF(FLAG.EQ.0.) GC TO 406
431  CONTINUE
      PRINT 505, E(3,2,1), E(3,2,2), E(3,2,3), E(3,1,1), (3,1,2), E(3,1
      1, 3)
406  CONTINUE
200  CONTINUE
C*FINISH ALL SUMS
C*HERE THE FIELDS ARE CORRECTED FOR TRANSVERSALITY
  EZEKIS=CCSPSI*SINTEY*E(3,1,1)+SINPSI*SINTEY*E(3,1,2)
  1 + COSTET*E(3,1,3)
  EZEVE=CCSPSI*SINTEY*E(3,2,1)+SINPSI*SINTEY*E(3,2,2)
  1 + COSTET*E(3,2,3)
  C1=E(3,1,1)-CCSPSI*SINTEY*EZEKIS
  C2=E(3,1,2)-SINPSI*SINTEY*EZEKIS
  C3=E(3,1,3)-COSTET*EZEKIS
  D1=E(3,2,1)-CCSPSI*SINTEY*EZEVE
  D2=E(3,2,2)-SINPSI*SINTEY*EZEVE
  D3=E(3,2,3)-COSTET*EZEVE
  CSTF1=CONJG(C1)
  CSTR2=CONJG(C2)
  CSTF3=CONJG(C3)
  DSTR1=CONJG(D1)
  DSTF2=CONJG(D2)
  DSTF3=CONJG(D3)
  IF(ANGLE(I).GE. MINANG.ANC.ANGLE(I).LE. MAXANG) GC TO 432
  IF(FLAG.EQ.0.) GC TO 401
432  CONTINUE
      PRINT 506

```



```

506  FORMAT(/,9X,*C1*,9X,*CSTR1*,9X,*C2*,9X,*CSTR2*,9X,*C3*,9X,
      1*CSTR3*)
      PRINT 505, C1,CSTR1,C2,CSTR2,C3,CSTR3
      PRINT 507
507  FORMAT(/,*          D1          /          DSTR1 /          D2          /
      1DSTR2 /          D3          /          DSTR3 *)
      PRINT 505, D1,DSTR1,D2,DSTR2,D3,DSTR3
401  CONTINUE
C
C*****
C*CCMFUTE IL MINUS IR
C*THIS GIVES THE CORRECT IL-IR FOR INCIDENCE ALCNG Z
C*****
C
      ILMIR(I)=(CSTR1*C1+CSTR2*D2+CSTR3*C3-(C1*CSTR1+C2*DSTR2
      1 +C3*DSTR3)) *(-2.*(0.,1.))
      ILPIR(I)=(C1*CSTR1+C2*CSTR2+C3*CSTR3+D1*DSTR1+D2*DSTR2
      1 + D3*DSTR3)*2.
C
C*****HERE CORRECT FOR SHARP DISCONTINUITIES DUE TO ZERO/ZERO RATIOS
      TEST1=ABS(ILMIR(I))
      TEST2=ABS(ILPIR(I))
      H=1.E-15
      IF(TEST1.LE.H.AND.TEST2.LE.H.AND.I.NE.1) GO TO 1500
      IF(TEST1.LE.H.AND.TEST2.LE.H.AND.I.NE.2) GO TO 1500
C
      CD(I)=ILMIR(I)/ILPIR(I)
      GO TO 1501
1500 CONTINUE
C
C
C*****
C*MCRE PRINTING ROUTINES
C**PRINT UNCORRECTED DISCONTINUITIES
C*****
      PRINT 1550
      PRINT 1550, ANGLE(I), ILMIR(I), ILPIR(I)
1550  FORMAT(/,* *,*ANGLE=*,F5.2,*IL-IR=*,E16.9,2X,*IL+IR=*,E16.9)
      CD(I)=100.
1501  CONTINUE
      IF(ANGLE(I).GE.MINANG.AND.ANGLE(I).LE.MAXANG) GO TO 433
      IF(FLAG.EQ.0.) GO TO 511
433  CONTINUE
      PRINT 512, ILMIR(I), ILPIR(I), CD(I)
512  FORMAT(/,* *,*ILPIR=*,E16.9,2X,*ILPIR=*,F16.9,2X,*CD=*,E16.9)
      PRINT 510
510  FORMAT(/,/,/,/)
511  CONTINUE
100  CONTINUE
C
C
C
C*GET THE MAXIMUM ABSOLUTE VALUE OF IL+IR
      MAXILM=0
      DO 1560 M=1,360
      AILPIR= ABS(ILPIR(M))
      MAXILM=AMAX1(AILPIR,MAXILM)
1560  CONTINUE
C*CORRECT CIDS FOR FALSE VALUES
      DO 1565 M=1,360
      AILPIR=ABS(ILPIR(M))

```

```

      TCD(M)=CD(M)
      FORM=AILPIR/MAXILM
      IF (FORM.LT.VALUE) TCD(M)=0.
1565 CONTINUE
C
C
C
C*PRINT ROUTINES
      PRINT 907, LENGTH
907  FCRMAT(/,/,*,*,* CD AND TOTAL SCATTER FOR HELIX LENGTH =*,F
      1  5.2,/)
      PRINT 7
7    FCRMAT(/, *APCLAR*, 8X,*CD(I)*, 8X, *IL-IR*,6X,*IL+IR*,8X,*
      1  CORRECTED CD*)
      DO 57 K=1, NANGLE
      ANGL= THETA(K)*180./PI
      IF (CD(K).EQ.100.) CC(K)= 0.5*(CD(K-1)+CD(K+1))
      PRINT 58 , ANGL, CD(K) , ILMIR(K), ILPIR(K),TCD(K)
58   FORMAT(* *, F9.4, 4), E12.5, 3(4X,E15.8))
57   CONTINUE
C
C****DETERMINE THE MAXIMUM VALUE FOR PLOTTING SUBROUTINE
      DO 109 I=1, NANGLE
      SMAX=AMAX1(ILPIR( I),SMAX)
109  CONTINUE
      RMAX=1.0
C
      DO 115 J=1, NANGLE
      PLOTSC(J)=ILPIR( J)/SMAX
115  CONTINUE
C*PLOT SCATTERING VERSUS THE POLAR ANGLE
C
C
C
      PRINT 151, RMAX, LENGTH
151  FCRMAT(/,*PLOT GRAPH WITH RMAX=*,F9.4,2X,*LENGTH =*,F5.2)
      PRINT 152,SMAX,LENGTH
152  FCRMAT(/,*PLOT GRAPH FOR TOTAL SCATTER DIVIDED BY SMAX=*,
      1  E16.8,2X,*LENGTH =*, F5.2)
C
C PLOT GRAPHS
      IF (NO PLOT.EQ.0) GO TO 600
C
C
C
C*IN PLOTTING SCATER=0. WILL PLOT CC, SCATER=1.0 WILL PLOT IL+IR/ MAX(IL+IR)
C
      SCATER=0.
      CALL PCLAR(ANGLE,CD,FMAX,LENGTH,PRATIO,A,SCATER)
      CALL PCLAR(ANGLE,TCD,RMAX,LENGTH,PRATIO,A,SCATER)
      SCATER=1.0
      CALL PCLAR(ANGL,PLOTSC,RMAX,LENGTH,PRATIO,A,SCATER)
600  CONTINUE
C
      STOP
      END
C
C
C
      SUBROUTINE POLAR(TH,P,RMA),AZIMUT,PRATIO,RADIUS,SCATER)
C*****
C*THIS SUBROUTINE MAKES PCLAR GRAPHS

```

```

C*THE ARGUMENT OF THE FUNCTIONS ARE MEASURED IN DEGREES.
C*THE INPUT OF THE ANGULAR VARIABLE HAS TO BE ENTERED IN RADIANS
C*ANGLES ARE POSITIVE IN THE CCOUNTERCLOCKWISE DIRECTION.
C*AN ANGLE OF ZERO IS HORIZONTAL AND TO THE RIGHT.
C*****
COMMON/IGSZZZ/Z(200)
DIMENSION R(400) , TH(400), Y(400)
DIMENSION YNEG(400)
EXTERNAL FONT2
DATA IRAD/2HR=/
DATA IPITCH/4HP/h=/
DATA ISENTE/3HNLN=/
DO 20 I=1, 360
YNEG(I)=0.0
Y(I)=ABS(P(I))
IF(R(I).LT.0.0) YNEG(I)=ABS(R(I))
20 CONTINUE
C INITIALIZES GRAPHIC SYSTEM
CALL MCODES(Z,6,4+CIDS)
23 CONTINUE
CALL VECIG(Z, FONT2,0)
CALL SETSMG(Z,51,1.)
C SET UP A VIEW PORT TO LEVEL TEN PERCENT BORDER
CALL OBJCTG(Z,10.,10.,90.,90.)
C SET THETA AXIS OFFSET
Z(185)=90.
C SET ANGLE OF R AXIS LABELS, MEASURED FROM THE HORIZONTAL
Z(186)=45.
C DEFINE THE SUBJECT SPACE FOR BOTH RADIAL AND ANGULAR VARIABLES
CALL PSUBJG(Z,0.,0.,FMAX,360.)
C DRAWS A GRID OF 30 DEGREES OF ANGULAR SPACING AND .2 OF RADIAL UNITS
CALL PGRIDG(Z,RMAX/10.0,30.,0,0)
CALL SETSMG(Z,45,1.0)
C SETS FORMAT FOR LABELLING
FMT=5.2
C LABEL RADIAL AXIS
CALL PLABELG(Z,0,FMAX/5.,0,FMT)
C SET LARGE CHARACTER SIZE
CALL SETSMG(Z,45,3.0)
C INDICATE THE FORMAT FOR THE LABELLING
FMT=6.2
C LABEL THETA AXIS
CALL PLABELG(Z,1,3(.,0,FMT)
CALL SETSMG(Z,45,1.0)
ENCODE(10,999,LABEL)ISENTE,AZIMUT
999 FORMAT(A3,F7.2)
CALL POLEG(Z,1,0493,170.,9,LABEL)
IF(SCATER.EQ.0.0)
1CALL POLEG(Z,1,1226,171.,22,22+LIGHT INCIDENT ALONG Z)
IF(SCATER.EQ.1.0)
1CALL POLEG(Z,1,1226,171.,22,22+TOTAL SCATTER ALONG Z)
ENCODE(10,997,LABEL2) IPITCH,PRATIO
997 FORMAT(A4,F6.4)
ENCODE(6,996,LABEL3)IRAD,RADIUS
996 FORMAT(A2,F4.2)
998 FORMAT(* *, *LABEL=*, A10, 2X, *LABEL2=*,A10)
PRINT 999 , LABEL,LABEL2
CALL SETSMG(Z,45,2.0)
CALL POLEG(Z,1,92,60.,6,LABEL3)
CALL POLEG(Z,1,70,45.,10,LABEL2)
CALL SETSMG(Z,45,1.)
C JOINS WITH A LINE THE POINTS THAT HAVE BEEN PLOTTED

```

```
CALL SETSMG(Z,30,3.)
CALL PLINEG(Z,360,Y,TH)
IF(SCATER.EQ.1.0) GO TO 40
CALL PLINEG(Z,360,YNEG,TH)
CALL PLINEG(Z,360,YNEG,TH)
CALL PLINEG(Z,360,YNEG,TH)
40 CONTINUE
C TO EXIT
CALL EXITG(Z)
PRINT 21, PMAX ,PRATIC
21 FORMAT(* *,*GRAPH HAS BEEN PLOTTED WITH RMAX=*, F 8.4,
1 4X, *PRATIO=*, F10.6)
RETURN
END
```

## III. PROGRAM COCO.

Calculates CIDS and total scattering for groups of point dipoles, forming a helical array, with uni-axial polarizabilities along the tangent to the helix. The incident electric field is corrected for dipole-dipole interaction among the point dipoles. The input parameters are: pitch, radius, angular separation between the groups, length of the helix and the band properties of the polarizability.

Deck set-up:

- (1) Control cards
- (2) Program                    {   Program INTERAC
- {   Subroutine POLAR
- (3) Input deck
- (4) End-of-job-card

```

COCC, 2, 3000, 55000, 449312, BUSTAPANTE
* NOSTAGE
SCP, A=2900.
SFL, 100000.
MNF, .
FETCHFS, SANDIA, SAND, SANLIB.
FETCHGS, IDOS/ULIBX, DATE=01NOV79, 15475.
FETCFBS, GPACBN7, GPAC, SCEN.
FBSIZE, SAND=0, ULIBX=0.
LINK, F=LGO, P=ULIBX, F=GFAC, P=SANC, X, PP=(LC=50000).
EXIT.
DUMP, 0.
SCP, A=0.
FETCFBS, IDOS, SYMTAB, SYMTAEX.
GRUPF.
FIN.
SCP, A=0.
SFL, 0.
REWIND(FILM)
COPY(FILM, CUT)
REWIND(FILM)
COPY(FILM, MORE)
DISPOSE, FILM=3M, M=MF.
DISPOSE, MCRE=3M, M=MF.
DISPOSE, CUT=MF, M=ME.

```

```

C*****
C*THIS PROGRAM COMPUTES THE TOTAL AND THE DIFFERENTIAL SCATTERING FOR A *
C*DISCRETE ARRAY OF POINTS FORMING A HELIX AND HAVING A POLARIZABILI *
C*TY TANGENTIAL TO THE HELIX. THE HELIX PARAMETERS ARE ARBITRARY. *
C*THE INPUT PARAMETERS ARE THEREFORE WAVELENGTH, PITCH, RADIUS, ANGLE *
C*OF ALTITUDE OF SCATTERING AND THE ELECTRONIC PARAMETERS OF THE POLARIZ *
C*ABILITY *
C*THIS PROGRAM CORRECTS THE INCIDENT FIELD OF THE LIGHT BY BY ADDING TO IT *
C*THE RADIATION FIELD OF ALL OTHER DIPOLES INDUCED IN THE ARRAY. *
C*IF THE PITCH OF THE HELIX IS GREATER OR EQUAL TO THE WAVELENGTH IT CALCUL *
C*LATES THE SCATTERING INTENSITIES AT EACH LAYER LINE. IF PITCH IS SMALLER *
C*THAN LAMBDA IT CALCULATES THE SCATTERING INTENSITIES AT FIXED ANGLES IN *
C*SPACE. *
C*****
C

```

```

PROGRAM INTERAC(INPLT, OUTPUT, TAPE5=INPUT, TAPE6=OUTPUT, FILM)

```

```

C
C
C
C*****
C*HERE WE DECLARE ALL VARIABLES AND ARRAYS USED IN THIS PROGRAM AND ALSO *
C*THE ALLOCATION FOR MEMORY IS DONE *
C*****
COMMON FMTT, FMPP, FMNN, TEG, PEO, NBO
REAL NBO
DIMENSION IN(4), PA(4)
REAL LAMBOT, LAMBCN, LAMEOF
REAL LENGTH
COMPLEX F(3,3,3), XPCN
COMPLEX XPONTL, SP, CN, TN, XPONT2

```

```

COMPLEX CE(3,3,3)
CCOMPLEX SUMMA(3,3,3)
COMPLEX ALPHAT,ALPHAN
CCOMPLEX ALPHAP
COMPLEX EXPONT
COMPLEX EYZETA, EYEKIS
CCOMPLEX C1,C2,C3,D1,D2,C3,CSTR1,CSTR2,CSTR3,DSTR1,DSTR2,DSTR3
DIMENSION QA(400,20)
LEVEL2,BJN
COMPCN/GIANT/BJN(81,400)
DIMENSION CD(400),PSI(400),PSISTR(400),BJ(41)
DIMENSION ILMIR(400),ILPIR(400),IL(400),IR(400),PLOTIL(400),
1PLCTIF(400)
DIMENSION PLOTSC(400)
REAL LYF
REAL ILMIR,ILPIR,LAMBDA,IL,IR
DIMENSION ANGLE(400)
DIMENSION PARAM(10)

C
C
C
307 CONTINUE
C*****
C*HERE WE INITIALIZE THE VALUES NEEDED FOR COMPLTATION. *
C*SIGN DETERMINES THE SENSE OF THE HELIX. SIGN=1. GIVES A RIGHT HANDED *
C*HELIX. SIGN=-1 GIVES A LEFT HANDED ONE. *
C*FMTT IS THE STRENGTH OF THE TANGENTIAL BAND *
C*LAMBOT IS THE POSITION OF THIS BAND *
C*GAMMAT IS THE HALF HEIGHT WIDTH OF THE BAND *
C*THE CORRESPONDING ELECTRONIC PARAMETERS FOR THE OTHER AXES OF THE POLAR *
C*IZABILITY ARE SET BUT NOT USED IN THE COMPUTATIONS. *
C*NAZIMP IS THE MAXIMUM NUMBER OF LAYER LINES THAT EXIST FOR A GIVEN *
C*RATIO OF P/LAMBDA. HERE A DEFAULT VALUE FOR THE CONTINUOUS CASE IS GIVEN *
C*A IS THE RADIUS OF THE HELIX *
C*PERIOD IS THE PITCH OF THE HELIX AND LENGTH THE NUMBER OF TURNS OF THE *
C*HELIX. *
C*NCPLCT WILL DECIDE THE MAXIMUM NUMBER OF PLOTS TO BE GENERATED BY THE *
C*PROGRAM. *
C*INITIA CONTROL THE INITIALIZATION OF THE POLAR PLOTS *
C*PCLZ=0. GIVES SCATTERING OF LIGHT POLARIZED IN THE X DIRECTION *
C*PCLY=0. GIVES SCATTERING OF LIGHT POLARIZED IN THE Z DIRECTION *
C*DEFAULT GIVES CIDS *
C*NLFR DETERMINES THE NUMBER OF LAYER LINES COMPUTED *
C*LYR DETERMINES THE ALTERNATIVE PLOTTING OF LAYER LINES OF ALTITUDE IN *
C*POLAR PLOTS *
C*INDEX DETERMINES THE MAXIMUM ORDER OF BESSEL FUNCTIONS USED IN THE SLPS *
C*FLAG IS AN OPTION THAT WHEN EQUAL TO 1 CONTROL THE PRINTING OF ALL *
C*INTERMEDIARY CALCULATIONS. IF EQUAL TO ZERO ONLY THE FINAL RESULTS ARE *
C*PRINTED *
C*TETC IS THE ANGULAR SEPARATION BETWEEN THE DIPOLES IS GIVEN IN RADIANS *
C*****
FLAG=C.0
C INITIALIZE VALUES
TETO=0.3
TETOSO=TETO*TFTO
SIGN=1.
FMTT=1.
FMPP=C. & FMNN=0.
LAMBOT=3.0
LAMBON=1.0 & LAMBOP= 1.0
GAMMAT=.15
GAMMAP=.15

```

```

GAMMAN=.15
NAZIMU=8
NOPL0T=2
PERIOD=1.0 $ A=1 $ LENGTH=20 $ LAMBDA= 1
INITIA=0
PCLX=1.0$ POLZ=1.0
NLYR=1.
LYR=0
INDEX1=-20
INDEX2=20
PI=3.1415926535897

C
C
C
311 CONTINUE
C*****
C*HERE THE COMMANDS FOR INPUT DATA ARE SET *
C*****
READ 999,((IN(J),PA(J)),J=1,4)
PRINT 998,((IN(J),FA(J)),J=1,4)
999 FORMAT(A9,F9.4,X,3(A9,X,F9.4,X))
998 FORMAT(/,/,4(A9,X,F9.4,X))
DC 301 I=1,4
IF (IN(I).EQ.9HPERIOD )PERIOD= PA(I)
IF (IN(I).EQ.9HLAMBDA )LAMBDA= PA(I)
IF (IN(I).EQ.9HRADIUS )A= PA(I)
IF (IN(I).EQ.9HLZEPON )LAMBON= FA(I)
IF (IN(I).EQ.9HLZEROP )LAMBOP = PA(I)
IF (IN(I).EQ.9HLZEPOT )LAMBOT= FA(I)
IF (IN(I).EQ.9HNCFMAL )LAMBON= PA(I)
IF (IN(I).EQ.9HTANGENT )LAMBOT= PA(I)
IF (IN(I).EQ.9HFMTT )FMTT= PA(I)
IF (IN(I).EQ.9HFMPF )FMPF= PA(I)
IF (IN(I).EQ.9HFMAN )FMNN= PA(I)
IF (IN(I).EQ.9HPERFEADIC)LAMBOP= PA(I)
IF (IN(I).EQ.9HLENGTH )LENGTH= PA(I)
IF (IN(I).EQ.9H+LAYER )ACPLCT=1+ PA(I)
IF (IN(I).EQ.9H-LAYER )NLYR= PA(I)
IF (IN(I).EQ.9HSIGN )SIGN= PA(I)
IF (IN(I).EQ.9HPOL )PCLX= PA(I)
IF (IN(I).EQ.9HPOLZ )PCLZ= PA(I)
IF (IN(I).EQ.9HINDEX1 )INDEX1= PA(I)
IF (IN(I).EQ.9HINDEX2 )INDEX2= PA(I)
IF (IN(I).EQ.9HSTCF )STOP
IF (IN(I).EQ.9HCOMPUTE ) GO TO 303
IF (IN(I).EQ.9HRESTART ) GO TO 307
301 CONTINUE
GO TO 311
303 CONTINUE
C
C HERE IS WHERE THE SIGN OF THE HELIX SENSE IS DETERMINED
P=PERIOD*SIGN
PSQR=(P/(2*PI))**2
PD2PI=P/(2*PI)
AP=SQRT(A*A+(P/(2*PI))**2)
C SMAX DETERMINES THE ACRPALIZATION FACTOR FOR THE TOTAL SCATTERING FOR EACH
C LAMBDA. IT MUST BE FOUND IN THIS DO LOOP
SMAX=0.0
SMAYL=0.0
SMAXR=0.0
COMAX=J.
C

```



```

C
C
C*****
C*HERE THE LORENTZIAN-SHAPED POLARIZABILITY IS DEFINED *
C*****
      ALPHAT=FPTT/((1/(LAMBOT**2))-1/(LAMBDA**2))+ (0.,1.)*GAMMAT/
      1(LAMBDA*((LAMBOT**2)-((GAMMAT**2)/4)))
      ALPHAP=FPPP/((1/(LAMBOP**2))-1/(LAMBDA**2))+ (0.,1.)*GAMMAP/
      1(LAMBDA*((LAMBOP**2)-((GAMMAP**2)/4)))
      ALPHAN=FPPN/((1/(LAMBON**2))-1/(LAMBDA**2))+ (0.,1.)*GAMMAN/
      1(LAMBDA*((LAMBON**2)-((GAMMAN**2)/4)))
      TEG=LAMBOT & PBQ=LAMBOP & NBQ=LAMBON
C
C      IF (FLAG.NE.0) PRINT 1505
1505  FORMAT(/,6X,*ALPHAT*,6X,*ALPHAN*,6X,*ALPHAP*)
      IF (FLAG.NE.0) PRINT 505,ALPHAT,ALPHAN,ALPHAP
C
C
C*****
C*THETA IS THE POLAR ANGLE OF SCATTERING *
C*THETA IS IN RADIANS *
C*PSI IS THE AZIMUTHAL ANGLE OF SCATTERING. IT IS COMPUTED HERE EVERY *
C*DEGREE BETWEEN 0 AND 360 *
C*DISCRT=0 IS FOR CONTINUOUS CASE (PERIOD LESS THAN LAMBDA), DISCRT=1 IS *
C*FOR DISCRETE CASE (PERIOD GREATER THAN LAMBDA) *
C*DELKZ IS THE Z PROJECTION OF THE VECTOR K-K0. ITS MAXIMUM VALUE IS *
C*2*PI/LAMBDA *
C*NAZIMU FOR P GREATER OR EQUAL TO LAMBDA IS CALCULATED HERE *
C*IF ONLY ONE LAYER LINE IS WANTED SET NAZIMU=2 *
C*****
      NANGLE=360
      NANGI=NANGLE+1
      DO 11 I=1,NANGI
      PSI(I)=(I-1)*PI/180.
      ANGLE(I)=PSI(I)*180./PI
11  CONTINUE
      DISCRT=0.
      IF (PERIOD.GE.LAMBDA) DISCRT=1.0
C
C
C
C
C COMPUTE THE MAXIMUM NO. OF LAYER LINES FOR DISCRETE CASE
C COMPUTE ALSO THE PARAMETER DELTA KZ IN TERMS OF THE AZIMUTHAL ANGLE
      IF (DISCRT.EQ.1) NAZIMU=INT (PERIOD/LAMBDA+2)
      SAFETY=25
      IF (NOPLCT.LE.NAZIMU) NAZIMU=NOPLCT
      DO 300 ITETA=2,NAZIMU
      IF (SAFETY.LE.NAZIMU) STCF
      LYR=ITETA-2
      DO 299 LP=1,2
C THIS CONTROLS THE NUMBER OF NEGATIVE LAYER LINES TO BE COMPUTED
      IF (ITETA.(T.(NLYR+2).AND.LP.EQ.2) GO TO 299
C THIS ASSURES ONLY ONE ZERO LAYER LINE COMPUTATION
      IF (LP.EQ.2 .AND. ITETA.EQ.2) GO TO 299
      IF (DISCRT.EQ.0) THETA=(PI/2.)-15.*(ITETA-2)*(PI/180.)
      IF (DISCRT.EQ.1) THETA=ACOS ((ITETA-2)*LAMBDA/PERIOD)
C THIS COMPUTES NEGATIVE ALTITUDE ANGLE FOR THE CONTINUOUS CASE
      IF (LP.EQ.2 .AND. DISCRT.EQ.0) THETA=(PI/2.)+15.*(ITETA-2)*(PI/180.)
C THIS COMPUTES ALL NEGATIVE LAYER LINES FOR DISCRETE CASE
      IF (LP.EQ.2 .AND. DISCRT.EQ.1) THETA=PI-ACOS ((ITETA-2)*LAMBDA/

```

```

1 PERIOD)
IF (LP.EQ.2.AND.DISCRT.EQ.1) LYR=-LYR
DFLKZ=(2*PI/(LAMECA))*COS(THETA)
APCLAR=THETA*180./PI
C*R IS THE PROJECTION OF THE CUTTING K VECTOR ONTO THE X-Y PLANE
R=(2.*PI/LAMBDA)*SIN(THETA)
C
C
C
C*****
C*HERE WE INITIALIZE AND CALCULATE THE PART OF THE ELECTRIC FIELD CCNTRI *
C*BY THE DIPOLES. THIS IS THEREFORE THE INTERACTION TERM.
C*J REPRESENTS THE MAXIMUM NUMBER OF NEAREST NEIGHBOR INTERACTIONS TAKEN *
C*INTO ACCOUNT AT EACH SIDE OF A DIPOLE
C*****
      SN=(0.0,0.0)*CN=(0.0,0.0) STN=(0.0,0.0)
      DO 202 J=1,10
      TETJ=J*TETO
      SINTEJ=SIN(TETJ)
      CCSTEJ=CCS(TETJ)
      D=2*A*A*(1-CCSTEJ)+FSQR*TETJ*TETJ
      AJN=(1/(C**1.5))*(A*A*CCSTEJ+PSQR-3*(A*A*SINTEJ+PSQR*TETJ)**2/D)
      ANG2=(2*PI*A/LAMECA)*SINTEJ
      SN=SN+(0.1,0)*(A*SINTEJ)*SIN(ANG2)*AJN*2.0
      CN=CN+(F/(2*PI))*CCS(ANG2)*AJN*2.0
      IF (FLAG.EQ.1)
C
C
C
C*****
C*HERE COME SOME PRINTING ROUTINES
C*****
      1PRINT 520,J
520  FCRMAT(*,*,*  SN  *,*  CN  *,*  TN  *,*J=*,I4
      )
      IF (FLAG.EQ.1)
      1PRINT 505,SN,CN,TN
202  CONTINUE
C
C
C
C*****
C*THE LOOP STARTING HERE AND ENDING IN 100 COMPLETE THE SCATTERING INTENSI *
C*TIES FOR EACH PSI ANGLE AND FOR A GIVEN VALUE OF THE ALTITUDE OR LAYER *
C*LINE.
C*ILAM IS A PARAMETER THAT ALLOWS FOR THE VARIATION OF THE HELIX PARAME *
C*TERS TO CALCULATE THE SCATTERING OF CONCENTRIC HELICES OF VARIOUS PITCH *
C*AND RADIUS. IF ILAM GOES FROM 1 TO 1 THEN ONLY ONE HELIX IS CALCULATED *
C*****
      DO 100 I=1,360
      IF (FLAG.EQ.1)
      1 PRINT 521, I, PSI(I)
521  FCRMAT(*,*,*I=*,I4,*  PSI(I)=*, F8.4)
      DO 699 II=1,3
      DO 698 JJ=1,3
      DO 697 KK=1,3
      SUMMA(II,JJ,KK)=(0.0,0.0)
697  CONTINUE
698  CONTINUE
699  CONTINUE
C
      DO 700 ILAM=1,1

```

```

C PLT PARAMETERS FOR RLNS BETWEEN THIS CARD AND NEXT CARD
C
C
C*****
C*HERE THE DIFFERENT VALUES OF THE ANGLE PSISTR RELATED TO THE AZIMUTHAL *
C*ANGLE PSI, ARE CALCULATED *
C*****
      QA(I,ILAM)=(2.0*FI*A/LAMBDA)*SQRT(1.0+(SIN(THETA))**2
1     -2.0*SIN(PSI(I))*SIN(THETA) )
      DUMMY1=QA(I,ILAM)
      IF(DUMMY1.EQ.0.) GO TO 20
      ALPHA= R*A*COS(PSI(I))/QA(I,ILAM)
      IF(ALPHA.GT.1.0)GC TO 20
C
C TAKE NEGATIVE AVLUE FOR PSISTR ANGLE
C
      PSISTR(I)=-ACOS(R*A*CCS(PSI(I))/QA(I,ILAM))
21  CONTINUE
      IF(FLAG.EQ.0.) GC TO 71
C HERE COME THE PRINTING STATEMENTS FOR ....
C POLAR ANGLE, QA, INDEXJ, PSISTR(I),
      PRINT35,APGLAR,(CA(J,ILAM),J=89,93),(PSISTR(J),J=88,93)
35  FCRMAT(/,* *,*APCLARH=*,F8.4,2X,*QA=*,5(2 X,F8.4),2X,*PSISTR=*,5
1     (2X,F8.4))
71  CONTINUE
      IF(FLAG.EQ.0.) GC TO 77
      PRINT 9
9    FORMAT(* *, *PSI*, F(10X, *QA*),/)
      PRINT 10,ANGLE(I),QA(I,ILAM)
10  FCRMAT(* *, F8.4,5X,F8.4)
77  CONTINUE
C
C
C*****
C*PROCEED TO COMPUTE CCNTINCLCS CD FOR LIGHT INCIDENT ALONG THE Y DIFFC*
C*TION *
C*COMPUTE NOW THE COMPCENTS FOR EACH OF THE POLARIZATIONS OF THE CORREC *
C*TION PART OF THE ELECTRIC VECTOR. THESE WILL BE SIMBOLIZED BY CE *
C*THEY ARE CE(DIRECTION,PCLAFIZATION,EACH OF THE THREE COMPCONENTS) *
C*EXAMPLE CE(2,1,3) MEANS THIFD COMPCENT OF CORRECTION FIELD TRAVELLING *
C*IN THE POSITIVE Y DIRECTION PCLAFIZED IN THE X DIRECTION *
C*****
      DC 1000 II=1,3
      DC 1001 JJ=1,3
      DC 1002 KK=1,3
      E(II,JJ,KK)=(0.0,0.0)
      CE(II,JJ,KK)=(0.0,0.0)
1002 CONTINUE
1001 CONTINUE
1000 CONTINUE
      DC 200 NN=1,361
      N=NN-131
      SINTN=SIN(N*TF TO)
      CCSTN=CCS(N*TF TO)
      ANG3=QA(I,ILAM)*CCS(N*TF TO-PSISTR(I))+ P*TF TO*N*(CELKZ/(2*PI))
      XPCNT2=CCS(ANG3)+(0.,1.0)*SIN(ANG3)
      CE(2,1,1)=CE(2,1,1)-(1/(AM**2))*XPCNT2*(ALPHAT**2)*(-A*SINTN*
1 TETO*TF TO)*SN
      CE(2,1,2)=CE(2,1,2)-(1/(AM**2))*XPCNT2*(ALPHAT**2)*( A*CCSTN*
1 TETO*TF TO)*SN

```

```

      CE(2,1,3)=CE(2,1,3)-(1/(AM**2))*XPONT2*(ALPHAT**2)*(P/(2*PI))*
1 TETO*TETC *SN
      CE(2,3,1)=CE(2,3,1)-(1/(AM**2))*XPONT2*(ALPHAT**2)*(-A*SINATN*
1 TETO*TETC)*CN
      CE(2,3,2)=CE(2,3,2)-(1/(AM**2))*XPONT2*(ALPHAT**2)*(A*COSTN)*
1 TETO*TETC*CN
      CE(2,3,3)=CE(2,3,3)-(1/(AM**2))*XPONT2*(ALPHAT**2)*(P/(2*PI))*
1 TETO*TETO*CN
      IF(FLAG.EQ.1)
1 PRINT 940
940  FCRMAT(* *,*      CE(2,3,1)      (CE(2,3,2,
1 CE(2,3,3)      CE(2,1,1)      CE(2,1,2)
1 CE(2,1,3)      *)
      IF(FLAG.EQ.1)
1 PRINT 505,CE(2,3,1),CE(2,3,2),CE(2,3,3),CE(2,1,1),CE(2,1,2) ,
1 CE(2,1,3)

C
C
C
C*****
C*NOW COME THE CORRESPONDING SCATTERED ELECTRIC FIELD WITHOUT THE CORREC*
C*TION. IMMEDIATELY AFTER THESE FIELDS SO OBTAINED ARE CORRECTED *
C*FACTOR IS A DUMMY INDEX THAT CAN BE USED TO ELIMINATE THE CORRECTION *
C*THAT IS FACTOR=0 OR TO LEAVE IT THERE THAT IS FACTOR=1 *
C*****
      SINNTC=SIN(N*TETC)
      COSNTC=CCS(N*TETC)
      ANG=QA(I,ILAM)*CCS(N*TETC-PSISTR(I))+P*TETO*N*(DELKZ/(2*PI))
      EXPONT=CCS(ANG)+(C.,1.0)*SIN(ANG)

C
C
C
C INCIDENCE Y POLARIZATION Z
      E(2,3,1)=E(2,3,1)+(-A*P/(2*PI*AM*AM))*EXPONT*SINNTC
1 *ALPHAT*TETO*AM
      E(2,3,2)=E(2,3,2)+(A**2/(2*PI*AM*AM))*EXPONT*COSNTC
1 *ALPHAT*TETO*AM
      E(2,3,3)=E(2,3,3)+((P/(2*PI*AM))**2)*EXPONT
1 *ALPHAT*TETO*AM

C
C INCIDENCE Y POLARIZATION X
C COMPUTE THE TERMS E(2,1,COMPONENTS 1,2 AND 3)
      E(2,1,1)=E(2,1,1)+((A/AM)**2)*EXPONT*(SINATO**2)
1 *ALPHAT*TETO*AM
      E(2,1,2)=E(2,1,2)+(-(A/AM)**2)*EXPONT*SINATO*COSNTC
1 *ALPHAT*TETO*AM
      E(2,1,3)=E(2,1,3)+(-A*P/(2*PI*(AM**2)))*EXPONT*SINNTC
1 *ALPHAT*TETO*AM
      IF(FLAG.EQ.0.) GC TC *CE
      IF(FLAG.EQ.1) PRINT 504
      PRINT 505, E(2,3,1),E(2,3,2),E(2,3,3),E(2,1,1),E(2,1,2),E(2,1,3)
406  CCNTINUF
200  CCNTINUF
      FACTOR=1.
      E(2,1,1)=E(2,1,1)*CE(2,1,1)*FACTOR
      E(2,1,2)=E(2,1,2)*CE(2,1,2)*FACTOR
      E(2,1,3)=E(2,1,3)*CE(2,1,3)*FACTOR
      E(2,3,1)=E(2,3,1)*CE(2,3,1)*FACTOR
      E(2,3,2)=E(2,3,2)*CE(2,3,2)*FACTOR
      E(2,3,3)=E(2,3,3)*CE(2,3,3)*FACTOR
      E(2,3,1)=E(2,3,1)*PCLZ
      E(2,3,2)=E(2,3,2)*PCLZ

```

```

E(2,3,3)=E(2,3,3)*PCLZ
E(2,1,1)=E(2,1,1)*PCLX
E(2,1,2)=E(2,1,2)*PCLX
E(2,1,3)=E(2,1,3)*PCLX
C PRINTING OF THE COMPONENTS OF THE ELECTRIC FIELD VECTOR
C CORRECTED BY THE DIPOLE-DIPOLE INTERACTION
C COMPUTE THE TERM E(X,Y,COMPONENTS 1,2,AND3)
IF( FLAG.EQ.0) GO TO 405
PRINT 504
504  FORMAT(/,*, E(2,3,1) / E(2,3,2) / E(2,3,3) /
1    E(2,1,1) / E(2,1,2) / E(2,1,3)*)
PRINT 505, E(2,3,1),E(2,3,2),E(2,3,3),E(2,1,1),E(2,1,2),E(2,1,3)
505  FORMAT(* *,6(1X,*(,F9.4,*,*,F8.4,*)*)
405  CONTINUE
C THIS ADDS THE ELECTRIC FIELDS FOR A SERIES OF CONCENTRIC HELICES WITH DIFF
C ERENT PARAMETERS FOR ONE GIVEN ANGLE OF SCATTERING.
DC 701 IF=1,3
DC 702 JF=1,3
DC 703 KF=1,3
SUMMA(IF,JF,KF)=SUMMA(IF,JF,KF)+F(IF,JF,KF)
703  CONTINUE
702  CONTINUE
701  CONTINUE
700  CONTINUE
DC 705 II=1,3
DC 706 JJ=1,3
DC 707 KK=1,3
E(II,JJ,KK)=SUMMA(II,JJ,KK)
707  CONTINUE
706  CONTINUE
705  CONTINUE
C*****
C*FINISH ALL SUMS
C*****
C
C
C*****
C*CORRECT FOR TRANSVERSALITY IN THIS SECTION
C*DEFINE THE TRIGONOMETRIC VALUES OF THE COMPONENTS OF THE SCATTERED WAVE
C*VECTOR K
C*****
SINPSI=SIN(PHI(I))
CCSPSI=CCS(PHI(I))
SINTET=SIN(THETA)
CCSTET=CCS(THETA)
C DEFINE EYEKIS= K DCTE(2,1,COMPONENTS)AND EYZETA= K DCTE(2,3,COMP)
EYZETA=CCSPSI*SINTET*E(2,3,1)+SINPSI*SINTET*E(2,3,2)+CCSTET*
1 E(2,3,3)
EYEKIS=CCSPSI*SINTET*E(2,1,1)+SINPSI*SINTET*E(2,1,2)+CCSTET*
1 E(2,1,3)
C FINISH COMPUTING CD(I) FOR ALL PHI(I)
IF(FLAG.NE.0)PRINT 517
517  FORMAT(* *,*EYEKIS*,8X,*EYZETA*)
IF(FLAG.NE.0) PRINT 515, EYEKIS,EYZETA
C
C*****
C*COMPUTE IL MINUS IR
C*****
C1=E(2,1,1)-CCSPSI*SINTET*EYEKIS
C2=E(2,1,2)-SINPSI*SINTET*EYEKIS
C3=E(2,1,3)-CCSTET*EYEKIS

```

```

D1=E(2,3,1)-COSPSI*SINTET*EYZETA
D2=E(2,3,2)-SINPSI*SINTET*EYZETA
D3=E(2,3,3)-COSTET*EYZETA
CSTR1=CONJG(C1)
CSTR2=CONJG(C2)
CSTR3=CONJG(C3)
DSTR1=CONJG(D1)
DSTR2=CONJG(D2)
DSTR3=CONJG(D3)
IF(FLAG.EQ.0.) GC TC *01

C
C
C PRINTING ROUTINES FOR INTERMEDIATE CALCULATIONS OF CD
PRINT 506
506 FCRMAT(/,9X,*C1*,9X,*CSTR1*,9X,*C2*,9X,*CSTR2*,9X,*C3*,9X,
1*CSTR3*)
PRINT 505, C1,CSTR1,C2,CSTR2,C3,CSTR3
PRINT 507
507 FCRMAT(/,* C1 / DSTR1 / D2 /
1DSTR2 / D3 / DSTR3 *)
PRINT 505, D1,DSTR1,D2,CSTR2,C3,DSTR3
401 CCATINUE
C
ILMIR(I)=(CSTR1*C1+CSTR2*D2+CSTR3*D3-(C1*CSTR1+C2*DSTR2
1 +C3*DSTR3))*(2.*(0.,1.))
EZ=D1*DSTR1+D2*DSTR2+D3*DSTR3
IL(I)=EZ
EX=C1*CSTR1+C2*CSTR2+C3*CSTR3
IR(I)=EX
ILPIR(I)=(C1*CSTR1+C2*CSTR2+C3*CSTR3+D1*DSTR1+D2*DSTR2
1 + D3*DSTR3)*2.
CD(I)=ILMIR(I)/ILPIR(I)
IF(FLAG.EQ.0.) GC TO 511
PRINT 512, ILMIR(I),ILPIR(I), CD(I),IL(I),IR(I)
512 FCRMAT(/,* *,*ILPIR=*,E16.9,2X,*ILPIR=*,E16.9,2X,*CD=*,E16.9,
12X,*IL=*,E16.9,2X,*IR=*,E16.9)
PRINT 510
510 FCRMAT(/,/,,/)
511 CCATINUE
100 CCATINUE
C
C IS THE SAME AS THAT OF C DEGREES
ANGLE(361)=360.
CD(361)=CD(1) & ILPIR(361)=ILPIR(1) & ILMIR(361)=ILMIR(1)
1 & IL(361)=IL(1) & IR(361)=IR(1)

C
C*****
C*HERE COME MORE PRINTING SUBROUTINES
C*****
PRINT 907 ,APCLAR,PERICC,A,LENGTH,LAMBDA
907 FCRMAT(/,/,* *,* CD AND TOTAL SCATTER FOR APCLARH ANGLE=*,F
1 : 5.2,2X,*PERICC=*,F5.2,2X,*RADIUS=*,F5.2,2X,*LEAGTH=*,F10.2,2X,
1 *LAMEDA=*,F5.2)
PRINT7
7 FCRMAT(/,* PSI*, 8X,*CD(I)*,12X,*IL-IR*,12X,*IL+IR*
1.15X,*POLZ*,15X,*POLX*)
DC 57 K=1, NANGL
ANGL=PSI(K)*180./PI
PRINT 58 , ANGL, CD(K) , ILMIR(K), ILPIR(K),IL(K),IR(K)
58 FCRMAT(* *, F8.4, 4X, E12.5, 4(4X,E15.8))
57 CCATINUE
C

```

```

C*****
C* DETERMINE THE MAXIMUM VALUE FOR PLOTTING SUBROUTINE *
C*****
      DO 109 I=1,NANGLE
      CDMAX=AMAX1(ABS(CC(I)),CDMAX)
      SMAX=AMAX1(ILPIR(I),SMAX)
      SMAXL=AMAX1(IL(I),SMAXL)
      SMAXR=AMAX1(IR(I),SMAXR)
109   CONTINUE
      IF(CDMAX.GE.0.2) CDMAX=1.
      DO 1115 J=1, NANGL
      CD(J)=CD(J)/CDMAX
      PLCTSC(J)=ILPIR(J)/SMAX
      PLCTIL(J)=IL(J)/SMAXL
      PLCTIR(J)=IR(J)/SMAXR
1115  CONTINUE
C PLOT SCATTERING VS PSI FOR DIFFERING AZIMUTHS.
C
C PLOT GRAPHS
      IF(NOPLOT.EQ.0) GO TO 600
      IF(DISCRT.EQ.0) LYR=100
C
C IN PLOTTING SCATER=0. WILL PLOT CD, SCATER=1.0 WILL PLOT IL+IR/MAX(IL+IR)
C SCATER=2.0 , PLOT IL/MAX(IL), SCATER=3 , PLOT IR/MAX(IR)
C
      RMAX=1.0
C
C
C
C*****
C*PLOT SCATTERING VS PSI FOR DIFFERING APOLAR ANGLES *
C*IN PLOTTING SCATER=0. WILL PLOT CD, SCATER=1.0 WILL PLOT IL+IR/MAX(IL+IR) *
C*SCATER= 2.0 , PLOT IL/MAX(IL), SCATER=3 , PLOT IR/MAX(IR) *
C*****
      IF(PCLX.EQ.0.OF.PCLZ.EQ.0) GO TO 605
      INITIA=INITIA+1
      APCLAF=90. - APOLAR
      PRINT 151,CDMAX,APOLAR
151   FORMAT(/,*GRAPH OF CD/CDMAX WITH CDMAX=*,F16.3,*ALITUDE=*,F5.2)
      APCLAF=INT(APCLAF)
      SCATER=0
      IF(CDMAX.LT.1.0) SCATER=-1
      CALL PCLAF(ANGLE,CD,FMAX,APCLAF,P,A,SCATER,LAMBDA,LENGTH,LYR,
1   INITIA)
605   CONTINUE
C
      RMAX=1.0
      INITIA=INITIA+1
      PRINT 152, SMAX,APOLAR
152   FORMAT(/,*PLOT GRAPH FOR TOTAL SCATTER DIVIDED BY SMAX=*,
1   E16.8,2X,*APCLAFH =*, F5.2)
      APCLAF=INT(APOLAR)
      SCATER=1.0
      CALL PCLAF(ANGLE,PLCTSC,RMAX,APOLAR,P,A,SCATER,LAMBDA,LENGTH,
1   LYR,INITIA)
      PRINT 153,SMAXL,APOLAR
153   FORMAT(/,*PLOT GRAPH FOR LEFT SCATTER DIVIDED BY SMAXL=*,F16.3,
1   2X,*APOLAR=*,F5.2)
      SCATER=2.0
      CALL PCLAF(ANGLE,PLCTIL,RMAX,APOLAR,P,A,SCATER,LAMBDA,LENGTH,
1   LYR,INITIA)
      PRINT 154,SMAYR,APOLAR

```

```

154  FORMAT(/,*PLOT GRAPH FOR RIGHTSCATTER DIVIDED BY SMAXR=*,E16.8,
      1 2X,*APOLAR=*,F5.2)
      SCATER=3.0
      CALL PCLAR(ANGLE,FLCTIR,RMAX,APOLAR,P,A,SCATEF,LAPBDA,LENGTH,
      1 LYF,INITIA)
      600 CONTINUE
C
299  CONTINUE
300  CONTINUE
      GO TO 311
      STOP
20   CONTINUE
      PSISTR(I)=0.0
      GO TO 21
      END
      SLBRCTINE POLAR(TH,F,RMAX,APCLAR,FRATIC,RADIUS,SCATEF,W,L,LYP,
      1 INITIA)
C*****
C*THIS SLBRCTINE MAKES PCLAR GRAPHS
C*THE ARGUMENT OF THE FUNCTIONS ARE MEASURED IN DEGREE&S.
C*THE INPUT OF THE ANGLAR VARIABLE HAS TO BE ENTERED IN RADIANS
C*ANGLES ARE POSITIVE IN THE COUNTERCLOCKWISE DIRECTION.
C*AN ANGLE OF ZERO IS HORIZONTAL AND TO THE RIGHT.
C*****
      COMMON FMTT,FMPP,FMNN,TEO,PBO,NBO
      REAL NBO
      COMMON/IGSZZZ/Z(200)
      DIMENSION R(400),TH(400),Y(400)
      REAL L,LYF
      INTEGER STB,SPB,SNB
      DIMENSION YNEG(400)
      EXTERNAL FONT2
      DATA IRAC/2HR=/
      DATA IPITCH/2HP=/
      DATA IWAVE/2HW=/
      DATA ISENTE/4FALT=/
      DATA ILYF/4HLYR=/
      DATA ILENGH/2HL=/
      INTEGER BLANK
      DATA ELANK/4H /
      DATA IPB/3HPB=/
      DATA INB/3HNB=/
      DATA ITB/3HTB=/
      DATA LOGLBL/3HLG=/
      DATA ICOPMA/1H./
      DATA LGFNT/3HLT=/
995  FORMAT(A3,I3)
996  FORMAT(A2,F4.2)
999  FORMAT(A4,F5.2)
      LOGLEN=10
      ENCODE(9,999,LABEL1)ISENTE,APCLAR
      IF(LYR.NE.100)ENCODE(9,999,LABEL)ILYR,LYP
      ENCODE(6,996,LABEL2)IPITCH,FRATIO
      ENCODE(6,996,LABEL3)IRAC,RADIUS
      ENCODE(6,996,LABEL5)IWAVE,W
      IF(L.GT.99.)LOGLEN=ALOG10(L)
      IF(L.LE.99)ENCODE(6,996,LABEL6)ILENGH,L
      IF(L.GT.99)ENCODE(6,995,LABEL)LOGLBL,LOGLEN
913  FORMAT(F4.2)
      ENCODE(4,913,STB)FMTT
      ENCODE(4,913,SPB)FMPP
      ENCODE(4,913,SNB)FMNN

```



```

911  FORMAT(A3,F4.2,A1)
      ENCODE(8,911,LABELT)ITB,TB0,ICOMMA
      ENCODE(8,911,LABELP)IPB,FB0,ICOMMA
      ENCODE(8,911,LABELN)INB,NB0,ICOMMA
      IF(FMTT.LT.0.01)LCGFMT=ALCG10(T90)
      IF(FMTT.LT.0.01)ENCCDE(8,911,LABELT)LGFMT,T9C,ICOMMA
912  FORMAT(A3,A4,A1)
      IF(FMTY.EQ.0)ENCCDE(8,912,LABELT)ITB,BLANK,ICOMMA
      IF(FMPP.EQ.0)ENCCDE(8,912,LABELP)IPB,BLANK,ICOMMA
      IF(FMNN.EQ.0)ENCCDE(8,912,LABELN)INB,BLANK,ICOMMA
C
C
C  HERE IS WHERE THE POSITIVE VALUES ARE SEPARATED FROM NEGATIVE VALUES
      DO 20 I=1, 361
      YNEG(I)=0.0
      Y(I)=ABS(R(I))
      IF(R(I).LT.0.0) YNEG(I)=ABS(R(I))
20   CONTINUE
C
C
C
C *****
C*IMPRTANT IMPRTANT IMPRTANT *
C*HERE IS WHERE THE PLOTTING FRTIME GETS INITIALIZED ONLY ONCE *
C *****
      IF(INITIAL.NE.1) GO TO 23
      CALL MCDESG(Z,6.4HCIDS)
23   CONTINUE
C
C
      CALL VECIG(Z,FONT2.0)
      CALL SETSPG(Z,51.1.)
C  SET UP VIEW PORT TO LEAVE 20 PERCENT BORDER
      CALL CBJCTG(Z,20.,20.,80.,90.)
C  SET THETA AXIS OFFSET
      Z(185)=90.
C  DEFINE THE SUBJECT SPACE FOR BOTH RADIAL AND ANGULAR VARIABLES
      CALL PSUEJG(Z,0.,0.,FMAX,360.)
C  DRAWS A GRID OF 30 DEGREES OF ANGLLAP SPACING AND .2 CF RADIAL UNITS
      CALL SETSPG(Z,173.0.C)
      CALL PGRIDG(Z,FMAX/5.0,30.,0.,0.)
C  SETS FORMAT FOR LABELLING
      CALL SETSPG(Z,30,2.)
      CALL SETSPG(Z,45,2.0)
      FMT=5.2
C  LABEL RADIAL AXIS
      CALL PCLEG(Z,.65,175.,4,4H0.60)
      CALL PCLEG(Z,1.05,175.,4,4H1.00)
C  SET LARGE CHARACTER SIZE
      CALL SETSPG(Z,45,3.0)
C  INDICATE THE FORMAT FOR THE LABELLING
      FMT=6.2
C  LABEL THETA AXIS
      CALL PLABELG(Z,1,30.,0,FMT)
      CALL SETSPG(Z,45,3.C)
      X8=FMAX*1.41
      CALL PCLEG(Z,X8 .211., 9,LABEL)
      X7=FMAX*1.7
      IF(SCATER.EQ.4.0)
1     CALL PCLEG(Z,X7,136.,7,7HCD/MAX )
      IF(SCATER.EQ.0.C)
1     CALL PCLEG(Z,X7,136.,7,7HCIDS Y)

```

```

      IF (SCATER.EQ.1.0)
1 CALL PCLEG(Z,X7,136.,7,7HSCATY Y)
      IF (SCATER.EQ.2.0)
1 CALL PCLEG(Z,X7,136.,7,7HI PCLZ )
      IF (SCATER.EQ.3.0)
1 CALL PCLEG(Z,X7,136.,7,7HI PCLX )
      PRINT998,LABEL,LABEL2,LABEL3,LABEL5,LABEL6
      PRINT998,LABELT,LABELP,LABELN
998 FCRMAT(* *,*HERE ARE THE LABELS *, 6(4X,A9))
      X3=RMAX*1.79
      CALL PCLEG(Z,>3 ,30.,6,LABEL3)
      X4=RMAX*2.2
      CALL PCLEG(Z,X4,45., 6,LABEL2)
      X5=RMAX*2.05
      CALL PCLEG(Z,X5 ,49., 6,LABEL5)
      X6=RMAX*1.61
      CALL PCLEG(Z,>6,33.,6,LABEL6)
      XTB=RMAX*1.73F
      CALL PCLEG(Z,>TB,339.,8,LABELT)
      IF (FMNN.EQ.0.AND.FMFP.EQ.0) GC TO 50
      XPB=RMAX*1.54
      CALL PCLEG(Z,XPB,335.,8,LABELP)
      XNB=RMAX*1.36
      CALL PCLEG(Z,XNB,332.,8,LABELN)
      XSTB=2.07*RMAX
      CALL PCLEG(Z,XSTE ,320.,4,STB)
      XSPB=1.92*RMAX
      CALL PCLEG(Z,XSPE ,317.,4,SPB)
      XSAB=1.79*RMAX
      CALL PCLEG(Z,XSNB ,312.,4,SNB)
50 CCNTINUE
C JCINS WITH A LINE THE PCINTS THAT HAVE BEEN PLOTTED
      CALL SETSPG(Z,30,2.)
      CALL PLINEG(Z,361,Y,TH)
      IF (SCATER.EQ.4) GC TO 41
      IF (SCATER.GE.1.0) GC TO 40
41 CCNTINUE
      CALL SETSPG(Z,30,4.)
      CALL PLINEG(Z,361,YNEG,TF)
40 CCNTINUE
      CALL SETSPG(Z,30,2.)
C MCVL TC NEW FRAME
      CALL PAGEG(Z,0,1,1)
C TC EXIT
      CALL EXITG(Z)
      PRINT 21,RMAX,PRATIC,W,RADIUS,L
21 FCRMAT(* *,*GPAH HAS BEEN PLOTTED WITH RMAX=*, F 8.4,
:4X,*PERICC=*,F10.6,2X,* WAVELENGTH=*,F9.4,2X,*RADIUS=*,F9.4
: ,2X,*LLENGTH=*,F9.4)
      RETURN
      END

```

